

MODELLING OF A SOLAR POND AS A COMBINED HEAT SOURCE AND STORE TO DRIVE AN ABSORPTION COOLING SYSTEM FOR A BUILDING IN IRAQ

A thesis submitted to The University of Manchester for the degree of

Doctor of Philosophy

in the Faculty of Science and Engineering

2017

Safwan Mohammed Jameel Ahmed Kanan

School of Mechanical, Aerospace and Civil Engineering

University of Manchester

Table of Contents

ABSTRACT.....	9
DECLARATION	10
COPYRIGHT STATEMENT	11
ACKNOWLEDGEMENT	12
LIST OF PUBLICATIONS	13
LIST OF TABLES	14
LIST OF FIGURES	15
NOMENCLATURE.....	20
CHAPTER 1. INTRODUCTION	22
1.1 BACKGROUND AND OVERVIEW	22
1.2 SOLAR POND.....	23
1.3 APPLICATIONS OF SOLAR PONDS	24
1.4 COMPARISON BETWEEN SOLAR POND AND FLAT PLATE SOLAR COLLECTOR	24
1.5 ABSORPTION REFRIGERATION SYSTEMS.....	25
1.6 SUGGESTED COOLING SYSTEM FOR BUILDINGS IN IRAQ	25
1.7 AIM AND OBJECTIVES.....	25
1.8 STRUCTURE OF THE THESIS	26
CHAPTER 2. FUNDAMENTALS AND LITERATURE REVIEW.....	29
2.1 INTRODUCTION	29
2.2 BUILDING COOLING LOADS	31
2.3 AIR CONDITIONING SYSTEMS.....	34
2.3.1 ALL -AIR SYSTEMS.....	35
2.3.2 ALL -WATER SYSTEMS	36
2.3.3 AIR- WATER SYSTEMS	37

2.3.4 UNITARY OR PACKAGE REFRIGERANT BASED SYSTEMS.....	37
2.4 REFRIGERATION SYSTEMS.....	37
2.5 CHILLERS.....	39
2.5.1 VAPOUR COMPRESSION CHILLER SYSTEM.....	39
2.5.2 VAPOUR ABSORPTION CHILLER SYSTEM	41
2.5.3 ADSORPTION CHILLER SYSTEM.....	43
2.5.4 DESICCANT DEHUMIDIFICATION	43
2.5.5 CHILLERS SUMMARY	44
2.6 SOLAR COOLING.....	45
2.7 SOLAR COLLECTORS.....	49
2.8 SOLAR POND.....	50
2.8.1 HISTORY	50
2.8.2 SALT GRADIENT SOLAR PONDS.....	51
2.9 OTHER TYPES OF SOLAR PONDS.....	52
2.9.1 PARTITIONED SOLAR PONDS	52
2.9.2 VISCOSITY STABILIZED SOLAR PONDS	53
2.9.3 MEMBRANE STRATIFIED SOLAR PONDS	54
2.9.4 SATURATED SOLAR PONDS.....	54
2.9.5 SHALLOW SOLAR PONDS	54
2.10 SALINITY GRADIENT SOLAR POND FUNDAMENTALS	55
2.10.1 SOLAR RADIATION WITH SOLAR POND.....	55
2.10.2 SALT GRADIENT SOLAR POND ZONES	59
2.10.3 CONSTRUCTION AND MAINTENANCE OF SALT GRADIENT	60
2.10.4 METHODS OF GRADIENT ESTABLISHMENT	61
2.10.5 THE SOLAR POND STABILITY	62
2.10.6 SALINITY GRADIENT SOLAR POND STABILITY	63

2.10.7 STATIC STABILITY	63
2.10.8 MOLECULAR DIFFUSION	64
2.10.9 STATIC STABILITY CRITERIA.....	64
2.10.10 DYNAMIC STABILITY CRITERION.....	66
2.11 SALT GRADIENT SOLAR POND CASE STUDIES.....	67
2.11.1 BET HA ARAVA SOLAR POND	69
2.11.2 PYRAMID HILL SOLAR POND	69
2.11.3 MARGHERITA DI SAVOIA SOLAR POND.....	70
2.11.4 BHUJ SOLAR POND, INDIA	70
2.11.5 ALICE SPRINGS SOLAR POND	71
2.11.6 UTEP HIGH – PERFORMANCE SOLAR POND	73
2.11.7 HEAT EXTRACTION AND REJECTION	74
2.11.8 CONVENTIONAL METHODS OF HEAT EXTRACTION.....	74
2.11.9 HEAT EXTRACTION FROM THE GRADIENT LAYER.....	76
2.11.10 SOLAR POND FOR BOTH HEAT EXTRACTION AND REJECTION	79
2.11.11 SUGGESTED SYSTEM FOR THIS RESEARCH.....	80
2.12 PRACTICAL DESIGN CONSIDERATION OF SOLAR PONDS	81
2.13 DIFFICULTIES AND LIMITATIONS OF SOLAR POND USE	81
2.14 MODELLING APPROACHES AND SOFTWARE.....	83
2.15 CONCLUSIONS.....	86
CHAPTER 3. DATA.....	88
3.1 INTRODUCTION	88
3.2 WEATHER DATA FOR SIMULATION PROGRAM.....	88
3.2.1 WEATHER DATA TYPES.....	88
3.2.2 TEST REFERENCE YEAR (TRY).....	89

3.2.3 TYPICAL METROLOGICAL YEAR (TMY).....	89
3.2.4 INTERNATIONAL WEATHER FOR ENERGY CALCULATIONS (IWEC).....	90
3.2.5 ENERGY PLUS WEATHER (EPW).....	90
3.2.6 IRAQ WEATHER DATA	91
3.3 SALINITY GRADIENT SOLAR POND DATA.....	96
3.4 GROUND HEAT LOSS	98
3.4.1 SOIL THERMAL PROPERTIES.....	98
3.4.2 DEPTH OF THE WATER TABLE.....	100
3.5 BUILDING DATA	101
3.6 EQUIPMENT DATA.....	104
3.7 TRNSYS	105
3.7.1 SOLAR POND DATA.....	105
3.7.2 HEAT EXCHANGER DATA	105
3.7.3 ABSORPTION CHILLER.....	106
3.7.4 COOLING TOWER.....	108
3.7.5 COOLING COIL	108
3.7.6 SINGLE SPEED FAN	109
3.7.7 PUMPS.....	110
3.7.8 THERMOSTAT.....	110
3.8 CONCLUSION	112
CHAPTER 4. MATHEMATICAL MODELLING	113
4.1 INTRODUCTION	113
4.2 METHODOLOGY.....	113
4.3 MATHEMATICAL FORMULATION	114
4.3.1 ASSUMPTIONS FOR FINITE DIFFERENCE MODEL	114

4.3.2 SOLAR RADIATION MODEL IN THE SOLAR POND	115
4.3.3 HEAT TRANSFER MODEL FOR SOLAR POND.....	116
4.3.4 HEAT TRANSFER MODEL FOR SOIL BELOW THE POND.....	120
4.3.5 MASS TRANSFER MODEL FOR SOLAR POND	122
4.3.6 FINITE DIFFERENCE METHOD.....	124
4.3.7 NUMERICAL SOLUTION OF SOLAR POND AND THE GROUND MODEL	127
4.4 TRNSYS 17	128
4.5 COMPLETE SYSTEM MODELLING	129
4.6 BUILDING DESCRIPTION	130
4.6.1 TRNSYS3D	130
4.6.2 TRNBUILD	131
4.6.3 IMPORTING THE BUILDING MODEL	133
4.7 ABSORPTION CHILLER MODEL	134
4.7.1 MODELLING OF TYPE 107	134
4.8 SOLAR POND MODEL.....	136
4.8.1 CALLING MATLAB TYPE 155	137
4.8.2 STRUCTURE OF THE M-FILE	139
4.8.3 CALLING SOLAR POND'S MATLAB CODE IN TRNSYS	140
4.9 COMPLETE SYSTEM COMPONENTS (TYPES).....	142
4.10 COUPLED SYSTEM DESCRIPTION	143
4.11 OUTPUTS FROM TRNSYS	146
4.11.1 SYSTEM OFF OUTPUTS.....	146
4.11.2 AMBIENT AND ROOM AIR TEMPERATURES.....	147
4.11.3 AMBIENT AND CHILLED WATER OUTLET TEMPERATURES...	149
4.12 THE REPRESENTATIVE YEAR.....	153
4.13 CONCLUSION	1525

CHAPTER 5. RESULTS AND DISCUSSION.....	155
5.1 INTRODUCTION	155
5.2 FEASIBILITY AND SIZING OF THE BASE CASE	155
5.2.1 SOLAR POND.....	156
5.2.2 HEAT EXTRACTION	160
5.2.3 HOT WATER INLET TEMPERATURE.....	162
5.2.4 ABSORPTION CHILLER.....	163
5.2.5 ROOM AIR TEMPERATURE.....	165
5.2.6 COOLING COIL AIR AND WATER TEMPERATURES	166
5.2.7 COOLING TOWER.....	168
5.3 VALIDATION.....	169
5.3.1 INTRODUCTION.....	169
5.3.2 VALIDATION OF THE SOLAR POND MODEL.....	169
5.3.3 VALIDATION OF THE ABSORPTION CHILLER.....	173
5.3.4 ENERGY BALANCE FOR THE SOLAR POND COOLING SYSTEM.....	174
5.4 PARAMETERS VARIATION	177
5.4.1 SELECTION OF REQUIRED SOLAR POND AREA.....	177
5.4.2 SOLAR POND AND GROUND CONDITIONS	180
5.4.3 SOIL TYPE.....	180
5.4.4 MOISTURE CONTENT.....	181
5.4.5 SANDY SOIL TEXTURE.....	182
5.4.6 DEPTH OF THE WATER TABLE.....	183
5.4.7 GROUND CONDITIONS SUMMARY	186
5.4.8 SOLAR POND OPTIMUM ZONE THICKNESSES	186
5.4.9 UCZ THICKNESS.....	187
5.4.10 NCZ THICKNESS.....	190

5.4.11 LCZ THICKNESS	192
5.4.12 OPTIMUM ZONE THICKNESSES SUMMARY	194
5.5 HEAT EXCHANGER EFFECTIVENESS	195
5.6 ELECTRICAL ENERGY CONSUMPTION	197
5.7 CONCLUSION	199
CHAPTER 6. CONCLUSIONS AND RECOMMENDATIONS	201
6.1 INTRODUCTION	201
6.2 CONCLUSIONS.....	201
6.2.1 CONTRIBUTION.....	201
6.2.2 METHOD AND VALIDATION	201
6.2.3 BASE CASE MAIN PARAMETER VALUES AND PERFORMANCE	202
6.2.4 KEY PARAMETER VARIATIONS AND EFFECT ON PERFORMANCE	204
6.2.5 PRACTICAL CONSIDERATIONS.....	205
6.2.6 OVERALL CONCLUSION	205
6.3 RECOMMENDATIONS	206
6.3.1 RECOMMENDATIONS AND PRACTICAL SUGGESTIONS.....	206
6.3.2 RECOMMENDATIONS FOR FURTHER RESEARCH	206
APPENDIX A: MATLAB CODES	208
APPENDIX B: DATA	217
APPENDIX C: PUBLISHED PAPERS	224
REFERENCES.....	251

Abstract

The University of Manchester

Safwan Mohammed Jameel Ahmed Kanan

Doctor of Philosophy (PhD)

Modelling of a solar pond as a combined heat source and store to drive an absorption cooling system for a building in Iraq

23 October 2016

This research studies the performance of a salinity-gradient solar pond driving an absorption cooling system, as an alternative to a conventional electrically-powered cooling system, to provide cool air for a modern single family house in the hot dry climate of Baghdad, Iraq.

The system comprises a salinity-gradient solar pond, a hot-water-fired absorption water chiller, a chilled-water cooling coil which cools the air in the house, and a cooling tower which rejects heat to the ambient air. Hot brine from the pond circulates through a heat exchanger, where it heats water that is then pumped to the chiller. This arrangement protects the chiller from the corrosive brine. The system is controlled on-off by a room thermostat in the house.

The system performance is modelled by dynamic thermal simulation using TMY2 hourly typical weather data. TRNSYS software is used for the main simulation, coupled to a MATLAB model of heat and mass transfer in the pond and the ground beneath it. The model of the pond and the ground is one-dimensional (only vertical transfers are considered). Radiation, convection, conduction, evaporation and diffusion are considered; the ground water at some depth below the pond is treated as being at a fixed temperature. All input data and parameter values in the simulation are based on published, standard or manufacturer's data.

Temperature profiles in the pond were calculated and found to be in good agreement with published experimental results.

It was found that a pond area of approximately 400 m² was required to provide satisfactory cooling for a non-insulated house of approximately 125 m² floor area.

It was found that varying the pond area, ground conditions and pond layer thicknesses affected the system performance. The optimum site is one that has soil with low thermal conductivity, low moisture content and a deep water table.

It is concluded that Iraq's climate has a potential for solar-pond-powered thermal cooling systems. It is feasible to use a solar-pond-powered cooling system to meet the space-cooling load for a single family house in the summer season. Improving the thermal performance of the house by insulation could reduce the required solar pond area.

Declaration

No portion of the work referred to in the thesis has been submitted in support of an application for another degree or qualification of this or any other university or other institute of learning.

Copyright Statement

i. The author of this thesis (including any appendices and/or schedules to this thesis) owns certain copyright or related rights in it (the “Copyright”) and s/he has given The University of

Manchester certain rights to use such Copyright, including for administrative purposes.

ii. Copies of this thesis, either in full or in extracts and whether in hard or electronic copy, may be made only in accordance with the Copyright, Designs and Patents Act 1988 (as amended) and regulations issued under it or, where appropriate, in accordance with licensing agreements which the University has from time to time. This page must form part of any such copies made.

iii. The ownership of certain Copyright, patents, designs, trademarks and other intellectual property (the “Intellectual Property”) and any reproductions of copyright works in the thesis, for example graphs and tables (“Reproductions”), which may be described in this thesis, may not be owned by the author and may be owned by third parties. Such Intellectual Property and Reproductions cannot and must not be made available for use without the prior written permission of the owner(s) of the relevant Intellectual Property and/or Reproductions.

iv. Further information on the conditions under which disclosure, publication and commercialisation of this thesis, the Copyright and any Intellectual Property and/or Reproductions described in it may take place is available in the University IP Policy (see <http://documents.manchester.ac.uk/DocuInfo.aspx?DocID=487>), in any relevant Thesis restriction declarations deposited in the University Library, The University Library’s regulations (see <http://www.manchester.ac.uk/library/aboutus/regulations>) and in The University’s policy on Presentation of Theses.

Acknowledgement

All praises to Almighty Allah who bestowed upon me the capabilities to complete this work. I extend my sincerest thanks to my praise worthy supervisor Dr. Jonathan Dewsbury for his precious time, valuable guidance, continuous support, constructive criticism, motivations and incredible encouragements.

I gratefully acknowledge Iraqi Cultural Attaché in London and Ministry of Higher Education and Scientific Research (MOHESR – Baghdad) and the Erbil Polytechnic University, who provided the required supports for this project.

Special thanks for my wife who was a great support for me when I was in this scholarship at Manchester University as well as to my three lovely kids, for their endless love and support during this study.

List of Publications

- **Kanan, S.**, Dewsbury, J. and Lane-Serff, G.F., 2016. Optimum zone thicknesses for a solar pond connected to a solar air-conditioning. Submitted to Solar Energy Journal.
- **Kanan, S.**, Dewsbury, J. and Lane-Serff, G.F., 2016. The effect of ground conditions under a solar pond on the performance of a solar air conditioning system. Energy Procedia, 91, pp.777-784.
- Asim, M., Dewsbury, J., **Kanan, S.**, 2016. TRNSYS simulation of a solar cooling system for the hot climate of Pakistan. Energy Procedia, 91, pp.702-706.
- **Kanan, S.**, Dewsbury, J. and Lane-Serff, G.F., 2015. Simulation of Solar Air-Conditioning System with Salinity Gradient Solar Pond. Energy Procedia, 79, pp.746-751.
- **Kanan, S.**; Dewsbury, J. ; Lane-Serff, G.F.,2014, A Simple Heat and Mass Transfer Model for Salt Gradient Solar Ponds, World Academy of Science, Engineering and Technology, International Science Index 85, International Journal of Mechanical, Aerospace, Industrial, Mechatronic and Manufacturing Engineering, 8(1), pp.27 - 33.

List of Tables

Table 2.1 Index of refraction for different medium	57
Table 2.2 Rabl and Nielsen's absorption data (1975)	58
Table 3.1 Different weather data sets	93
Table 3.2 Range of several thermophysical properties of sodium chloride solutions	97
Table 3.3 Soil thermal properties	100
Table 3.4 Soil thermal properties with a different texture	100
Table 3.5 Building geometrical dimensions	101
Table 3.6 Building data	103
Table 3.7 Heat exchanger data	106
Table 3.8 Inputs for (7 TR) absorption chiller	107
Table 3.9 Closed circuit cooling tower data.....	108
Table 3.10 Cooling Coil data (Type 697)	109
Table 3.11 Existing pumps data from Wilo Company.....	110
Table 4.1 values of spatial layer thickness and time steps with the maximum LCZ temperature.....	126
Table 4.2 Complete system components (Types) used in TRNSYS simulation	143
Table 5.1 The Bundoora experimental pond and current simulation pond model.....	170
Table 5.2 Annual input and output energies for all components.....	175
Table 5.3 Number of hours for chilled water outlet temperature at 7°C with different ground conditions.....	186
Table 5.4 Zone thicknesses for simulations.....	187
Table 5.5 Number of hours for chilled water set point temperature of (7°C) achieved by varying zone thicknesses.....	194
Table B.1 Absorption chiller energy balance.....	219
Table B.2 Solar pond cooling system energy balance for the second year.....	220
Table B.3 Vapour compression air cooled chiller and heat pump from YORK.....	223

List of Figures

Figure 1.1 Schematic view of the salt gradient solar pond	27
Figure 1.2 Absorption chiller system diagram	27
Figure 1.3 Monthly mean dry bulb temperature and global horizontal radiation for Baghdad	28
Figure 2.1 World Primary energy consumption 1989-2014	30
Figure 2.2 World carbon dioxide emission 1965-2035	31
Figure 2.3 Origin of Difference Between Magnitude of Instantaneous Heat Gain and Instantaneous Cooling Load.	33
Figure 2.4 Electricity consumption by economic groups	34
Figure 2.5 All air heating and cooling system	36
Figure 2.6 Schematic representation of refrigeration system.....	38
Figure 2.7 Heat Transfer Loops in a typical Refrigeration System	38
Figure 2.8 Vapour compression cycle: principal system components and simple pressure–enthalpy diagram.	40
Figure 2.9 Schematic of a single effect LiBr-water absorption system	42
Figure 2.10 Desiccant dehumidification	44
Figure 2.11 Alternative routes from solar energy into cooling effect	48
Figure 2.12 Refraction and Reflection of solar radiation	56
Figure 2.13 Variation of radiation intensity with depth of solar pond as calculated on the basis of two different correlations given by Equations. (2.4) and (2.5).	59
Figure 2.14 Bet Ha Arava Solar pond power station in the Dead Sea	69
Figure 2.15 3000 m ² solar pond at Pyramid Hill, Australia.	70
Figure 2.16 Solar pond, Bhuj, India	71
Figure 2.17 Alice Springs Solar Pond, Australia	72
Figure 2.18 ORC Engine at Alice Springs.....	72
Figure 2.19 El Paso Solar Pond, Texas, USA	73

Figure 2.20 Conventional method of heat extraction using an internal heat exchanger	75
Figure 2.21 Conventional method of heat extraction using an external heat exchanger	75
Figure 2.22 53 m2 Bundoora experimental solar pond	76
Figure 2.23 In pond heat exchanger for gradient layer and LCZ	78
Figure 2.24 Schematic heat extraction system in solar pond	78
Figure 2.25 Solar pond connect to absorption chiller	79
Figure 3.1 Baghdad temperature comparison (WMO, TMY2, and NASA).....	92
Figure 3.2 Iraq cities maximum average temperature from TMY2	94
Figure 3.3 Iraq cities average global horizontal radiation from TMY2.....	94
Figure 3.4 Iraq cities average relative humidity from TMY2.....	95
Figure 3.5 Iraq cities average wind speed from TMY2	95
Figure 3.6 Density temperature variation for the different salinity of NaCl solution from (Lide and Bruno, 2004) compared with the linear density approximation	96
Figure 3.7 Whole building isometric plan view.	102
Figure 3.8 Annual cooling load for building in Baghdad, Iraq.....	104
Figure 3.9 Yazaki WFC – SC10 performance data file.....	107
Figure 3.10 Set Point Definition	111
Figure 4.1 Solar pond and ground mathematical model	117
Figure 4.2 Temperature profiles with different time steps at the end of July 2 nd year, layer thickness =0.01m.....	126
Figure 4.3 Temperature profiles with different layer thicknesses at the end of July 2 nd year, and different time steps.....	127
Figure 4.4 Diagram of complete system	130
Figure 4.5 Architecture view of house in Iraq	131
Figure 4.6 Building Zone in TRNBuild.....	133
Figure 4.7 Wall Layers Definition	133
Figure 4.8 Multi-zone building model (Type 56) with all required connections	135
Figure 4.9 Solar pond (Type 155) weather data inputs	139

Figure 4.10 Solar pond (Type 155) heat exchanger return data inputs	139
Figure 4.11 Calling solar pond's MATLAB code in TRNSYS	141
Figure 4.12 Complete TRNSYS simulation system for solar pond with absorption chiller and building	145
Figure 4.13 Ambient and room air temperatures during two years	147
Figure 4.14 Ambient and room air temperatures during first period system OFF ..	148
Figure 4.15 Ambient and room air temperatures during second period system OFF.	148
Figure 4.16 Ambient and room air temperatures during third period system OFF .	149
Figure 4.17 Ambient and chilled water outlet temperatures during two years	150
Figure 4.18 Ambient and chilled water outlet temperatures during first period system OFF	151
Figure 4.19 Ambient and chilled water outlet temperatures during second period system OFF	151
Figure 4.20 Ambient and chilled water outlet temperatures during third period system OFF	152
Figure 4.21 TLCZ and TUCZ for three year simulation time.....	153
Figure 4.22 Difference between TLCZ3 (third year) and TLCZ2 (second year) for summer season.....	153
Figure 5.1 Pond lower and upper zones temperature with ambient temperature with simulation time	157
Figure 5.2 Temperature distribution for a solar pond and the ground underneath at the end of January, April, July, and October in the second simulation year	158
Figure 5.3 Solar pond monthly average efficiency for the second simulation year	159
Figure 5.4 Concentration profiles of the solar pond for a month to five years	160
Figure 5.5 Heat extraction from the solar pond	161
Figure 5.6 Pond outlet and inlet temperatures.	161
Figure 5.7 Hot water inlet temperature to the absorption chiller	162
Figure 5.8 Chilled water outlet temperature	163
Figure 5.9 Chilled water inlet and outlet temperatures	164
Figure 5.10 Coefficient of performance for absorption chiller	165
Figure 5.11 Ambient and room air temperatures for two years	166

Figure 5.12 Inlet and outlet air temperature for cooling coil	167
Figure 5.13 Inlet and outlet water temperature for cooling coil	167
Figure 5.14 Inlet and outlet water temperatures of the cooling tower	168
Figure 5.15 Simulated (MATLAB code) and experimental (Leblanc et al., 2011) temperature distributions for Bundoora solar pond on 1st February 2008	170
Figure 5.16 Simulated and experimental (Leblanc et al., 2011) temperature distributions for El Paso solar pond on 1 st September 1999.....	173
Figure 5.17 Simulated and experimental (Leblanc et al., 2011) annual LCZ temperature profile of the El Paso solar pond and ambient temperature with TMY2.....	173
Figure 5.18 Yazaki chiller cooling capacity and simulation model.....	174
Figure 5.19 Yazaki chiller heat medium input and simulation model.....	175
Figure 5.20 Energy balance of the solar pond cooling system	177
Figure 5.21 Annual input and output energy distribution	177
Figure 5.22 Chilled water outlet temperature with different pond area	180
Figure 5.23 Chilled water outlet temperature with different types of soil under solar pond	182
Figure 5.24 Chilled water outlet temperature with different moisture content for clay and silt 2 soil under the solar pond	182
Figure 5.25 Chilled water outlet temperature with dry sand soil texture under the solar pond	183
Figure 5.26 Chilled water outlet temperature with different depth of the water table under the solar pond	185
Figure 5.27 Chilled water outlet temperature with different depth of the water table under the solar pond for May to October in the 2 nd year.	185
Figure 5.28 Effect of varying UCZ thickness on the chilled water outlet temperature with NCZ=1.25 m and LCZ=0.7 m	189
Figure 5.29 Effect of varying NCZ thickness on the chilled water outlet temperature with UCZ=0.3 m and LCZ=0.7 m	191
Figure 5.30 Effect of varying LCZ thickness on the chilled water outlet temperature with UCZ=0.3 m and NCZ=1.25 m	193

Figure 5.31 Effect of varying heat exchanger effectiveness on the chilled water outlet temperature	196
Figure 5.32 Effect of varying heat exchanger effectiveness on the solar pond efficiency.....	197
Figure 5.33 Monthly electrical energy consumption for solar pond cooling system	199
Figure B.1 Iraq global horizontal irradiation.....	218
Figure B.2 Yazaki absorption chiller performance spreadsheet (part 1 of 2).....	221
Figure B.3 Yazaki absorption chiller performance spreadsheet (part 2-of 2).....	222

Nomenclature

A_p	Area of the pond (m^2)
C	salt concentration (kg/m^3)
C_p	specific heat capacity of salt water ($J/kg\ ^\circ C$)
C_{pg}	specific heat capacity of soil ($J/kg\ ^\circ C$)
C_s	specific heat of moist air ($kJ/kg\ ^\circ C$)
D	coefficient of salt diffusion (m^2/s)
Fr	Fresnel reflection
g	gravity acceleration (m/s^2)
G_r	Grashof number
h	local time
h_{LCZ}	Heat transfer coefficient in the LCZ ($W/m^2\ ^\circ C$)
h_c	convection heat transfer coefficient ($W/m^2\ ^\circ C$)
H_o	monthly average insolation incident on horizontal surface (W/m^2)
H_x	incoming radiation flux at depth x (W/m^2)
J	diffusion flux ($kg/m^2\ s$)
k	thermal conductivity of the solution ($W/m\ ^\circ C$)
LCZ	lower convective zone
L_e	Lewis number
L	Length of the solar pond
L_c	characteristic length
L_v	Latent heat of evaporation of water (kJ/kg)
m	Brine mass flowrate (kg/s)
max t	maximum time (s)
MC	moisture content (%)
n	number of cells in the NCZ
$n1, n2$	index
N	the day of the year
NCZ	non-convective zone
P_a	partial pressure of water vapour in ambient air at temperature T_a (mmHg)
P_l	vapour pressure of water at surface temperature T_l
P_r	Prandtl number
$q'(x, t)$	solar radiation energy absorbed in the body of the pond (W/m^2)
q_c	Heat transfer by convection (W/m^2)
q_e	Heat transfer by evaporation (W/m^2)
q_{ext}	Heat extracted from the pond (W/m^2)
q_g	Heat loss to the ground (W/m^2)
q_{loss}	Heat loss to the environment (W/m^2)
q_r	Heat transfer by radiation (W/m^2)
q_{cond}	Heat transfer by conduction (W/m^2)
Q_{up}	heat loss from LCZ to NCZ (W)
Ra	Rayleigh number
Ra_T	Thermal Rayleigh number
Ra_s	Solutal Rayleigh number
Ra_I	Internal Rayleigh number
RH	Relative humidity
$S(x, t)$	Salinity
t	Time (s)

T	temperature ($^{\circ}\text{C}$)
T_a	ambient temperature ($^{\circ}\text{C}$)
TR	ton of refrigeration
T_{sky}	Sky temperature ($^{\circ}\text{C}$)
V	Wind speed (m/s)
x	depth (m)
X_{LCZ}	thickness of the LCZ (m)
X_{NCZ}	thickness of the NCZ (m)
X_{UCZ}	thickness of the UCZ (m)

Greek symbols

α	Brine thermal diffusivity (m^2/s)
α_g	soil thermal diffusivity (m^2/s)
β_T	Thermal expansion coefficient ($1/^{\circ}\text{C}$)
β_s	Salinity expansion coefficient (m^3/kg)
Δt	time step (s)
Δx	space step (m)
ΔH_x	difference between the solar radiation within the element (W/m^2)
δ	declination angle
ϵ_w	Emissivity of water
ν	Kinematic viscosity (m^2/s)
μ	viscosity ($\text{kg}/\text{m}\cdot\text{s}$)
μ_i	average extinction coefficient for <i>ith</i> portion of solar spectrum (m^{-1})
ρ	Density (kg/m^3)
η_i	fraction of solar radiation
θ_r	angle of refraction at the pond surface (deg)
θ_i	radiation incident-angle over pond's surface (deg)
λ	wavelength of light travelling through respective medium
σ	Stefan-Boltzmann constant $\text{W}/\text{m}^2\text{K}^4$
τ	dimensional mesh Fourier number
ϕ	latitude angle (deg)
ω	hour angle

Subscripts

o	reference
amb	ambient
b	base
c	corrected
d	dry
g	ground
LCZ	lower convective zone
NCZ	non-convective zone
UCZ	upper convective zone
w	water

Chapter 1. Introduction

1.1 Background and Overview

The greatest advantage of solar energy as compared with other forms of energy is that it is clean and can be supplied without environmental pollution. Solar energy is freely usable; merely it wants a collection system to harness it. The intermittent nature of its supply often makes it necessary to have a storage system so that it can be used conveniently whenever there is a need for it. At present, conventional collection and storage systems are quite expensive and often uneconomic. To make it more economically feasible, it is necessary to reduce the cost of collection and storage systems. It should be mentioned that the material cost of a conventional collection and storage system is close to 75% of the total cost and, as such, the prospect of reducing the price of a conventional system does not seem to be very bright. The solar pond is a relatively cheap form of collection and storage system that is especially suitable for rural areas and can be used for heating, cooling, drying, solar power generation as well as for other purposes (Hawladar, 1981).

The Iraqi climate has hot, dry summers, cold winters, and a pleasant spring and autumn. Roughly 90% of the annual rainfall occurs between November and April, most of it in the winter months from December through March. The remaining six months, particularly the hottest ones of June, July, and August, at approximately 40°C on average, are dry. The influence of the Gulf on the climate of Iraq is very limited. In the south of Iraq and near the Gulf the relative humidity is higher than in other parts of the country. (Iraq-Climate, 1988)

Due to this hot and dry summer and cold winter, buildings in Iraq need cooling in summer and heating in winter. The monthly mean dry-bulb temperature and global horizontal radiation for Baghdad is shown in Figure 1.3. It may be seen that the climate is favourable for solar cooling, as the solar radiation is abundant (mean over 300 W/m² from May to August) and nearly in phase with the dry-bulb temperature. Iraq receives a high level of solar radiation: Baghdad averages 7.56 kWh/m² day in June and 5.02

kWh/m² day annually (Surface meteorology and solar energy, 2016). On the other hand, the impacts of a stop in investment in the power sector and rapidly increasing electricity demand have created a shortage and desperate need for reliable power. This, in turn, affected the using of the heating and cooling systems for buildings.

1.2 Solar Pond

A solar pond is an artificial large body of water that collects and stores solar thermal energy. It is about 1 to 3 metres deep, and the bottom of the pond is usually painted black. The solar radiation landing on the surface of the pond penetrates the liquid and falls on the blackened bottom which is thereby heated. In the normal case, if the liquid is homogeneous, convection currents will be set up and the heated liquid, being lighter, will travel towards the surface dissipate its heat to the atmosphere. In a solar pond these convection currents are prevented by having a density gradient of salt, the solution's density being highest at the bottom and lowest at the top. Typically a pond is composed of three zones as shown in Figure 1.1. The first zone is the Upper Convective Zone (**UCZ**), which is cold, close to the ambient temperature, and has low salt concentration (almost fresh water). The thickness of this surface layer varies from 0.1 to 0.4 m. The second zone is the Non-Convective Zone (**NCZ**) (or insulation layer), where the salt density increases with depth. The thickness of the NCZ ranges from 0.6 to 1.5 m. Hot water in the NCZ cannot rise because it has a greater salt content than the water above and is therefore denser. Similarly, cool water cannot fall because the water below it has a higher salt content, therefore a greater density. Therefore, convection motions are hindered and heat transfer from the third hot zone, the Lower Convective Zone (**LCZ**) (or storage layer) to the cold UCZ can only happen through conduction. Given the fairly low conductivity of water, the NCZ layer acts as a transparent insulator, permitting solar radiation to be trapped in the hot bottom layer, from which useful heat is withdrawn. LCZ thickness depends on the temperature and the amount of the thermal energy to be stored. (Angeli and Leonardi, 2004), (El-Sebaei et al., 2011).

1.3 Applications of Solar Ponds

Because of the massive storage of heat and negligible diurnal fluctuation in temperature, solar ponds have a variety of applications such as electrical power generation, water desalination, heating and cooling of buildings and industrial process heating.

Because of the large heat storage capability in the lower convective zone (LCZ) of the solar pond, it has an ideal use for house heating, even for several cloudy days. The solar pond may be operated in conjunction with a heat pump. The heat pump could serve as an air conditioner in summer (Kamal, 1992).

1.4 Comparison Between Solar Pond and Flat Plate Solar Collector

The daily calculation of heat collected from solar pond and comparison to the performance of a flat-plate solar collector has been investigated by Kooi in 1979. On a sunny day, the flat-plate collector collected more heat than the solar pond because the effective absorptivity-transmissivity for the flat-plate collector is higher than for the solar pond. On a cloudy day, the solar pond collected slightly more heat than the flat-plate collector since its heat-loss factor is lower. The loss factor depends on the thermal conductivity of water and on the thickness and insulation of the NCZ. The pond is expected to perform better than the flat-plate collector at high temperature difference or low solar radiation (Kooi, 1979). The advantage of the pond's low loss factor is reduced by night-time losses. The pond cannot be turned off when the heat collected becomes zero, so it loses heat continuously. On the other hand, the flat-plate collector is turned off when heat collected become zero and does not lose heat continuously. However, it requires some heat in the morning to warm it up, which Kooi does not account for in his calculation, so that its useful collected heat is somewhat less than the calculated value. Under reasonably sunny conditions, the solar pond would be expected to collect less heat per unit area than a flat-plate collector, so that its advantage would have to be its lower cost and its ability to store heat.

1.5 Absorption Refrigeration Systems

A vapour absorption chiller is a machine that produces chilled water using a heat source such as solar energy rather than power input (usually electrical) as in the more familiar vapour compression system. The system diagram is shown in Figure 1.2.

Both vapour compression and absorption refrigeration cycles accomplish the removal of heat through the evaporation of a refrigerant at a low pressure and the rejection of heat through the condensation of the refrigerant at a higher pressure. The primary difference is that a vapour compression chiller employs a compressor to create the pressure differences necessary to circulate the refrigerant, whereas an absorption chiller uses a heat source and (usually a liquid pump). The differences cause an absorption system to use very little work input, but energy must be provided as heat. This makes the system very attractive when there is a cheap source of heat at a suitable temperature, such as solar thermal or waste heat from electricity or heat generation. (Bhatia, 2015)

1.6 Suggested Cooling System For Buildings In Iraq

A solar pond connected to a heat pump (absorption chiller) is therefore suggested as a cooling system for buildings in Iraq and that could reduce energy consumption. Due to the cost and practical difficulty of experimental work, the feasibility of such a system will be investigated by simulation. This appears to be the first research into the use of a solar pond connected to the solar air conditioning system for a building in Iraq and countries with the same weather conditions.

1.7 Aim and Objectives

The aim of this study is to develop a simulation model for a solar pond connected to an absorption chiller and to use it to assess its suitability for cooling buildings in a typical hot, dry climate such as Iraq. In order to satisfy this aim, a number of objectives are addressed:

1. Review and explain the concepts of solar pond thermal performance with the various equations necessary for assessing the performance.

2. Develop a simulation model of a solar pond to understand heat and mass transfer within the solar pond.
3. Develop an extended simulation model for solar pond and ground heat loss with varying ground conditions.
4. Develop a coupled simulation of a solar pond, an absorption chiller and a building.
5. Investigate the effect on system performance of solar pond parameters such as pond area, layer thicknesses and ground conditions.

1.8 Structure of the Thesis

This thesis is composed of six chapters.

- Chapter One starts with introduction in which solar pond and absorption chiller are presented. Solar pond applications and comparison between solar ponds and other solar collectors are also presented. Finally, the aims and objectives of this work are given.
- Chapter Two provides principles of solar ponds and a review of the most pertinent literature published in the area of solar ponds, air conditioning systems and absorption chiller systems.
- Chapter Three gives information about weather data for Baghdad in Iraq (the location of the proposed solar pond), salinity gradient solar ponds, soil thermal properties data, equipment data and building data.
- Chapter Four describes the mathematical models of solar pond and the ground underneath it. MATLAB codes are programmed to solve pond and ground equations. Solar air conditioning systems that include absorption chiller and building are modelled and simulated by using TRNSYS software.
- Chapter Five shows the results from MATLAB code for solar pond and ground model. Overall system simulation results from TRNSYS for solar pond and ground model with solar air conditioning system are given.
- Chapter Six presents the conclusions drawn from this work and recommendations for future work.

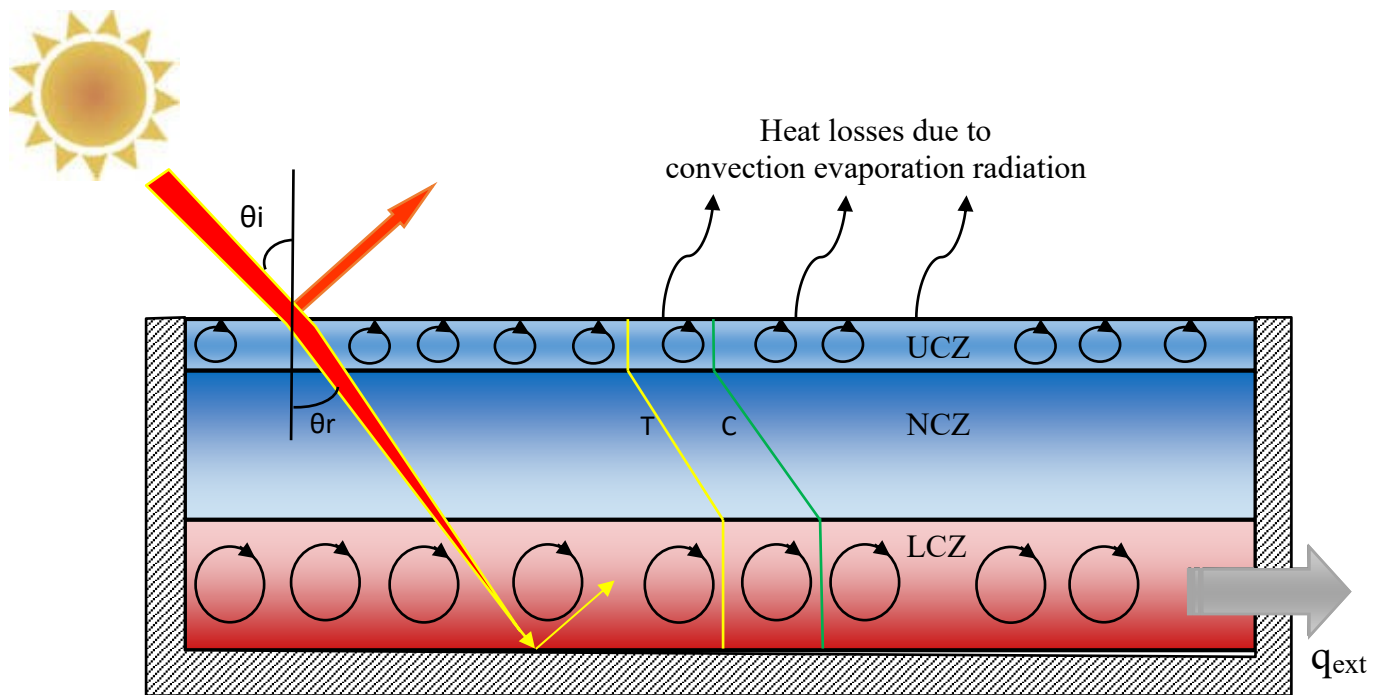


Figure 1.1 Schematic view of the salt gradient solar pond

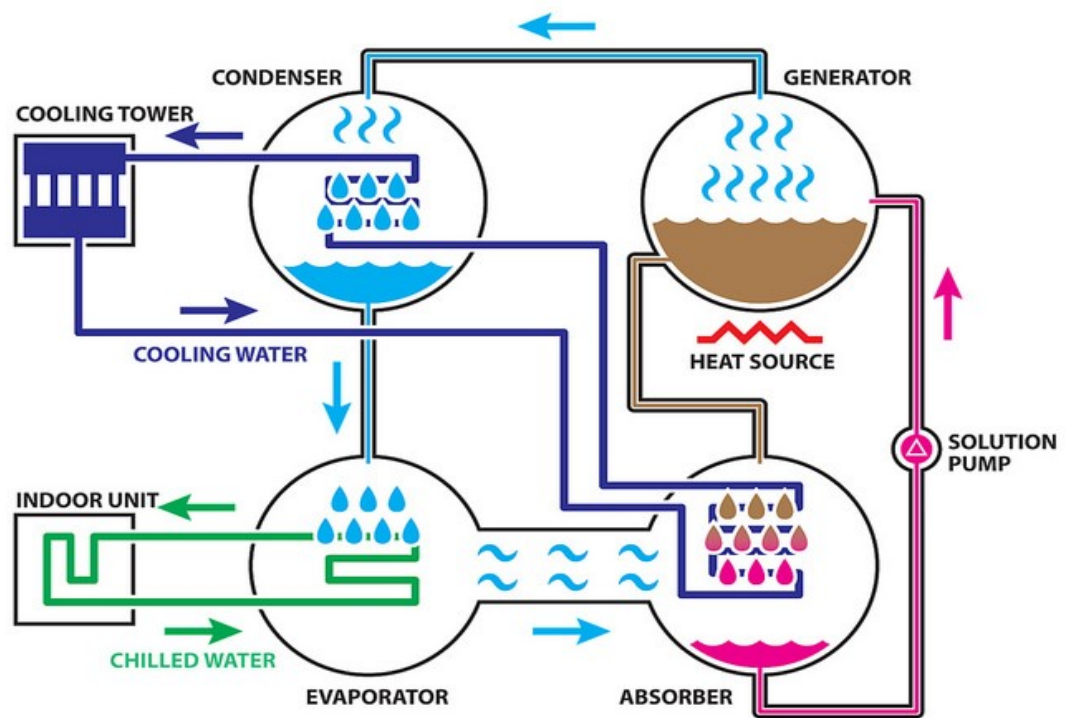


Figure 1.2 Absorption chiller system diagram. (www.r718.com)

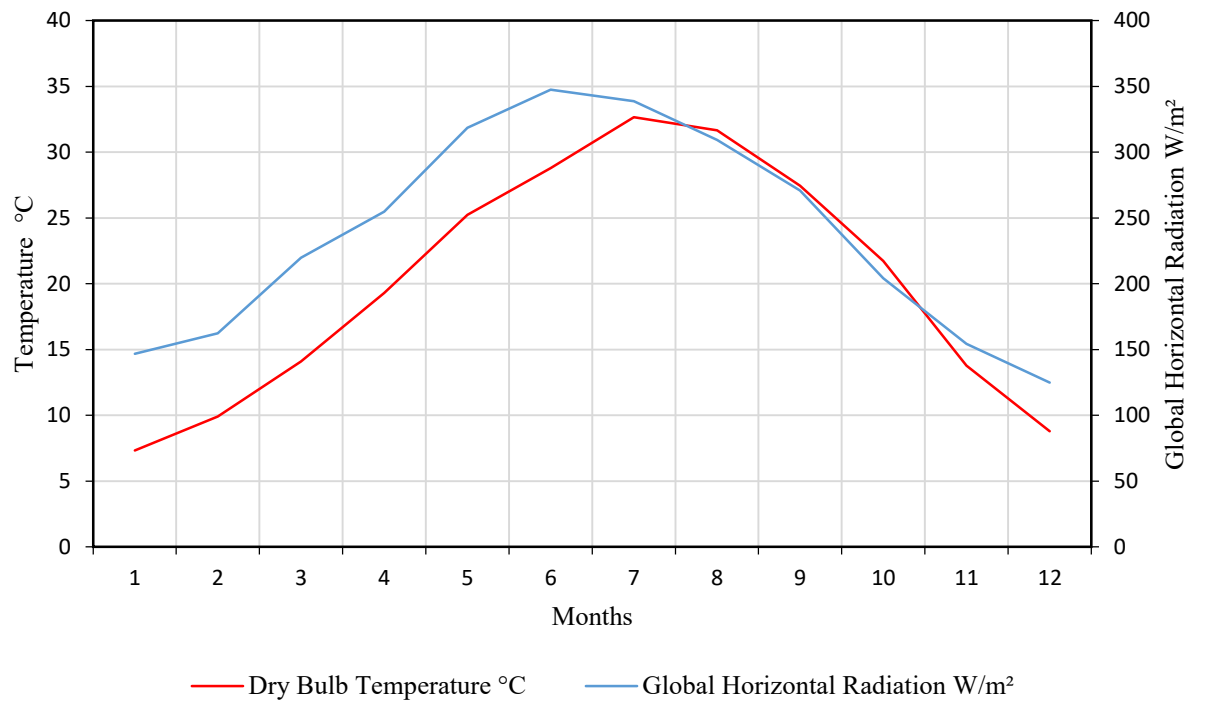


Figure 1.3 Monthly mean dry bulb temperature and global horizontal radiation for Baghdad (Klein, 2010)

Chapter 2. Fundamentals and literature review

2.1 Introduction

In this chapter, the World energy consumption, building cooling loads, air conditioning systems, chillers, and solar collectors are explained briefly. Solar ponds, being the main topic of the thesis are described in detail.

World energy demand is supplied by exploiting the energy sources that exist in nature as primary energy. Primary energy may be found in the form of fossil based fuels such as oil, gas and coal, or renewable sources like the wind and the sun or radioactive sources such as uranium.

Figure 2.1 shows world primary energy consumption from 1989-2014. It may be seen that the greatest portion of the world energy consumption depends on fossil fuels while the rest rely on the renewable sources. (BP Statistical Review of World Energy, 2015)

As reported by BP's Energy Outlook 2035, published in 2016, world primary energy demand is expected to increase by 34% from 2014 to 2035, with an annual average growth rate of 1.4%. The major consumer is expected to be the residential sector, in the form of electricity consumption. Global CO₂ emissions from energy use continue to grow, increasing by 20% between 2014 and 2035.

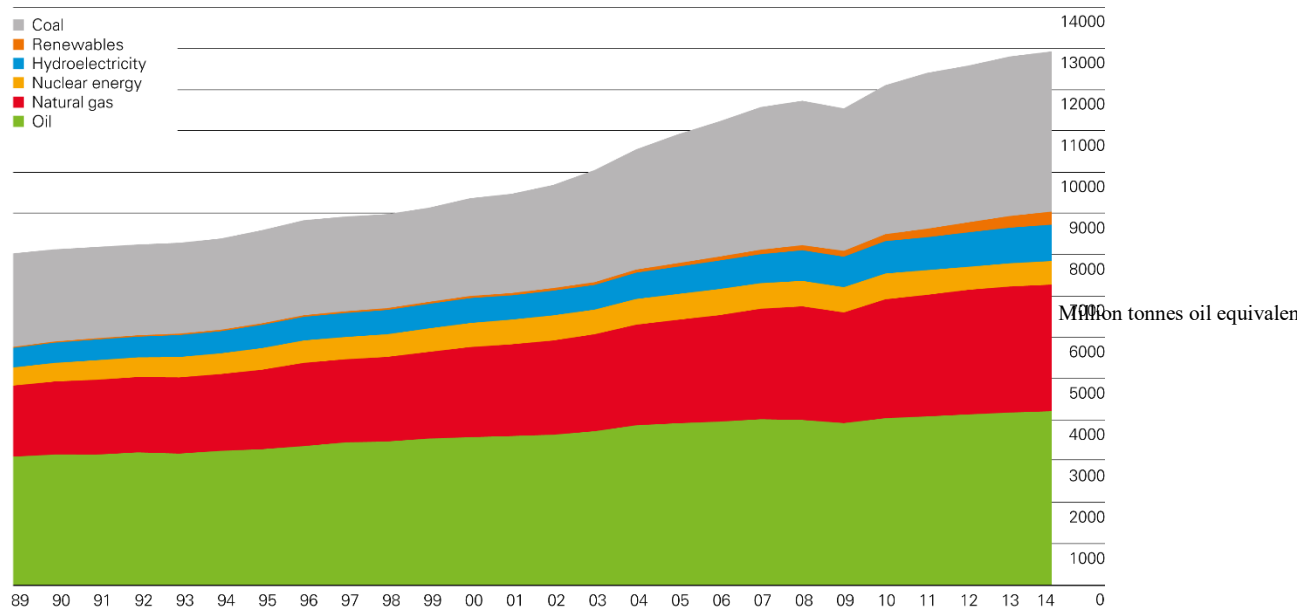


Figure 2.1 World Primary energy consumption 1989-2014

Million tonnes oil equivalent (BP Statistical Review of World Energy, 2015)

One of the large energy consuming sectors is buildings, which account for more than 30% of global total final energy consumption. For example, in 2012 residential and commercial buildings consume 84% of all grid electricity generation in Saudi Arabia, 65% of which was consumed by air conditioners (IEA, 2015). If absorption chillers driven by solar energy are employed, they will lead to significant electricity savings.

The predominant sources of energy for our modern society are fossil fuels, and this will depend mainly on the cost of fossil fuels (oil, gas and coal). Crude oil prices showed significant instabilities over the last 40 years. Crude oil prices increased from 2000 to 2014, except in 2009 due to the economic crises. It fell by 48% in nominal terms between 2014 and 2015, a drop of 46 US dollar per barrel. Although the increasing trend and decreasing trend (during some periods) in the oil prices, global oil consumption grew by 0.8 million barrels per day, a little below its recent historical average, and significantly weaker than the increase of 1.4 million barrels per day seen in 2013 (BP Statistical Review of World Energy, 2015).

Due to rising fossil fuel prices, some countries keep spending much more of their incomes on fossil fuels instead of spending for the improvement of the sustainable solutions for energy consumption. Fossil fuel consumption emits CO₂ to the

atmosphere and is the main cause of global warming. Carbon dioxide emissions due to the burnt fossil fuels (oil, gas and coal) experienced a great increase (from 11 billion tonnes CO₂ to 38 billion tonnes CO₂) since 1965. Amount of CO₂ emissions resulting from burnt fossil fuels are given in Figure 2.2 (BP Energy Outlook, 2016)

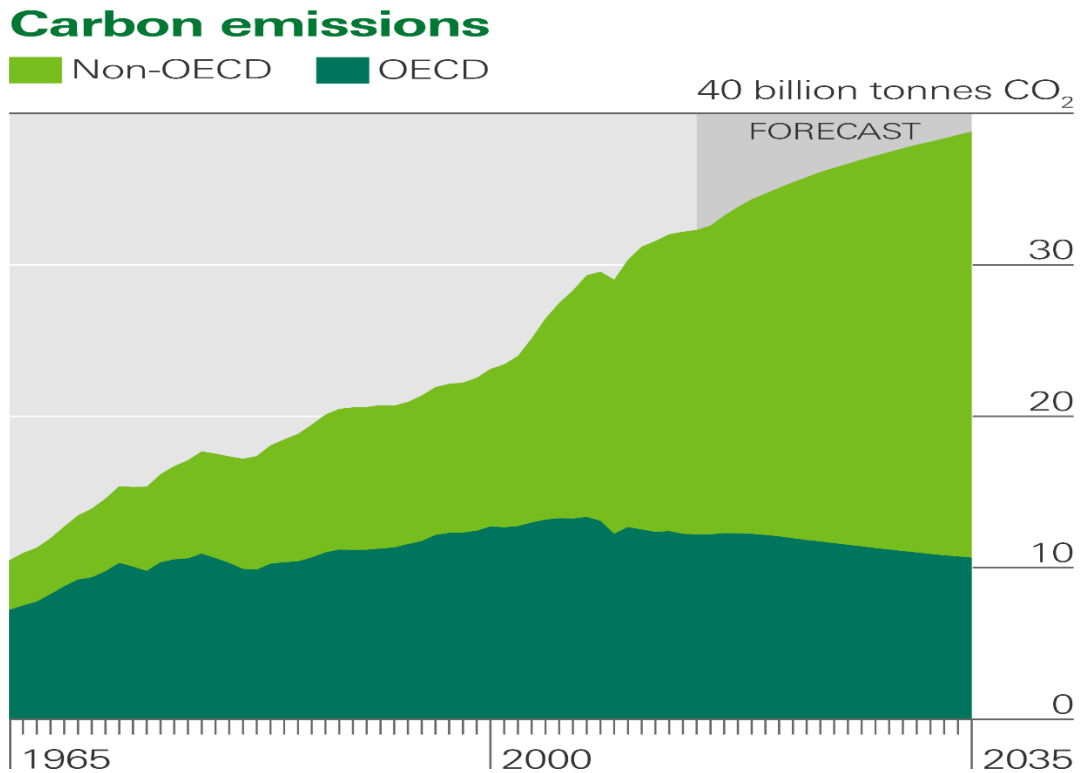


Figure 2.2 World carbon dioxide emission 1965-2035 (BP Energy Outlook, 2016).

Energy consumption is increasing dramatically, and a significant portion of that is used in commercial and domestic buildings as electrical energy. Studies should be carried out in improved buildings and building services systems to reduce their energy consumption and CO₂ emissions.

In hot and dry areas such as Middle East, air conditioning is a major consumer of energy and therefore an important topic for research.

2.2 Building Cooling Loads

The space cooling load is the rate at which energy must be removed from a space to maintain a desired space condition. The purpose of cooling load calculations is to provide information for equipment selection and HVAC system design. For estimating

cooling loads, one has to consider the unsteady state processes, as the peak cooling load occurs during the daytime and the outside conditions also vary significantly throughout the day due to solar radiation. Also, all internal sources add on to the cooling loads and neglecting them would lead to underestimation of the required cooling capacity and the possibility of not being able to maintain the required indoor conditions. Thus, cooling load calculations are inherently more complicated than heating load calculations, for which many of these factors may be neglected. (Rudoy, 1979)

The space heat gain is the algebraic sum of the heat flow rates entering the space and can be classified by:

1. Solar radiation through transparent surfaces such as windows.
2. Heat conduction through exterior walls and roofs.
3. Heat conduction through interior partitions, ceilings and floors.
4. Heat generated within the space by occupants, lights, appliances, equipment and processes.
5. Loads as a result of ventilation and infiltration of outdoor air.
6. Other miscellaneous heat gains such as printers.

The types of heat gain are sensible and latent. Sensible heat load is total of:

- a. Heat transmitted through floors, ceilings, walls.
- b. Occupant's body heat.
- c. Appliance and light heat.
- d. Solar heat gains through glass.
- e. Infiltration of outside air.
- f. Air introduced by ventilation.

The latent heat load is total of:

- a. Moisture-laden outside air from infiltration & ventilation.
- b. Occupant respiration & activities.
- c. Moisture from equipment & appliances.

The heat received from the heat sources (conduction, convection, solar radiation, lightning, people, equipment, etc...) does not go immediately to heating the room air. Only a small fraction of radiant energy is absorbed by the air in the conditioned space

instantaneously, leading to a minute change in its temperature. The majority heats the surfaces of the room and its contents. When these surfaces and objects become warmer than the surrounding air, some of their heat is transferred to the air by convection. The composite heat storage capacity of these surfaces and objects determines the rate at which their respective surface temperatures increase for a given radiant input, and thus governs the relationship between the radiant portion of heat gain and its corresponding part of the space cooling load (Figure 2.3) (ASHRAE Handbook Fundamentals, 2005).

As mentioned in the preceding sections, cooling load and the resulting fossil fuel energy consumption could be reduced if there are improvements in the building and building service system. One of the possible improvements is to reduce the heat gains by, for example insulating the building envelope, or using blinds to reduce solar heat gain through windows. Another option is to find a sustainable source such as solar energy to drive an air conditioning system.

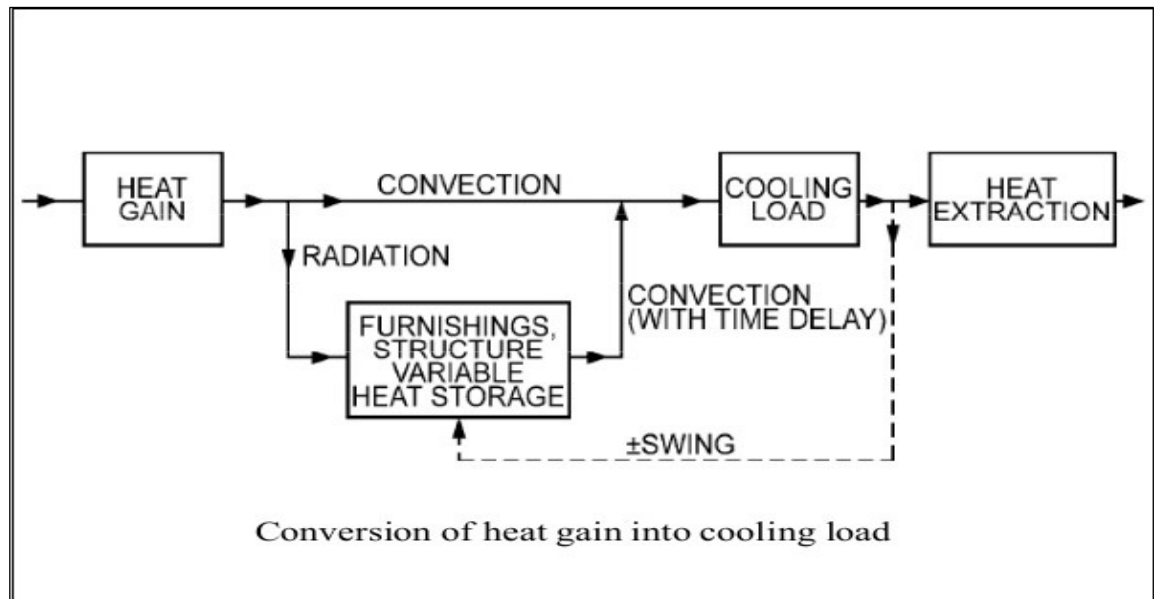


Figure 2.3 Origin of Difference Between Magnitude of Instantaneous Heat Gain and Instantaneous Cooling Load. (ASHRAE Handbook Fundamentals, 2005)

Current buildings in Iraq have problems such as poor thermal comfort in peak summer and winter seasons, high cooling and heating loads, and poor energy efficiency. They typically have no insulation and single glazing (Mohamed et al., 2015).

According to the Ministry of Electricity in Iraq, residential buildings in Iraq are the primary source of consumption, consuming 48 % of the total electricity used (Alsammarae, 2005), as shown in Figure 2.4.

Energy can be saved in existing buildings by insulation of the building envelope (walls, roof, and ground floor), glazing of windows, installation of energy efficient heating and cooling systems, annual service of appliances, installation of temperature controllers and thermostats.

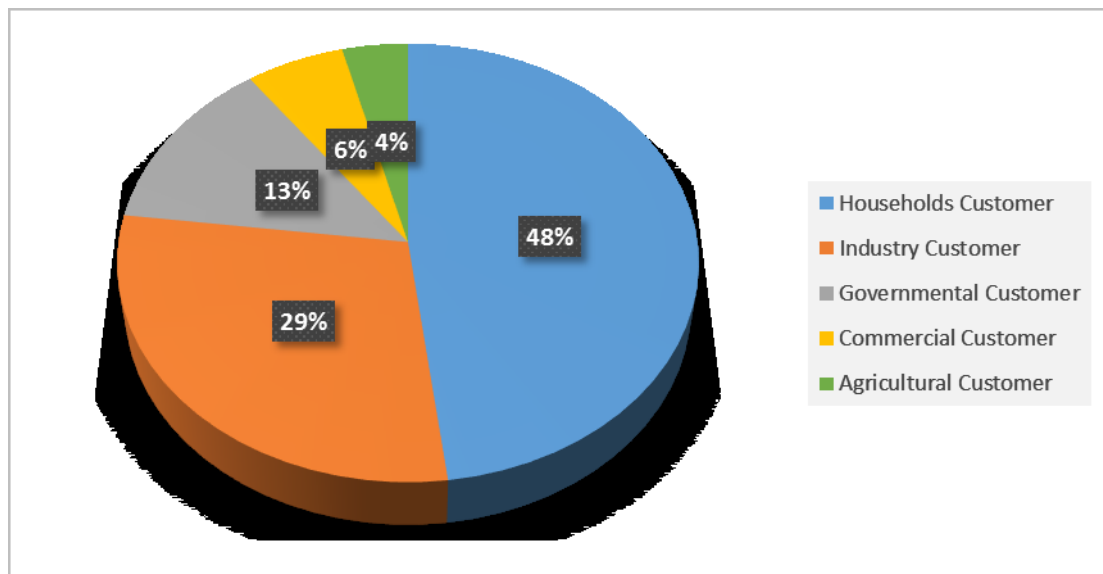


Figure 2.4 Electricity consumption by economic groups (Alsammarae, 2005)

2.3 Air Conditioning Systems

Air conditioning can be defined as the process of treating air to meet the requirements of a conditioned space by controlling its temperature, humidity, cleanliness, and distribution. There are seven main processes required to achieve full air conditioning, heating, cooling, humidifying, dehumidifying, cleaning, ventilating and air distribution.

Most air conditioning systems are used for improving some industrial and manufacturing process, and to provide human comfort.

Heat is transferred naturally from a warmer to a cooler area. In winter, there are continual heat losses from within the building to the outdoors. If the building inside

air is maintained at a comfortable temperature, heat must be continually supplied to the building. The equipment that provides the heat required is called a heating system. In summer, heat continuously enters the building from outside. To maintain the building air at a comfortable temperature, heat must be continually removed from the building. The equipment that removes heat is called a cooling system (ASHRAE Handbook Fundamentals, 2005).

An air conditioning system could provide heating, cooling or both. Air conditioning system size and complexity may range from a small single space heater or window unit for a single room to a huge and complex system for commercial buildings. All systems work on the same basic principles.

Based on the fluid media used in the thermal distribution system, air conditioning systems can be classified as all-air systems, all-water systems, air-water systems and unitary or package refrigerant based systems (ASHRAE Handbook Fundamentals, 2005).

2.3.1 All -Air Systems

An all-air system uses air to heat and cool rooms. The system may also have the capability of adding humidity and fresh air ventilation. A typical all-air heating and cooling system is shown in Figure 2.5. Air is heated by a heating coil which is connected to the heat source such as boiler. The heated air is circulated by a fan and through a supply duct. The supply air enters the room through outlets called air diffusers that are designed to provide proper air distribution in the room. Thus, the air in the room is heated. In winter, a humidifier may be included to maintain a comfortable room humidity.

In summer, air is cooled when it flows through a cooling coil, usually a coil of tubing containing fluid cooled by the refrigeration system. When the supply cooled air enters the room, the room is cooled. The same volume of supply air that enters the room must also exit by return air duct. Fresh outdoor air may be provided for increasing air quality. Similarly, the same volume of air must be exhausted.

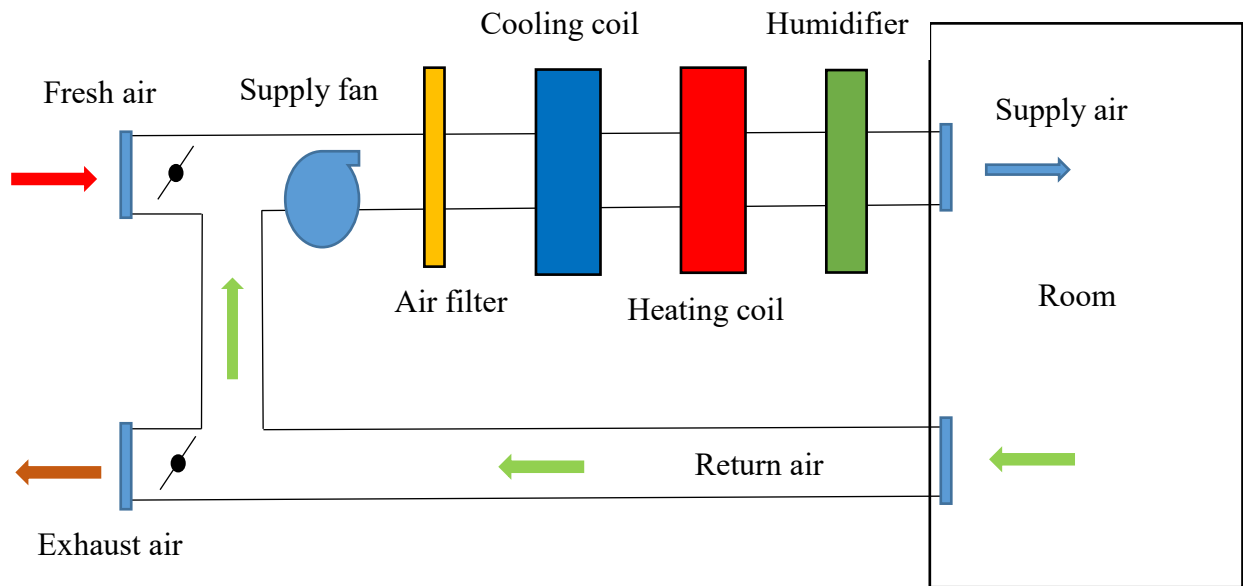


Figure 2.5 All air heating and cooling system

2.3.2 All -Water Systems

In an all-water system, water is used in the thermal distribution system; i.e., water transports energy between the conditioned space and the air conditioning plant. In summer, when cooling is required in the conditioned room, cold water is circulated between the conditioned room and the plant, while, in winter, hot water is circulated through the distribution system when heating is required. Since only water is transported to the conditioned space, provision must also be made for supplying required amount of treated, outdoor air to the conditioned space for ventilation purposes.

Heat transfer between the cold/hot water and the conditioned space takes place either by convection, conduction or radiation or a combination of these. The cold/hot water may flow through bare pipes located in the conditioned space, or one of the following equipment can be used for transferring heat:

- a. fan coil units
- b. convectors

c. chilled ceilings

d. radiators etc.

2.3.3 Air- Water Systems

In air-water systems, both air and water are used for providing the required conditions in the conditioned space. The air and water are cooled or heated in a central plant. The air supplied to the conditioned space from the central plant is called primary air, while the water supplied from the plant is called secondary water. The complete system consists of a central plant for cooling or heating of water and air, a ducting system with fans for conveying air, water pipelines and pumps for circulating water and a room terminal. The room terminal may be in the form of a fan coil unit, an induction unit or a radiation panel.

2.3.4 Unitary or Package Refrigerant Based Systems

Unitary refrigerant based systems consist of several separate air conditioning units with individual refrigeration systems. These systems are factory assembled and tested to standard specifications, and are available in the form of package units of varying capacity and type. Each package consists of refrigeration and/or heating units with fans, filters, controls, etc. Depending upon the requirement these are available in the form of window air conditioners, split air conditioners, heat pumps, and ductable systems with air cooled or water cooled condensing units. The capacities may range from a fraction of TR to about 100 TR for cooling. Depending upon the capacity, unitary refrigerant based systems are available as single units which cater to a single conditioned space, or multiple units for several conditioned spaces (IIT Kharagpur, 2009).

2.4 Refrigeration Systems

Refrigeration systems are used to cool products or a building environment. The refrigeration system transfers heat from a cooler reservoir to a warmer reservoir (Figure 2.6).

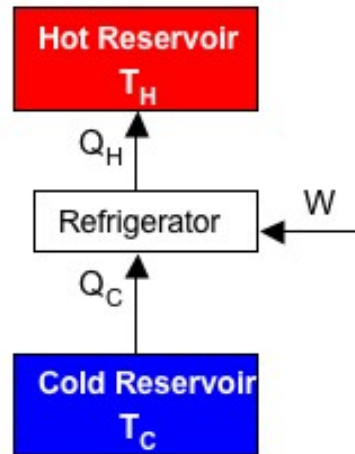


Figure 2.6 Schematic representation of refrigeration system

There are several heat transfer loops in a typical refrigeration system as shown in Figure 2.7. Thermal energy moves from left to right as it is extracted from space and expelled into the outdoors through five loops of heat transfer:

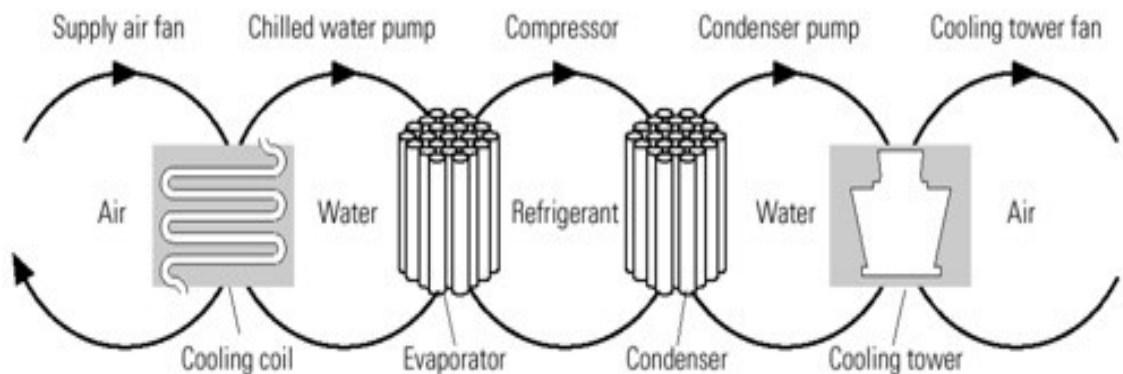


Figure 2.7 Heat Transfer Loops in a typical Refrigeration System

(Bureau of Energy Efficiency, 2004)

Indoor air loop. In the left loop, indoor air is driven by the supply air fan through a cooling coil, where it transfers its heat to chilled water. The cool air then cools the building space.

Chilled water loop. Driven by the chilled water pump, water returns from the cooling coil to the chiller's evaporator to be re-cooled.

Refrigerant loop. Using a phase change refrigerant, the chiller's compressor pumps heat from the chilled water to the condenser water.

Condenser water loop. Water absorbs heat from the chiller's condenser, and the condenser water pump sends it to the cooling tower.

Cooling tower loop. The cooling tower's fan drives air across a flow of the hot condenser water, transferring the heat to the outdoors. (Bureau of Energy Efficiency, 2004)

2.5 Chillers

Air conditioning systems are one of the most important applications of refrigeration system or “chillers”. HVAC chillers are classified primarily on the basis of the cycle on which they work.

- Vapour compression chillers.
- Vapour absorption chillers.

Other types of chillers such as adsorption chiller system and desiccant dehumidification are also explained briefly.

2.5.1 Vapour Compression Chiller System

In a vapour compression refrigeration system, a working fluid (refrigerant) evaporates at low temperature and pressure. The temperature stays constant while the enthalpy of evaporation or latent heat is absorbed from the space or product to be cooled. The vapour is compressed to a high pressure, which raises its temperature so that heat can be rejected to the surroundings and vapour condensed and returned back to absorb heat.

The essential components of the vapour compression cycle are compressor, condenser, expansion device and evaporator as shown in Figure 2.8.

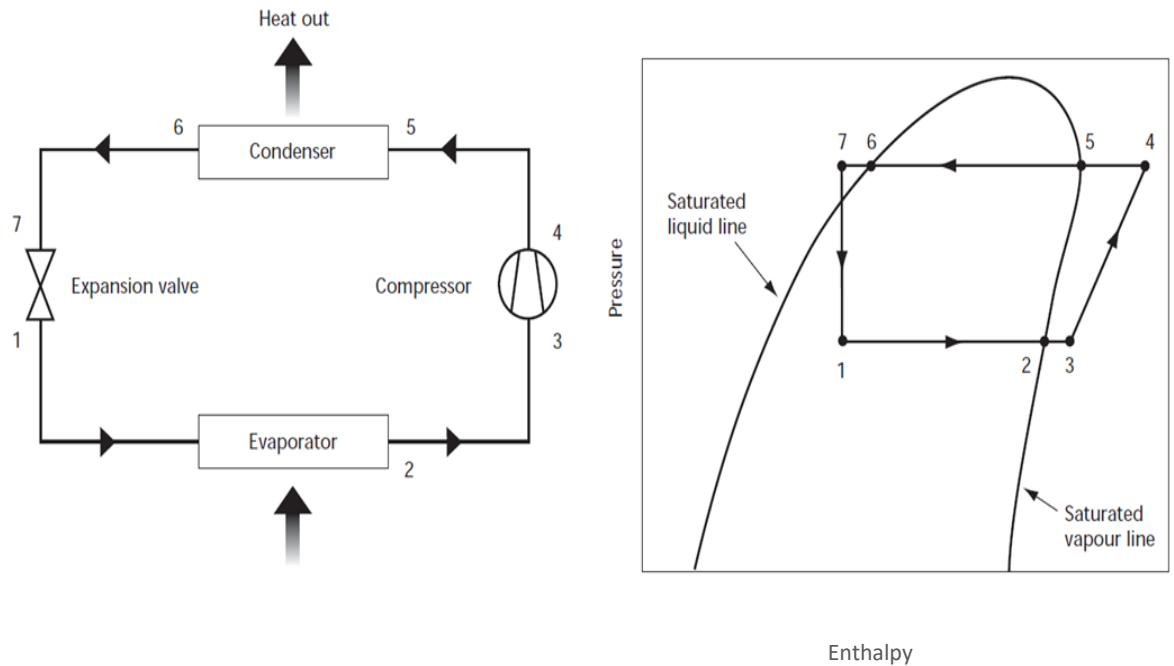


Figure 2.8 Vapour compression cycle: principal system components and simple pressure–enthalpy diagram. (CIBSE Guide B, 2016)

The stages in the cycle are: from 1 to 2: low-pressure liquid refrigerant in the evaporator absorbs heat from the medium to be cooled (usually air or water and evaporates). From 2 to 3: the refrigerant vapour absorbs more heat and may be superheating of vapour inside evaporator, as well as in the pipework joining the evaporator to the compressor. From 3 to 4: the superheated vapour is compressed, increasing its temperature and pressure. From 4 to 5: the hot superheated vapour enters the condenser and de-superheated partly or wholly within the condenser rather than the pipework. From 5 to 6: the hot vapour is condensed back to a saturated liquid at constant temperature and pressure. Heat is rejected to a suitable heat sink, such as ambient air.

From 6 to 7: further cooling may take place to sub cool the liquid before it enters the expansion valve (this may occur in the pipework connecting and the condenser with the expansion valve). From 7 to 1: liquid passes through an expansion device causing a reduction in its temperature and pressure (CIBSE Guide B, 2016).

2.5.2 Vapour Absorption Chiller System

Absorption refrigeration systems are based on extensive development and experience in the early years of the refrigeration industry, in particular for ice production. From the beginning, its development has been linked to periods of high energy prices. Recently, however, there has been a great resurgence of interest in this technology not only because of the rise in the energy prices, but mainly due to the social and scientific awareness about the environmental impact of fossil fuel use.

Absorption systems are similar to vapour compression systems, but differ in the pressurisation stage. Compared to an ordinary refrigeration cycle the basic idea of an absorption system is to avoid compression work. This is done by using a suitable combination of refrigerant and an "absorbent" which can absorb the refrigerant vapour. The most usual combinations include lithium bromide-water ($\text{LiBr-H}_2\text{O}$) where water is the refrigerant and ammonia-water ($\text{NH}_3\text{-H}_2\text{O}$) where ammonia is the refrigerant.

The pressurization is achieved by dissolving the low-pressure refrigerant from the evaporator in the absorbent, in the absorber section. Subsequently, the solution is pumped to a high pressure with an ordinary liquid pump. Heat is then added in the generator to separate the refrigerant from the solution at the higher pressure, and the high-pressure refrigerant vapour then flows to the condenser. Any heat source at suitable temperature can be used: e.g. waste heat, solar heat. In this way, the refrigerant vapour is compressed without the need of large amounts of mechanical energy that the vapour compression air conditioning systems demand.

As shown in Figure 2.9, when the refrigerant vapour is coming from the evaporator (10) it is absorbed in a liquid (1). This liquid is pumped to higher pressure (1-2), where the refrigerant is boiled out of the solution by the addition of heat (3-7). Subsequently, the refrigerant goes to the condenser (7-8) as in an ordinary cooling cycle. Finally, the liquid with less refrigerant returns back to the absorber (6) (Herold et al., 1996). The remainder of the system consists of a condenser, expansion valve and evaporator, which function in a similar way as in a vapour compression air conditioning system.

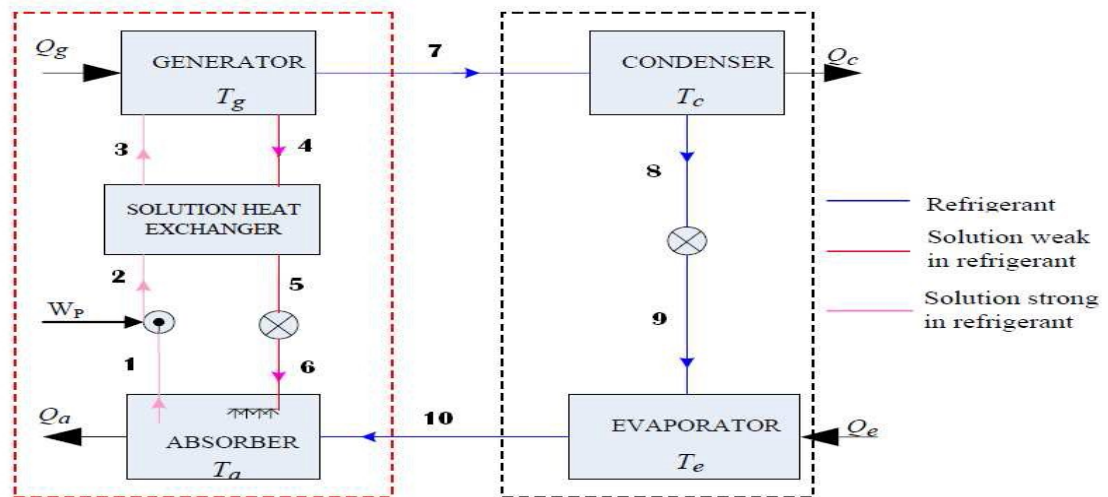


Figure 2.9 Schematic of a single effect LiBr-water absorption system (Herold et al., 1996)

The $\text{NH}_3\text{-H}_2\text{O}$ system is more complicated than the $\text{LiBr-H}_2\text{O}$ system since it needs a rectifying column that assures that no water liquid enters the evaporator where it could freeze. The $\text{NH}_3\text{-H}_2\text{O}$ system requires generator temperatures in the range of 125°C to 170°C with air cooled absorber and condenser and 80°C to 120°C when water cooling is used. These temperatures cannot be obtained with flat plate solar collectors. The coefficient of performance (COP), which is defined as the ratio of the cooling effect to the heat input, is 0.6 to 0.7. In the $\text{LiBr-H}_2\text{O}$ system water is used as a coolant in the absorber and condenser and has a higher COP than the $\text{NH}_3\text{-H}_2\text{O}$ systems. The COP of this system is between 0.6 and 0.8 (Duffie and Beckman, 1980). A disadvantage of the $\text{LiBr-H}_2\text{O}$ systems is that the evaporator cannot operate at temperatures much below 5°C since the refrigerant is water vapour.

Commercially available absorption chillers for air conditioning applications usually operate with a solution of lithium bromide in water and use steam or hot water as the heat source. In the market, two types of chillers are available: the single and the double effect.

The single-effect absorption chiller is mainly used for building cooling loads, where chilled water is required at $6\text{-}7^\circ\text{C}$. The COP will vary to a small extent with the heat source and the cooling water temperatures. Single-effect chillers can operate with heat source temperatures ranging from about 80°C to 150°C . (Florides et al., 2002).

Water fired absorption chillers LiBr-H₂O are available that can operate with inlet hot water temperature between 70°C and 95°C (Yazaki, 2008). These temperatures can be achieved by solar collectors; therefore these chillers are potentially usable for solar cooling systems.

A double-effect absorption chiller has two stages of generation to separate the refrigerant from the absorbent. Thus the temperature of the heat source needed to drive the high stage generator is essentially higher than that needed for the single-effect machine and is in the range of 155 to 205°C. Double effect chillers have a higher COP of about 0.9-1.2 (Dorgan, 1995). Although double-effect chillers are more efficient than the single-effect machines they are obviously more expensive to purchase and the heat source temperatures required cannot be achieved by the common types of solar collectors (flat plate, evacuated tube or solar pond), as described in section 2.8. However, every individual application must be considered on its merits since the resulting savings in capital cost of the single-effect units can largely offset the extra capital cost of the double effect chiller.

2.5.3 Adsorption Chiller System

The adsorption chiller system depends on the phenomena called adsorption which is the result of the interaction between a solid and a fluid based on physical or chemical reaction. There are several possible adsorbent–adsorbate working pairs that can be used in adsorption refrigeration systems (Fernandes et al., 2014) such as Silica Gel-Water. The performance of the adsorption system is affected by the chosen working pair. The adsorption system is simple and can be operated without any moving parts. This result leads to silent operation. When one fixed adsorbent bed is used, operations on an intermittent cycle. Two or more adsorbent beds are required for continuous cycle operation.

2.5.4 Desiccant Dehumidification

Two methods can achieve dehumidification of the air:

- 1- Cooling the air below its dew point and removing moisture by condensation.
- 2- Sorption by a desiccant material.

Desiccants in either solid or liquid forms have a natural affinity for removing moisture. As the desiccant eliminates the moisture from the air, desiccant releases heat and warms the air, i.e., latent heat becomes sensible heat. The dried warm air can then be cooled to desired comfort conditions by sensible coolers (e.g., evaporator coils, heat exchangers, or evaporative coolers). To reuse the desiccant, it must be regenerated or reactivated by a process in which moisture is driven off by heat from an energy source such as electricity, waste heat, natural gas, or solar energy.

For air conditioning applications, the most appropriate dehumidifier is the rotary wheel (as shown in Figure 2.10). The humid air enters the system, comes into contact with the material of the desiccant wheel, and exits as hot and dry air. The wheel rotates so that the portion of the desiccant wheel which has taken up moisture is exposed to hot air and its moisture removed. In cooling applications, the hot and dry air needs to be cooled by a standard vapor compression cooling coil or direct evaporative cooler (Pesaran, 1994).

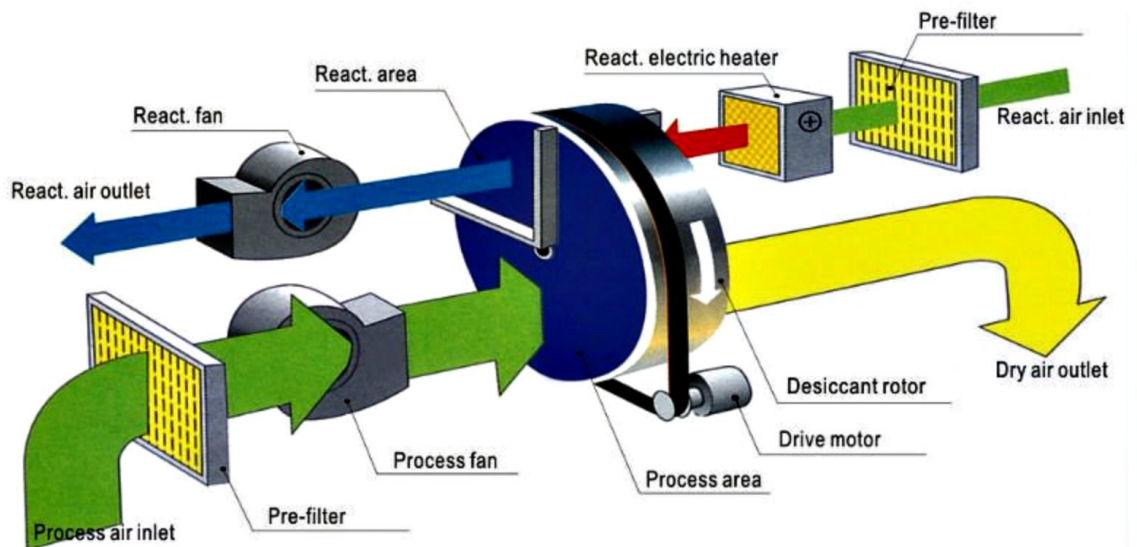


Figure 2.10 Desiccant dehumidification (Source: CtrlTech, 2014)

2.5.5 Chillers Summary

From the literature presented on chiller systems, the primary difference is that a vapour compression chiller employs a compressor to create the pressure differences necessary

to circulate the refrigerant, whereas an absorption chiller uses a heat source and liquid pump. The differences cause an absorption system to use very little work input, but energy must be provided as heat. This makes the system very attractive when there is a cheap source of heat at a suitable temperature, such as solar thermal energy or waste heat from electricity or heat generation.

The adsorption chiller was not selected as a cooling system for this research because it has a lower COP than absorption chiller, relatively higher initial costs, and requires a high vacuum tightness of the container (Sarbu and Sebarchievici, 2013), (Allouhi et al., 2015).

The disadvantages of liquid desiccant cooling systems include a relatively larger size, and reduced efficiency due to air leaks (Ghafoor, and Munir, 2015). Therefore, a desiccant cooling system is not adopted in this research.

2.6 Solar Cooling

The cooling demand of a building depends on the internal gains such as number of people and appliances and external gains such as outside high temperature and solar radiation intensity. Therefore, solar cooling, that is the use of solar energy in summer to satisfy cooling loads of the buildings can be considered as a logical solution. Solar cooling can be achieved by two alternative routes (thermal and electric). The two options of solar cooling can be seen in Figure 2.11 (Noro and Lazzarin, 2014).

Solar cooling technologies were developed or demonstrated with many projects since the 1970s, after the 1973 energy crisis (Ward, 1976, 1979), (Nakahara, 1977). A variety of solar cooling technologies was developed, and many of them are available in the market (Balaras et al., 2007), (Henning, 2007). Most review articles in the past were limited to solar thermal, especially sorption cooling technologies (Grossman, 2002); (Zhai and Wang, 2009). More recently, other authors presented reviews with a broader overview including solar electric (Hwang et al., 2008) ;(Henning and Döll, 2012).

Since the first decades after the energy crisis and till very recently, the PV (photovoltaic) option was excluded from research because of the high cost of the

modules. Therefore, solar thermal collectors have been widely developed in the last decades to improve efficiency and durability and decrease cost.

Little literature is available as academic published research on solar cooling systems in Iraq. Most of the research work carried out is on flat plate collectors with absorption cooling technology.

Joudi, (2003) carried out research on simulation for a solar cooling system and development of solar cooling design charts. A transient simulation program is developed for simulating the Iraqi solar house cooling system, using TRNSYS as a design tool. The solar guest house in Baghdad was the first full scale project undertaken by the Iraqi Solar Energy Research Center in the field of solar air conditioning applications. It was built in 1981 (Al-Karaghoul et al., 1989). It has a total area of 600 m² with a solar air conditioned area of 400 m². It includes a reception room, a dining room, four bedrooms, two bathrooms, a kitchen and a machinery room. The house is well insulated and the total heat loss coefficient was calculated as 0.66 W/m² °C for the exterior walls and 0.573 W/m² °C for the roof.

The solar cooling system consists of

- 128 flat plate collectors with a single glass cover of 1.89 m² area each, with a total effective area of 243 m².
- 20 m³ stainless steel hot water storage tank.
- 10 tons (TR) lithium bromide-water absorption chiller.

Joudi, (2003) proposed a general design procedure for solar cooling systems, presented in a graphical form called the cooling *f*-chart. Using this design chart simplifies the designer's task for predicting the long term cooling energy supplied from a solar collector array serving an absorption chilled water system.

The *f*-chart method provides a mean for estimating the annual thermal performance of active heating systems common in residential applications, using air, or liquid as a working fluid. The *f*-chart is used to estimate the fraction of a total heating load that can be provided by a solar system. The *f*-chart was developed by (Klein et al., 1976) and (Beckman et al., 1977).

Joudi, (2003) work is an attempt to develop a method, similar to the heating *f*-chart, for use in designing solar cooling systems. The proposed work is a numerical study

with lot of limitations including no details for chiller operation and performance parameters, chiller integration with solar thermal and cooling systems for building. These limitations make use of f -charts unsuitable for current detailed research.

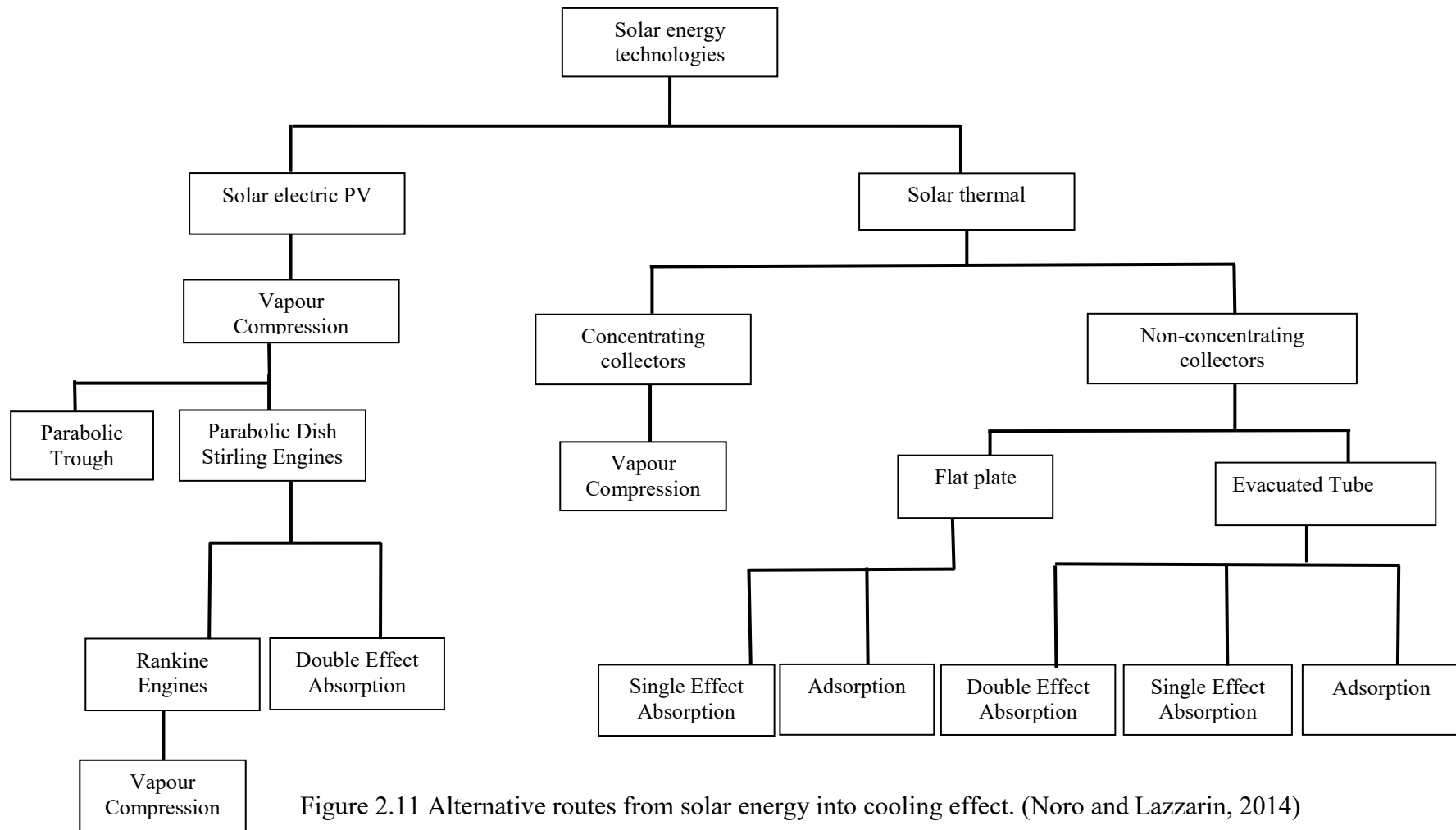


Figure 2.11 Alternative routes from solar energy into cooling effect. (Noro and Lazzarin, 2014)

2.7 Solar Collectors

A solar collector is a device that converts solar radiation into thermal energy. Solar thermal collectors can be classified according to their collecting characteristics, the way in which they are mounted and the type of transfer fluid that they use.

a) Collecting characteristics: Non-concentrating solar collectors such as FPC (Flat plate collector) and ETC (Evacuated tube collector) are ones in which the absorbing surface for solar radiation is essentially flat with no means for concentrating the incoming solar radiation.

Concentrating or focusing collectors are ones which contain reflectors or other optical means to concentrate the energy falling on the aperture onto a heat exchanger of surface area smaller than aperture such as PDC (parabolic dish collector), and PTC (parabolic trough collector).

b) Mounting: A collector can be mounted to remain stationary, be adjustable as tilt angle (measured from the horizontal) to follow the change in solar declination or be designed to track the sun.

c) Types of fluid: A collector will usually use either a liquid or a gas as the transfer fluid. The most common liquids are water or water-ethylene glycol solution. The most common gas is air.

The history of the thermal collectors' development for solar cooling technologies has been reported by Lazzarin (2014). The report discussed both concentrating PDC, PTC and non-concentrating ETC, FPC technologies are shown in Figure 2.11.

In the concentrating collectors' side in Figure 2.11, collectors allow use of thermodynamic cycles (mainly Stirling and Rankine engines) to drive a vapour compression chiller, because of the high temperature produced that allows a reasonable engine efficiency. In the non-concentrating collectors' side, collectors allow the use of the sorption cooling system only. Single and double effect absorption chillers are very widely used. In a recent study (Choudhury et al., 2013) ;(Sekert, 2012) an adsorption chiller was used after some main drawbacks had been solved. The problem was the poor heat exchange between solid adsorbent and the cooling or

heating fluids. Other sorption technologies are available and allow good energy performance (open cycle systems like liquid and solid rotating desiccant) (Grossman, 2002; Gomme and Grossman, 2007; Henning, 2007), but they treat directly the air introduced into the rooms: therefore, it is difficult to equip an existing building with such systems, even if they allow good energy performance.

All types of solar collectors need storage to store solar thermal energy and with large area required to collect a substantial quantity of energy. Therefore, they require a very large investment of capital and material resources to realize a world economy based on renewable energy. If this goal is to be approached, an option of low-cost large area solar collectors, is the solar pond, which combines low-cost collection with long-term storage for a variety of low temperature thermal applications.

2.8 Solar Pond

2.8.1 History

The phenomenon of natural solar ponds was first discovered by Von Kálcinsky in natural occurring lakes in a salt region of Transylvania (Hungary) (Hull and Nielsen, 1989). This lake had a temperature of 70°C at a depth of 1.32m at the end of the summer; even in the early spring, the minimum temperature recorded was about 26°C. The bottom of this lake had a salt (NaCl) concentration of 26 percent. Similar phenomena have been reported by (Anderson, 1958) in Oroville (Washington State) where a temperature of 50 °C at a depth of 2 m was recorded during the summer season.

The idea of creating artificial solar ponds was proposed by Bloch in 1954 and a research director of the Dead Sea works suggested the study of solar lakes with a view to world practical utilization. It was expected that higher temperature and useful collection efficiencies could be achieved in an artificial pond. In experiments with a 1200 m² pond, temperatures greater than 103 °C were measured and collection efficiencies of greater than 15 per cent for extraction at 70 °C to 90 °C were achieved (Tabor, 1981).

Theoretical and experimental observations on the laboratory scale solar ponds for understanding the physics of the solar pond were carried out by Weinberger (1964),

Elata and Levin (1965), Tabor (1965) and Hirschmann (1961) and Stolzenbach, (1986) have developed numerical methods to predict temperature distributions within a solar pond. Some theoretical investigations on solar ponds have been carried out by Usmanov (1969, 1971).

There are several types of solar ponds such as salt gradient solar ponds, partitioned solar ponds, viscosity stabilized solar ponds, membrane stratified solar ponds, saturated solar ponds, membrane viscosity stabilized solar ponds, and shallow solar ponds. These types will be discussed briefly in the following sections.

2.8.2 Salt Gradient Solar Ponds

A salt gradient solar pond is a large area of saline water designed as a low-cost device for collecting solar energy and storing it in the water as thermal energy. The pond surface area may vary from a few square meters to thousands of square meters. The salinity is not uniform but increases linearly downwards until it reaches saturation near the bottom. The density gradient is large enough to suppress convection and prevent the formation of any large scale convection cells. The result of this is that solar radiation is trapped in the lower region. The useful thermal energy is then withdrawn from the solar pond in the form of hot brine. The pre-requisites for establishing solar ponds are: a large tract of land, solar radiation, and cheaply available salt such as sodium chloride. It is important to maintain the clarity of a solar pond to allow as much solar radiation as possible to reach the lower zone (Alagao, 1994). The salinity gradient must also be maintained for it to perform efficiently as a store of solar energy.

This simplicity of the solar pond and its capability of generating sustainable heat with a temperature around 100 °C make it attractive for a lot of applications. The energy stored and collected in a solar pond is low grade heat at temperatures limited by the boiling point of the bottom zone brine.

Salinity gradient solar ponds are, in principle, very straightforward and inexpensive systems for the collection and storage of solar energy (Hull et al., 1989). The solar pond consists of a containment volume, a salinity stratified solution contained therein, and associated equipment.

The essential components of a salinity gradient solar pond are dissolved salt and water. To establish a salinity gradient, it requires a very concentrated brine, and a low salinity brine or fresh water. The availability of low-cost brines or salts having suitable chemical and physical properties strongly affects the overall economics of solar ponds. NaCl is wide available, relatively inexpensive, and has well known properties. Therefore, it is the frequently used salt in solar ponds. Pond brine uses a refined NaCl salt and water to produce highly transparent solutions. Ponds utilizing such brines have demonstrated a high degree of clarity during the year following initial establishment.

To select an appropriate location for a solar pond, there are essential requirements that must be satisfied:

- Use for the heat or power produced
- Access to salt
- Access to water

In addition to the stated essential requirements, there are desirable characteristics for solar pond sites such as:

- High insolation
- Deep water table
- Low wind speed
- Relatively flat site
- Soil with good cohesion for walls

2.9 Other Types Of Solar Ponds

2.9.1 Partitioned Solar Ponds

(Tabor, 1961) has found the following problems that occurred during the operation of solar pond: (i) biological growth of algae, (ii) decreasing the transparency by dirt falling in it; (iii) high concentration at the top of the pond caused by evaporation;

(iv) disturbance of the concentration gradient while extracting heat.

Adding chemicals can prevent biological growth (Rabl and Nielsen, 1975). The other problems may be overcome by installing two transparent partitions one on top or few centimeters below the surface of the pond and the other at a depth of 1–2 m. A thin water layer above the top partition brings both advantages and disadvantages. On the negative side, especially in windy locations, include evaporative cooling and increased reflectivity due to wave action. The advantage is a decrease in reflective losses because the water has a lower index of refraction than plastics, so that reflective losses at a water plastics boundary are small. The lower partition separates the insulating layer from the convective layer. It improves the stability of the pond and facilitates the extraction of heat. Instabilities due to buoyancy can be prevented either by making the lower partition stiff for example (glass panes) or if a flexible partition for example (Tedlar sheet) is used, by filling the convection zone with salt water. To improve convection, heat is extracted just below the partition either by removing hot water or brine directly or by running fresh water through a network of heat exchanging plastic pipes. The Tedlar sheet may be preferable if brine is used in the convective zone (Rabl and Nielsen, 1975).

2.9.2 Viscosity Stabilized Solar Ponds

In gel or viscosity stabilized solar ponds, the non-convective layer consists of a viscous polymer gel positioned by transparent films. The gel is located in the upper part of the solar pond, is less dense than water and is optically clear. It provides insulation against heat loss, and allows the sun to heat the bulk of the water below the gel. The gel is viscous enough to prevent convection and also has low thermal conductivity. It uses high viscosity rather than a salinity gradient to suppress convection.

Materials suitable for viscosity stabilized solar ponds should have high transmittance for solar radiation, high efficiency of the chosen thickness and should be capable of performing at temperatures up to 60 °C. Polymers such as locust bean gum, starch and gelatin are all potentially useful materials. The ideas of viscosity stabilized solar pond appear to be promising but presently are not economically competitive with salt gradient solar pond (Garg, 1987).

2.9.3 Membrane Stratified Solar Ponds

A membrane stratified solar pond is a type of non-salt solar pond, which is a body of liquid using closely spaced transparent membranes. The membrane space for inhibiting convection should be very small and a large number of high transparent films are required (Taga, 1990). The buoyancy effect is balanced by the weight of water so that solar radiation is converted into sensible heat (Ouni, 1998). Three types of membranes are proposed for the membrane stratified solar pond, which are horizontal sheets, vertical tubes, and vertical sheets (Hull, 1980).

2.9.4 Saturated Solar Ponds

The problems of maintenance density maintaining gradient in the conventional salt gradient solar pond can be overcome by making the pond saturated at all levels, with a salt whose solubility increases with temperature. Such saturated ponds have no apparent diffusion problems and the gradients are self-sustaining depending on local temperature; thus the main advantage of such a pond is its inherent stability. In such a pond, vertical diffusion of salt is prevented and the density gradient is stable; thus making the pond maintenance free (Subhakar, 1993).

Although the advantages of maintenance free for the saturated pond, it was decided not to adopt it in this research because literature concerning theoretical and experimental studies on saturated solar ponds is scarce.

Vitner et al. (1988) reported that insufficient heating from the bottom of the saturated solar pond causes solute crystallization, which in time reduces heat transfer rate, thus causing further crystallization.

2.9.5 Shallow Solar Ponds

The shallow solar pond is a solar energy collector that is intended to supply large amounts of heat for industrial applications at a cost that is competitive with fossil fuels. Its use for the conversion of solar energy into low grade thermal energy has been a subject of intensive investigations for a number of years, especially by the solar energy group at Lawrence Livermore Laboratory (USA) (Dickinson et al., 1976). The name implies that the depth of water in the shallow solar pond is very small, typically only a few centimeters, which is like a conventional solar still consisting of a blackened tray holding some water in it. The still takes advantage of evaporation of salt water by

solar heat. In the shallow solar pond the shallow level is covered by a plastic film, in such a way that the film is in contact with the top surface of the water, and thus prevents the cooling effect due to evaporation. It is capable of heating a large quantity of water to appreciable temperature, and, because of its simplicity in working, it holds out promise for one of the cheapest known methods for harnessing solar energy. A shallow solar pond is essentially a large water bag or pillow placed within an enclosure with a clear upper glazing. Water is placed within the bag, which is generally constructed from clear upper plastic film and a black lower plastic film. The depth of the water within the bag is normally in the range of 4–15 cm. The solar energy collection efficiency is directly proportional to water depth, whereas the water temperature is inversely proportional to water depth. Solar energy is converted to thermal energy by heating the water during the day. The water is withdrawn from the shallow solar pond before sunset (or more precisely when the collection efficiency approach zero) for utilization or storage (Garg, 1982).

Salt gradient solar ponds have advantages for long-term energy storage. In contrast, non-salt solar ponds such as membrane stratified ponds and shallow solar ponds are more suitable for short-term energy storage because the temperature rise of the pond water is rapid.

2.10 Salinity Gradient Solar Pond Fundamentals

2.10.1 Solar Radiation with Solar Pond

When solar radiation falls on the surface of the water, some of the sunlight is reflected back to the sky, and part is absorbed in the bottom of the solar pond, as shown in Figure 2.12. The long wavelengths of solar radiation are mostly absorbed by the upper convective zone, while the shorter wavelengths reach the lower convective zone.

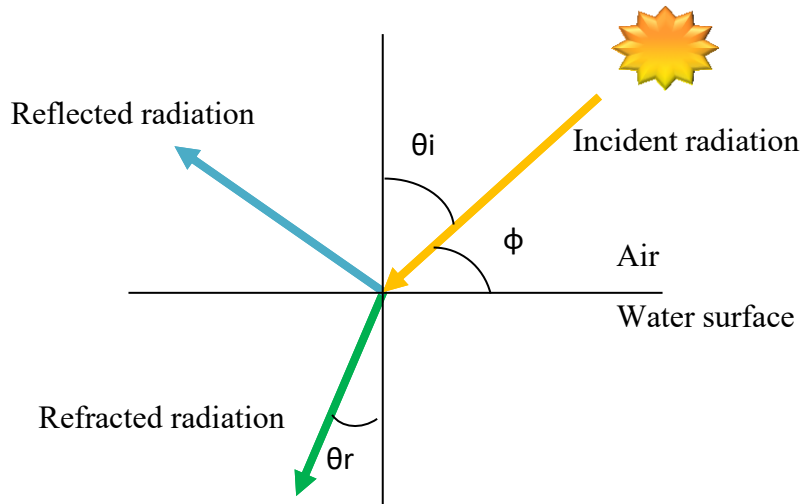


Figure 2.12 Refraction and Reflection of solar radiation

Sunlight Reflection

The amount of reflected solar radiation towards the sky depends on the position of the sun and the condition of the water's surface. A rough surface tends to absorb more sunlight, and a glass like surface reflects more (Cengel and Özişik, 1984). When the surface of water is not turbulent or is only slightly turbulent, then the fraction of direct radiation reflection can be calculated by Fresnel's equation (Wang and Akbarzadeh, 1983):

$$Fr(\theta_i) = \frac{1}{2} \left[\frac{\sin^2(\theta_i - \theta_r)}{\sin^2(\theta_i + \theta_r)} + \frac{\tan^2(\theta_i - \theta_r)}{\tan^2(\theta_i + \theta_r)} \right] \quad (2.1)$$

The Fresnel reflection (Fr) computes the ratio of the amount of reflected ray to the incident beam.

Sunlight Transmission

Some part of the full solar radiation, Ho , reaching the pond surface, is reflected back. The remainder Hp , is obtained from:

$$Hp = (1 - Fr)Ho \quad (2.2)$$

The remaining part is refracted into the water medium. This refraction of the incident solar radiation can be predicted by Snell's Law for an air and water interface:

$$\frac{\sin \theta_i}{\sin \theta_r} = \frac{n_2}{n_1} = \frac{v_1}{v_2} = \frac{\lambda_1}{\lambda_2} = 1.333 \quad (2.3)$$

Table 2.1 shows index of refraction for different medium.

The solar radiation travels deeper in the water for many metres, depending upon the transparency and clearness of the water. Water impurities may scatter and/or absorb the beam; clear water allows it to travel further, and therefore the water should be maintained as clear as possible.

Medium	Vacuum	Air	Water	Ethanol	Glycerine	Crown Glass*	Quartz	Flint Glass*	Diamond	Salt water
Index	1.00	1.0003	1.33	1.36	1.47	1.50-1.62	1.54	1.45-2.00	2.42	1.33-1.38

* Varies slightly due to inconsistencies in the glass

Table 2.1 Index of refraction for different medium (Clintberg, 2005)

Sunlight Absorption

The propagated light within a medium of water is attenuated by absorption and scattering. The latter is caused mainly by the presence of biological organisms and suspended particles (Elhadidy and Nimmo, 1983), while water molecules themselves cause a minor effect in terms of scattering.

The absorption of solar radiation is a complicated process, and there is very little available data on sunlight attenuation and transmission in water (Garg, 1987). Several researchers have attempted to derive formulae to describe it, but it has been found that solar radiation absorption in a body of water cannot be described by a single exponential equation, as such absorption varies from one wavelength to another. For example, the near infrared wavelength can be absorbed within the first decimetre of the water's surface and most of the visible light band can be absorbed within 10 metres, but short wavelengths may travel up to 150 m; none passes further than this depth, even in very clear water conditions (Rabl and Nielsen, 1975); (Garrison, 2007).

Rabl and Nielsen, (1975) divided the wavelength spectrum between 0.2 and 1.2 μm into four bands, and then determined the fraction of solar radiation and average extinction coefficient in each band. They considered that water is practically opaque to wavelengths greater than the infrared range (1 μm).

This classification is illustrated in Table 2.2.

Rabl and Nielsen (1975)			
i	η	$\mu(\text{cm}^{-1})$	Wavelength (μm)
1	0.237	0.32×10^{-3}	0.2-0.6
2	0.193	4.5×10^{-3}	0.6-0.75
3	0.167	0.03	0.75-0.9
4	0.179	0.35	0.9-1.2

Table 2.2 Rabl and Nielsen's absorption data (1975).

The total of the solar radiation fractions based on Rabl and Nielsen's approximation is 0.776, which represents 77.6% of the propagated sunlight in the water. The rest (22.4%) is assumed to be absorbed within the first few centimetres of the upper layer of the water's surface, as it is a far-infrared wavelength, i.e. greater than 1.2 μm .

The solar radiation, penetrating into the water body, decays exponentially with depth, as fluid layers absorb energy. The rate of decay or transmissivity is a function of the wavelength of the radiation and for the whole spectrum of wavelengths.

The data in Table 2.2 can be used to predict the fraction of the solar radiation at depth (x) by the following equation. (Rabl and Nielsen, 1975)

$$\frac{H_x}{H_o} = \sum_{i=1}^4 \eta_i \exp\left(\frac{-\mu_i x}{\cos \theta_r}\right) \quad (2.4)$$

where η is the fraction of solar radiation and μ is the average extinction coefficient for the i th portion of the solar spectrum (m^{-1}).

An alternative exponential formula (Equation 2.5) was proposed by Bryant and Colbeck, (1977).

$$\frac{H_x}{H_o} = \left\{ 0.36 - 0.08 \ln \left(\frac{x}{\cos \theta_r} \right) \right\} \quad (2.5)$$

Figure 2.13 presents the graph for the extent of the solar energy absorption inside the pond with the depth by using Equations 2.4 and 2.5. As evident from the trends, the predictions made by the two correlations is quite close. It is noted that the absorption of the incident radiation shows an initial sharp and then slow trend with respect to the depth of the pond. At a depth of 1 m, only 35% of the radiation entering the pond is available while at a depth of 2 m this value is reduced to 30%. Solar radiation intensity has a direct effect on the temperature of the pond.

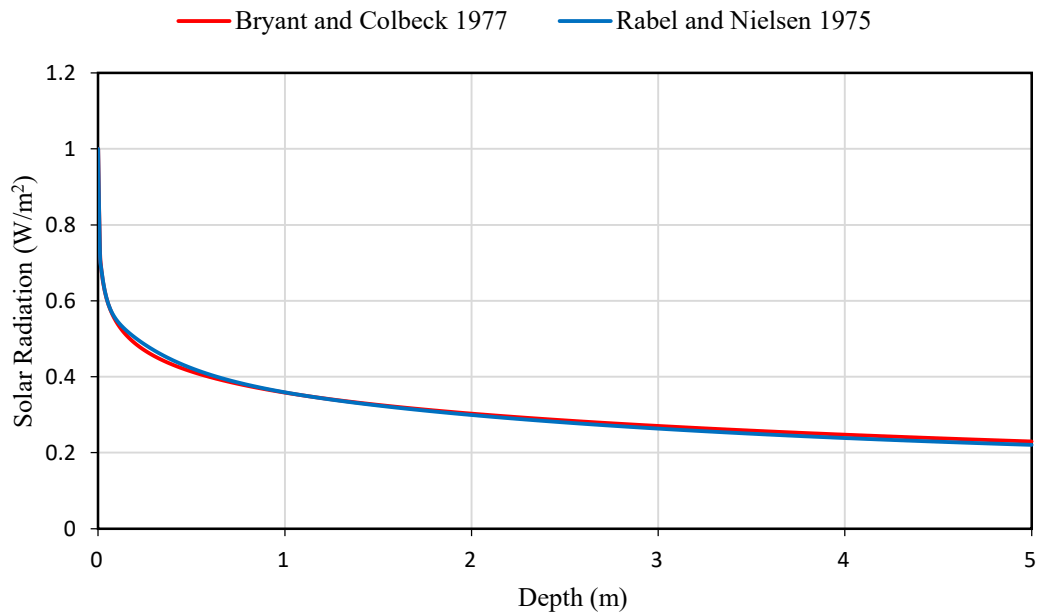


Figure 2.13 Variation of radiation intensity with depth of solar pond as calculated on the basis of two different correlations given by Equations. (2.4) and (2.5)

2.10.2 Salt Gradient Solar Pond Zones

The salt gradient solar pond consists of three thermally distinct zones; the upper convective zone (UCZ) or insulating layer with fresh or slightly saline water at around ambient temperature; a non-convective zone (NCZ) with a gradually increasing

salinity, and temperature; and a lower convective zone (LCZ), called the storage zone, which is hot and very salty (Hull et al., 1988).

The Upper Convective Zone

An upper convective zone, typically 0.3 m thick (Hull et al., 1988), consists of water with almost uniform low salinity, which is generally close to ambient temperature. The UCZ is situated on the top of the pond where the incident solar radiation is partially absorbed and the rest is transmitted to the zone below. The UCZ is the result of evaporation, wind induced mixing, and surface flushing. It protects the rest of the pond from external influences such as rain and wind.

The Non-Convective Zone

The non-convective zone has a salt concentration gradient, is much thicker than the upper convective zone and occupies more than half the depth of the pond. Both salinity and temperature increase with depth. The salinity gradient in the NCZ inhibits convection, and thus the NCZ provides thermal insulation. A weak salt gradient allows convection in the solar pond, which leads to energy loss through the surface layer of the pond.

The Lower Convective Zone

This is a homogenous layer, relatively high salinity at a high temperature and serves as the heat storage zone. The LCZ is almost as thick as the non-convective zone. Solar energy is absorbed, stored and extracted from this region in a solar pond. In addition, heat may be transferred to or from the NCZ to the LCZ and to or from the earth underneath the floor of the pond. The method of extracting heat from a solar pond is to draw the heat from the LCZ. Extraction can be accomplished using an internal heat exchanger located in this LCZ or by pumping hot brine from the upper region of LCZ through an external heat exchanger, where heat is delivered to the applications (such as heating or and cooling systems) and then returning the brine to the lower region of the LCZ.

2.10.3 Construction and Maintenance of Salt Gradient

The successful solar pond depends on salt gradient's establishment and maintenance of stratified regions on the solar pond which acts as transparent insulation (Zangrando, 1991). The gradient layer contains two profiles in parallel, one of temperature and

other of salinity. Both temperature and salinity increase as a function of depth. The slopes of these gradients are positive as a function of depth, but they are rarely constant. The salinity gradient must be established artificially; the temperature gradient is formed naturally after some time by the absorption of incident solar energy. Increasing the temperature results in a decrease in density, whereas increasing the salinity increases the density. Whilst increasing concentration with depth enhances the stability of a solar pond, increase in temperature has a reverse effect on it.

2.10.4 Methods of Gradient Establishment

The salt concentration gradient in the pond can be constructed by various methods dependent on different local requirements. These methods include natural diffusion, stacking, redistribution and falling.

In the natural diffusion method, the lower half is filled with water and salt and the upper half is filled with water; top and bottom concentrations are kept constant by regularly washing the surface and adding salt in the bottom. Owing to the upward diffusion of salt, a salinity gradient will be established. This is a very slow method of establishing the salt gradient and should be considered if the pond is very large or if the starting time could be unlimited (Zangrando, 1991).

Stacking involves the filling of the pond with a storage layer of highly concentrated solution and several other layers of salt solutions of differing concentration. The concentration of salt in successive layers is changed in steps from near saturation at the bottom to fresh water at the top. For a typical pond of about 1 m depth, one might use about 10 layers. The turbulent mixing generated during filling and continuous molecular diffusion modifies the stepwise type concentration profile into a nearly linear concentration profile (Chepurniy and Savage, 1975). The practical approach for stacking used in most solar ponds is that the bottom layer is filled first and successively lighter layers are floated upon the lower denser layers. However, some experimental ponds in Australia (Golding, 1982), have been built by injecting in the bottom successively denser layers which lifted the lighter layers filled previously.

Redistribution is considered to be the most convenient for larger ponds (Nielsen et al., 1977). When fresh water is injected at some level into homogeneous brine it stirs and uniformly dilutes the brine from a few centimeters below the injection level to the surface. Hence, the artificial pond is filled with high salinity brine to half of its total

depth and then fresh water is added through a diffuser. Initially, the diffuser is placed at the bottom and the water is added in the pond, flowing in as under current and the level in the pond increases. The diffuser is moved upward continuously or in steps. Timing of the movement is so adjusted that the diffuser and water surface reach the final level at same time. At the completion of this process it has a nearly uniform salt concentration gradient in the pond (Zangrando, 1991).

The salt gradient can also be maintained by periodically adding a saturated salt solution at the bottom and washing the surface with fresh water. A more efficient approach, which does not require the continual addition of salt, is the falling pond concept (Tabor, 1961), wherein hot brine is withdrawn from the bottom layer without causing disturbance to the layer above. This is possible, since in a fluid system stratified with a density gradient, selective flow of the bottom layer can be accomplished without requiring a mechanical separation between the flowing and stable regions of the system (Tabor, 1981). The hot brine withdrawn from the solar pond is passed through the flash evaporator to remove some of its water. The solution now having a high concentration and smaller volume is re-injected in the pond bottom and the removed water is replaced into the surface layer; consequently, the concentration gradient would be maintained. The fall in surface level due to evaporation is also restored by the addition of fresh water to keep both the pond depth and the surface concentration constant. In this process, the gradient tends to be displaced downwards. It is acute that the brine circulation rate and the location of the suction diffuser with respect to the lower interface must be selected carefully in such a manner that withdrawal and re-injection of brine does not disturb the salinity gradient (Kumar and Kishore, 1999).

2.10.5 The Solar Pond Stability

The stability of solar ponds has been extensively studied by Huppert and Turner (1976), Leshuk et al. (1978), Zangrando (1980) and Sundaram (1974). The density of liquid in the solar pond depends on the salt concentration and temperature of the liquid. Weinberger (1964) indicated that there will be no vertical thermal convection or the pond will be stable when the density gradient on account of the salt concentration gradient is greater than the negative density gradient produced by the temperature

gradient i.e. the total derivative of density with respect to depth is greater than or equal to zero, as shown in Equation (2.6).

$$\frac{d\rho}{dx} = \frac{\partial\rho}{\partial C} \frac{\partial C}{\partial x} + \frac{\partial\rho}{\partial T} \frac{\partial T}{\partial x}, \quad \frac{d\rho}{dx} > 0 \rightarrow \frac{\partial\rho}{\partial C} \frac{\partial C}{\partial x} \geq -\frac{\partial\rho}{\partial T} \frac{\partial T}{\partial x} \quad (2.6)$$

The details of solar pond stability are discussed in the next section.

2.10.6 Salinity Gradient Solar Pond Stability

An essential factor in gradient solar pond stability is maintaining the gradient profile in the non-convective middle zone of the pond. A salt gradient solar pond (SGSP) cannot operate efficiently without an internally stable non-convective zone (NCZ). The main design consideration for the successful operation of an SGSP is to maintain the stable state of the NCZ boundaries and level of the salt gradient. Moreover, the state of the NCZ can be affected by the UCZ and LCZ, causing erosion to the integrity of its boundaries; erosion leads to a reduction in the thickness of the NCZ and, ultimately, the destruction of the pond (Zangrando, 1980).

This aim of stability will not be achieved unless the salt concentration gradient is correctly built and the salt diffusion inside a non-convective solar pond is successfully controlled. The density of this highly saline water is a function of salt concentration and temperature. The saline concentration and temperature should both increase downward and, although the solution density decreases as temperature increases, the direct proportion with salinity concentration has a greater effect. Several internal and external factors can affect solar pond stability or could destroy the gradient zone of the SGSP. The minimum requirement for gradient pond stability is that the salt density in the gradient layer increases downward to avoid any gradient mix or overturn.

2.10.7 Static Stability

The internal stability of a salinity gradient solar pond is based on a low rate of salt diffusion from the storage zone toward the upper zone of the pond. Diffusion can be defined as the movement or migration of an individual component within a mixture solution medium. The primary cause of diffusion is the different concentrations or the concentration gradient of a component in a fluid. Such fluids tend to become internally

stable through equalizing the concentrations, and, consequently, the molecules travel from the high concentration area to the lower one. If there is no applied pressure or forced diffusion in a binary or multi component fluid, the mass flux in the mixture is primarily dependent on the concentration difference and the temperature gradient. The former is known as molecular (ordinary) diffusion. Unfortunately, molecular diffusion works against the stability of salinity gradient solar ponds. Therefore, salt management is absolutely essential for monitoring and operating a gradient solar pond.

2.10.8 Molecular Diffusion

Molecular diffusion happens mainly as a result of the concentration gradient in a solution, and this kind of diffusion occurs according to Fick's law. Fick's law states that the rate of diffusion of chemical species at a location in a gas mixture (or liquid or solid solution) is proportional to the concentration gradient of that species at the location (Cengel et al., 1998). The salt concentration in a bottom zone of a salinity gradient solar pond is about 230 g/l of sodium chloride (NaCl), and this amount of salt may represent 20% of the lower zone's saline water while the upper zone may contain between 0 and 2% salinity (Chepurniy and Savage, 1975).

If the molecular diffusion is only considered in a solar pond study, then Fick's law can be expressed as the following:

$$J = -D \frac{\partial C(x,t)}{\partial x} \quad (2.7)$$

2.10.9 Static Stability Criteria

The salt density gradient resulting from salt concentration difference magnitude in a solar pond is sometimes called a positive gradient, as it contributes to forming the desired shape of the gradient profile. Inside a non-convective layer within a solar pond, for example, the salinity gradient is concentrated downward. On the other hand, the density gradient may create a reversed profile in the salinity gradient due to the Soret effect; this is not actually desired and it may be called a negative gradient. These counter effects of positive and negative density gradient should be investigated to predict the static stability in a gradient pond, and if a negative stratification dominates

the positive gradient, convection may gradually take place inside the gradient zone; this gradient will then be destroyed or at least the performance of the pond will be reduced. In other words, the net concentration at any point in a salinity gradient pond must be lower than at any point underneath to suppress vertical convection in the gradient zone (Elwell, 1977). This stability condition was first suggested by (Weinberger, 1964), and it has been widely accepted and adopted by the most researchers. The condition can be expressed by the following formula (Weinberger, 1964):

$$\beta_T \frac{dT}{dx} \leq \beta_s \frac{dc}{dx} \quad (2.8)$$

$$\beta_T = -1/\rho_o [\partial \rho / \partial T]_c \quad \text{and} \quad \beta_s = -1/\rho_o [\partial \rho / \partial c]_T \quad (2.9)$$

Consequently, the density change with depth must satisfy this equation to indicate that a solar pond is sufficiently stable:

$$\frac{d\rho}{dx} = \beta_T \frac{dT}{dx} + \beta_s \frac{d\rho_s}{dx} > 0 \quad (2.10)$$

Alternatively, the above correlation can be expressed by a finite difference approach:

$$\frac{\Delta \rho}{\Delta x} = \beta_T \frac{\Delta T}{\Delta x} + \beta_s \frac{\Delta \rho_s}{\Delta x} > 0 \quad (2.11)$$

The stability criterion can also be viewed by another formula based on thermal and saline Rayleigh number. It is a dimensionless number resulted by multiplying the Grashof number, which expresses the relation between buoyancy and viscosity in a fluid, by the Prandtl number, which describes the relationship between momentum and thermal diffusivities. Thus, the Rayleigh number may be considered as the product of the ratio of buoyancy and viscosity forces and the ratio of momentum diffusivity and thermal diffusivity. Hence;

$$Ra = G_r \cdot P_r \quad (2.12)$$

Garg (1987) stated that convection takes place only when the Rayleigh number (Ra) in the above relation is higher than 2000.

The thermal Rayleigh number Ra_T is:

$$Ra_T = g \beta_T \Delta T L_c^3 / (\alpha \nu) \quad (2.13)$$

and the saline Rayleigh number Ras is:

$$Ra_s = g\beta_s \Delta C Lc^3 / (\alpha \nu) \quad (2.14)$$

The density ratio of the thermal and salinity Rayleigh number ($R\rho$), which may determine the stability behaviour, can be represented by the following correlation: (Garg, 1987), (Elwell, 1977).

$$R\rho = \frac{Ra_s}{Ra_T} = \frac{\beta_s \Delta C}{\beta_T \Delta T} \quad (2.15)$$

2.10.10 Dynamic Stability Criterion

When the above static stability condition is obtained and the salinity gradient is sufficiently large to suppress vertical convection, the solar pond tends to be stable. However, there are several external perturbation factors, such as the wind, falling particles, rainfall, evaporation, heat loss, etc., which may support the Soret thermal gradient to rebel against the salinity gradient suppression force.

This may occur due to the potential energy stored in the inverted temperature profile and, if the transmitted external energy together with the profile potential energy is stronger than the viscous damping, then vertical convection will be initiated and will grow with time, leading to the mixing of the solar pond layers. It has been found that heat diffusivity is 100 times faster than salt diffusivity (Elwell, 1977). In a laboratory experiment, the internal oscillation was identified as having a tiny value, but then it grew gradually until it was ultimately supported by convection; shortly afterwards, the saline gradient was debilitated by the mass transfer resulting from this oscillation (Shirtcliffe, 1969 ; Wright, 1976).

The dynamic stability condition equation for a gradient solar pond was introduced by (Weinberger, 1964). The proposed formula can maintain the gradient sufficiently to avert any oscillatory movement effects developing with time, and the following relationship may express this condition:

$$(v + \alpha) \frac{\partial \rho}{\partial T} \frac{\partial T}{\partial x} + (v + D) \frac{\partial \rho}{\partial S} \frac{\partial S}{\partial x} \geq 0 \quad (2.16)$$

where α and D are thermal and salinity diffusion coefficients, respectively. The above equation can be rewritten in another suggested way (Meyer, 1981):

$$\frac{\Delta T}{\Delta x} < \left(\frac{Pr+Le}{Pr+1}\right)\left(\frac{\beta_S}{\beta_T}\right)\left(\frac{\Delta S}{\Delta x}\right) \quad (2.17)$$

where the Prandtl number (Pr) and the Lewis number (Le) are:

$$Pr = \nu/\alpha \quad \text{and} \quad Le = \alpha/D$$

Most investigators have adopted the above equations, and they have been used widely to investigate gradient solar pond stability. Equation (2.17) is employed to carry out the stability calculation from the top to the bottom of a solar pond, including both convective and non-convective zones. In the case of one-dimensional instability (Schladow, 1988) suggested a simplification of the above equation:

$$R_\rho = \frac{Pr+1}{Pr+Le} \quad (2.18)$$

The mathematical analysis of thermohaline (double-diffusive) diffusion in a gradient study may predict the marginal stability, and can be represented in this equation (Hull, 1985):

$$Ra_T = \frac{\nu+D}{\nu+\alpha} Ra_S + \left(1 + \frac{D}{\alpha}\right)\left(1 + \frac{D}{\nu}\right)\left(\frac{27\pi^4}{4}\right) \quad (2.19)$$

The salinity and thermal Rayleigh correlations have an effect much larger than the second term on the right-hand side of Equation (2.19); hence, the latter term can be neglected, leading again to the Weinberger dynamic stability criterion in Equation (2.16); this simplification is commonly assumed. For a typical salinity gradient solar pond, Hull and Kasza (1985) stated that the Lewis number usually varies from 30 to 140 and that the Prandtl number is expected to be between 3 and 10. It was confirmed in the same report that the salt concentration gradient should be far greater than that obtained through the dynamic stability correlation to ensure that the marginal stability is strong enough to keep a gradient zone in a fixed position.

2.11 Salt Gradient Solar Pond Case Studies

Solar pond technology is one of the renewable energy sources. This technology has a number of advantages. Compared to other sources of renewable energy, the solar pond approach is much cheaper, economical in operation and heat can be stored for up to

six months. Solar pond technology is particularly attractive for remote and rural areas, especially in developing countries. Very large area collectors can be set up for just the cost of the clay or plastic pond liner.

The simplicity of the solar pond and its capability of generating sustainable low grade heat make it attractive for a variety of applications. Heat from solar ponds can be used for desalination, process heating, electrical power production, salinity mitigation, production of chemicals and in aquaculture and biotechnology.

Sodium chloride based solar ponds are primarily an established technology for low temperature applications. The operation of the 300 m² Ohio State University Pond by Nielsen, (Hull et al., 1988) successfully demonstrated the use of a NaCl pond for heat production. High temperature applications of NaCl ponds also have been successful, but these applications require more careful pond operation and maintenance procedures. Several ponds have operated at temperatures more than 80°C (Hull et al., 1988).

According to the above information, the salinity gradient solar pond is considered in this current study.

A large number of experimental solar ponds have been constructed around the world. There have also been a considerable number of demonstration solar ponds constructed in Australia, India, USA and Israel which are supplying heat.

2.11.1 Bet Ha Arava Solar Pond

The world's first commercial scale solar pond power plant was installed at Ein Boqek in Israel (Tabor, 1981). The plant was commissioned in December 1979 and was connected to the grid in 1984 (Figure 2.14). The pond generated 150 KW power for 7 years between 1979 and 1986. Here, two solar ponds, with a combined area of the 250000 m², supplied the required thermal energy input to the power plant.



Figure 2.14 Bet Ha Arava Solar pond power station in the Dead Sea

Source: (MOTHER and Publications, 1980)

There has been renewed interest in solar ponds in Israel in recent years, but the focus has shifted from electricity generation to direct low temperature heating applications, such as industrial process heating, space heating and desalination (Akbarzadeh et al., 2005).

2.11.2 Pyramid Hill Solar Pond

In 2000- 2001, a solar pond project was set up at Pyramid Hill Salt Pty Ltd. It is a collaborative project involving RMIT University, with two industry partners: Geo-Eng. Australia Pty Ltd and Pyramid Salt Pty Ltd. The Project was supported by funding from the Australian Greenhouse Office under the Renewable Energy Commercialization Program. The project focused on the use of solar ponds for industrial process heating and in particular for the drying process in commercial salt

production. The pond is located in northern Victoria and is approximately 200 km north of Melbourne on the Pyramid Hill – Boort Road (Figure 2.15).

This 3000 square metre solar pond supplies up to 60 kW of process heat for commercial salt production. (Leblanc et al., 2011).



Figure 2.15 3000 m² solar pond at Pyramid Hill, Australia. (Chinn et al., 2001)

2.11.3 Margherita di Savoia Solar Pond

Folchitto (1991) has described the Margherita di Savoia solar pond. The pond was 25,000 square metre and 4 metre deep. 500 kW of process heat were extracted from the pond for 8000 hours. The pipes were of high density PVC and high density polyethylene for seawater, and of insulated fiberglass for carrying hot brine from and to the LCZ in the solar pond. (Hull et al., 1988)

2.11.4 Bhuj Solar Pond, India

A 6000 square meter solar pond (Figure 2.16) was constructed and operated at the Kutch dairy, Bhuj, India. The pond supplies hot water to the dairy plant. The pond

attained a maximum temperature of 99.8 °C under stagnation in May 1991 (Kumar and Kishore, 1999).

The heat extraction system incorporates an external heat exchanger with brine suction and discharge diffusers.



Figure 2.16 Solar pond, Bhuj, India (Kumar and Kishore, 1999)

2.11.5 Alice Springs Solar Pond

Sherman and Imberger (1991) analysed the performance of the 1600 square meter solar pond in Alice Springs shown in Figures 2.17 and 2.18. Temperatures of the storage zone between 85 and 90°C were consistently maintained and a solar to thermal efficiency of 12 to 15 % was achieved when heat was extracted from late January to March 1989. Heat extraction helped to maintain the storage zone temperature within the desired range. The pond was used to supply heat to run a developmental 20 kW organic vapour screw expander Rankine cycle engine and generator (Figure 2.18).

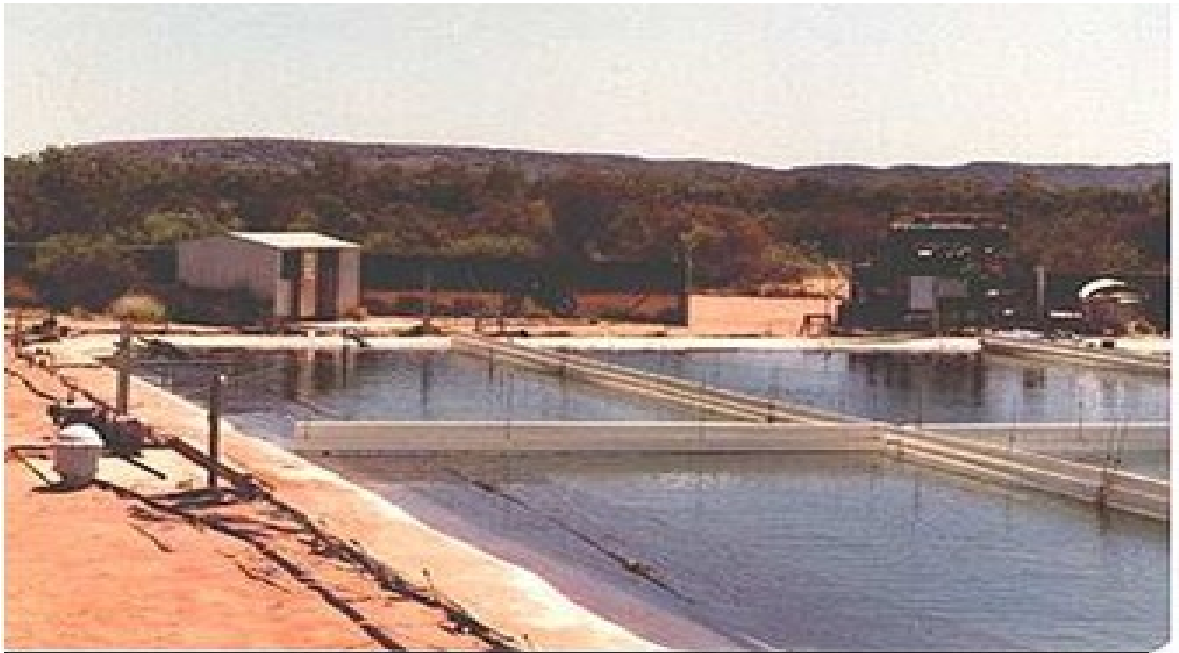


Figure 2.17 Alice Springs Solar Pond, Australia (Collins and Fredrickson, 1985)



Figure 2.18 ORC Engine at Alice Springs (Collins and Fredrickson, 1985)

2.11.6 UTEP High – Performance Solar Pond

The University of Texas at El Paso (UTEP) has designed and operated a high performance solar pond (0.37 hectare) at a food processing facility located 20 km northwest of downtown El Paso since the late 1980s (Figure 2.19). The solar pond efficiency and thermodynamic conversion efficiency (heat to power) were found to be 16, 5.5% respectively. The pond generated 150 kW power for 7 years.



Figure 2.19 El Paso Solar Pond, Texas, USA (Leblanc et al., 2011)

The plant has been in operation since 1983 and has reached a maximum pond temperature of 93 °C. Heat extracted upon demand has been used to power an organic Rankine cycle heat engine (ORC) for electricity production to supply hot water and to supply heat to operate a spin flash desalting unit and a Licon desalting unit for fresh water production. The pond was used to generate electrical power at 100 kW from September 1986. Problems with liner failure have been encountered. In 1992, during the summer, a maximum electric power of 120 kW was achieved using an ORC engine coupled to the pond (Akbarzadeh et al., 2005). The El Paso solar pond experience has

demonstrated that reliable high performance operation requires continuous automatic monitoring of the key pond data to maintain profiles that do not require speedy attention to any instability in the salinity gradient that might otherwise develop.

It can be concluded that these examples show that solar ponds are practical and reliable system that can produce significant amounts of energy.

2.11.7 Heat Extraction And Rejection

The performance of a solar pond depends substantially on the amount of solar energy that is input to the solar pond and the amount of heat loss (or heat extraction) from the pond. The solar energy is derived from the incident solar radiation, which can be converted into useful heat by such ponds.

The heat extraction is the main aim when constructing a solar pond, but it is a form of heat loss as it reduces the storage zone temperature.

2.11.8 Conventional methods of heat extraction

Heat has generally been successfully extracted from the lower convective zone (LCZ) of solar ponds by two main methods. In the first, a heat transfer fluid circulates in a closed cycle through an in-pond heat exchanger, as used in the Pyramid Hill solar pond, in Victoria, Australia. In the second method, hot brine from the LCZ is circulated through an external heat exchanger, as tested and demonstrated in El Paso solar pond.

1) The conventional method of heat extraction from a solar pond is to draw the heat from the LCZ only. This can be done using an in-pond heat exchanger located in the LCZ. A heat transfer fluid circulates in a closed cycle through the internal heat exchanger and transfers its thermal energy through an external heat exchanger. Figure 2.20 shows such a system for a heating application.

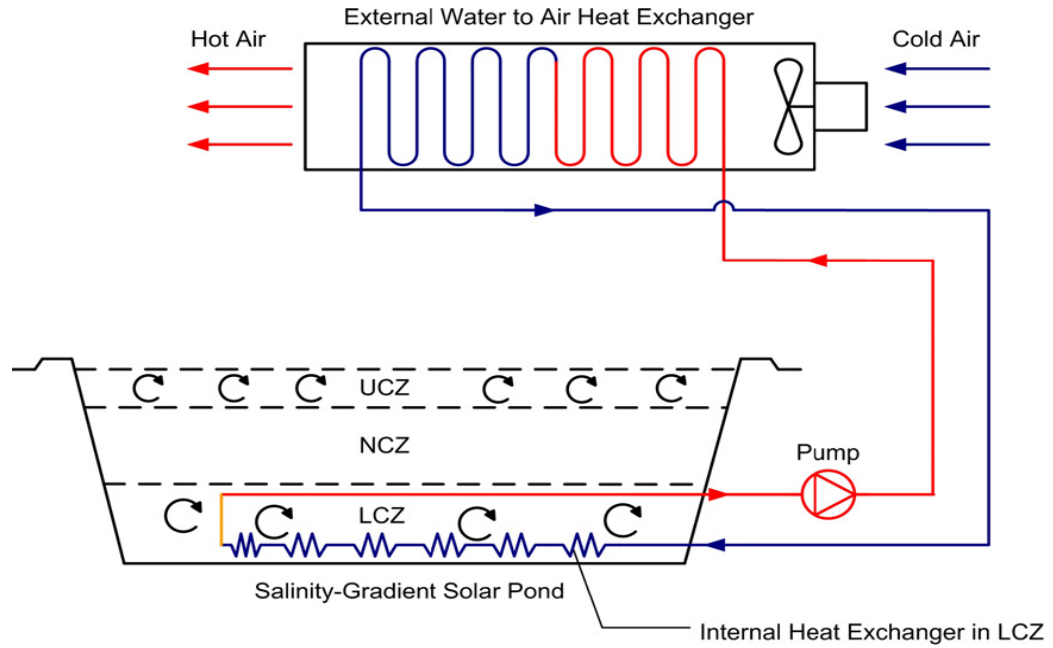


Figure 2.20 Conventional method of heat extraction using an internal heat exchanger (Leblanc et al., 2011).

2) Heat extraction can also be performed by pumping the hot brine from the top of the LCZ through an external heat exchanger and then returning the brine at a reduced temperature to the bottom of the LCZ (Figure 2.21). The velocity of the brine being pumped needs to be regulated to prevent erosion of the gradient layer.

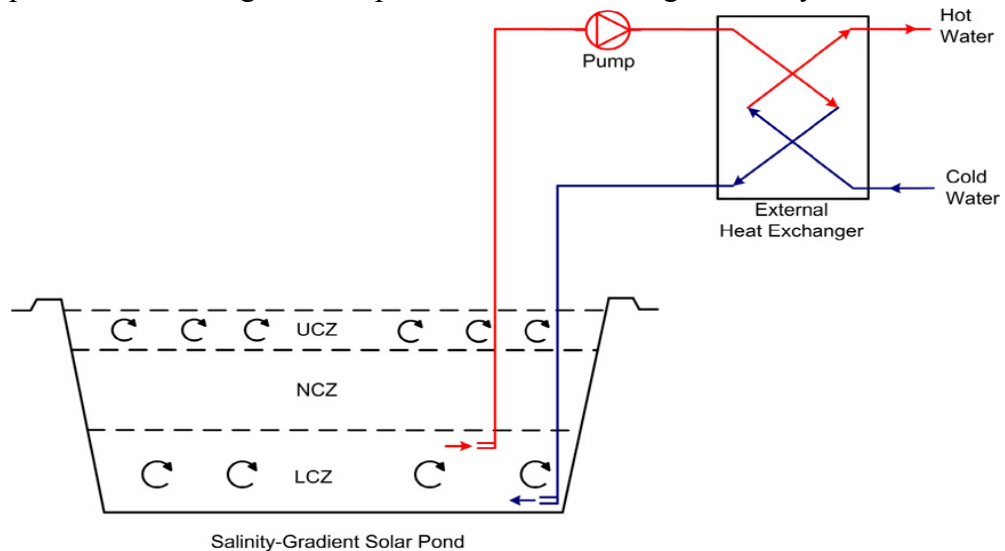


Figure 2.21 Conventional method of heat extraction using an external heat exchanger (Leblanc et al., 2011).

2.11.9 Heat extraction from the gradient layer

An alternative way of extracting heat from solar ponds has been investigated both theoretically and experimentally with the aim of improving the overall energy efficiency. In this method, heat is extracted from the NCZ as well as, or instead of, the LCZ (Akbarzadeh et al., 2005), (Leblanc et al., 2011).

A 53 square metre experimental salinity gradient solar pond was constructed in 1998 at the Renewable Energy Park of the School of Aerospace, Mechanical and Manufacturing Engineering, RMIT University located in Melbourne, Australia. The circular solar pond, as shown in Figure 2.22 is 8.2 m in diameter. The level of water in the pond is fixed at 2.05 m from the bottom using an overflow system. Its wall and base are made of reinforced concrete with a thickness of 0.2 m. The surface of the concrete is coated with a 1 mm layer of epoxy resin to protect the concrete against corrosion and possible chemical reactions. (Leblanc et al., 2011)



Figure 2.22 53 m² Bundoora experimental solar pond (Leblanc et al, 2011).

Heat is extracted from the gradient layer as well as from the LCZ at the bottom of the pond. Using an in-pond heat exchanger covering the entire thickness of the gradient layer as shown in Figure 2.23 and Figure 2.24. A heat transfer fluid enters this heat exchanger at a low temperature (equal or close to ambient) and is heated as it travels down through the heat exchanger towards the upper boundary of the LCZ. The fluid leaves the heat exchanger having a temperature close to the bottom zone temperature. This method of heat extraction will be especially suitable for applications where it is desired to heat a heat transfer fluid from ambient temperature to the temperature available in the lower regions of solar ponds. As with the conventional method of heat extraction, the heat obtained may be used for applications such as water heating, air heating, power generation or desalination.



Figure 2.23 Inpond heat exchanger for gradient layer and LCZ (Leblanc et al, 2011).

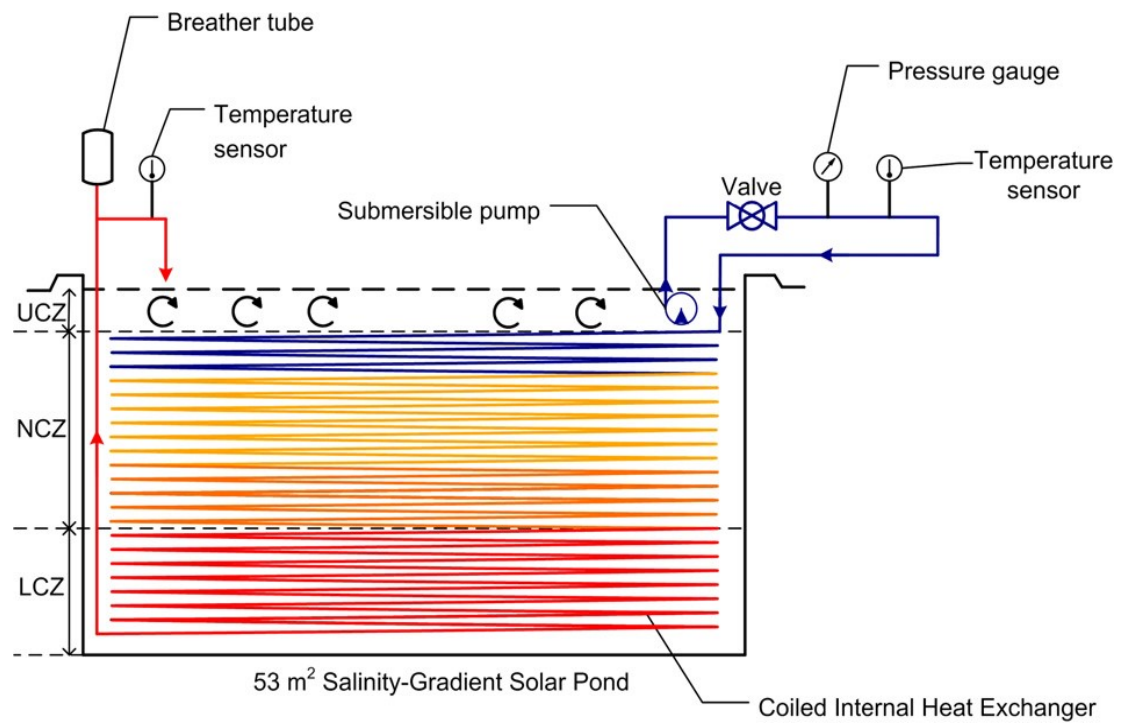


Figure 2.24 Schematic heat extraction system in solar pond (Leblanc et al., 2011).

2.11.10 Solar Pond For Both Heat Extraction And Rejection

The possibility of using solar ponds as low-cost solar collectors combined with conventional absorption chillers in a large scale solar cooling design was investigated by Tsilingiris (1992). Figure 2.25 details the working principle of this system. The lower convection zone (LCZ) of the solar pond provides the hot brine to the generator while the upper convection zone (UCZ) provides the low temperature water to the condenser and absorber so that the cooling tower is avoided.

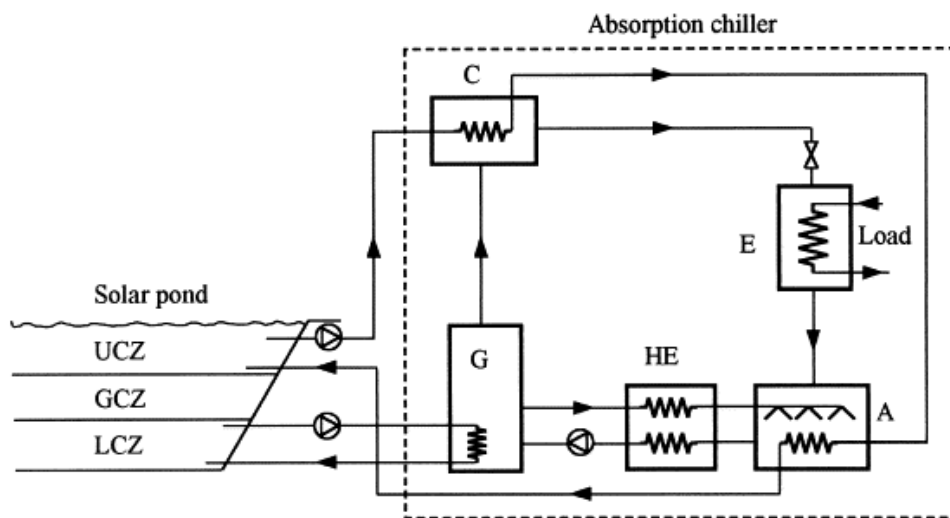


Figure 2.25 Solar pond connect to absorption chiller (Tsilingiris, 1992)

The flow rate of brine through the chiller should be designed carefully and is limited to a velocity of less than 1 m/s, so not to disturb the gradient in the NCZ layer. The experiments from both the small and large size ponds have shown that the lateral separation of withdrawal and injection heat extraction flow distributors can be located at the same side of the pond adjacent to the power plant, since a small temperature drop is sufficient to separate the flows vertically. Therefore, the assumption of well mixed convection zones will not always be realized in practice, since return flow from the condenser and absorber will form a warmer surface region within the UCZ and a cooler fluid region within the LCZ, respectively. Fortunately, both these effects have a favorable influence on chiller capacity by decreasing the heat flux to the soil and increasing the flux to the environment.

The difficulties involved with the construction of large scale solar cooling at a competitive cost are related to the prohibitively high costs of advanced technology high temperature collectors. The optimum pond area at which capital cost is minimized has been reported for a given chiller size. The derived cost per unit kW depends mainly

on salt cost and ranges from about \$300-500/kW in 1992, figures which are almost an order of magnitude lower than those corresponding to a large scale cooling installation using evacuated tube solar collectors. The comparison of the solar pond with flat plate collectors also shows that the solar pond is more effective at higher temperatures with built-in heat storage at substantially lower cost (Kooi, 1979).

The disadvantages of this kind of system may be the corrosion by salt in the heat exchanger of the chiller, which decreases the heat transfer from the solar pond to the chiller.

The limitations of this study are:

- The analysis is based on the combination of a steady state solar pond mathematical model with the operational characteristics of a commercial absorption chiller.
- Assuming condenser heat rejection in the upper convective zone (UCZ) which could disturb the NCZ layer.
- Assuming yearly mean values of weather conditions such as total incident radiation, ambient, and groundwater temperatures.
- No building model integrated with the solar pond and absorption chiller.

2.11.11 Suggested System For This Research

According to previous sections, the suggested system for the current study is a transient simulation model of salinity gradient solar pond and the ground underneath it, connected to an absorption chiller to serve the building as an air conditioner during summer. The heat extracted from the LCZ in the solar pond is used as a heat input to the generator of absorption chiller to produce a cooling air for building in Baghdad under hot and dry real weather conditions.

2.12 Practical Design Consideration of Solar Ponds

In evaluating a particular site for solar pond application, several factors need to be considered (Kalogirou, 2013). The main ones are:

- Since solar ponds are horizontal solar collectors, sites should be at low to moderate northern and southern latitudes e.g. latitudes between $\pm 40^\circ$.
 - Each potential site has to be evaluated for soil characteristics because the underlying earth structure should be free of stresses, strains, and fissures, which could cause differential thermal expansions, resulting in ground movement if the structure is not homogeneous.
 - Since the thermal conductivity of soil increases significantly with moisture content, the water table of the proposed site should be at least a few metres below the bottom of the pond to minimize heat losses.
 - A source of cheap salt or seawater should be available locally.
 - The site should be fairly flat to avoid moving large quantities of earth.
 - A cheap source of water must be available to make up for evaporation losses.
- (Kalogirou, 2013).

2.13 Difficulties and Limitations of Solar Pond Use

The salt gradient solar ponds are like any other technology in that they have some limitations, but the most common problem in any solar energy application is the absence of sunlight at night and cloudy days. Solar ponds, however, are less affected by this problem as they store heat cumulatively.

The main challenge in using most solar energy applications is heat loss. Therefore, good insulation is vital. The storage zone in salt gradient solar pond is insulated from the top by the gradient layer, which suppresses convection, but heat loss can still occur from the sides and the bottom if they are not well insulated. The bottom energy losses can be a serious problem if there is an aquifer beneath.

Most solar ponds are uncovered, and thus they are exposed to dust and impurity fouling. This fouling is an inherent problem in such ponds, which can considerably

reduce the irradiation reaching the lower zone. Consequently, the pond's efficiency will be reduced. Open surface ponds can be affected by wind shear, which can create waves on the surface of the solar pond; this movement can exacerbate heat loss and increase the evaporation rate. Although rainfall in adequate amounts is desirable to recover the evaporated water, it could adversely affect the pond's temperature. Moreover, it may dilute the saline water in the pond and cause it to overflow.

The growth of algae on the surface or within the pond is a problem that may impair the transparency of the water of the solar pond. However, Al-Mutaz and Alenezi (1999) reported that because the alkalinity of their water had been increased to above pH9, all the algae that had been apparent entirely disappeared from the precipitators, channels, and filters in the Salboukh RO Water Treatment Plant.

Gasulla et al. (2011) reported that both chlorine and copper ethylamine complex can prevent the growth of algae.

One of the most serious problems in a saline gradient solar pond is the upper-temperature limit. The temperature in these ponds should not rise to the boiling point of saline water. Otherwise the gradient layer will be destroyed. This problem occurred in El Paso Solar Pond in the early years of construction (Lu et al., 2001). This issue can be avoided by continuous heat removal from the storage zone. The boiling temperature of MgCl_2 near saturated water is 117°C , and the boiling temperature of NaCl saturated water is 108°C (Tabor, 1965)

Preparing a concentrated solution (brine), building the layers, and heat accumulation are all time consuming processes. In the El Paso Solar Pond it took five months to prepare the brine by adding 1100 tons of salt (Kumar and Kishore, 1999). In India, a separate system was developed to accelerate the dissolving process, and the dissolving of 3200 tons of NaCl was accomplished within two and a half months during the first phase. Due to some maintenance works, it was essential to rebuild the layers, but further improvements were made to the dissolving system, and the preparation process was reduced to just one month.

Establishing the gradient used to take a considerable amount of time (Dickinson et al., 1976). However, due to recent technological improvements, it now takes only a few days. For instance, it took four days in El Paso's 3000 m^2 solar pond (Lu et al., 2001) and 115 hours in the 6000 m^2 solar pond at Kutch, India. The temperature starts to rise

immediately after building the salinity gradient, and the pond's temperature increases by 1°C per day on average (Lu et al., 2001). In a salt gradient solar pond, the temperature of the storage zone can reach 80°C in about two months (Lu and Swift, 2004). These examples illustrate how much time is needed to rebuild the salt gradient solar pond layers if any of the layers are destroyed.

Solar pond research and operations have been halted several times in different parts of the world, as they have proved to be uncompetitive with other technologies in commercial projects. Nevertheless, operating solar ponds coupled with other technologies, such as salt gradient solar pond coupled with absorption chiller for air condition purposes, seems to be more promising than using fossil fuel to produce electricity to drive the conventional cooling systems.

2.14 Modelling Approaches and Software

The study of solar ponds, including experimental, and numerical investigations, has received much attention from numerous researchers.

One of the first experimental work of solar pond was carried out by Weinberger, (1964) using 25 m² of pond area. Some other researchers also presented experimental results for exists solar pond or laboratory one such as (Zangrando, 1979; Hull et al., 1984; Kurt et al., 2000, 2006). Karakilcik et al., (2006) have investigated experimentally and numerically the thermal performance of an insulated salt gradient solar pond.

Due to the cost and practical difficulty of experimental work, the feasibility of such a system will be investigated by numerical simulation.

Numerical modeling of solar pond has been reported by many investigators to predict the temperature and salinity profiles in the pond, as well as the prediction of the stability of the solar ponds. Most of these investigations used a one-dimensional model and use either a finite difference method (FDM) or finite element method (FEM).

The use of numerical methods for studying the solar pond was first suggested by Tybout, (1967). However, only since 1980 the finite difference models have been published. Hull, (1980) first used the FDM to investigate the validity of the assumptions employed by Weinberger (1964) and Rabl and Nielson (1975). Since

then, various numerical models have been developed. Most of these numerical models were one-dimensional and treated the problem in simplified ways. The models in general rely on the one-dimensional unsteady equation for heat transfer by conduction, with a source term representing heat absorbed by the pond from solar radiation. Also a one-dimensional transient mathematical model is used for the density gradient in a solar pond. The governing differential equations are solved numerically using the finite difference formulation with appropriate initial conditions. Different numerical techniques are available to solve the governing partial differential equations. An implicit-explicit finite difference scheme was developed by Rubin et al. (1984). The Crank-Nicolson method has been utilized by Hawalder and Brinkworth, (1981).

Boudhiaf, et al (2012) have numerically studied the problem of hydrodynamic, heat and mass transfer and stability in a two-dimensional salt gradient solar pond. The governing equations were solved using the finite volume method. It was concluded that the buoyancy ratio has a very important effect is preventing convective motions induced by solar radiation absorption and stabilizing the layers of the salty water in the solar pond. It was concluded that the increase of the thickness of UCZ would increase the UCZ temperature. The thickness of the NCZ has a very important effect in the reduction of the upwards heat losses, which causes in this case a rise in the temperature of the LCZ.

Mehdizadeh and Ahmadi (2014) developed a two-dimensional unsteady computational fluid dynamic (CFD) model for numerical stability analysis of the pond, as well as heat and mass transfer in salt gradient solar ponds. ANSYS-Fluent was used as the CFD solver. The heat extraction from the pond was studied by extracting the hot brine from the LCZ. The corresponding temperature and velocity field were evaluated.

Suarez et al. (2010) studied numerically the effects of double-diffusive convection on the heat performance and stability of a solar pond using a fully coupled two-dimensional model. ANSYS-Fluent was used as the CFD solver for the problem.

In the solar pond CFD model, a set of Navier-Stokes equations for a 3-dimensional space is derived using conservation of momentum, energy, and mass (salinity). The 3-

dimensional model is necessity of describing the convective vortices, which occur naturally in a fluid when the temperature of a lower layer is higher than the one above it. These convective motions lead to relatively fast transport of heat, leading the temperature to be distributed homogenously throughout the fluid.

However, in solar ponds, inside the non-convective zone (NCZ) in particular, the convective motions are eliminated (fluid is stationary), due to the density increasing with depth. Thus, the full three-dimensional solution is no longer necessary. The transport of thermal energy and salinity is then limited to diffusive motions, which occur over longer period of time.

For the cooling system and building, the techniques available for the study of solar cooling systems are by experiment or by dynamic simulation.

Experimental studies have been carried out on solar cooling using various types of collectors, such as flat plate collector and evacuated tube collector (Lizarte, et al., 2013; Schwerdt, 2014; Martinez et al., 2012; Fasfous et al., 2013). All the experimental studies were carried out to evaluate the potential of solar cooling systems, the economics, the parametric analysis, the efficiency of solar thermal collectors and cooling systems for a specific location. Most of the systems were building integrated and used for both heating and/or cooling purposes.

Simulation studies of the solar cooling system have been carried out for thermal performance, design, optimisation, and sensitivity analysis of solar cooling systems and comparisons of different solar cooling systems (Hartmann et al., 2011 ;Fong et al., 2010 ;Noro and Lazzarin, 2014 ;Wrobel et al., 2013). Most simulation research has been carried out on solar cooling systems based on an absorption chiller, for which integrated systems were built with different collectors, energy and carbon emission saving with solar cooling systems. However, none of the studies in the literature cover the salinity gradient solar pond cooling system.

Therefore, in this research, a salinity gradient solar pond is suggested as a collector to drive an absorption chiller, to provide cool air for a house during hot and dry weather. As there is no experimental solar pond absorption cooling system facility anywhere around the world, a dynamic simulation will decide first as a methodology for this research.

According to the literature referred to above (Hartmann et al., 2011 ;Fong et al., 2010 ;Noro and Lazzarin, 2014 ;Wrobel et al., 2013), TRNSYS is the most widely used simulation program for dynamic simulation of the solar cooling system.

Many programs have been developed for modelling and simulation of solar energy systems. The most popular programs are WATSUN, Polysun, and f-Chart. Many other software for building energy simulation such as Energy Plus and IES-VE have been developed. These software products were not used for this research because they cannot simulate solar cooling systems and building energy together at one simulation.

TRNSYS is used for both solar energy and building energy systems so its details are presented in sections 3.7 and 4.4. TRNSYS provides the flexibility of detailed simulation and performance investigation. However, TRNSYS lacks a solar pond model, but it can be linked to other software by other models which is not exist.

It is then decided to use TRNSYS as a main simulation software and to write a solar pond model in another language. MATLAB was chosen as a suitable language for solar pond model because it is capable of solving a required equations and the author is already familiar with the MATLAB programming.

Finally, a coupled simulation between MATLAB and TRNSYS has been used to develop a model for a solar pond cooling system.

2.15 Conclusions

This chapter explained the principles of building cooling loads, air conditioning systems, chillers, solar collectors and solar ponds.

A wide range of research was carried out for the building loads, chillers, solar cooling and solar pond. Different types of solar collectors with the various types of chillers are used together to produced cold air for buildings. The process called a solar cooling.

As described in section 2.11.11, the suggested system for the current study is a coupled simulation model of salinity gradient solar pond and the ground underneath it,

connected to an absorption chiller to serve the building as an air conditioner during summer. The heat extracted from the LCZ in the solar pond is used as a heat input to the generator of absorption chiller to produce a cooling air for a household located in a region with a hot climate, such as Baghdad, Iraq, is chosen for analysis of the system performance.

Coupled simulation between MATLAB and TRNSYS has been used to develop a model for a solar pond cooling system.

Chapter 3. DATA

3.1 Introduction

In the previous chapter, it was decided to study a salinity gradient solar pond to drive an absorption chiller and to produce a cool air for a building in hot and dry weather. According to section 2.15, a simulation method will be used to solve the problem of this project, therefore collecting and investigating data is one of the primary steps. At the beginning of this chapter, brief information about existing weather datasets is given. Subsequently, salinity gradient solar pond and soil thermal properties data are investigated in detail. Finally, equipment and building data are explained briefly.

3.2 Weather Data for Simulation Program

Weather conditions and building loads are the main factors that affect cooling system performance. Heating and cooling loads in buildings are dependent on weather conditions and also other factors such as heat gain/lost and internal load. Meteorological data, including ambient temperature, solar radiation and wind speed, wind direction, and relative humidity are measured at weather recording stations around the world (Duffie and Beckman, 1980; Forejt et al., 2006).

3.2.1 Weather Data Types

For simulation of solar cooling systems, weather data with the important system parameters (chiller capacity and building cooling loads) and derived data is used. All simulations in this research are performed with real meteorological data, and it is important to select a suitable data set (Duffie and Beckman, 1980). The data set type depends on the simulation program to be used. To compare the full range of system performance, it is best to use a full year of data or an entire season of data if the process is seasonal (Forejt et al., 2006). Klein (1976) developed the concept of a design year for the first time, which helped to create different types of weather data for building energy calculations.

The available data sets differ according to the process by which they are compiled, the amount and type of data presented. A brief description of some important weather data sets are presented here.

3.2.2 Test Reference Year (TRY)

The earliest hourly weather data set specifically designed for use in building energy simulation is the Test Reference Year (TRY) derived from measured data at the National Climatic Data Centre (NCDC). The data was available for 60 locations in the US for the period from 1948-1975. The limitations of the TRY were the exclusion of solar radiation and extremely high or low temperatures (Forejt et al., 2006).

3.2.3 Typical Metrological Year (TMY)

Hall et al. (1978) detailed a study of 23 years of data for solar radiation at 26 stations in the US which resulted in the generation of typical meteorological year data for those and other locations. This TMY data was used to simulate heating and cooling systems and added data which was not available with TRY (Duffie and Beckman, 1980).

A TMY is a data set of hourly values of meteorological elements and solar radiation for one year. It consists of typical months of real weather data selected from different years and combined to form a data set of a year of typical weather. It provides hourly data for meteorological elements that contribute to performance comparisons for different types of single or multiple locations. It is not a good indicator for predicting the system parameters for the next one or five years, as selected data is data for a typical month. It is useful to represent typical conditions judged for a longer period such as 30 years. It is not useful to design systems and their components to fulfil extreme weather conditions for a location, as it represents typical conditions instead of extreme conditions. A typical meteorological year is classified into three categories (Agyenim et al., 2010; Armanasco, et al. 2015).

- TMY: This consists of data sets derived from the NCDC of National Oceanic and Atmospheric Administration (NOAA) with measured data for 26 USA locations from years 1952-1975.
- TMY 2: This consists of data sets derived from years 1961-1990, from the National Solar Radiation Data Base (NSRDB) of USA National Renewable Energy Laboratory for 239 stations.

- TMY3: This consists of data sets derived from years 1991-2005, from the NSRDB of the US National Renewable Energy Laboratory for 1,020 stations worldwide.

The TMY, TMY2, and TMY3 data sets cannot be used interchangeably due to differences in time (local versus solar), formats, data types, and units (Duffie and Beckman, 1980 ; Hong et al., 2013).

3.2.4 International Weather for Energy Calculations (IWECC)

IWECC was generated as a result of the ASHRAE research project RP-1015 for the ASHRAE technical committee. The purpose was to represent more typical weather than a single representative year could give. These files contain typical weather data suitable for use in building energy simulation software for 227 locations outside Canada and the US. (Forejt et al., 2006; Thevenard and Brunger, 2002)

All files of IWECC data are derived from 18 years (1982-1999) of DATASAV3 hourly weather data originally archived in the US at the National Climatic Data Centre (NCDC). The solar radiation data is estimated on an hourly basis from earth-sun geometry and hourly weather elements particularly cloud amount data (EnergyPlus Weather data sources, 2016).

Like TMY files, the IWECC files are typical years that avoid extreme conditions. Sizing of heating, ventilation, and air conditioning systems that require the consideration of extreme conditions cannot use the IWECC files.

3.2.5 Energy Plus Weather (EPW)

Energy Plus Weather (EPW) data is generated by the United States Department of Energy. EPW is compiled from TMY, TMY2, TMY3, IWECC and other international data sets. This format data is now available on the Energy Plus website for more than 2,100 locations: 1,042 locations in the US, 71 in Canada and more than 1,000 locations in another 100 countries throughout the world (EnergyPlus Weather data sources, 2016).

The EPW format has generalised weather data for use in energy simulation programs. The data includes dry-bulb, dew-point temperature, relative humidity, station pressure, solar radiation (global, extra-terrestrial, horizontal, direct and diffuse), illuminance, wind direction and speed and cloud cover.

Each EPW file is named using an ISO standard three letter country code, followed by the location name, World Meteorological Organization (WMO) and the source format such as California Climate Zones 2 (CTZ2), Canadian Weather for Energy Calculations (CWECC).

There are three files associated with each location: energy plus weather files (EPW), a summary report on data (STAT) and a compressed file (zip) which contains the EPW, STAT and Design Day Data (DDY) files for the location (EnergyPlus Weather data sources, 2016).

3.2.6 Iraq Weather Data

Official weather data for Iraq is recorded and maintained by the Iraqi Meteorological Organization and Seismology Department. It is a scientific and public service department managed by the Ministry of Transportation to provide meteorological data services. Data available is not in any of the standards described in the previous section, which can be used for building energy simulation programs.

The available data is for 41 weather stations deployed in all provinces in Iraq and contains ambient temperature, wind speed, humidity and solar radiation only (Iraqi Meteorological Organization and Seismology, 2013).

In a solar cooling simulation program, two important weather data sets used are Energy Plus Weather (EPW) and Typical Meteorological Year (TMY). There is no Energy Plus Weather (EPW) data set for Iraq, the only available type of standard hourly data set is the Typical Meteorological Year (TMY), which is described here.

A TRaNsient SYstems Simulation program (TRNSYS) is supplied with TMY2 weather data files for three main cities in Iraq along with 1,036 cities worldwide. This weather data is provided by METEONORM (Klein, 2010). The data is for the years 1961-90 and was obtained from about 7,400 stations worldwide. This data contains mean air temperature, humidity, and solar radiation (Forejt, 2006).

The World Meteorological Organization (WMO) is producing a large volume of monthly temperature, precipitation and pressure data from hundreds of stations around the world. The WMO uses a 33 year period, which is long enough to filter out any

interannual variation in the climatic trends (World weather information service home, 2014).

Satellite data for many locations across the world with parameters for solar energy calculations are provided by National Aeronautics and Space Administration (NASA), Surface meteorology and Solar Energy (SSE) for the 22-year period July 1983 to June 2005. Air temperature is for 10 m above the ground (Surface meteorology and solar energy, 2014).

Figure 3.1 compares the WMO data, TMY2, and NASA dry bulb temperatures for Baghdad. This shows a difference of 3 to 5 °C on average maximum data values for three sets. Minimum values are in good agreement for WMO and TMY2 data sets. The difference may be due to the data dates range, methods used to provide the data and monthly or hourly based time as shown in Table 3.1. In recent years, increasing values of carbon dioxide into the atmosphere have increased the temperature of the Earth and caused changes in weather data (Seinfeld et al., 2016). The WMO and NASA weather data are monthly based values, while TMY2 is the hourly based values. The fair agreement between the three data sets gives confidence that the TMY2 data can be used to perform the valid simulation.

It was therefore decided to adopt TMY2 data set for the calculations in this research.

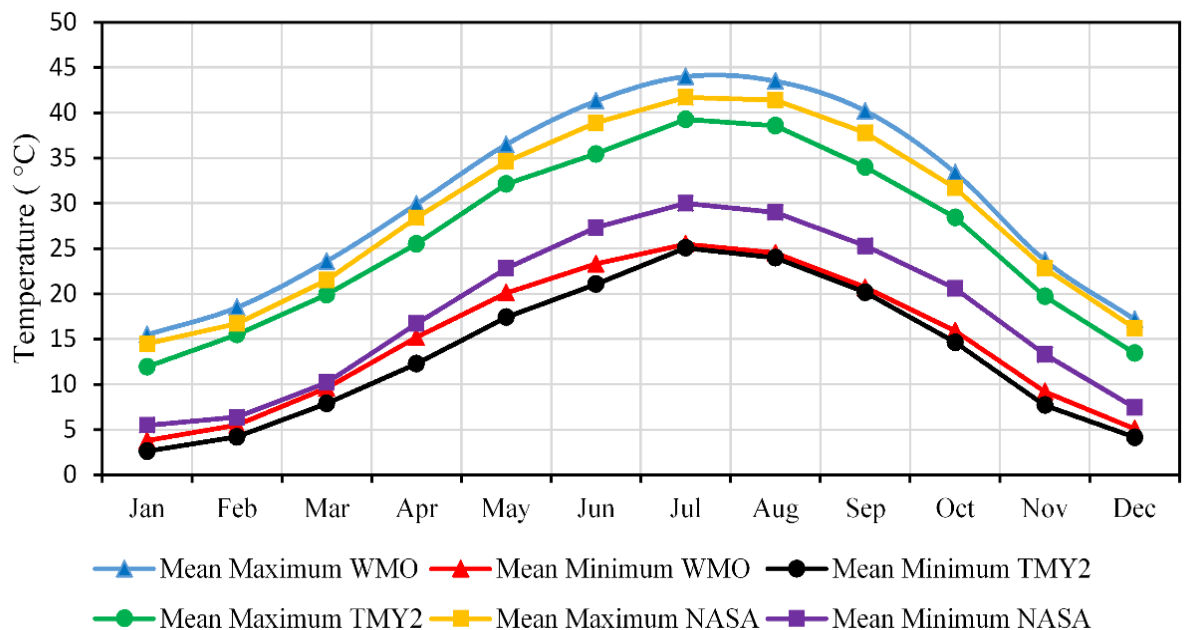


Figure 3.1 Baghdad temperature comparison (WMO, TMY2, and NASA)

Data set	Dates range	Method	Monthly or Hourly based	Note
WMO	1976-2008	Monthly data from weather stations	Monthly averaged	
NASA	1983- 2005	Satellite data	Monthly averaged	10m above ground
TMY2	1961-1990	Hourly values for typical months and combined to typical year from stations	Hourly based	

Table 3.1 Different weather data sets

A comparison of TRNSYS available TMY2 data of mean maximum dry bulb temperature, average global horizontal radiation, average relative humidity, and average wind speed for the three major cities in Iraq was carried out to analyse the climatic conditions in these cities and is shown in Figures 3.2, 3.3, 3.4 and 3.5.

The analysis of the data shows that Baghdad has a mean maximum dry bulb temperature compare to Mosul and Basra (cities in Iraq). Baghdad also has high solar radiation during summer, which is suitable to represent typical conditions for solar cooling applications. Relative humidity for Baghdad is similar to other cities. Baghdad has low wind speed. Therefore, data for Baghdad is suitable for use as typical weather data for Iraq.

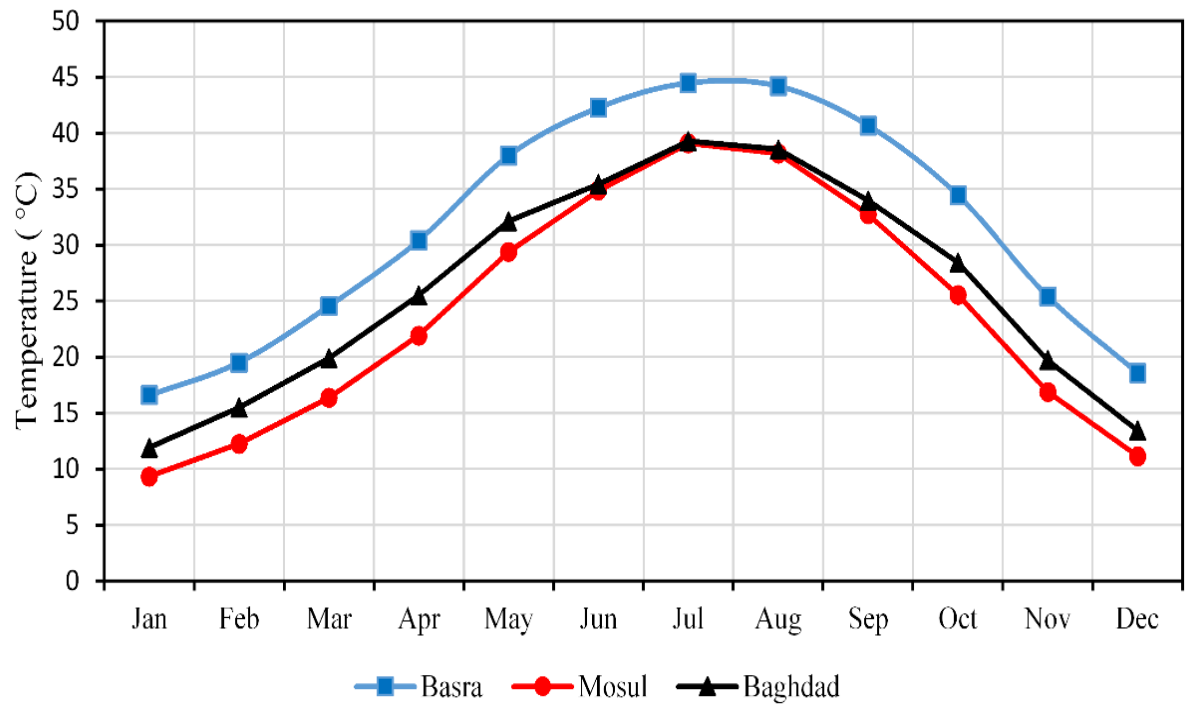


Figure 3.2 Iraq cities maximum average temperature from TMY2

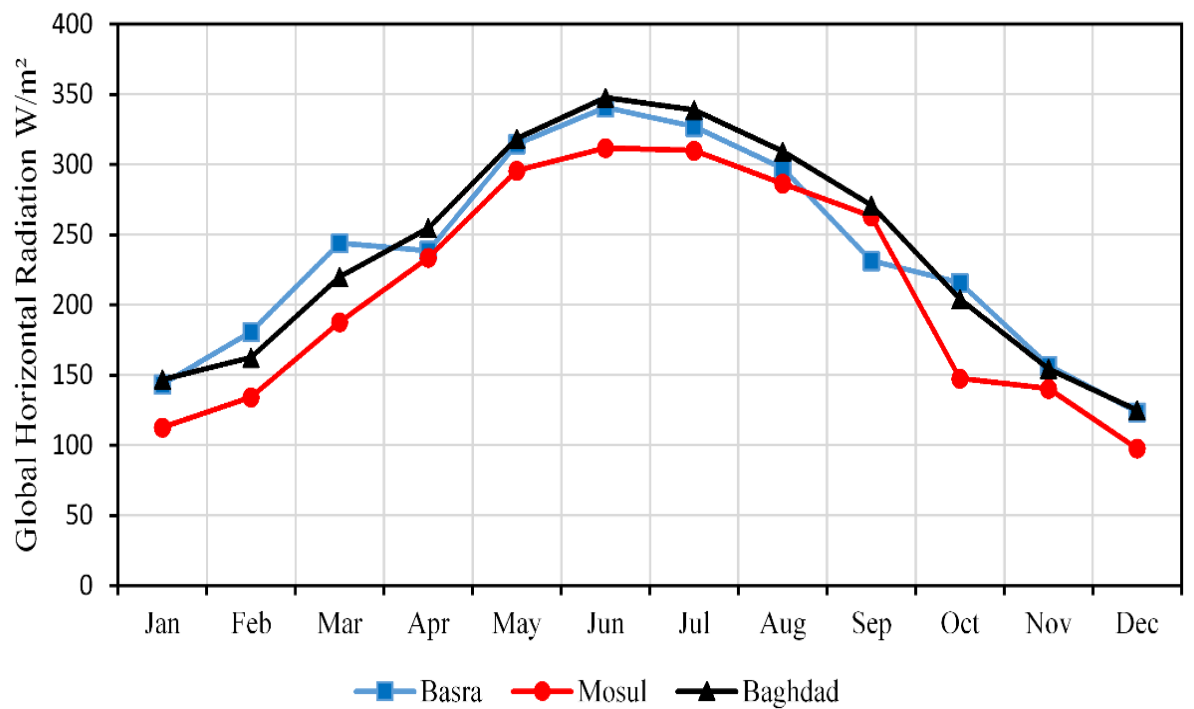


Figure 3.3 Iraq cities average global horizontal radiation from TMY2

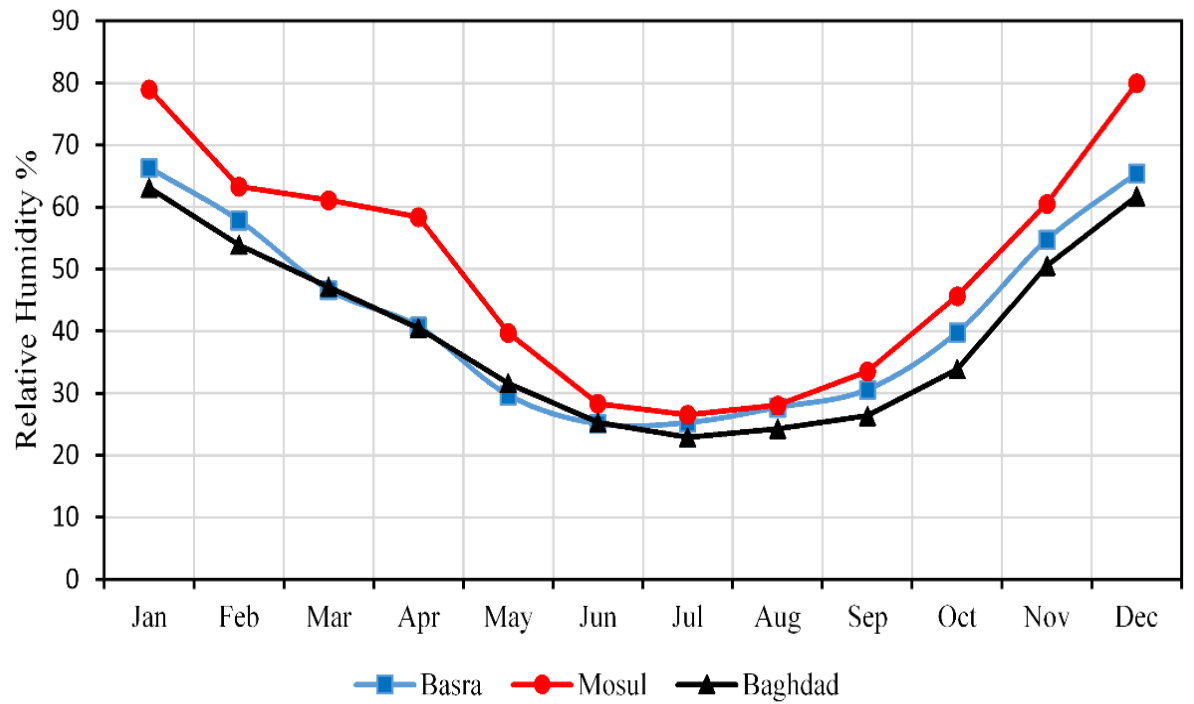


Figure 3.4 Iraq cities average relative humidity from TMY2

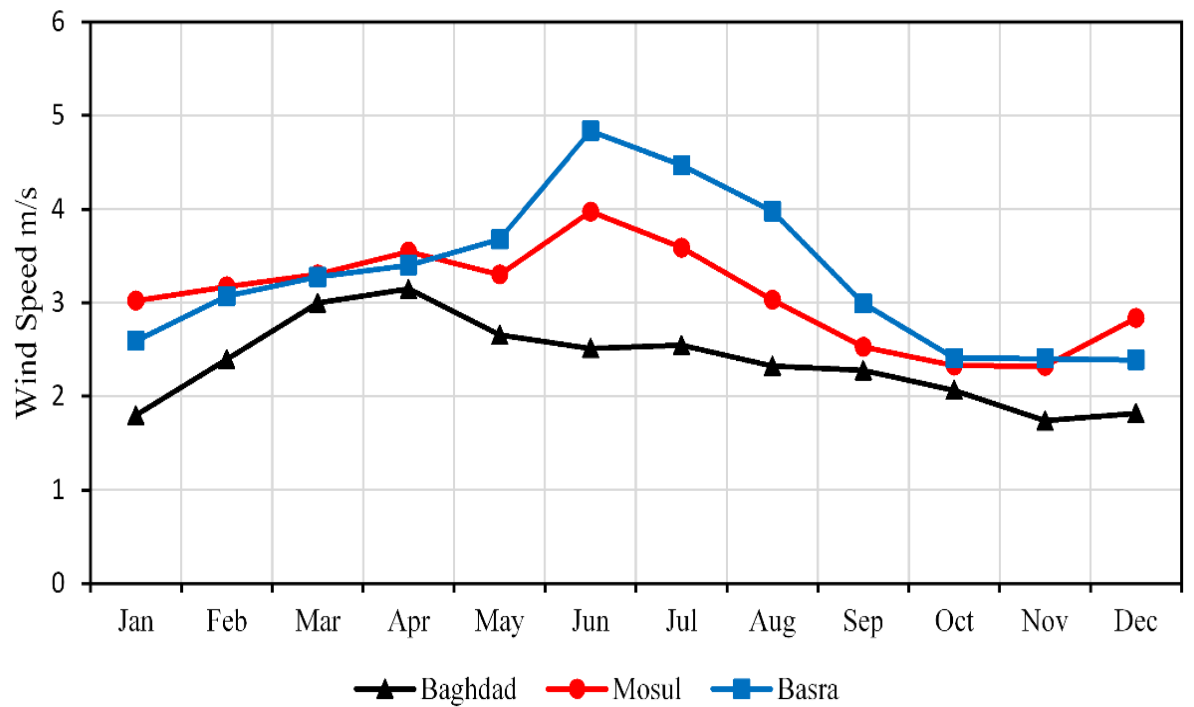


Figure 3.5 Iraq cities average wind speed from TMY2

3.3 Salinity Gradient Solar Pond Data

The thermophysical properties of an aqueous solution of sodium chloride are important for the thermal performance and efficiency of a salinity gradient solar pond. Properties such as specific heat capacity, thermal conductivity, diffusion coefficient, and density are used as input data in program as shown in Appendix A. The properties are found from (Suarez et al., 2010; Giestas et al., 2009; Rebai et al., 2006; Lide and Bruno, 2004; Zangrando, 1991; Hull et al., 1988). Suarez et al. (2010) summarises the data as $\rho_0 = 1088.6 \text{ kg/m}^3$, $T_0 = 60^\circ\text{C}$ and $S_0 = 15\% \text{ NaCl by mass}$, where these are the reference density, temperature and salinity respectively, and $\beta_T = 5.24 \times 10^{-4} \text{ }^\circ\text{C}^{-1}$ and $\beta_S = 6.82 \times 10^{-3} \text{ \%}^{-1}$ where these are the thermal and solutal expansion coefficients respectively. This data is taken from (Hull et al., 1988).

A linear approximation for the variation with temperature of the density of aqueous sodium chloride solution is used by a wide range of the above researchers.

Figure 3.6 shows that the linear approximation of density for sodium chloride is in excellent agreement with data values from (Lide and Bruno, 2004).

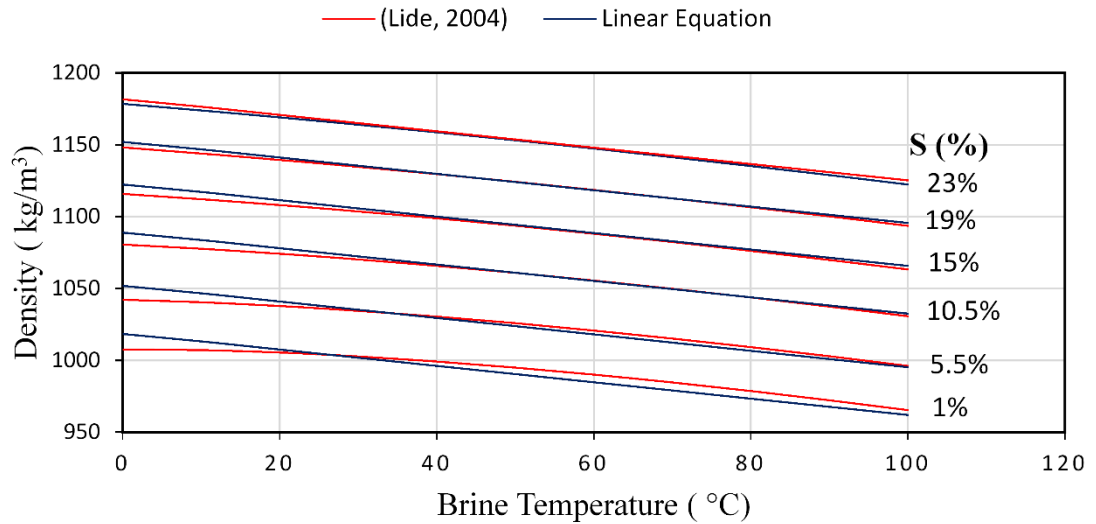


Figure 3.6 Density temperature variation for the different salinity of NaCl solution from (Lide and Bruno, 2004) compared with the linear density approximation.

The thermophysical properties of pure NaCl solutions have been investigated (Elwell, 1977). Table 3.2 gives the range of values for some of the thermophysical properties of sodium chloride solutions (Hull et al., 1988).

Units	Property	Range	Values at S=15%,T=60°C
kg/m ³	Density	957-1207	1088.6
J/kg. °C	Heat capacity	3300-4200	3570
W/m. °C	Thermal conductivity	0.54-0.68	0.637
m ² /s	Kinematic viscosity	(2.4-25)*10 ⁻⁷	5.81*10 ⁻⁷
m ² /s	Thermal diffusivity	(1.3-1.8)* 10 ⁻⁷	1.64*10 ⁻⁷
m ² /s	Solutal diffusivity	(0.9-6.0)* 10 ⁻⁹	3.23*10 ⁻⁹
1/°C	Thermal expansion coefficient	(0.3-7.4)* 10 ⁻⁴	5.24*10 ⁻⁴
1/%	Solutal expansion coefficient	(6.7-7.5)* 10 ⁻³	6.82*10 ⁻³

Table 3.2 Range of several thermophysical properties of sodium chloride solutions (Hull et al., 1988)

The thermal conductivity, density and specific heat of NaCl solution are given by the following correlations (Wang and Akbarzadeh, 1983).

These correlations depend on the temperature and concentration of NaCl solution.

$$k = 0.5553 - 0.0000813 C + 0.0008(T - 20) \quad (3.1)$$

$$\rho = 998 - 0.4(T - 20) + 0.65 C \quad (3.2)$$

$$C_p = 4180 - 4.396 C + 0.0048 C^2 \quad (3.3)$$

where T in °C and C in kg/m³ The linear approximation for density of sodium chloride is also used.

It was therefore decided to adopt linear approximation of density for sodium chloride for the calculations in this research as an input for the mass transfer MATLAB code.

The averaged values of thermal conductivity, density, specific heat and thermal diffusivity from Table 3.2 are used in this research as inputs for the heat transfer MATLAB code. The reason for using averaged values was due to a limit of the TRNSYS software parameter definition, which is a value that is constant over the entire length of the simulation. For example, in the heat exchanger between the solar pond and the absorption chiller, specific heat of sodium chloride solution (the heat source side fluid) is a TRNSYS parameter which has to be a constant value of (3570 J/kg. °C).

Subhakar and Murthy, (1993) investigated the average thermophysical properties and varying them with temperature and concentration for magnesium chloride. It was found that the change in LCZ temperature was only 1°C in a magnesium chloride solar pond.

Therefore, in the calculation of this research, the averaged thermophysical properties were chosen.

3.4 Ground Heat Loss

3.4.1 Soil Thermal Properties

Ground heat loss may be significant, particularly if the bottom of the pond is non-insulated. It plays a role in determining the minimum size of the technically and economically feasible pond. Heat loss from the solar pond to the ground depends on the properties of the soil underneath the solar pond.

Soil is a porous medium and is thus composed of solids and pores. The solids comprise mineral substances and organic matter; the pores may be filled with air or water in any of its three phases (liquid, vapour or ice) (Behari, 2006).

Heat loss from the solar pond to the ground is by unsteady conduction and is affected by the soil's thermal conductivity, density and specific heat (Ochsner, et al., 2001). Obtaining accurate values for thermal properties of the soil requires a detailed site survey. Thermal properties of granular soils (sand, clay, silt) may be estimated from

the sand and clay content, dry density, and moisture content. Experimental soil thermal properties for Baghdad were found from AlMaliky (2011).

The thermal conductivity of the soil (k_g) was calculated from the equations given by Hepbasli (2002) as follows:

$$k_g = 0.14423(0.9 \log MC - 0.2) 10^{0.000624 \rho_{gd}} \quad \text{for silt and clay soils} \quad (3.4)$$

$$k_g = 0.14423(0.7 \log MC + 0.4) 10^{0.000624 \rho_{gd}} \quad \text{for sand soils} \quad (3.5)$$

The dry specific heat (Cp_{gd}) and dry soil density (ρ_{gd}) of the soil must be corrected for moisture content as follows (Hepbasli, 2002):

$$Cp_{gc} = [MC Cp_w + (100 - MC)Cp_{gd}]/100 \quad (3.6)$$

$$\rho_{gc} = [MC \rho_w + (100 - MC)\rho_{gd}]/100 \quad (3.7)$$

All values are used in this study are listed in Tables 3.3 and 3.4 There is a wide variation of thermal conductivity with soil type and, especially, moisture content. There is less variation of density and specific heat.

The soil moisture content are assumed to be 5% and 10% from the whole soil weight. 5% and 10% soil moisture content were found to be around the experimental values of moisture content in the soil found in the literature (AlMaliky, 2011).

The calculated and experimental values show good agreement, so it was decided to use both values for this research as they could then be easy to explore the effect of changes to soil conditions.

				Calculated soil properties			Experimental soil properties	
		Unit	Clay and Silt 2 (Hepbasli, 2002)	Clay and silt 2 (calculated) 5% moisture	Clay and silt 2 (calculated) 10% moisture	Sandy soil (Yari, 2007)	Clay and sandstones (AlMaliky ,2011)	Clay and silt1 (AlMaliky ,2011)
Thermal conductivity	k_g	W/m.°C	2.941	1.932	3.152	1.082	1.7	2.15
Dry density	ρ_{gd}	kg/m ³	2395	2395	2395	1382	-	
Moisture	ω	%	8.87	5	10	7.9	4.4	5.6
Dry specific heat	Cp_{gd}	kJ/kg.°C	0.84	0.84	0.84	0.84	-	
Corrected density	ρ_{gc}	kg/m ³	2271	2325.25	2255.5	1352	1470	1350
Corrected specific heat	Cp_{gc}	kJ/kg.°C	1.137	1.007	1.175	1.105	2.0	1.137

Table 3.3 Soil thermal properties. (Hepbasli, 2002;Yari and Javani, 2007;AlMaliky, 2011)

Soil type	Moisture content %	Density kg/m ³	Thermal conductivity W/m. °C	Specific heat kJ/kg .°C
Coarse sand(dry)	0	1800	0.25	0.800
Coarse sand (sat.)	20.2	2080	3.72	1.483
Fine sand (dry)	0	1600	0.15	0.800
Fine sand (sat.)	24.6	2010	2.75	1.632

Table 3.4 Soil thermal properties with a different texture. (Clarke, et al., 2008)

3.4.2 Depth of the Water Table

Heat loss from the pond to the ground also depends on the depth of the water table, which act as a heat sink. Researchers have explored this aspect also (Saxena, et al. 2009; Zhang and Wang, 1990).

Saxena et al. (2009) developed a computer program to estimate the temperature of the LCZ over a duration of three years. Varying the depth of the water table in the range

from 5 m to 25 m from the bottom of the pond. It was found that the deeper the water table, the less the heat losses and the higher is the temperature achieved by the pond. Secondly, there is a significant depth of water table below which, further depression does not have a significant impact on the thermal performance of pond. The numerical value of this significant depth depends on the ambient parameters, soil properties, and pond dimensions.

In this study, the depth of the water table was varied from 1m to 10m measured from the bottom of the solar pond. These values are range of the depth of the water table in Baghdad and surrounding area (Jassim and Goff, 2006).

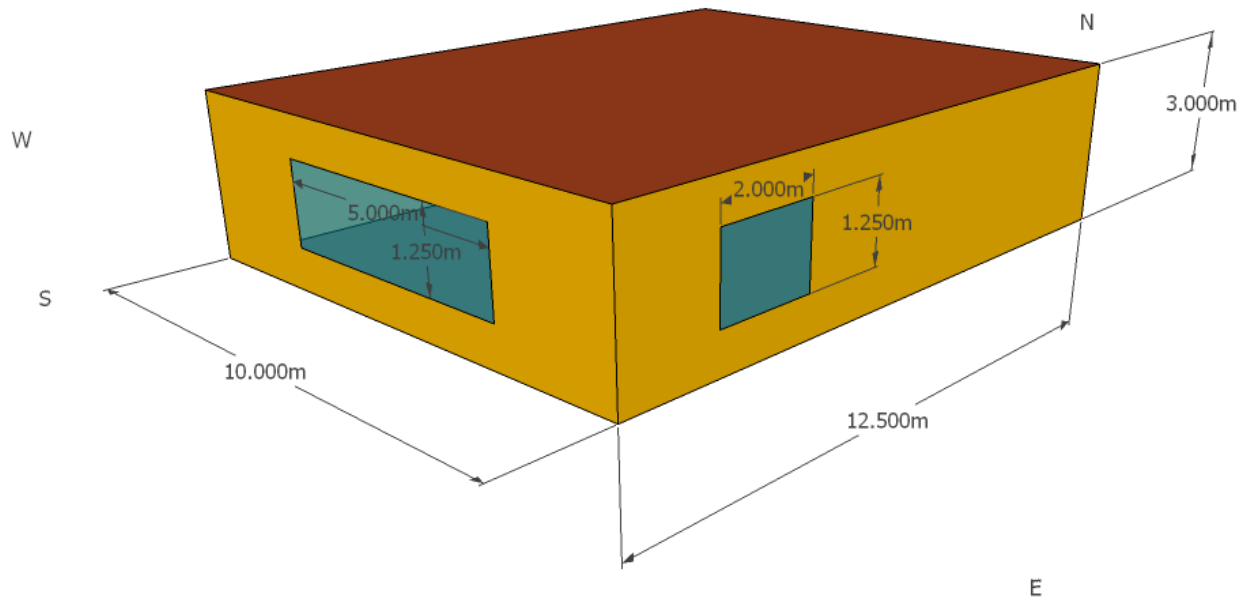
3.5 Building Data

The building model selected for this research is based on a real typical modern single-family house situated in Baghdad, Iraq designed by Aryo Company, (2012). The model is shown in Figure 3.7. It has one storey, a flat roof, a total land area of 200 m² and a floor area of 125 m². The building height is 3 m. It is constructed of uninsulated concrete with single glazed windows. The building has six windows, two of them are merged in the model for the sake of simplicity as shown in Figure 3.7.

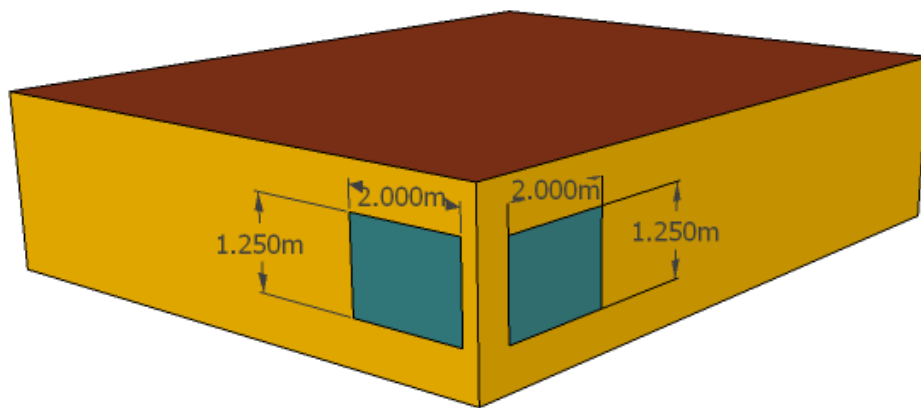
The orientation of the building is towards the south. The building has two bedrooms, living room, hall and kitchen as conditioned spaces. Table 3.5 presents the geometrical description.

No.	Space	Floor dimensions(m ²)	Windows area(m ²)
1	Bed room 1	19.18	2*1.25
2	Bed room 2	17.00	2*1.25
3	Living room	30.40	2.5*1.25
4	Hall	35.12	2.5*1.25
5	Kitchen	14.80	1.25*1.25
6	Bath room and toilet	8.50	0.55*1.25
	Total	125	13.5

Table 3.5 Building geometrical dimensions



(Front View)



(Back View)

Figure 3.7 Whole building isometric plan view.

The whole building envelope is constructed according to very common standard walls, floors, and roofs in Iraq. Walls are built as multi-layer from gypsum plaster, concrete block and cement mortar. The floor is also built as multi-layer from tile and concrete. The roof consists of gypsum plaster, concrete and tile. Windows are single glazed. The house is occupied and air conditioned continuously. Table 3.6 presents the building data.

Name	Value	Unit	Material	Thickness (m)
No. of storeys	1			
Opaque Wall Area	135	m ²		
Glazed Wall Area	13.5 m ²	m ²		
U-value				
Floor	3.753	W/m ² .K	tile and concrete	0.175
Walls	2.295	W/m ² .K	gypsum plaster, concrete block and cement mortar	0.22
Roof	3.655	W/m ² .K	gypsum plaster, concrete, and tile	0.185
Windows	5.68	W/m ² .K	Glass	0.004
Surface finish				
Walls	White paint			
Roof	Yellow tiles			
Inside set point temperature (cooling)	25	°C		
Inside relative humidity	50%			
Infiltration	0.6	l/hr		
Internal loads				
Occupancy	4	person		
Fridge	416	Watt		
Lights	500	Watt		

Table 3.6 Building data

The TRNSYS Type 56 simulation component was used to model the building and calculate the building cooling load. The building data, such as construction details, walls, floor, roof, windows, infiltration, ventilation and internal loads are set as INPUTS to the TRNSYS simulation software. Figure 3.8 shows the simulated annual cooling load for the building. The peak load is 21 kW, so the chiller capacity was chosen to be 24.6 kW (7 tons of refrigeration) to allow a realistic margin. The other components of the cooling and air conditioning system were sized to match the chiller.

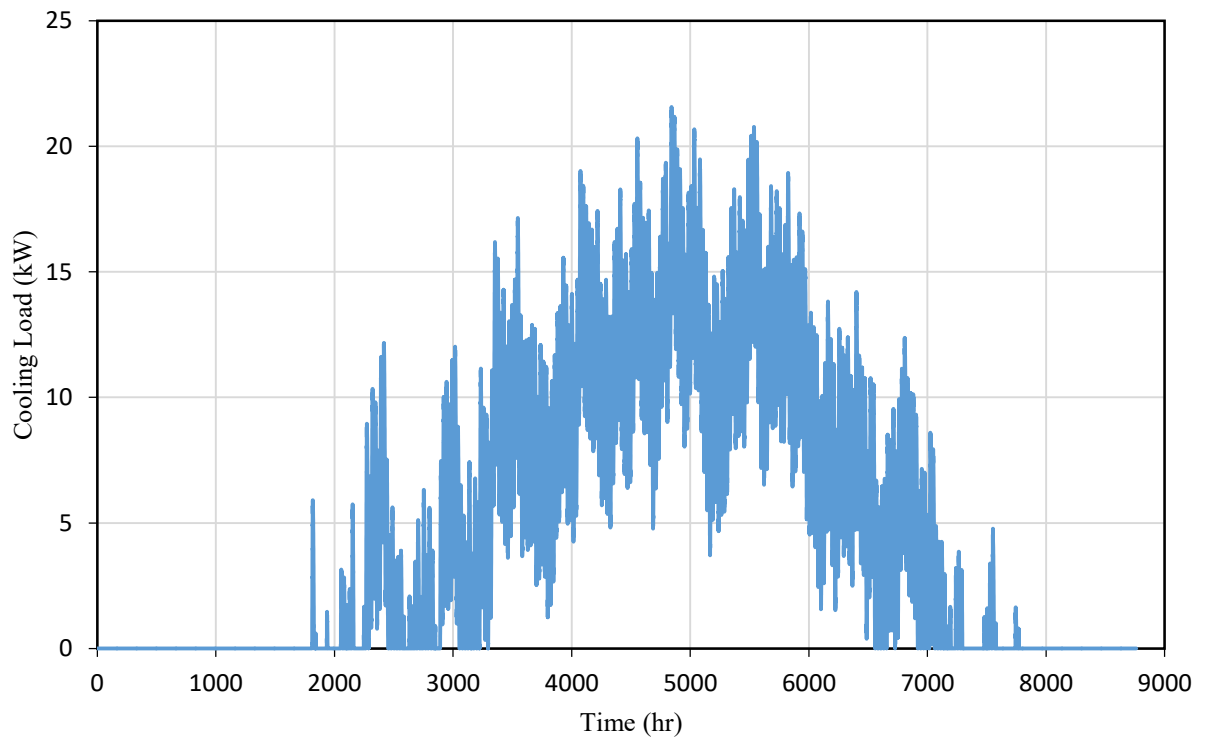


Figure 3.8 Annual cooling load for building in Baghdad, Iraq.

3.6 Equipment Data

A solar thermal cooling system consists of four basic components: a thermal collector, thermal storage (both are represented by the solar pond), thermal chiller, and heat exchanging system to exchange heat with a conditioned space (Sarbu and Sebarchievici, 2013; Ullah, et al. 2013). The other components typically required are the hot water pump, chilled water pump, condenser water pump, cooling tower, fan, cooling coil, heat exchanger and controller thermostat (Duffie and Beckman, 1980).

In this study, hot brine is pumped from the lower convective zone of the solar pond and passed through an external heat exchanger, where it transfers heat to hot water; the brine is then returned to the lower convective zone. The hot water is pumped to the chiller, gives up the heat and is returned to the heat exchanger. Thus, heat is transported from the solar pond to the chiller while the chiller is isolated from the corrosive brine.

Cooling water circulates between the chiller and a wet cooling tower which rejects heat to the environment.

Chilled water circulates between the chiller and the air cooling coil. Air flows from the inside of the house, through the cooling coil and back into the house.

3.7 TRNSYS

In the present study, the solar thermal cooling system is modelled using the TRAnsient SYstem Simulation (TRNSYS) thermal process dynamic simulation program. TRNSYS has the capability to interconnect system components in any desired manner, solving differential equations and providing information output. Given OUTPUT from one component can be used as an INPUT to other components (Kalogirou, 2004). Each component has a unique TYPE number, and components from the standard library of TRNSYS were validated (Almeida, et al., 2014).

3.7.1 Solar Pond Data

A solar pond Type does not exist in TRNSYS software. Therefore, a MATLAB code was written to represent a solar pond Type in TRNSYS. The data of the solar pond model was explained in section 3.3.

3.7.2 Heat Exchanger Data

A heat exchanger of Type 91 is used. This Type is modeled a heat exchanger with constant effectiveness which is independent of the system configuration. The effectiveness is the ratio between the actual heat transfer rate and the maximum possible heat transfer rate for the given fluid inlet temperatures, flow rates, and specific heats. The value of heat exchanger effectiveness used is 0.8 which is recommended by Barron (1999).

The specific heat capacity of source side fluid (hot brine) is 3570 J/kg.°C, taken from Table 3.2 (Hull et al, 1988). And the specific heat capacity of the load side fluid (water) is 4190 J/kg. °C (Holman, 2010). Heat exchanger data is shown in Table 3.7.

Name	Value	Unit
Specific heat of source side fluid	3570	J/kg.K
Specific heat of load side fluid	4190	J/kg.K
Source side flow rate	7874	kg/hr
Load side flow rate	6038	kg/hr
effectiveness	0.8	-

Table 3.7 Heat exchanger data

3.7.3 Absorption Chiller

The absorption chillers are the most commonly used chillers with solar cooling systems. A single effect vapour absorption water chiller with rated capacity of 7 TR (24.64 kW), the heat input required is (35.2 kW) and the rated coefficient of performance (COP) of 0.7 was modelled by TRNSYS using Type 107. A commercially available chiller (Yazaki WFC – SC10, Yazaki, 2008) was selected as a basic as it had appropriate hot, chilled and cooling water temperatures. As this has a rated capacity of 10 TR, the manufacturer’s performance data was adjusted by assuming that all temperatures were unchanged, while energy flow changed in proportion.

TRNSYS contains a performance data file for the Type 107 chiller. However, the data provided does not correspond to the operation range of the Yazaki WFC – SC10 absorption chiller; e.g. the hot water inlet temperature range is 106°C – 116°C instead of 70°C – 95°C. A new data file was therefore created based on the Yazaki manufacturer’s data. The fraction of design load is varied from 0 to 1 in steps of 0.1. The chilled water outlet temperature ranges from 5.5°C – 11.667°C, the cooling water inlet temperature from 25°C – 32°C, and the hot water inlet temperature from 70°C –

95°C. A part of the data file is shown in Figure 3.9. The primary inputs of the absorption chiller after selected and designed are shown in Table 3.8.

0.00	0.1	0.2	0.3	0.4	0.5	0.6	0.7	0.8	0.9	1		! Fraction of design load		
5.500	6.500	7.000	7.500	8.500	9.500	11.667						! Chilled water outlet temperature		
25.000	26.000	27.000	29.500	31.000	32.000							! Cooling water inlet temperature		
70.00	75.00	80.00	85.00	90.00	95.00							! Hot water inlet temperature		
0.63	0	!Capacity and Design Energy Input Fraction at									0	5.5	25	70.00
0.86	0	!Capacity and Design Energy Input Fraction at									0	5.5	25	75.00
1.06	0	!Capacity and Design Energy Input Fraction at									0	5.5	25	80.00
1.16	0	!Capacity and Design Energy Input Fraction at									0	5.5	25	85.00
1.3	0	!Capacity and Design Energy Input Fraction at									0	5.5	25	90.00
1.33	0	!Capacity and Design Energy Input Fraction at									0	5.5	25	95.00
0.58	0	!Capacity and Design Energy Input Fraction at									0	5.5	26	70.00
0.8	0	!Capacity and Design Energy Input Fraction at									0	5.5	26	75.00
0.99	0	!Capacity and Design Energy Input Fraction at									0	5.5	26	80.00
1.09	0	!Capacity and Design Energy Input Fraction at									0	5.5	26	85.00
1.22	0	!Capacity and Design Energy Input Fraction at									0	5.5	26	90.00
1.27	0	!Capacity and Design Energy Input Fraction at									0	5.5	26	95.00
0.53	0	!Capacity and Design Energy Input Fraction at									0	5.5	27	70.00
0.74	0	!Capacity and Design Energy Input Fraction at									0	5.5	27	75.00
0.92	0	!Capacity and Design Energy Input Fraction at									0	5.5	27	80.00
1.01	0	!Capacity and Design Energy Input Fraction at									0	5.5	27	85.00
1.14	0	!Capacity and Design Energy Input Fraction at									0	5.5	27	90.00
1.21	0	!Capacity and Design Energy Input Fraction at									0	5.5	27	95.00
0.24	0	!Capacity and Design Energy Input Fraction at									0	5.5	29.5	70.00
0.48	0	!Capacity and Design Energy Input Fraction at									0	5.5	29.5	75.00
0.7	0	!Capacity and Design Energy Input Fraction at									0	5.5	29.5	80.00
0.88	0	!Capacity and Design Energy Input Fraction at									0	5.5	29.5	85.00
1.01	0	!Capacity and Design Energy Input Fraction at									0	5.5	29.5	90.00
1.07	0	!Capacity and Design Energy Input Fraction at									0	5.5	29.5	95.00
0.13	0	!Capacity and Design Energy Input Fraction at									0	5.5	31	70.00
0.42	0	!Capacity and Design Energy Input Fraction at									0	5.5	31	75.00
0.65	0	!Capacity and Design Energy Input Fraction at									0	5.5	31	80.00
0.8	0	!Capacity and Design Energy Input Fraction at									0	5.5	31	85.00
0.92	0	!Capacity and Design Energy Input Fraction at									0	5.5	31	90.00
0.92	0	!Capacity and Design Energy Input Fraction at									0	5.5	31	95.00
0	0	!Capacity and Design Energy Input Fraction at									0	5.5	32	70.00

Figure 3.9 Yazaki WFC – SC10 performance data file.

Name	Value	Unit
Chilled water inlet temperature	12.5	°C
Cooling water inlet temperature	31.0	°C
Hot water inlet temperature	70-90	°C
Chilled water temperature set point	7.0	°C
Chilled water flow rate	3846	kg/hr
Cooling water flow rate	12851	kg/hr
Hot water flow rate	6038	kg/hr

Table 3.8 Inputs for (7 TR) absorption chiller

3.7.4 Cooling Tower

The closed circuit cooling tower Type 510 is used to model and cool the liquid stream by evaporating water from the outside of coils containing the working fluid. The working fluid is completely isolated from the air and water in this type of system. Closed circuit cooling towers are often referred to as indirect cooling towers or indirect evaporators. The Counter Flow Induced Draft Cooling Tower Model T-220 is selected from CTS cooling tower systems (Systems, 2007) with a rated capacity of 70.4 kW and the heat capacity of fluid is 4.190kJ/kg. K. The rated water flow rate is 13173 kg/hr, which is greater than the required cooling water flow rate 12851 kg/hr. The data of the cooling tower is shown in Table 3.9.

Name	Value	Unit
Design inlet fluid temperature	35	°C
Design outlet fluid temperature	29.44	°C
Design fluid flow rate	12851	kg/hr
Design ambient air temperature	35	°C
Design wet bulb temperature	23.88	°C
Design air flow rate	13002	kg/hr
Rated fan power	1342	kJ/hr
Desired outlet temperature	31	°C

Table 3.9 Closed circuit cooling tower data

3.7.5 Cooling Coil

A cooling coil model Type 697 is used in TRNSYS to model building air cooling through chilled water received from a chiller. Type 697 models a simple air cooling device that removes energy from an air stream according to performance data found

in a combination of three external data files and based on the flow rates and inlet conditions of the air stream and a liquid stream. In Type 697, three data files are required. The first provides water temperature correction factor performance data. The second provides correction factor data for the performance, based on varying air temperatures while the third provides correction factor data for the performance based on varying airflow rates. The values are used as INPUTS to TRNSYS shown in Table 3.10. The total cooling capacity is 19.34 kW (69633 kJ/hr), and the sensible cooling capacity is 15.31 kW (55126 kJ/hr). These settings are by chiller performance to maintain room temperature below the set point. For the Type 697, the TRNSYS default ratio of total cooling capacity to sensible cooling capacity is 1.26.

At each time step, Type697 performs a call to the TRNSYS psychrometric routine to obtain air properties for the inlet air stream not specified by the user among the component's inputs.

Name	Value	Unit
Rated volumetric air flow rate	870	L/s
Rated volumetric liquid flow rate	0.870	L/s
Total cooling capacity	69633	kJ/hr
Sensible cooling capacity	55126	kJ/hr

Table 3.10 Cooling Coil data (Type 697)

3.7.6 Single speed fan

Type 112b was selected to model a fan to transfer air from cooling coil Type 697 to building Type 56. It is simple model of a fan which spins at a single speed and maintains a constant mass flow rate of air. Type 112b sets the flow rate based on its rated flow rate parameter and the current value of its control signal input which must have a value of 1 or 0.

The inputs to the fan are humidity mode, rated flow rate, rated power, motor efficiency and motor heat loss fraction. The fan calculation depends on the humidity mode, which is by default a percentage of relative humidity. The component passes pressure, temperature and either relative humidity or humidity ratio to the TRNSYS

PSYCHROMETRICS routine, which returns values of temperature, relative humidity, and enthalpy. The air flow rate is 4356 kg/hr (3618 m³/hr), sufficient to maintain room temperature below a set point. The rated power is 432.15 W, and the default standard motor efficiency and heat loss fraction were selected. The default standard motor efficiency is 0.90 and the motor heat loss fraction is zero.

3.7.7 Pumps

Type 3d was chosen to simulate the pumps in TRNSYS. It is a simple, single speed and constant flow pump with only inputs of fluid flow and pump electrical power. The TRNSYS library contains multiple pump types which are complex and meet different criteria. Type 3d pump model computes a constant mass flow rate using a variable control function, which must have a value of 1 or 0. The pump will be on when it is 1 and off when it is 0. Type 3d sets the flow rate for the rest of the components in the flow loop by multiplying the maximum flow rate from the control signal. All the four pumps used for brine flow rate in the solar pond and the heat exchanger loop, the water flow rate in the heat exchanger and the absorption chiller loop, the absorption chiller, and the cooling coil loop and the absorption chiller to the cooling tower loop are Type 3d pumps. All pumps were selected from the manufacturer data as shown in Table 3.11.

Loop and Pump Type	Flow required m ³ /hr	Max. Flow m ³ /hr	Head m	Rated power W	Power Consumption W
Cooling Loop, Wilo-Stratos 40/1-4	12.8	12.9	5	100	9-125
Heating loop, Wilo-Stratos 25/1-6	6	7.6	6.5	65	9-80
Chilled loop, Wilo-Stratos 25/1-4	3.8	5.5	4.4	30	9-38
Pond loop, Wilo-Stratos 25/1-10	7.8	8	10.8	140	9-190

Table 3.11 Existing pumps data from Wilo Company (WILO, 2013)

3.7.8 Thermostat

Room thermostat Type 108 was selected for the current simulation in TRNSYS. This is the only thermostat controller in the TRNSYS library. Type 108 is a five stage room thermostat modeled to give five output ON/OFF control functions that can be used to

control a system with a two stage heating system, an auxiliary heater and a two-stage cooling system. The controller commands first stage cooling at moderately high room temperatures and second stage cooling at room temperatures higher than the 1st stage. First stage heating starts at a low room temperature, second stage heating at a lower room temperature, and auxiliary heating at an even lower room temperature. Heating and cooling stages with set point definition are shown in Figure 3.10. There is an option to disable first stage heating during the second stage, disable both first and second stage heating during auxiliary heating, and disable first stage cooling during second stage cooling.

The first stage heating, second stage heating, and third stage heating were set to be OFF. The first and second stage cooling were set to be ON. The first and second stage cooling set points temperatures were 20.5°C and 35 °C respectively. The monitored room temperature was set to 25°C. If the monitored temperature rises to a certain temperature, the absorption chiller comes on to bring the zone temperature back.

Type 108 used to control fan, pumps, absorption chiller, cooling tower fan. All system is ON or OFF at the same time.

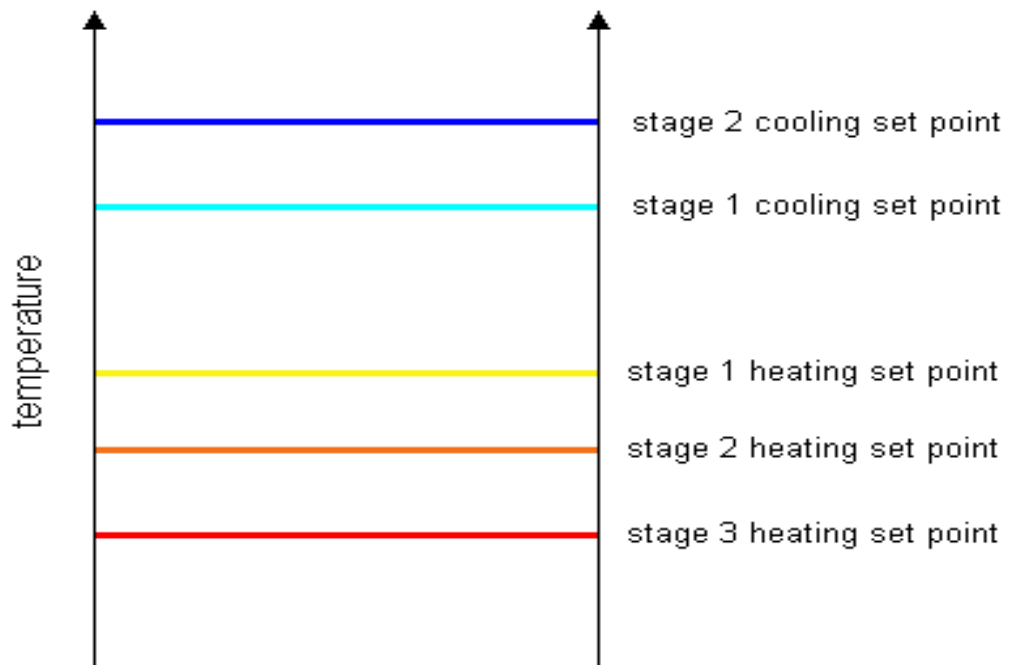


Figure 3.10 Set Point Definition (TRNSYS 17, Mathematical Reference Manual)

3.8 Conclusion

This chapter started with a brief information about the existing weather datasets. TRNSYS weather dataset (TMY2) has been decided to adopt for the calculations in this research. It was also found that Baghdad is suitable for the solar pond location compared with two cities in Iraq. The salinity gradient solar pond and soil thermal properties data have been investigated in detail. It has been decided to adopt a linear approximation for the density of sodium chloride solution for the calculations in this research. The building data has been explained briefly. The TRNSYS Type 56 simulation component has been used to model the building and calculate the building cooling load. The peak cooling load was found to be 21 kW; therefore the chiller capacity has been chosen to be 24.6 kW (7 tons of refrigeration) to allow a realistic margin.

Equipment such as an absorption chiller has been modelled by TRNSYS using Type 107. A new data file has been created based on Yazaki manufacturer's data. Finally, the rest of the cooling system components data have been explained.

Chapter 4. Mathematical modelling

4.1 Introduction

This chapter explains the mathematical model of a salinity gradient solar pond with the ground underneath it, absorption cooling system and building. The model used throughout the thesis, starting with the governing equations of heat and mass transfer of the solar pond. The model uses the solar radiation equation as a source for the energy equation of the solar pond. The equations obtained from the model are solved numerically by using the finite difference method. MATLAB codes were written to solve the equations. The solar cooling system, including the absorption chiller and building, is simulated by the TRNSYS software. A coupled simulation between MATLAB and TRNSYS are described. Finally, the output results from TRNSYS simulation are explained.

4.2 Methodology

The techniques available for the study of solar pond cooling systems are by experiment or by dynamic simulation. To the best of the author's knowledge, there is no experimental or installed solar pond absorption cooling system facility anywhere around the world; dynamic simulation will therefore be the adopted methodology for this research.

For dynamic simulation of a solar pond integrated absorption cooling system with a realistic 3D building model using actual building construction will be chosen and the solar pond powered cooling system will be sized so that it can maintain the room temperature level at the required set point all the time.

The problem in designing a new solar cooling facility (solar pond cooling system) is that there are no standard specifications and configurations to follow due to variation in climatic conditions and building characteristics. Every case is specific, and a detailed study is required to achieve maximum efficiency of the system.

The procedure used to perform the dynamic simulation of solar pond cooling system with building is explained here step by step.

1. Identify the building which needs air conditioning and draw a 3D building model by Trnsys3d software. Then import the building model in the TRNSYS.
2. Evaluate building cooling load. Internal and external gains are considered.
3. Select the absorption cooling system capacity for the most efficient configuration and operation parameters depending on the building cooling load.
4. Design the solar pond model depending on heat input to the chiller, and hot water inlet temperature operation range by writing a MATLAB program.
5. Select and size the rest of the cooling system components depending on the size of chiller and the pond.
6. Use Type 155 to link TRNSYS and MATLAB to create coupled simulation.
7. After appropriately linking all components, TRNSYS produces solutions based on the successive substitution method.
8. Adjust the system design by trial and error to minimise the component sizes while maintaining the desired performance.

A limitation of this methodology was the time taken, as there is no specific standard for solar cooling systems to guide the choice of parameter values. To obtain the final results hundreds of different combinations were simulated and analysed to find the best configuration.

4.3 Mathematical Formulation

Solar pond and ground model

4.3.1 Assumptions for finite difference model

The solution of the heat equation for a salt gradient solar pond used the following assumptions (Weinberger, 1964; Rabl and Nielson, 1975; Hull, 1980; Rubin et al. 1984; Tundee et al., 2010; Leblanc et al., 2011).

1. The pond consists of three zones; the upper convective zone (UCZ), the non-convective zone (NCZ) and lower convective zone (LCZ).
2. The horizontal temperature variations are considered small enough so that they are negligible. Therefore, the temperature and salinity distributions within the pond are one-dimensional.
3. Mass transfer is one-dimensional.

4. The temperatures and density in the upper convective zone and in the lower convective zone are uniform and perfectly mixed.
5. The heat losses from the walls are neglected.
6. The bottom surface is blackened in order to maximize the radiation absorption. Therefore, the radiation energy reaching the LCZ is completely absorbed by the solution and the bottom of the pond.
7. The upper surface of the solar pond is subjected to heat losses by convection, evaporation and radiation.
8. No insulation between solar pond and the ground underneath it.
9. Heat transfer through the ground is assumed to be one-dimensional.
10. The ground lower boundary condition is a fixed ground water temperature at the water table depth.

4.3.2 Solar Radiation Model In The Solar Pond

The solar radiation, penetrating into the water body, decays exponentially with depth, as fluid layers absorb energy. The rate of decay is a function of the wavelength of the radiation and for the whole spectrum of wavelengths. An exponential formula was proposed by (Bryant and Colbeck, 1977) and seems to be in very good agreement with (Rabl and Nielsen, 1975) model as described in the section 2.10.1:

$$\frac{H_x}{H_o} = \left\{ 0.36 - 0.08 \ln \left(\frac{x}{\cos \theta_r} \right) \right\} \quad (4.1)$$

where H_o is the insolation incident on horizontal surface in W/m^2 and H_x is the incoming radiation flux at depth x in W/m^2 .

θ_r = angle of refraction at the pond's surface, which can be calculated from Snell's Law (Jaefarzadeh, 2004).

$$\frac{\sin \theta_i}{\sin \theta_r} = 1.333 \quad (4.2)$$

where θ_i is the angle of incidence of direct radiation to a horizontal plane with normal (zenith angle).

$$\cos \theta_i = \cos \delta \cos \phi \cos \omega + \sin \delta \sin \phi \quad (4.3)$$

Here, δ is the angle of declination, ϕ the angle of latitude, and ω the hour angle. The declination angle δ is defined in degrees by (Jaefarzadeh, 2004).

$$\delta = 23.45 \sin\left(\frac{360(284+N)}{365.25}\right) \quad (4.4)$$

N is the day of the year.

The hour angle ω is an angular measure of time considered from noon based on local time h , and is defined as:

$$\omega = \frac{2\pi(h-12)}{24} \quad (4.5)$$

4.3.3 Heat transfer model for solar pond

A vertical system of coordinates is used, with (x) measured as positive downward and $x = 0$ at the surface of the pond, as shown in Figure 4.1. The mathematical model developed in the present work is based upon an energy balance over a fluid layer. Incoming energy to the layer and radiant energy absorbed by the layer equals the loss of energy from the layer and energy accumulation in the layer with time. The pond and the ground beneath it down to the water table are divided into layers. The UCZ and LCZ are each treated as a single layer while the NCZ and the ground are each divided into a number of layers. For each layer, an energy balance is constructed for each time step in the simulation. Based upon energy conservation, the energy balances for UCZ, NCZ and LCZ are expressed as follows.

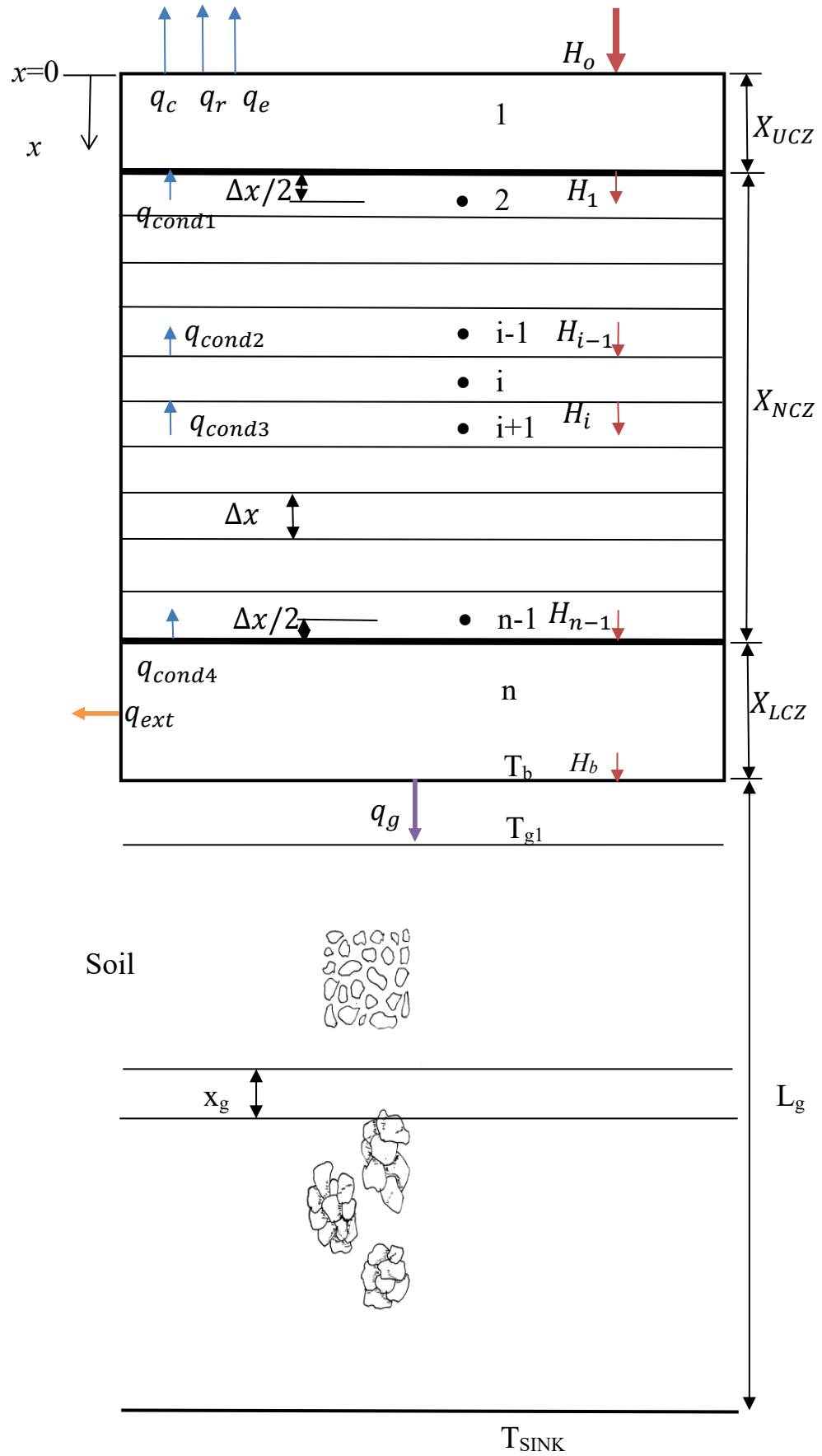


Figure 4.1 Solar pond and ground mathematical model

1. Energy Balance for the UCZ

The energy flows in solar pond's surface can be written as:

Energy in = Energy out + Energy stored

$$[H_o + q_{cond1}] = [H_1 + q_{loss}] + \rho C_p \frac{\partial T}{\partial t} X_{UCZ} \quad (4.6)$$

where q_{loss} is the total heat loss from the pond's surface due to convection, evaporation and radiation.

$$q_{loss} = q_c + q_r + q_e \quad (4.7)$$

The convection heat transfer from the upper layer to the atmosphere depends mainly on the wind speed and the temperature difference between the atmosphere and the pond's water surface.

$$q_c = h_c(T_1 - T_a) \quad (4.8)$$

where convection heat transfer coefficient is given by (Kishore and Joshi, 1984).

$$h_c = 5.7 + 3.8 V \quad (4.9)$$

where V is the wind speed in m/s and can be found in the TMY2 weather data.

The radiation heat loss equation may be written as the following:

$$q_r = \sigma \epsilon_w \{(T_1 + 273)^4 - (T_{sky} + 273)^4\} \quad (4.10)$$

where ϵ_w is the emissivity of water which is assumed to be 0.83 and σ is Stefan-Boltzmann constant (5.67×10^{-8}) W. m. K⁻⁴.

The sky temperature value may be found by several equations, such as (Kurt et al., 2000):

$$T_{sky} = T_a (0.55 + 0.061 \sqrt{P_a})^{0.25} \quad (4.11)$$

where T_a and T_{sky} in °C and P_a in mmHg. However, the sky temperature is found in the TMY2 weather data.

The heat loss from the surface due to the evaporation phenomenon is given by (Kishore and Joshi, 1984).

$$q_e = \frac{L_v h_c (P_1 - P_a)}{1.6 C_s P_{atm}} \quad (4.12)$$

where

$$P_1 = \exp \left(18.403 - \frac{3885}{T_1 + 230} \right) \quad (4.13)$$

$$P_a = RH * \exp \left(18.403 - \frac{3885}{T_a + 230} \right) \quad (4.14)$$

The finite difference equation for the upper convective zone heat equation (4.6) can be written as:

$$T_1^{j+1} = T_1^j + \frac{\Delta t}{\rho C_p X_{UCZ}} \left[(H_o - H_1) + k \left(\frac{T_2^j - T_1^j}{\frac{\Delta x}{2}} \right) - q_{loss}^j \right] \quad (4.15)$$

Where (i), (j) represent space and time, ρ , C_p and k are density, specific heat and thermal conductivity of sodium chloride brine. Equation (4.15) is the first upper boundary condition for the solar pond as defined in Figure 4.1.

2. Energy Balance for the NCZ

The NCZ is divided into (125) layers from (2 to n-1) each layer has 1 cm thickness. Δx has to be small enough so that the difference in the pond outlet temperature is negligible. Δx and Δt should match the stability criterion for explicit method as will be described later in section 4.3.6. The energy balance for the i th layer in the NCZ can be written as:

$$[H_{i-1} + q_{cond3}] = [H_i + q_{cond2}] + \rho C_p \frac{\partial T}{\partial t} \Delta x \quad (4.16)$$

The temperature for any layer in the NCZ in finite difference form can be obtained from Equation (4.16) as:

$$T_i^{j+1} = T_i^j + \frac{\Delta t}{\rho C_p \Delta x} \left[(H_{i-1} - H_i) + k \left(\frac{T_{i+1}^j - T_i^j}{\Delta x} \right) - k \left(\frac{T_i^j - T_{i-1}^j}{\Delta x} \right) \right] \quad (4.17)$$

The temperatures of the NCZ can be calculated from the above equation as internal nodes for the solar pond model.

3. Energy Balance for the LCZ

From Figure 4.1, the energy conservation equation for the LCZ with a thickness of X_{LCZ} can be written as:

$$[H_{n-1}] = [q_{cond4} + q_{ext} + q_g] + \rho C_p \frac{\partial T}{\partial t} X_{LCZ} \quad (4.18)$$

In Equation (4.18), the left hand side is the radiation energy entering the control volume of LCZ, and, in the right hand side, the first term is the heat loss to the non-convective zone at the interface, the second term is the useful heat extracted from the solar pond, the third term is the heat loss to the ground, the fourth term is the energy stored within the LCZ layer. The conduction heat loss from LCZ to NCZ at the interface is given by:

$$q_{cond4} = -k \frac{\partial T_n^j}{\partial x} \Big|_{x=X_{UCZ}+X_{NCZ}} \quad (4.19)$$

The ground heat loss can be calculated from the heat conduction through soil (Equation 4.22) as follows in the next section.

4.3.4 Heat transfer model for soil below the pond

Heat transfer through the solar pond's bottom is significant when solar pond is non-insulated, as shown in Figure 4.1, the heat flow equation within ground is: (Sodha et al., 1981).

$$\rho_g C_{p_g} \left(\frac{\partial T_g}{\partial t} \right) = k_g \left(\frac{\partial^2 T_g}{\partial x_g^2} \right) \quad (4.20)$$

Equation (4.20) will solve with one initial and two boundary conditions as will be described in section 4.3.7. The initial ground temperature was assumed to be 25°C at the beginning of the simulation. The ground underneath the solar pond is divided into 50 layers from 1 to n. where each layer has 10 cm thickness if the depth is 5 m and it varies with the depth of the water table. Δx_g has to be small enough so that the difference in the ground temperature is negligible. Δx_g and Δt should match the stability criterion for explicit method as will described later in section 4.3.6.

The two boundary conditions are:

- 1- Energy balance at the bottom of solar pond, (interface between solar pond and ground).

$$k_g \left(\frac{\partial T_b}{\partial x_g} \right) + h_{LCZ} (T_b - T_{LCZ}) = H_b \quad \text{BC1 (4.21)}$$

where h_{LCZ} is the heat transfer coefficient as will be explained later in this section, H_b is the radiation energy absorbed by the bottom of pond, which is partly imparted to the LCZ by convection and the remainder is transferred to the ground through conduction. The first term on the left hand side of Equation (4.21) is the heat loss from solar pond to the ground by conduction as follows:

$$q_g = k_g \frac{(T_b - T_{g1})}{\Delta x_g} \quad (4.22)$$

Equation (4.22) should be included in the LCZ boundary condition for the solar pond.

Using Equations (4.19) and (4.22) in Equation (4.18) and after simplifying, gives the pond LCZ temperature explicitly at the time of $j+1$, as follows:

$$T_n^{j+1} = T_n^j + \frac{\Delta t}{\rho C_p X_{LCZ}} \left[(H_{n-1}) - k \left(\frac{T_n^j - T_{n-1}^j}{\frac{\Delta x}{2}} \right) - q_{ext}^j - k_g \frac{(T_b - T_{g1})}{\Delta x_g} \right] \quad (4.23)$$

Equation (4.23) is the lower boundary condition of the pond.

The second term on the right hand side of Equation (4.21) is heat transfer by convection, h_{LCZ} is the heat transfer coefficient and it can be defined as:

$$h_{LCZ} = \frac{Nu \, k}{L_c} \quad (4.24)$$

where Nu is Nusselt number and L_c is a characteristic length, which is the pond's surface area divided by pond's perimeter. Nu is defined in terms of Rayleigh number, the following equations correlate experimental data as (Kreith et al., 2010), pp. 311:

$$Nu = 0.27 Ra^{1/4} \quad (10^5 \leq Ra \leq 10^{10}) \quad (4.25)$$

For $T_b > T_n$ lower surface hot or upper surface cool.

$$Nu = 0.54 Ra^{1/4} \quad (10^5 \leq Ra \leq 10^7) \quad (4.26)$$

$$Nu = 0.15 Ra^{1/3} \quad (10^7 \leq Ra \leq 10^{10}) \quad (4.27)$$

For $T_n > T_b$ upper surface hot or lower surface cool.

2- The second boundary condition is the constant temperature for ground water table at different depth from the bottom of the pond.

$$T_{g_{end}} = T_{SINK} = T_{Ground\ water\ table} \quad \text{BC2} \quad (4.28)$$

The heat extracted from the pond per unit area is given by Equation (4.29):

$$q_{ext}^j = m C_p (T_{out}^j - T_{in}^j) / A_p \quad (4.29)$$

where m is the brine mass flowrate, T_{out}^j is the outlet temperature from the LCZ which is assumed to be equal to T_n^j the LCZ temperature, and T_{in}^j is the inlet returned temperature from heat exchanger to the LCZ layer.

4.3.5 Mass transfer model for solar pond

There are several physical processes occurring in the operation of a solar pond. Convective mass transfer occurs in the LCZ and UCZ and diffusive mass transfer in the NCZ. The density gradient could develop by molecular diffusion. In this model, the total mass of the system in the control volume is constant, and the mass transfer takes place as a result of molecular diffusion. The mass transfer processes are independent of the thermal processes. Based upon these assumptions, one-dimensional mass diffusion in the x -direction for a differential volume element of thickness, Δx , is given as follows:

$$J_x - J_{x+\Delta x} = \left(\frac{\partial \rho(x,t)}{\partial t} \right) \Delta x \quad (4.30)$$

$$- \left(\frac{J_{x+\Delta x} - J_x}{\Delta x} \right) = \frac{\partial \rho(x,t)}{\partial t} \quad (4.31)$$

$$- \frac{\partial J}{\partial x} = \frac{\partial \rho(x,t)}{\partial t} \quad (4.32)$$

By Fick's law of diffusion, the diffusion flux J is related to the density gradient by

$$J = -D \frac{\partial \rho(x,t)}{\partial x} \quad (4.33)$$

Substituting from Equation (4.32) into Equation (4.31) and assuming a constant D the salt diffusivity, the following equation can be obtained:

$$\frac{\partial}{\partial x} \left(D \frac{\partial \rho(x,t)}{\partial x} \right) = \frac{\partial \rho(x,t)}{\partial t} \quad (4.34)$$

The salinity can be defined as the ratio of concentration to density of the salt water (Angeli and Leonardi, 2004).

$$S(x, t) = \frac{C(x,t)}{\rho(x,t)} \quad (4.35)$$

so that Equation (4.33) can be written as

$$\frac{\partial}{\partial x} \left(D \frac{\partial C(x,t)}{\partial x} \right) = \frac{\partial C(x,t)}{\partial t} \quad (4.36)$$

where S is the salinity % and C is the salt concentration, kg/m^3 , the diffusion coefficient of salt (D) is $3 \cdot 10^{-9} \text{ m}^2/\text{s}$, according to Srinivasan (1993).

The mass transfer partial differential (4.36) can be discretized as

$$D \frac{C_{(i-1)}^j - 2 \cdot C_{(i)}^j + C_{(i+1)}^j}{\Delta x^2} = \frac{C_{(i)}^{j+1} - C_{(i)}^j}{\Delta t} \quad (4.37)$$

Then

$$C_{(i)}^{j+1} = \frac{D \Delta t}{\Delta x^2} \left[C_{(i-1)}^j - 2 \cdot C_{(i)}^j + C_{(i+1)}^j \right] + C_{(i)}^j \quad (4.38)$$

This equation represents a concentration profile for internal nodes in the NCZ. The initial conditions are assumed to be 1 kg/m^3 at the UCZ and 212 kg/m^3 at the LCZ with linear distribution in the NCZ.

For the mass transfer equation, the two boundary conditions are:

At the top of the pond, the mass balance gives:

$$D \frac{\partial C}{\partial x} = \frac{\partial C}{\partial t} X_{UCZ} \quad \text{BC1 (4.39)}$$

At the bottom of the pond

$$-D \frac{\partial C}{\partial x} = \frac{\partial C}{\partial t} X_{LCZ} \quad \text{BC2 (4.40)}$$

4.3.6 Finite Difference Method

The heat flow equation for the solar pond in the NCZ is given by Equation (4.41) (Rubin et al., 1984).

$$\rho C_p \left(\frac{\partial T}{\partial t} \right) = k \left(\frac{\partial^2 T}{\partial x^2} \right) - \frac{\partial H(x,t)}{\partial x} \quad (4.41)$$

The equation is classified as a parabolic, second order, partial differential equation. One of the methods for the solution of this kind of equation is the so-called explicit method (Cengel et al., 1998).

In Figure 4.1, the NCZ is divided into n layers, and for a node located at

$$x(i) = (i-1) * \Delta x + x_{ucz} ,$$

where (i= 2,3,...,n) at time ($t = j * \Delta t$), j= 1,2,3,...max t.

Equation (4.41) can be discretized as

$$\frac{T_{(i-1)}^j - 2 * T_{(i)}^j + T_{(i+1)}^j}{\Delta x^2} + \frac{H_{(i-1)} - H_{(i)}}{k * \Delta x} = \frac{1}{\alpha} \left(\frac{T_{(i)}^{j+1} - T_{(i)}^j}{\Delta t} \right) \quad (4.42)$$

Then gives

$$T_{(i)}^{j+1} = \tau \{ T_{(i-1)}^j - 2 * T_{(i)}^j + T_{(i+1)}^j \} + \frac{\Delta x \tau}{k} \{ H_{(i-1)} - H_{(i)} \} + T_{(i)}^j \quad (4.43)$$

Where the thermal diffusivity $\alpha = k / \rho C_p$ and the non-dimensional mesh Fourier number is $\tau = \alpha \Delta t / \Delta x^2 \leq 0.5$ which is the stability criterion for explicit method. (Cengel et al., 1998), so for $\Delta x = 0.01$. when $\alpha = 1.64 * 10^{-7} \text{ m}^2/\text{s}$ from (Hull et al., 1989).

$$\Delta t \leq 0.5 \Delta x^2 / \alpha$$

$$\Delta t \leq (0.5 * (0.01)^2) / 1.64 * 10^{-7}$$

$\Delta t \leq 304.87 \text{ sec.}$ So **300 sec** was selected.

The time step and layer thickness are justified by comparing two different time steps 75 sec and 300 sec and three different layer thicknesses 0.005 m, 0.01 m ,and 0.02 m. Figure 4.2 shows temperature profiles for two different time steps at the end of July 2nd year temperature profile with layer thickness 0.01 m. It may be seen that the difference between temperature profiles of 75 sec and 300 sec time steps is small. The shorter time step the longer the computational time. With 300 sec the computational time for two years is 37 minutes while with 75 sec the computational time is approximately 2.5 hour.

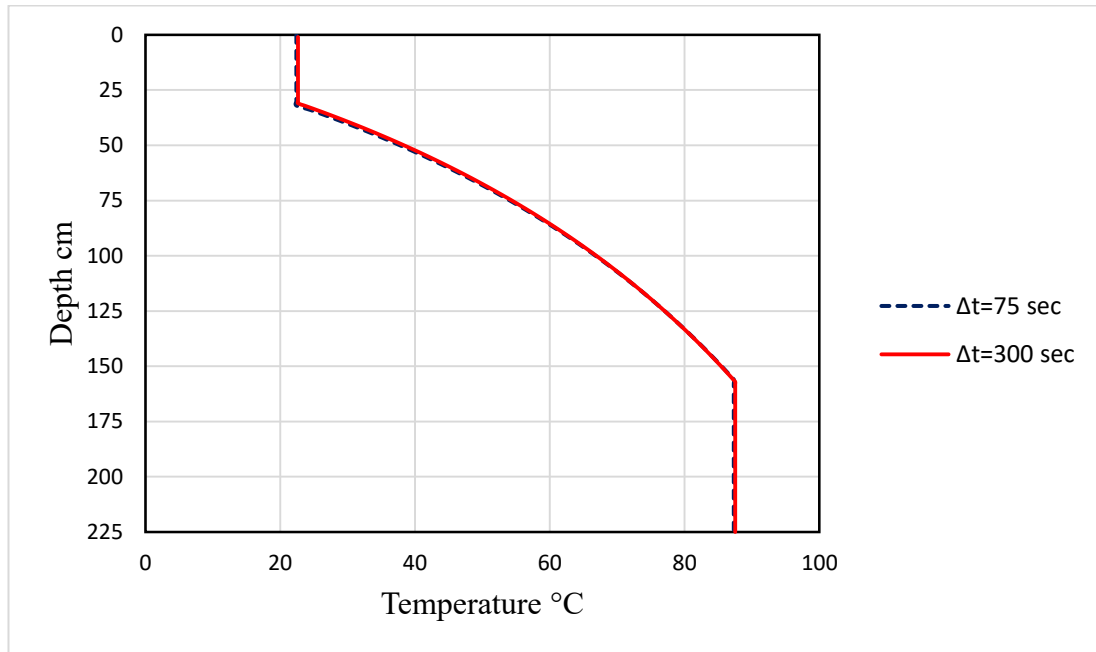


Figure 4.2 Temperature profiles with different time steps at the end of July 2nd year, layer thickness =0.01m

Figure 4.3 shows temperature profiles with three different layer thickness at the end of July 2nd year with time steps 300 sec and 75 sec. It can be seen that the differences between the temperature profiles are small. The difference between the LCZ temperatures for 0.01 m and 0.02 m thickness is only 0.105 °C and the difference between the LCZ temperatures for 0.005 m and 0.01 m thickness is 0.317 °C. 0.01m layer thickness was selected as a compromise between accuracy and computational stability. Table 4.1 shows the values of layer thickness and time steps and the resulting maximum LCZ temperatures.

With 0.02 m, LCZ temperature is a bit higher than the LCZ with 0.01m. However, the 0.01 m is selected because the small mesh is better and accurate than large mesh in the numerical solutions.

It is decided that the suitable time step is 300 sec and the suitable layer thickness is 0.01 m for the calculation of this research.

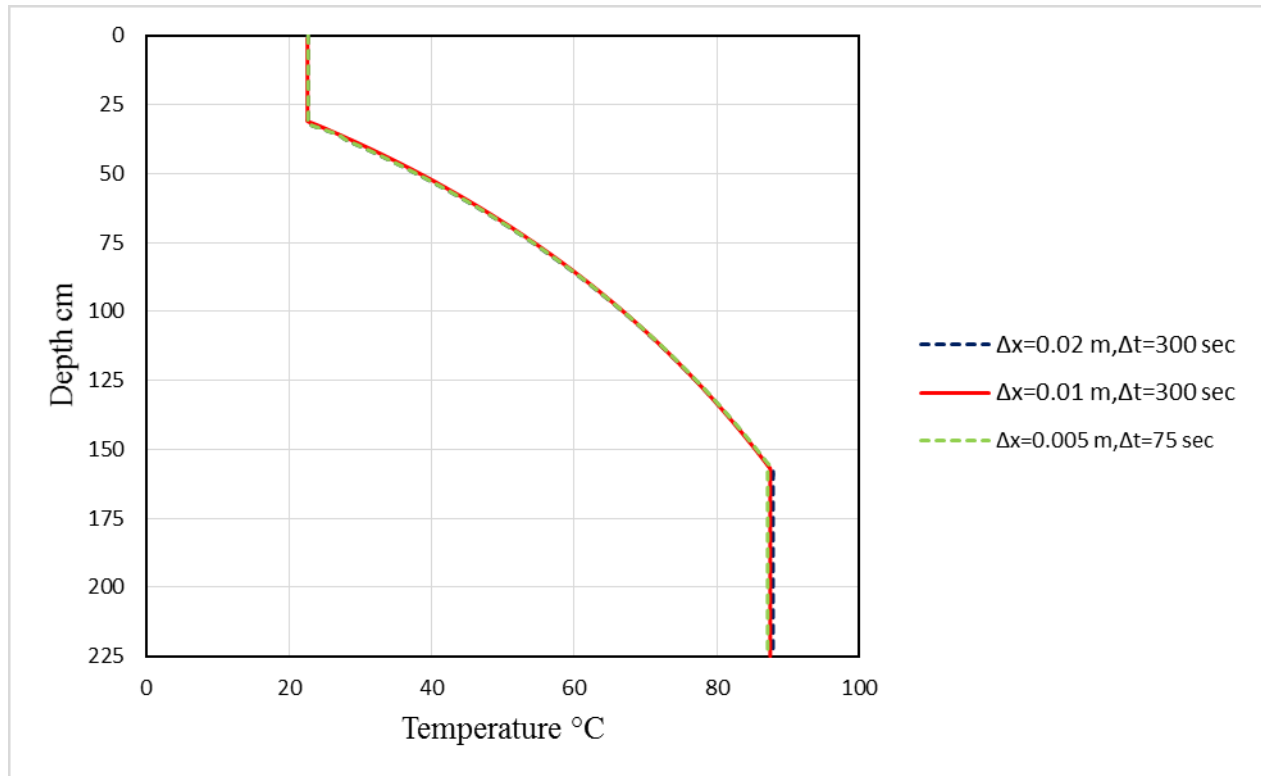


Figure 4.3 Temperature profiles with different layer thicknesses at the end of July 2nd year, and different time steps

Δt (sec)	Δx (m)	MaxTLCZ (°C)
75	0.01	87.302
75	0.005	87.202
300	0.01	87.519
300	0.02	87.624

Table 4.1 values of spatial layer thickness and time steps with the maximum LCZ temperature

Equation (4.42) will be used to calculate the temperature distribution for internal nodes in the NCZ.

The heat transfer through ground, Equation (4.20) can be discretized as

$$\frac{T_{g(i-1)}^j - 2 * T_{g(i)}^j + T_{g(i+1)}^j}{\Delta x_g^2} = \frac{1}{\alpha_g} \left(\frac{T_{g(i)}^{j+1} - T_{g(i)}^j}{\Delta t} \right) \quad (4.44)$$

Then

$$T_{g(i)}^{j+1} = \tau \left\{ T_{g(i-1)}^j - 2 * T_{g(i)}^j + T_{g(i+1)}^j \right\} + T_{g(i)}^j \quad (4.45)$$

The mass transfer Equation (4.36) can be discretized as

$$D \frac{C_{(i-1)}^j - 2 * C_{(i)}^j + C_{(i+1)}^j}{\Delta x^2} = \frac{C_{(i)}^{j+1} - C_{(i)}^j}{\Delta t} \quad (4.46)$$

Then

$$C_{(i)}^{j+1} = \frac{D \Delta t}{\Delta x^2} \left[C_{(i-1)}^j - 2 * C_{(i)}^j + C_{(i+1)}^j \right] + C_{(i)}^j \quad (4.47)$$

This equation represents a concentration profile for internal nodes in the NCZ.

4.3.7 Numerical Solution of Solar Pond and Ground Model

The governing equations (4.15), (4.17), and (4.23) of the solar pond heat transfer, Equations (4.39), (4.36), and (4.40) of the solar pond mass transfer and equation, and Equations (4.21), (4.20), and (4.28) of the ground heat loss are solved numerically to determine the temperature and concentration distribution for solar pond and ground temperature profile within soil below the pond. A finite difference form of the differential equation for solar pond and ground is used. MATLAB codes were written to solve differential equations for solar pond and ground as shown in Appendix A. In the simulation, input data for solar pond are 0.637 W/m °C thermal conductivity of brine. The brine density and specific heat at constant pressure at 60°C and salinity 15% NaCl by mass are 1088.6 kg/m³, 3570 J/kg. °C respectively. The thermal diffusivity is 1.64*10⁻⁷ m²/s at the same temperature and salinity (Hull et al., 1988).

The numerical stability criterion for the explicit formulation is $\tau = \alpha \Delta t / \Delta x^2 \leq 0.5$ for solar pond and $\tau = \alpha_g \Delta t / \Delta x_g^2 \leq 0.5$ where α is thermal diffusivity for brine and α_g

is soil thermal diffusivity (Cengel et al., 1998). So for $\Delta x = 0.01$ m, $\Delta t = 300$ sec. when $\alpha = 1.64 \times 10^{-7}$ m²/s

For ground heat loss with the same time step ($\Delta t = 300$ sec) and different soil thermal properties as described in section 3.4.1, different Δx_g was adopted depending on the depth of water table underneath solar pond.

With 5 m depth of the water table and 50 layers, so that $\Delta x_g = 10$ cm. With 10 m depth of the water table and 50 layers, $\Delta x_g = 20$ cm.

The simulation solution starts by solving Equation (4.23) to find T_n^{j+1} then Equation (4.17) for T_i^{j+1} and Equation (4.20) is solved for determining T_g^{j+1} . Finally Equation (4.21) is solved to find T_b^{j+1} for specific time step. In the next time step, temperatures are calculated on the basis of previous time step. It is assumed that for short time step it will not cause a significant error. The mass transfer Equation (4.36) with two boundary conditions Equations (4.39), and (4.40) are solved in a separate code as shown in Appendix A.

4.4 TRNSYS 17

TRNSYS (TRaNsient SYstem Simulation) is a modular simulation program that allows the modelling of various energy systems, including HVAC analysis, multi-zone airflow analyses, electric power simulation, solar design, building thermal performance, analysis of control schemes, etc. TRNSYS-17 manual, (Klein et al., 2010).

TRNSYS operates in a graphic interface environment called Simulation Studio. In this environment, icons of ready-made components are dragged and dropped from a list and connected together according to the real system configuration (Kalogirou, 2013). The standard library includes approximately 150 models ranging from photovoltaic panels, multizone buildings, solar collectors, storage tanks, weather data processors and HVAC equipment (Almeida, et al., 2014).

In addition to the main TRNSYS components, an engineering consulting company specialising in the modelling and analysis of innovative energy systems and buildings, Thermal Energy System Specialists (TESS), developed libraries of components for use with TRNSYS. The TESS library includes more than 500 TRNSYS components (Kalogirou, 2013).

TRNSYS consists of a Graphical User Interface, a simulation kernel and different simulation components (Types). After appropriately linking all components, TRNSYS produces solutions based on the successive substitution method, which is the process where the outputs of a component are fed/substituted as the inputs to another component. A component is called only if its inputs change during a particular time step, and convergence is reached when the outputs vary within the tolerance limits defined by the solver.

The simulation time step can be as short as 1/1000 of an hour (3.6s) and can be helpful for detailed instantaneous micro analysis. The short time step (less than one hour) can be useful as it may be necessary for computational stability in the simulation and it can be used to simulate the dynamic response of the systems that respond faster in seconds or minutes. (Klein, and Beckman, 1971; Klein et al., 1975)

4.5 Complete System Modelling

To have a clear view of the whole system, it has been divided into three main sections namely: solar pond as a source, absorption chiller, and building. These parts are interconnected as described in Figure 4.4.



Figure 4.4 Diagram of complete system

4.6 Building Description

The building being used for this work is a single family house situated in Baghdad the capital of Iraq. This kind of house is common in Iraq and is shown in Figure 4.5. According to the report from Ministry of Construction and Housing, Iraq will need to build 3.5 million new housing units by 2015 to meet the population growth and housing need. (Ministry of Construction & Housing, 2009). Depending on that more house will be built and more cooling and heating systems are needed.

The building data was explained in section 3.5. The details about drawing and importing building model in TRNSYS will be explained in the next sections.



Figure 4.5 Architecture view of house in Iraq. (Aryo-group, 2012)

4.6.1 Trnsys3d

In version 17, TRNSYS includes Trnsys3d, which can plug-in with Google Sketch Up, that allows multizone buildings to be drawn, and imports the geometry directly from the Sketch Up interface into TRNSYS.

The procedure to draw the building in Trnsys3d is similar to the drawing in Google Sketch Up, except that all drawing will be in the 'active' Trnsys3d zone. Creating the geometry step by step may be found in the Trnsys3d Manual (Klein et al., 2010).

The final building zone with all fenestrations (windows) was shown in Figure 3.7 in Chapter Three.

4.6.2 TRNBuild

TRNBuild is the tool used to enter data for multizone buildings. It is allowed to specify all the building structure details, as well as everything that is needed to simulate the thermal behavior of the building, such as windows' optical properties, heating and cooling schedules, etc. (Klein et al., 2010).

A TRNBuild interface for the model materials is shown in Figures 4.4 and 4.5.

A dynamic 3D-building simulation was carried out by TRNSYS using the 3D drawing capabilities of Trnsys3d for Google Sketch-up, then importing the geometrical information into the Type 56 (Multi-zone building model).

Type 56 needs a great amount of building data to calculate the thermal behaviour of the building. This includes geometry data, wall construction data, and windows data...etc. in addition to weather data information such as: radiation, ambient temperature, humidity, etc. Furthermore, it needs information such as SCHEDULE which may define the gain from the occupants during the day with intervals representing the time being occupant from the building owners.

The Trnsys3d geometry which was drawn by SketchUp, was written out on the Trnsys3d file called: *.idf file, which has all geometrical information about the modelled building.

The information about walls within a zone is displayed in the left lower part of the AIRNODE window. Here, the user can add, delete or edit the walls of an AIRNODE. A box in the upper part provides an overview of all defined walls. By clicking on a wall within this overview box, the definition of the selected wall is displayed below and can be edited in Figure 4.6.

Figure 4.7 shows the wall layers from the program library which can be selected. Creating the construction started from the “inside” surface (front) of the wall to the “outside” (back). The building structures are built according to the U-values that provided from the project owner.

Zone: 1F5197 - Airnode: 1F5197

Airnodes

1F5197

1F5197

number: 1

Airnode Regime Data

volume: 375 m³

capacitance: 450 kJ/K

Therm. Zone

Walls

Surf	Type	Area	Category
1	IRAQGROUND	125.00	BOUNDARY
2	IRAQWALL	30.00	EXTERNAL N_180_90
3	SIRAQWALL	30.00	EXTERNAL S_0_90
4	WIRAQWALL	37.50	EXTERNAL W_90_90
5	EIRAQWALL	37.50	EXTERNAL E_270_90
6	IRAQROOF	125.00	EXTERNAL H_0_0

Windows

Surf	Type	Area	Category	u-Value	g-Value
9	SINGLE	3.00	EXTERNAL	5.68	0.895

Walls

wall type: IRAQWALL <- new ...

area: 30 m² incl. windows

category: EXTERNAL

geosurf: 0 2

wall gain: 0 kJ/h

orientation: N_180_90 H_0_0

view fac. to sky: 0.5

Windows

window type: SINGLE <- new ...

area: 3 m²

category: EXTERNAL

geosurf: 0 9

gain: 0 kJ/h

orientation: N_180_90 H_0_0

view fac. to sky: 0.5

Figure 4.6 Building Zone in TRNBuild

New Wall Type

"Wall Type" Manager

new wall type: WALL001

Layer

front / inside

No.	Layer	Thickness	Type
1	GYPSUM_PLA	0.010	massive
2	BLOCK_MASS1	0.200	massive
3	CEMENT_MOR	0.010	massive

back

total thickness: 0.220 m

u - value: 2.295 W/m² K for reference only
(incl. alpha_i=7.7 W/m² K and alpha_o=25 W/m² K!)

Solar Absorptance of Wall

front: 0.6

back: 0.6

Longwave Emission Coefficient

front: 0.9

back: 0.9

Convective Heat Transfer Coefficient of Wall

front

☒ userdefined ☐ internal calculation

11 kJ/h m² K

back

☒ userdefined ☐ internal calculation

64 kJ/h m² K

Note.
The emissivity of inside surfaces are applied by the detailed longwave radiation mode only!
For the standard model fixed values of 0.9 are used.

Figure 4.7 Wall Layers Definition

4.6.3 Importing The Building Model

The TRNSYS simulation studio offers the opportunity to automatically set up a simulation by importing the 3D-building model. After selecting the file, a simulation with the important links for the first run are automatically generated as shown in Figure 4.8. A great advantage of the 3D-Building Wizard is that all orientations of the Building are linked automatically. This reduces errors and time used to link this information manually (Klein, et al., 2010).

Due to the complexity of a multi-zone building, the parameters of TYPE 56 are not defined directly in the TRNSYS input file, instead, a so-called building file is assigned containing the required information. TRNBuild has been developed to create the building file which contains the basic project information, and user thermal zones description. (All information imported and defined).

In TRNbuild, non-geometric objects, such as materials, constructions, schedules, internal heat gains, heating cooling etc. are added to the project. Then the user can provide required information to the project to have finally the desired outputs.

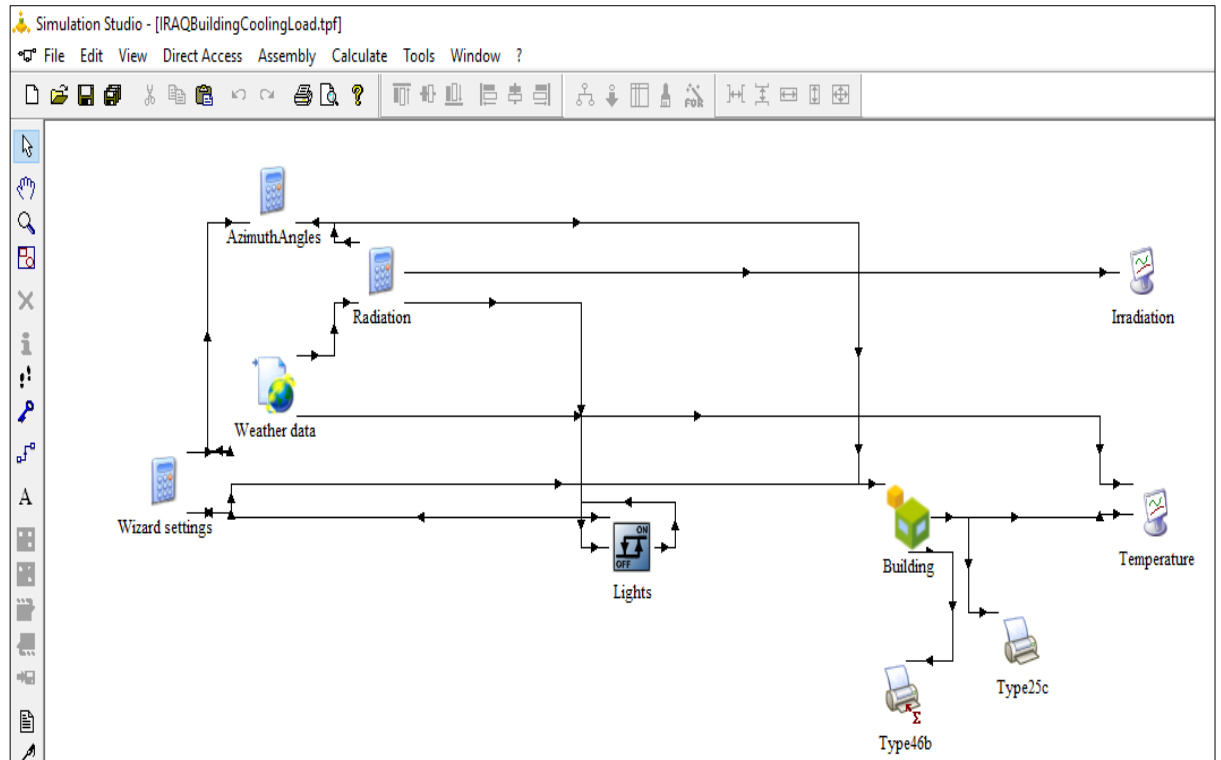


Figure 4.8 Multi-zone building model (Type 56) with all required connections

4.7 Absorption Chiller Model

The details and review of the absorption chiller were described in the section 2.5.2 and 3.7.3. To model the absorption chiller Type 107 was used.

4.7.1 Modelling of Type 107

Type 107 is based on ordinary calculation and on external data (performance data) which supply the required values: normalized fraction of full load capacity (the normalized value of energy that is available to chill at current working conditions) and fraction of design energy input (the normalized value of heat input required to reach the value fraction of nominal capacity). The depended values depend on fraction of design load, chilled water set point temperature (°C), entering cooling water temperature (°C), and hot water temperature (°C) which are independent values. TRNSYS17 Manual, (Klein et al., 2010).

Type107 requires a single data file, which is to be specified in the standard TRNSYS data format for the Dynamic Data subroutine. In this research, a new data file was created based on manufacturer's data. The data file is discussed in section 3.7.3.

In the beginning, Type107 determines the fraction of design load at which it must operate first by calculating the amount of energy that must be removed from the chilled water stream in order to bring it from its entering temperature to the set point temperature:

$$Q_{remove} = m_{chw} C_{pchw} (T_{chw,in} - T_{chw,set}) \quad (4.48)$$

The required energy removal is then divided by the machine's capacity to determine the fraction of design load at which the machine is required to operate:

$$f_{Design\ Load} = \frac{Q_{remove}}{Capacity_{Rated}} \quad (4.49)$$

Then Type 107 calls the dynamic data subroutine with the specified chilled water set point temperature, entering cooling water temperature, inlet hot water temperature, and fraction of design load and return the fraction of full load capacity and fraction of design energy input for the specific values in the external data file at current work condition.

After that, Type 107 calculates the machine capacity at the given time:

$$Capacity = f_{FullLoadCapacity} * f_{NominalCapacity} * Capacity_{Rated} \quad (4.50)$$

When dynamic data returns the fraction of design energy input, then Type 107 calculates the energy delivered to the chiller by the hot water stream:

$$Q_{hw} = \frac{Capacity_{Rated}}{COP_{Rated}} f_{DesignEnergyInput} \quad (4.51)$$

The hot water stream outlet temperature is then:

$$T_{hw,out} = T_{hw,in} - \frac{Q_{hw}}{m_{hw}Cp_{hw}} \quad (4.52)$$

The chilled water outlet temperature, which should be the set point temperature but may be greater if the machine is capacity limited, is then calculated as:

$$T_{chw,out} = T_{chw,in} - \frac{MIN(Q_{remove}, Capacity)}{m_{chw}Cp_{chw}} \quad (4.53)$$

In this stage, Type 107 can balance the chiller energy by calculating the energy rejection to the cooling water from the following equation:

$$Q_{cw} = Q_{chw} + Q_{hw} + Q_{aux} \quad (4.54)$$

Here term Q_{aux} is counting for the energy needed by auxiliary components on the entire system and it is used regardless of whether the machine works in a full capacity or not.

The temperature of the outlet cooling water stream can be calculated using the following equation:

$$T_{cw,out} = T_{cw,in} + \frac{Q_{cw}}{m_{cw}Cp_{cw}} \quad (4.55)$$

Finally, the chiller COP can be calculated by the Equation (4.56):

$$COP = \frac{Q_{chw}}{Q_{aux} + Q_{hw}} \quad (4.56)$$

4.8 Solar Pond Model

As solar pond Type does not exist in TRNSYS software. A MATLAB code was written to represent a solar pond Type in TRNSYS, as shown in Appendix A.

In order to achieve a complete system model for connecting solar pond model with absorption chiller and building, solar pond MATLAB code should be called inside

TRNSYS simulation for each time step. Type 155 is a component which is used to link MATLAB and TRNSYS software.

The main input parameters to the code are: solar pond parameters such as layer thicknesses and pond area, initial temperatures, thermophysical properties of brine, brine mass flowrate, thermophysical properties of soil, and TMY2 weather data from TRNSYS.

The main outputs from the MATLAB code at the end of each time step are: LCZ temperature (pond outlet temperature), UCZ temperature, pond bottom temperature, soil temperatures, and heat extraction per unit pond area.

4.8.1 Calling MATLAB Type 155

TRNSYS Type 155 implements a link with MATLAB. The connection uses the MATLAB engine, which is launched as a separate process. The FORTRAN routine communicates with the MATLAB engine through a Component Object Model (COM) interface. Type 155 can have different calling modes (e.g. iterative component or real-time controller). There are no specific limits on the number of inputs, outputs, or instances of Type 155 in a simulation (Klein et al., 2010).

In order to use Type 155 a specific steps should be done.

- Install MATLAB in your computer with specific MATLAB Releases are supported, only the 32-bit versions are supported.
- Add MATLAB\bin\win32 folder to Windows search path.
- Select a specific (Type 155.DLL) for your MATLAB version from (TRNSYS17\Exe\DLLs) folder.
- Copy the Type 155.DLL file to (TRNSYS17\Exe) folder.
- From (MATLAB\extern\lib\win32\lcc) folder find and copy these files (libeng.lib, libmat.lib, libmex.lib and libmx.lib) to (TRNSYS17\SourceCode\Optional folder.
- Copy (Type 155.DLL) file to (TRNSYS17\UserLib\ReleaseDLLs) folder.
- Run MATLAB as an administrator.

- Finally, write (regmatlabserver) command in MATLAB's Command Window to register the desired MATLAB session as an automation server.

The pond is connected to the weather data Type 15 and heat exchanger Type 91. Inputs to Type 155 are dry bulb temperature, effective sky temperature, percent relative humidity, wind velocity, total horizontal radiation, angle of incidence for horizontal are shown in Figure 4.9.

The heat exchanger outlet temperature (which is inlet temperature to the pond), and heat exchanger outlet mass flowrate of brine, are shown in Figure 4.10.

The main outputs from Type 155 are LCZ temperature (pond outlet temperature), UCZ temperature, solar pond bottom temperature, soil temperatures, and heat extraction per unit pond area.

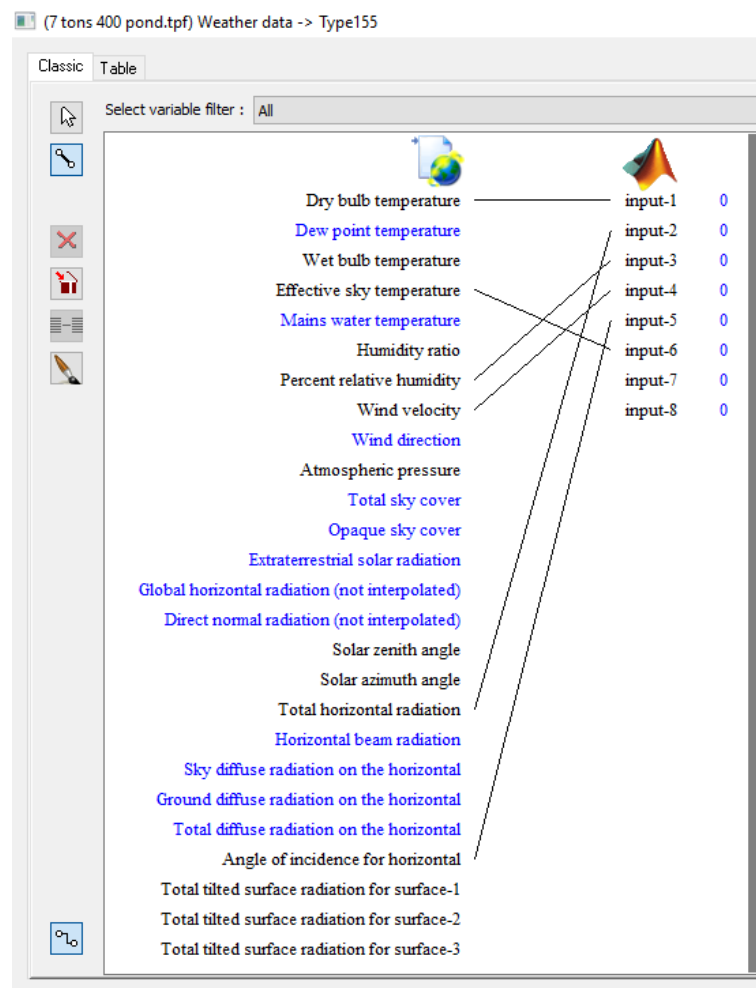


Figure 4.9 Solar pond (Type 155) weather data inputs

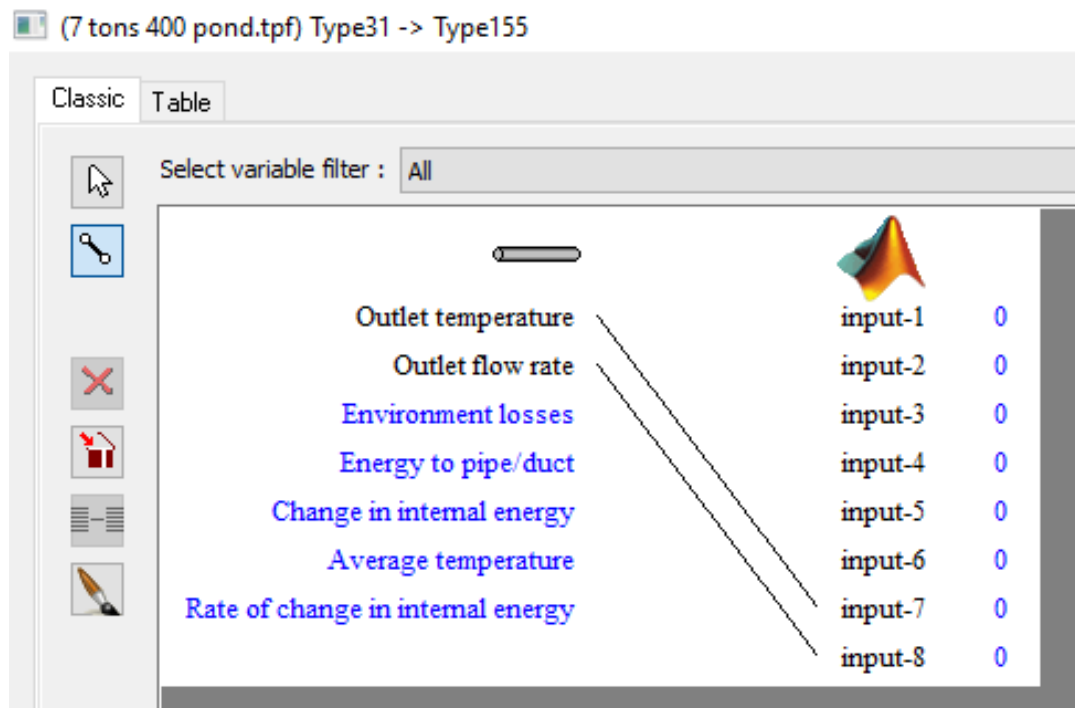


Figure 4.10 Solar pond (Type 155) heat exchanger return data inputs

4.8.2 Structure of the m-file

The m-file is a simple text file where MATLAB commands are placed. The m-file will be called at each call to MATLAB. Thus, the m-file must deal with the different TRNSYS calls, similar to what a TRNSYS Type is doing. (Klein et al., 2010). The m-file called by Type 155 is a MATLAB "batch file", not a function i.e. the MATLAB code in the Appendix (A) will not run in MATLAB software but it needs to connect with TRNSYS software to start the calling process properly.

The main structure of MATLAB code includes the following points:

- The code starts with the solar pond and ground parameters.
- MATLAB does not only receive the weather data, pond inlet temperature, and water inlet flow rate as the inputs in (trnInputs) but also other information about the simulation such as:

- trnInfo (The Info array is an integer array of 15 values. It contains an information about the UNIT that is currently being called by the kernel). (TRNSYS Manual, Volume 7) (Klein et al., 2010).
 - trnTime (simulation time)
 - trnStartTime (simulation start time)
 - trnStopTime (simulation stop time)
 - trnTimeStep (simulation time step)
 - mFileErrorCode (see here below)
- Setting the variable initial values at the first iteration.
 - Storing the values at the post convergence call.
 - Calculating the solar pond performance by solving the governing equations.
 - MATLAB return outputs such as pond outlet temperature, ground temperature and heat extracted from the pond in (trnOutputs). TRNSYS creates the output array (trnOutputs) with the correct size before running the m-file to prevent memory access violations in case the m-file fails.
 - All errors are found in the result file.

Another mechanism is implemented to prevent TRNSYS from continuing a simulation in case the m-file fails:

- Before running the m-file, TRNSYS creates a variable called mFileErrorCode which is initialized to 1
- If the value of that variable is not zero when MATLAB returns, the simulation will stop and TRNSYS will display an error message with the value of mFileErrorCode. This can be used by the m-file to give a hint about what happened if the value of mFileErrorCode is incremented at different places in the m-file.

4.8.3 Calling solar pond's MATLAB code in TRNSYS

A solar pond's MATLAB code is called inside TRNSYS by using Type 155 component as shown in Figure 4.11 below:

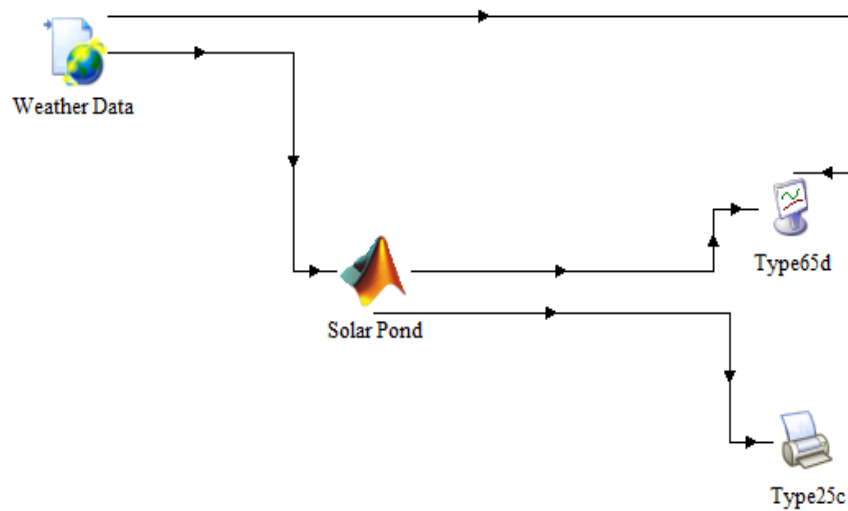


Figure 4.11 Calling solar pond's MATLAB code in TRNSYS

The types which have been used to model the solar pond system are the followings:

- Type 155 to link MATLAB and TRNSYS. It include parameters, inputs and outputs. Inputs are used in solar pond's MATLAB code to calculate outputs.
- Type 15-6. This component serves the purpose of reading data at regular time intervals from an external weather data file, interpolating the data (including solar radiation for tilted surfaces) at time steps of less than one hour, and making it available to other TRNSYS components. The model also calculates several useful terms including the mains water temperature, the effective sky temperature, and the heating and cooling season forcing functions.

This version of Type 15 reads data in the format generated by Meteonorm, which is identical to the Typical Meteorological Year (version 2) standard form.

- Type 25c, the printer component is used to output (or print) selected system variables at specified (even) intervals of time. In this mode, unit descriptors (kJ/hr, deg C) are NOT printed to the output file with each column heading. Output can be printed in even time intervals starting relative to the simulation start time or can be printed in absolute time. If relative printing is chosen with a one hour print interval and the simulation starts at time 0.5, values will be

printed at times 0.5, 1.5, 2.5, etc. If absolute printing is selected, for the same simulation, values will be printed at times 0.5, 1.0, 2.0, 3.0, etc. Type 25 is also able to print simulation information as a header to the output file (name of input file, and time of simulation run). It is further able to append new data to an existing file or can be set to overwrite the existing file.

- Type 65d. The online graphics component is used to display selected system variables while the simulation is progressing. This component is highly recommended and widely used, since it provides valuable variable information and allows users to immediately see if the system is not performing as desired. The selected variables will be displayed in a separate plot window on the screen. In this instance of the Type 65 online plotter, no output data file is generated.

4.9 Complete System components (Types)

The complete system components used in TRNSYS simulation are shown in Table 4.2, (TRNSYS Manual, Volume 4), (TESS Manual, Volume 6). (Klein et al., 2010).

No.	Type	TRNSYS Name	Real Component
1	Type 155	Calling MATLAB	Solar Pond
2	Type 91	Effectiveness Heat Exchanger	Heat Exchanger
3	Type 107	Single Effect Hot Water Fired Absorption Chiller	Absorption Chiller
4	Type 697	Performance Map Cooling Coil	Cooling Coil
5	Type 510	Closed Circuit Cooling Tower	Cooling Tower
6	Type 56	Multi-Zone Building and TRNBuild	Building
7	Type 108	Five Stage Room Thermostat	Thermostat

8	Type 15	Weather Data Processor	Weather Data,TMY2
9	Type 112b	Single Speed Fan/Blower with Relative Humidity Inputs	Fan
10	Type 3d	Single Speed Pump	Pumps
11	Type 31	Pipe Or Duct	Pipes and Ducts
12	Type 2	ON/OFF Differential Controller; Old Control Strategy	Controller
13	Type 65d	Online Plotter With Out File	Online Graphical Plotter
14	Type 25c	Printer, Unformatted ,No Units	Printer

Table 4.2 Complete system components (Types) used in TRNSYS simulation

4.10 Coupled System Description

The building is a typical modern single-family house situated in Baghdad, Iraq. It has one storey, a flat roof, and a floor area of 125 m². It is constructed of uninsulated concrete with single glazed windows. The house is occupied and air conditioned continuously.

The solar pond has an area of 400 m² and a depth of 2.25 m.

The solar cooling system comprises a hot water fired absorption chiller, four water circulating loops and a building air loop.

Hot brine is withdrawn from the lower convective zone of the solar pond and passed through an external heat exchanger where it transfers heat to hot water; the brine is

then returned to the lower convective zone. The hot water is pumped to the chiller, gives up the heat and is returned to the heat exchanger. Thus, heat is transported from the solar pond to the chiller while the chiller is isolated from the corrosive brine.

Cooling water circulates between the chiller and a wet cooling tower which rejects heat to the environment.

Chilled water circulates between the chiller and the air cooling coil. Air flows from the inside of the house, through the cooling coil and back into the house.

The system is controlled by an on-off room thermostat with a set point of 25°C. If the thermostat is satisfied, then the chiller and all pumps and fans are off. The chilled water set point temperature from the chiller is 7°C. If the temperature of the hot water supplied from the heat exchanger is below 70°C, the chiller does not operate.

The house and cooling system are modelled in the TRNSYS simulation software (TRaNsient SYstem Simulation) , which calls the MATLAB code at each simulation time step to model the solar pond (Klein et al., 2010). The complete TRNSYS model is shown in Figure 4.12; the lines in the Figure represent logical connections in the model, not necessarily physical connections such as pipes. The red lines shown represent the hot brine and hot water loops, the blue lines represent the chilled water loop, the sky blue line represents cooling water, and green lines represent the ducts between building and cooling coil loop. The pink line represents the weather data connections. The thin red lines are for representation of control signals from the controller to the equipment. The remaining black lines are the output data from the system to the online plotter and printer.

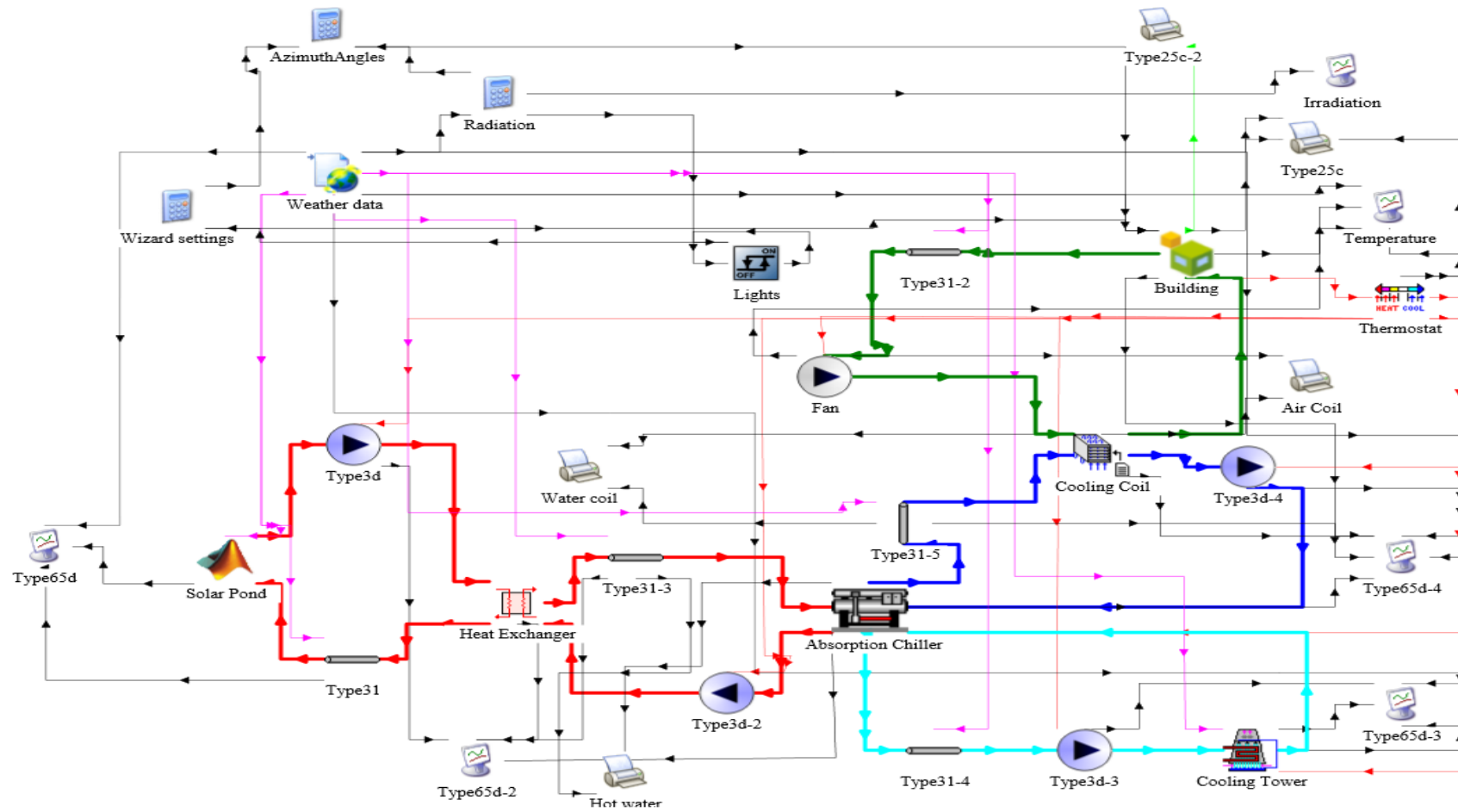


Figure 4.12 Complete TRNSYS simulation system for solar pond with absorption chiller and building

4.11 Outputs from TRNSYS

TRNSYS has many components which can be connected together according to the real system configuration. Each component of the system has a unique TYPE number and requires a set of INPUTS (from other components or data files) and a set of constants PARAMETERS, specified by the user. Each component has its own set of OUTPUTS, which can be saved in a file, plotted, or used as input for other components. Output values can be seen on an online plotter as the simulation progresses. (Almeida et al., 2014)

Heating, Ventilation and Air Conditioning equipment needs a control system to regulate the operation of a heating and/or air conditioning system. Usually a sensing device is used to compare the actual state (e.g. temperature) with a target state. Controller Type 108 (thermostat) was used for the current TRNSYS simulation, to control the fan air flow from building to the cooling coil. Type 108 is the only thermostat controller in the TRNSYS library. Type 108 is a room thermostat modeled to give output ON/OFF control functions that can also be used to control the whole system. In the current TRNSYS simulation, Type 108 was used to control fan, pumps, absorption chiller, and cooling tower fan. All system is ON or OFF at the same time, depending on the internal conditions of the building.

When the system is ON, which means fan, pumps, absorption chiller and cooling tower are ON, and the inlet conditions are in the range of design conditions, the output temperatures are maintained at the required set points temperature all the time.

4.11.1 System OFF Outputs

The system is OFF when the room temperature is below the cooling set point temperature, this will happen continuously during the late of autumn and winter and could happen sometimes during spring and summer nights.

In order to clarify the TRNSYS output results when the system is OFF, two examples of results are explained in detail.

4.11.2 Ambient and Room Air Temperatures

Figure 4.13 shows two years' TRNSYS simulation output results of ambient and room air temperatures for the solar pond cooling system located in Baghdad, Iraq. It can be seen that the room temperature is controlled during summers in such a way that the system maintains room temperature at less than 25°C during the second representative year. It might be unclear that the room temperatures are less than 5°C in some periods. These periods of time are mostly in winters and when the system is OFF. Figures 4.12, 4.13, and 4.14 show the first, second and third periods in the simulation ranges in hours (0-1000, 8000-9000, and 16520-17520) respectively. These figures illustrate that when the all system is OFF, the room temperatures are in the same pattern of the ambient temperature. It may be noticed that the room temperature lags behind the ambient temperature, that the fluctuations in room temperature are smaller than the fluctuations in ambient temperature, and that the average room temperature is higher than the average ambient temperature. This is what would be expected as the effects of the building's thermal capacity, resistance to heat loss, and solar and internal heat gains. The behaviour of the coil air outlet temperature is the same as the behaviour of room temperature with ambient temperature.

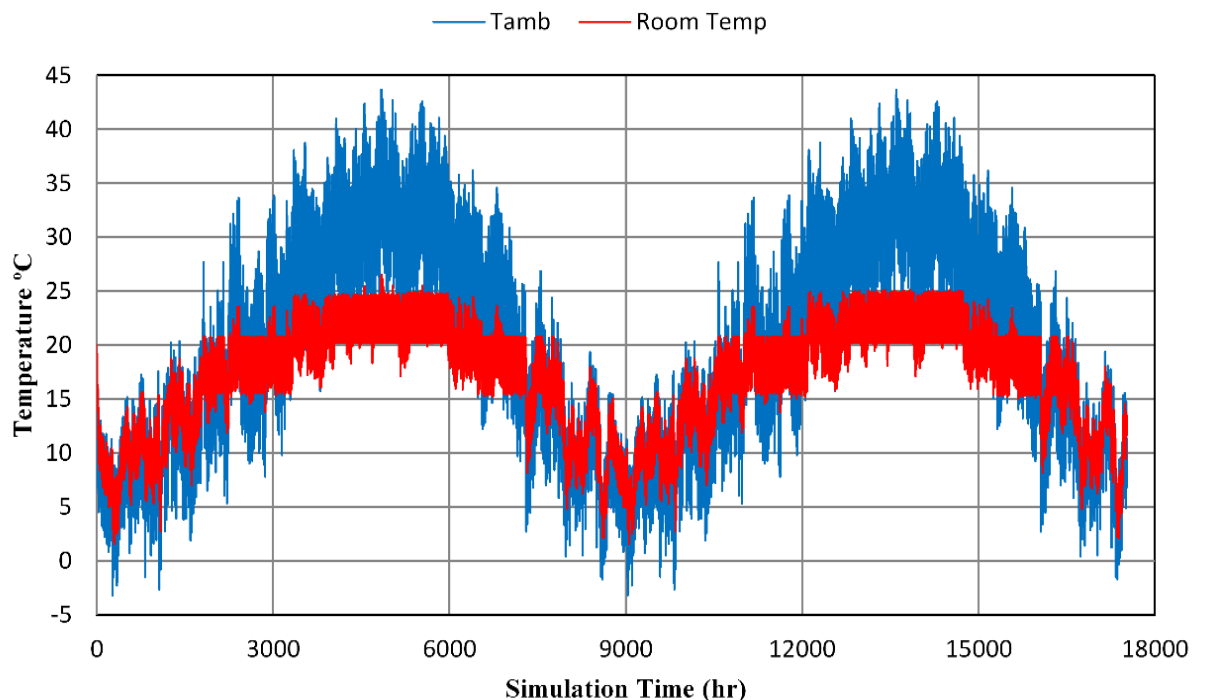


Figure 4.13 Ambient and room air temperatures during two years

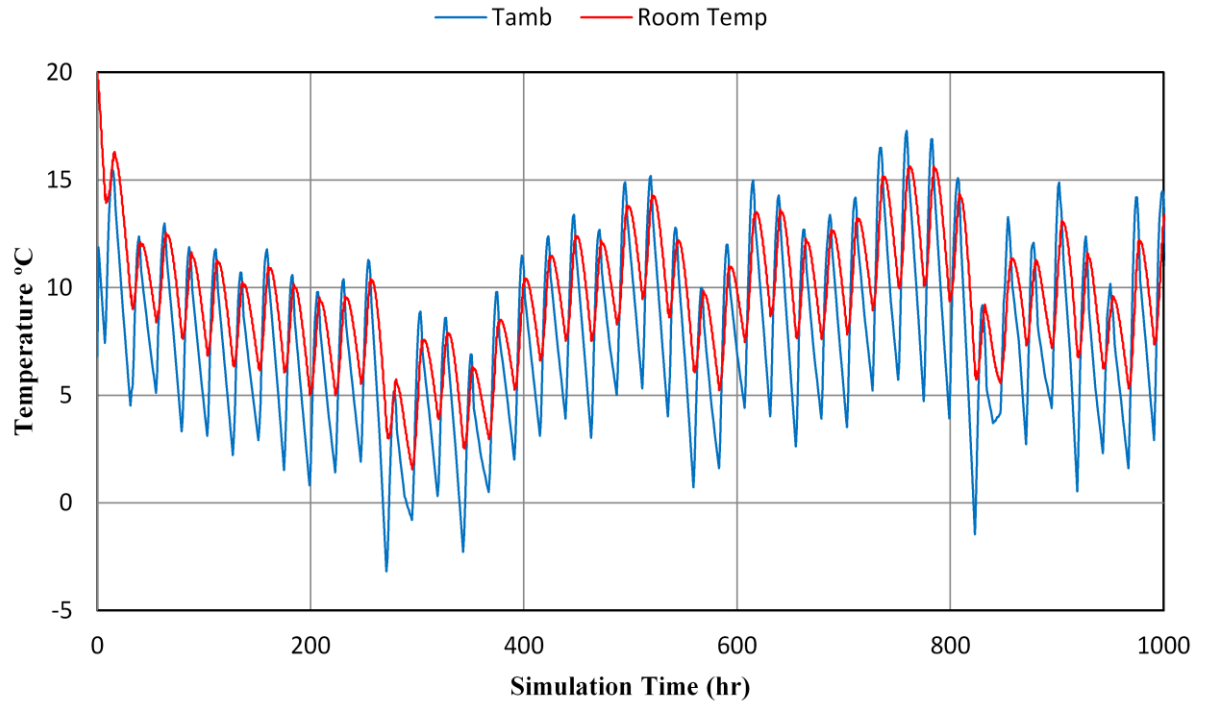


Figure 4.14 Ambient and room air temperatures during first period system OFF

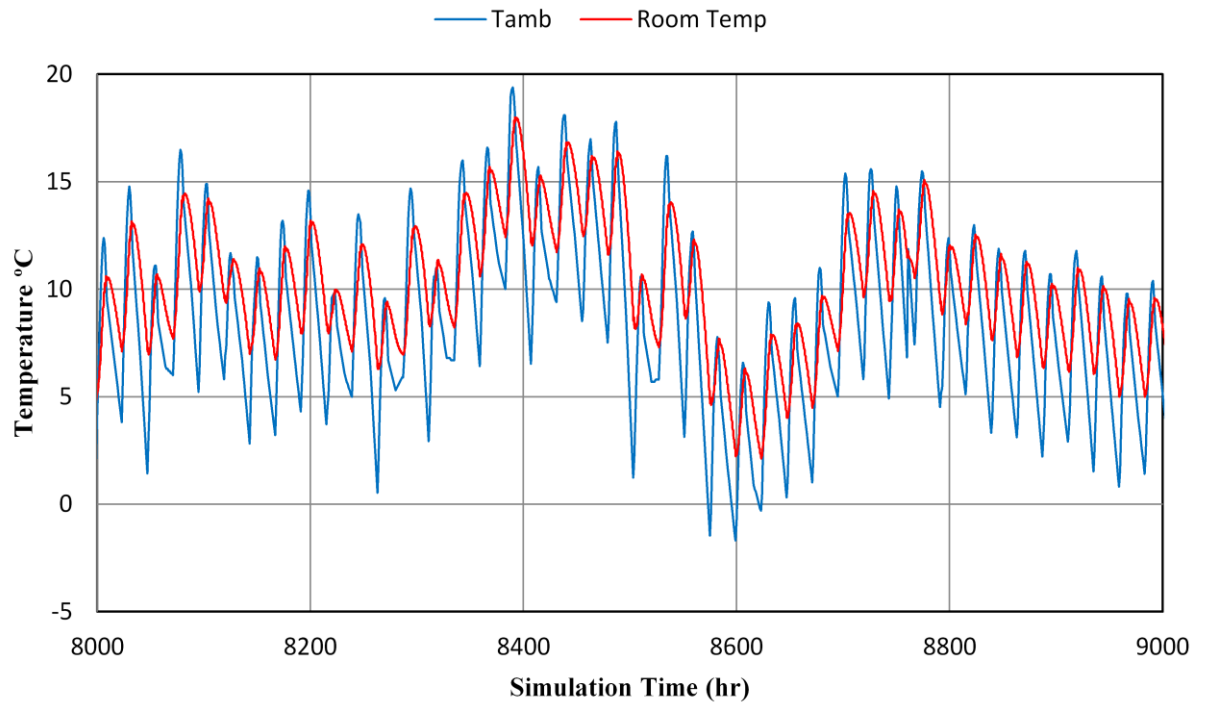


Figure 4.15 Ambient and room air temperatures during second period system OFF

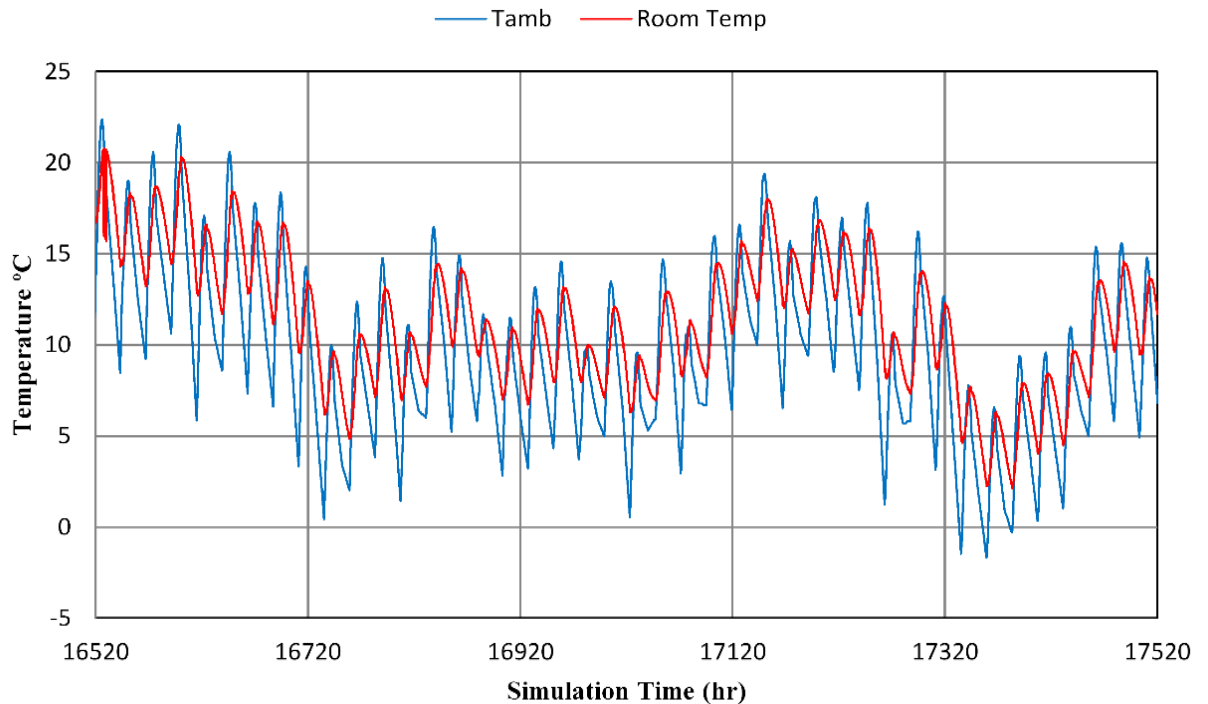


Figure 4.16 Ambient and room air temperatures during third period system OFF

4.11.3 Ambient and Chilled Water Outlet Temperatures

Figure 4.17 shows two years TRNSYS simulation output results of ambient temperature and chilled water outlet temperatures from the absorption chiller. In the second representative year, the chilled water outlet temperature is equal to the chiller set point temperature which is 7°C. This is because the chiller has the capacity to meet the current load, the chiller will modulate to meet the load and chilled water stream will leave at this temperature.

Again during winters, it might be incorrect to have a chilled water outlet temperature equal to or less than 5°C, which is less than the set point temperature. Figure 4.17 has three OFF periods, similar to Figure 4.13. These periods are shown in Figures 4.16, 4.17, and 4.18. These figures illustrate that when the all system is OFF, the chilled water outlet temperatures seem to be an average of the ambient temperature. It also noticed that the chilled water outlet temperatures lags behind the ambient temperature, and this lagging is increased from first period to the third period.

The behavior of hot water inlet and outlet temperatures, cooling tower inlet and outlet temperature, coil water inlet and outlet temperature, and water temperature are the same as behaviour of the chilled water outlet temperature.

To summarise, when the system is OFF, the TRNSYS output results will always relate to the pattern of the ambient temperature for air temperatures (room and coil air temperatures). The inlet and outlet water temperatures from any equipment in the system appear to be a moving average of the ambient temperature. The TRNSYS documentation does not explain how these temperatures are assigned when the system is OFF.

In Chapter five, the results will present the TRNSYS outputs when the system is ON and OFF for two years' simulation time.

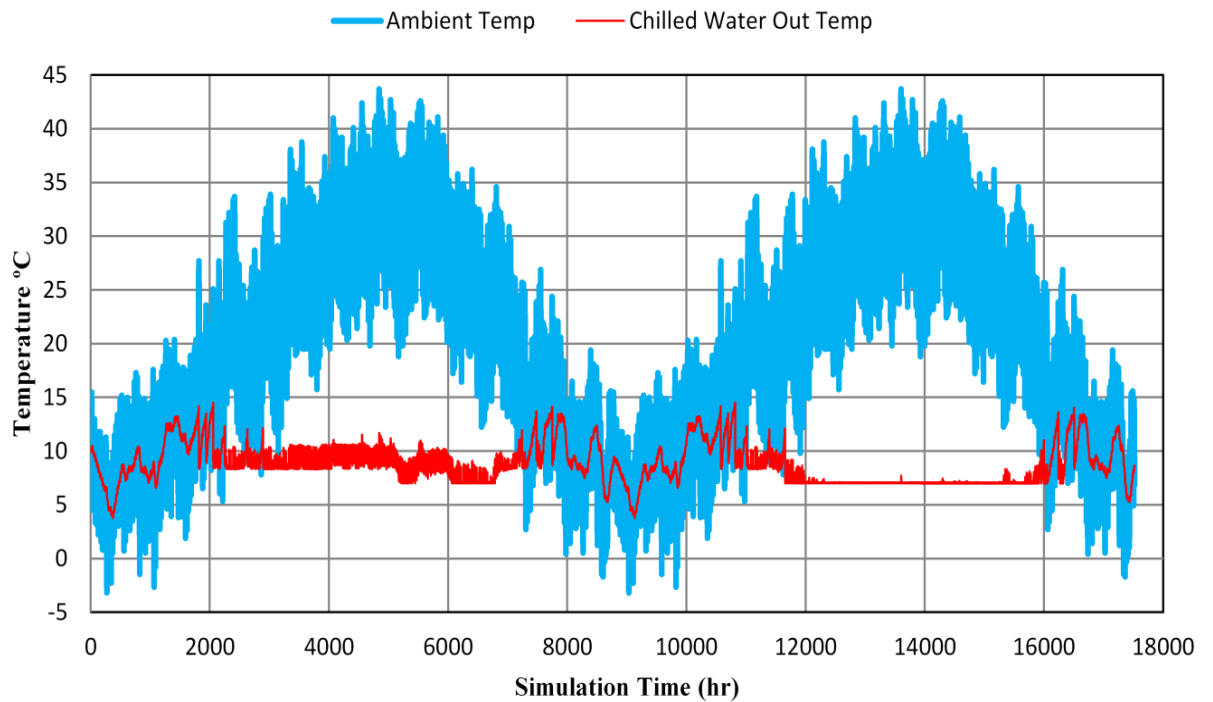


Figure 4.17 Ambient and chilled water outlet temperatures during two years

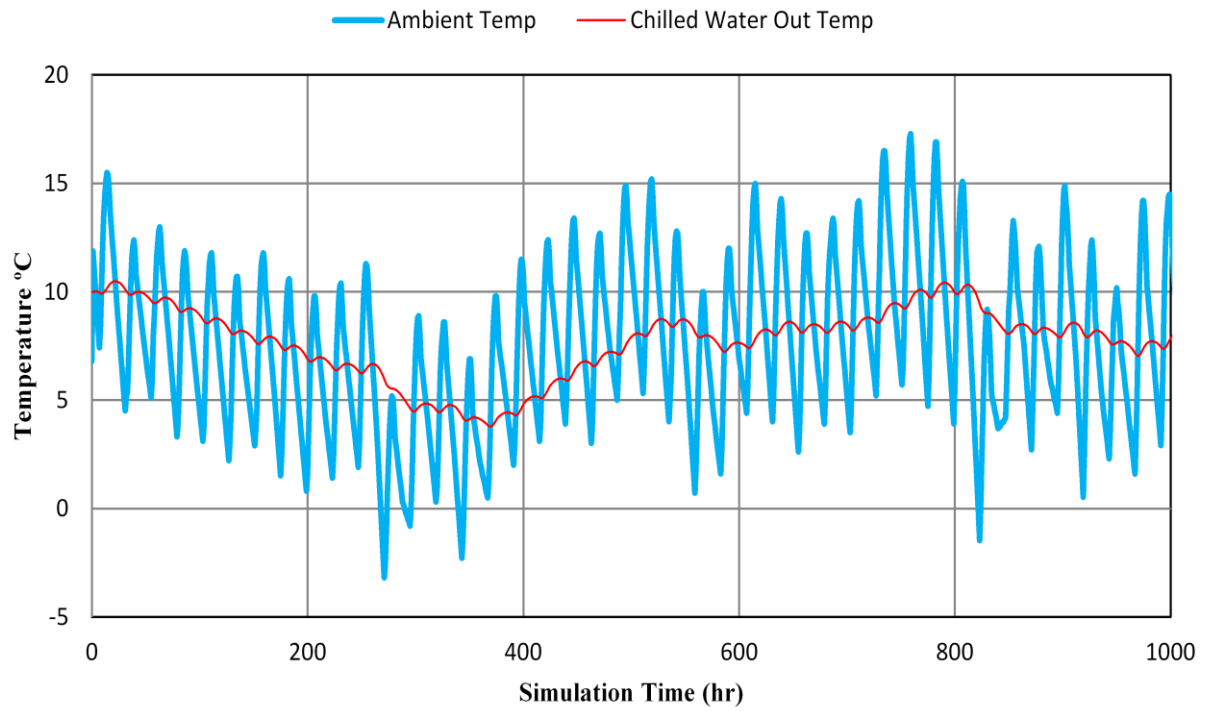


Figure 4.18 Ambient and chilled water outlet temperatures during first period system OFF

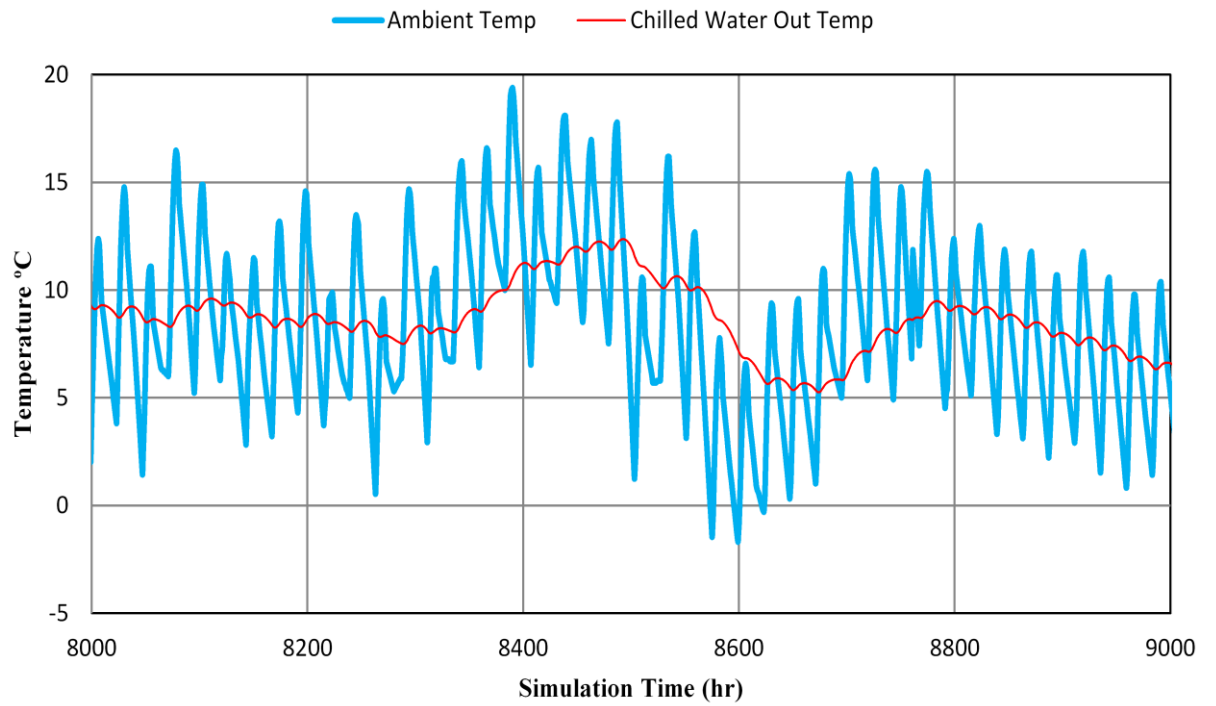


Figure 4.19 Ambient and chilled water outlet temperatures during second period system OFF

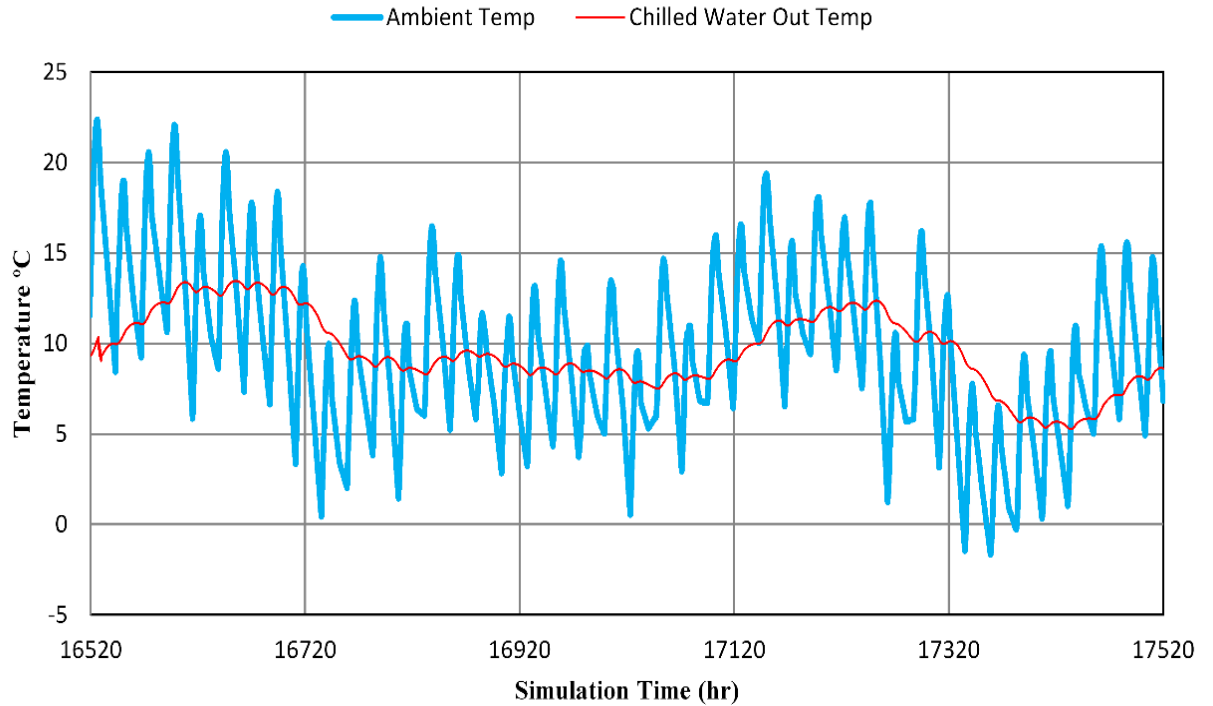


Figure 4.20 Ambient and chilled water outlet temperatures during third period system OFF

4.12 The Representative Year

The TRNSYS Simulation can be run for many years from the start year; however the least number of years will save computational time. The simulation was run for three years in order to select the representative year from the three years. Figure 4.21 shows the three years TRNSYS simulation output results of (TLCZ) the lower convective zone temperature and (TUCZ) the upper convective zone temperature. It can be seen that the first year is a warm up year, while the second and third year are very similar. Figure 4.22 shows the difference between TLCZ3 in the third year and TLCZ2 in the second year. It can be seen that the difference between TLCZ3 and TLCZ2 is small during the summer season (May to end of September). Therefore, the second year will be selected as a representative year, because the temperatures are similar to the third year and this choice will save the computation time. Most of the results in the thesis will be based on the second year as a representative year.

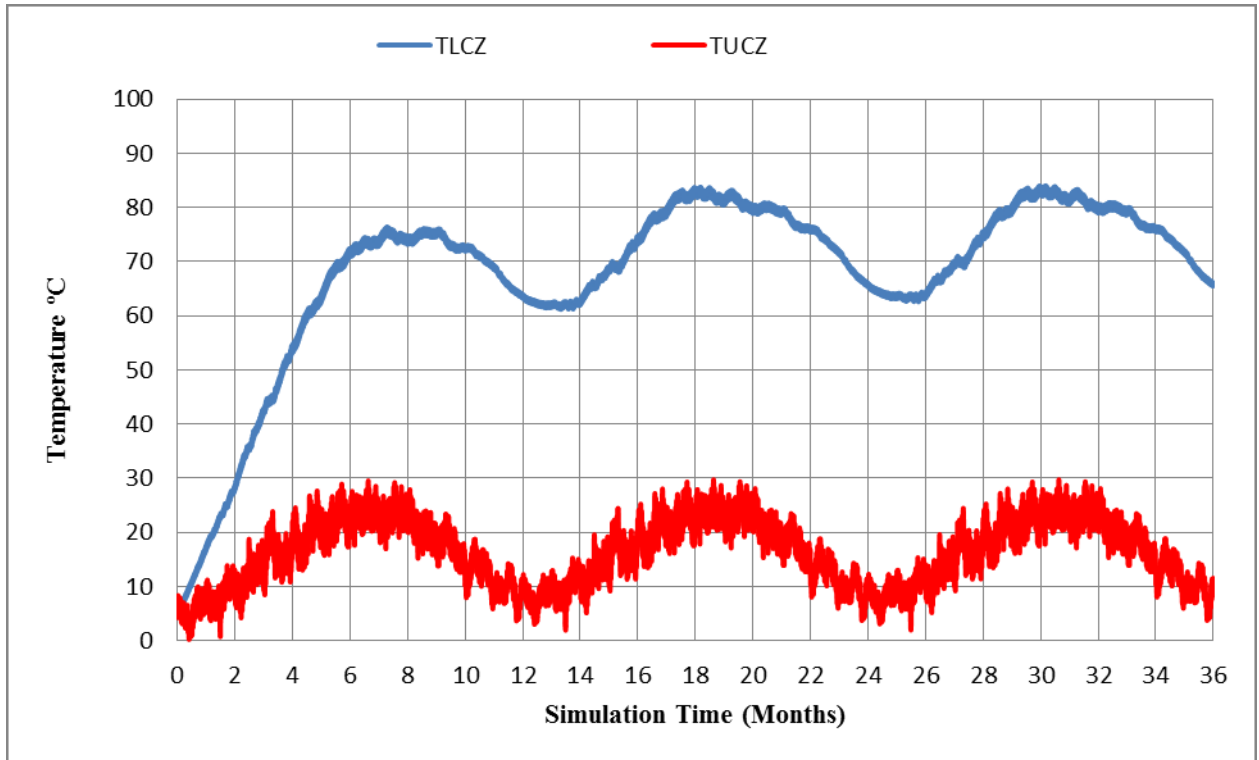


Figure 4.21 TLCZ and TUCZ for three year simulation time

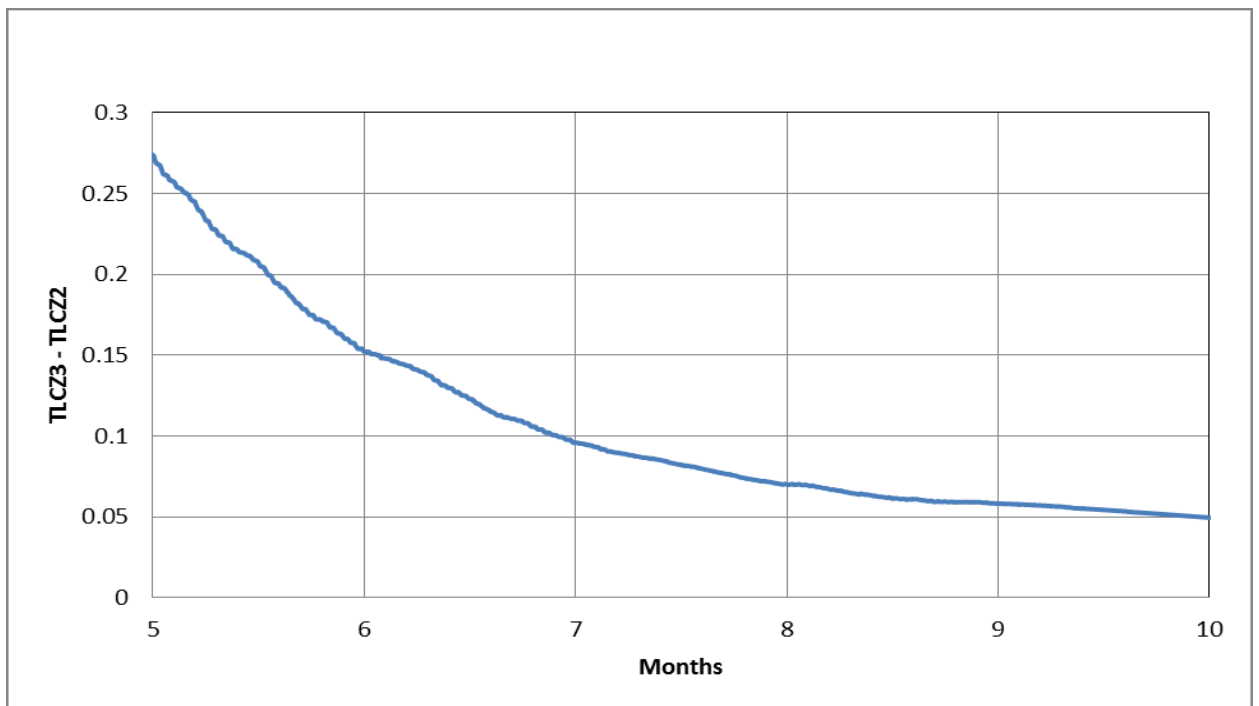


Figure 4.22 Difference between TLCZ3 (third year) and TLCZ2 (second year) for summer season

4.13 Conclusion

This chapter began with explanations of the mathematical model of a salinity gradient solar pond with the ground underneath it, absorption cooling system and building.

The solar radiation is modelled and its equation used as a source for the energy equation of the solar pond. The model equations have been solved numerically by using the finite-difference method. The problem has been solved by writing a MATLAB program.

The complete solar cooling system, including the absorption chiller, cooling coil, cooling tower, etc. and building have been simulated by TRNSYS. The solar pond cooling system components (Type) have been presented. A coupled simulation between MATLAB and TRNSYS has been explained. Finally, when the system is off, the sample of output results from TRNSYS simulation has been described.

Chapter 5. Results and discussion

5.1 Introduction

This chapter describes the simulation results of the salinity gradient solar pond, absorption cooling system and building. The first section deals with the feasibility and sizing of the base case of the solar pond absorption cooling system. The second section deals with the validation of the solar pond, absorption chiller and energy balance for the system. This chapter further describes the effect of varying parameter values on the system performance. The parameters under study are: solar pond area, ground conditions and solar pond layer thickness.

In this chapter, Figure axes are not calendar months, but artificial months of equal length, each month has 730 hours/month. Which is $\frac{365 \text{ days/yr} \times 24 \text{ hrs/day}}{12 \text{ months/yr}}$.

5.2 Feasibility and Sizing of the Base Case

The methodology design procedure used in this research started with creation of a building model of a typical single family house in Baghdad, Iraq as described in Chapter Four. The building model was imported in to TRNSYS and was assigned typical materials, heat gains, and inside operational conditions to calculate the cooling load. According to the cooling load a solar thermal cooling system was designed and connected to the building model to maintain the desired set point during the peak summer time. An important system performance criterion is that it would be designed to meet the cooling load without an auxiliary energy source, other than electricity for pumps; fan etc. The system design was adjusted by trial and error to minimise the component sizes while maintaining the desired performance. This was done by changing system parameters and repeating simulations till find the best parameter values to achieve maximum efficiency of the system. The final results are presented for the system.

According to section 3.5, the building peak cooling load is 21 kW as shown in Figure 3.8. Therefore, the absorption chiller capacity was chosen to be 24.64 kW (7 TR tons of refrigeration) to be sufficient for thermal comfort during the peak summer season. Once the chiller capacity has been set, every pump/fan flow rate and HVAC unit capacity has to be set according to the chiller type's design requirements. The heat

input required to drive the absorption chiller was 35.14 kW. As will be described later in the section 5.4.1, it was found that a solar pond area of approximately 400 m² is required to produce heat input to the absorption chiller and provide satisfactory cooling for the house with a floor area of approximately 125 m².

The simulation was run for two simulated years to allow the system to approach its long-term performance. The second year (representative year) results are adopted because the first year was assumed to be a warm up year. The simulation started from 1st of January in the first year. In TRNSYS a 300 sec time step was used, which was the same time step as for the solar pond MATLAB code. The short time step can be useful as it may be necessary for computational stability in the simulation and it can be used to simulate the dynamic response of the systems that respond faster in seconds or minutes.

5.2.1 Solar Pond

Temperature Profile

The TRNSYS-MATLAB simulation outputs include the lower convective zone temperature (TLCZ), upper convective zone temperature (TUCZ), salt concentration distribution and ground temperature profile. The base case pond area is 400 m² to meet the building cooling load. Figure 5.1 shows the lower convective zone temperature, upper convective zone temperature and ambient temperature during two simulation years, starting from 1st of January.

It is clear that the zone temperatures vary with the simulation time of the two years, depending on the outside air temperature and incoming solar radiation. The temperatures of the zones generally increase with increase in the incident solar energy per unit area. For the zones, the temperature of the UCZ is observed to be a maximum of 29.7°C in July in the second year. Similarly, the temperature of the LCZ is observed to be a maximum of 83.8°C in July in the second year while the ambient temperature is observed to be a maximum of 43.7°C in July.

UCZ temperature close to ambient in winter, but lower in summer. As expected, since ambient relative humidity is high in winter and low in summer hence evaporation is low in winter and high in summer.

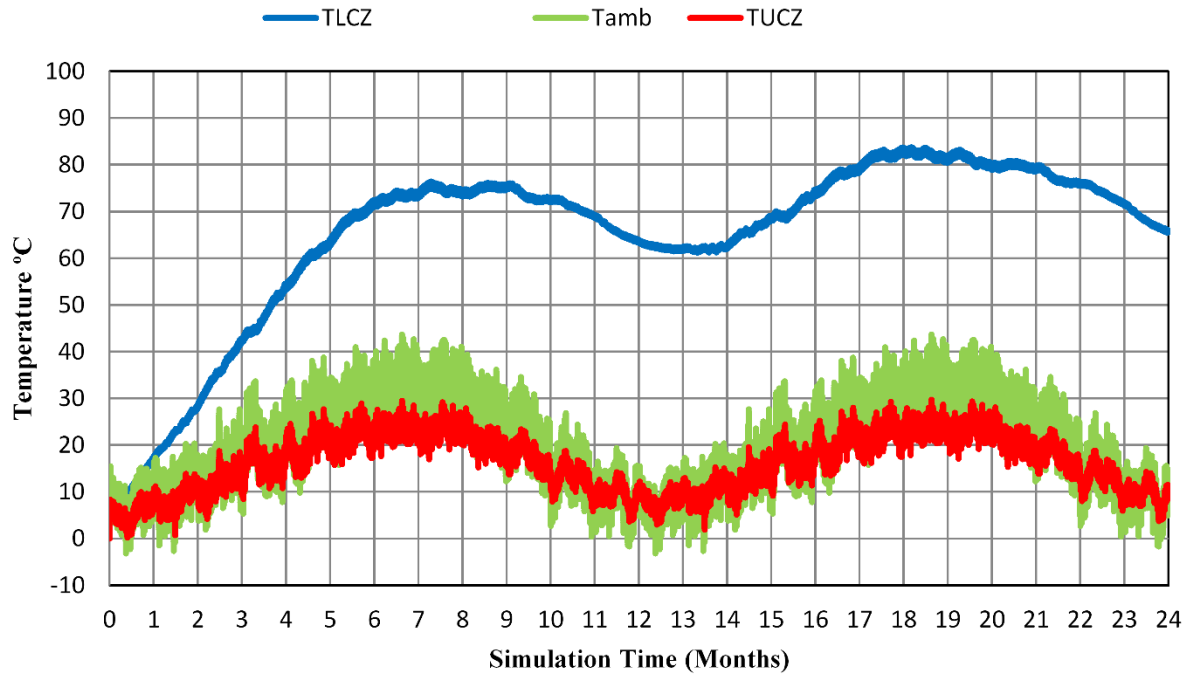


Figure 5.1 Pond lower and upper zones temperature with ambient temperature with simulation time

In the first simulation year, starting from 1st of January, the LCZ temperature reaches 70°C during June. This temperature is the minimum required temperature to drive the Yazaki absorption chiller. In the second year, the LCZ temperature reaches 70°C at the beginning of April. In addition, during the second year, it was found that the LCZ temperature range was 61°C to 83.8°C in January and July respectively. Therefore, the first year was considered to be a warm-up time of the solar pond and the second year was considered as a representative year of the solar pond results.

According to the range of LCZ temperature achieved during the second simulation year, the salinity gradient solar pond could be used to drive an absorption chiller and produce cool air for a single family house during the summer period in Iraq.

The temperature distribution of the solar pond and ground as a function of the depth at the end of January, April, July, and October in the second year are shown in Figure 5.2. The ground water table is assumed to be at 5 m depth, with a constant temperature of 25°C which is close to the annual average ambient temperature of Baghdad (Hussen et al., 2010). The UCZ temperature is found to be 22°C at the end of July. It is observed that, as intended, the temperature increases with depth in the gradient zone (NCZ). The LCZ temperature at the end of July is found to be 83.8°C. The temperature profile of soil underneath the solar pond is also shown in the Figure 5.2.

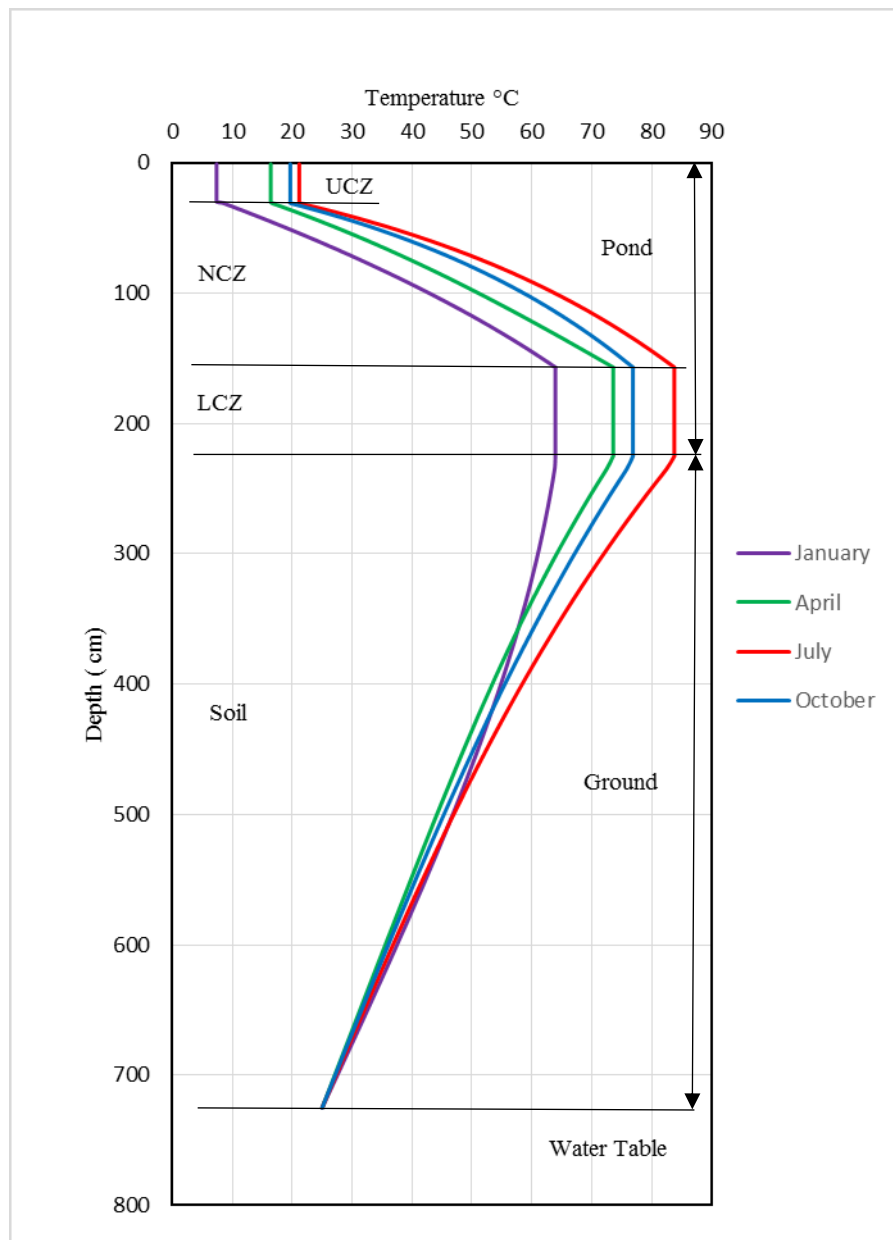


Figure 5.2 Temperature distribution for a solar pond and the ground underneath at the end of January, April, July, and October in the second simulation year

The monthly average solar pond efficiency for the second year is shown in Figure 5.3. The solar pond efficiency is defined as the monthly average pond heat extraction divided by the monthly average incident solar radiation. The calculated maximum efficiency for the solar pond is 19.5 % in July in the second year. This general pattern is as would be expected from the heat extraction and incident solar radiation in Figure 5.5 and Figure 1.3. Figure 5.1 shows that the pond takes several months to warm up, so heat storage is significant in the lower convective zone.

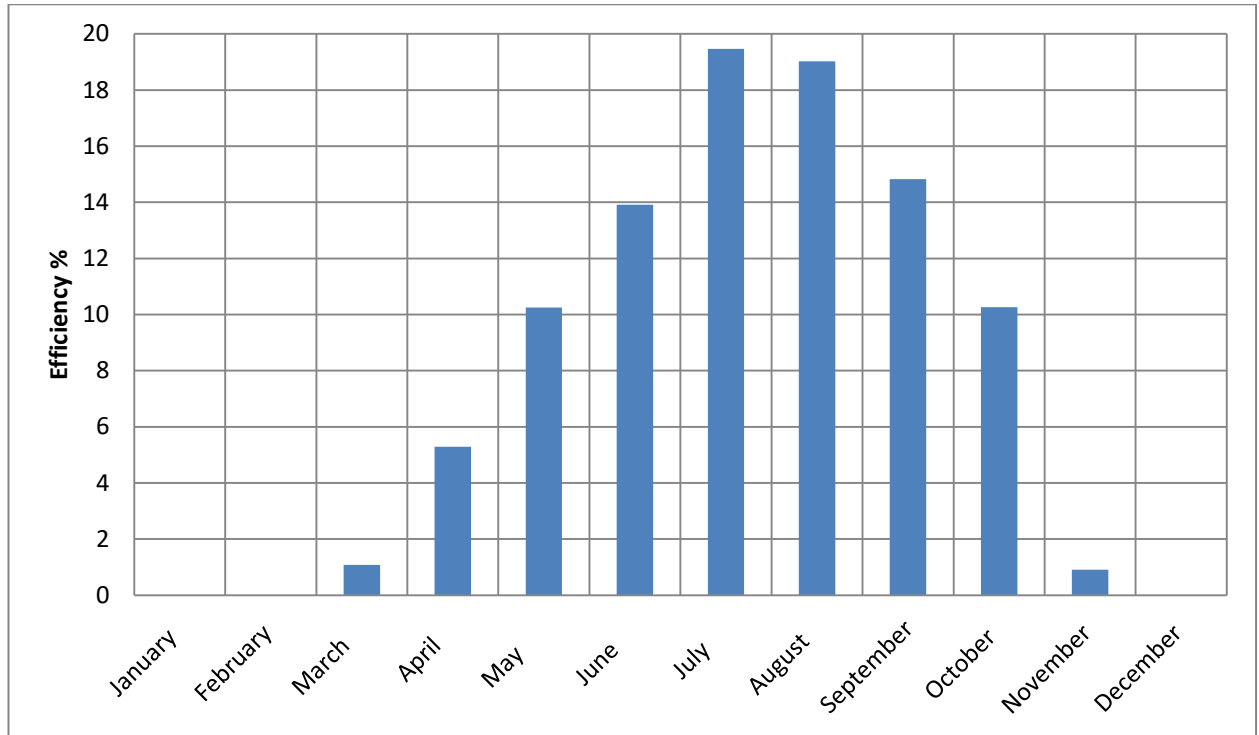


Figure 5.3 Solar pond monthly average efficiency for the second simulation year

Salt Concentration Profile

The salt concentration is designed to be low in the UCZ, high in the LCZ, and to vary linearly in the NCZ. Figure 5.4 shows the salt concentration profile of the solar pond over 5 years, assuming no maintenance except replacing evaporation loss from the UCZ, disturbances or water movement. It may be seen that the salt concentration gradually tends to become uniform with depth. This is because of the diffusion of salt inside the pond from high concentration to low. If this phenomenon is permitted in reality, the stratification of the NCZ layer will be disturbed. Therefore the salt

concentration of the solar pond needs occasional maintenance by flushing the UCZ with water and adding saturated brine to the LCZ.

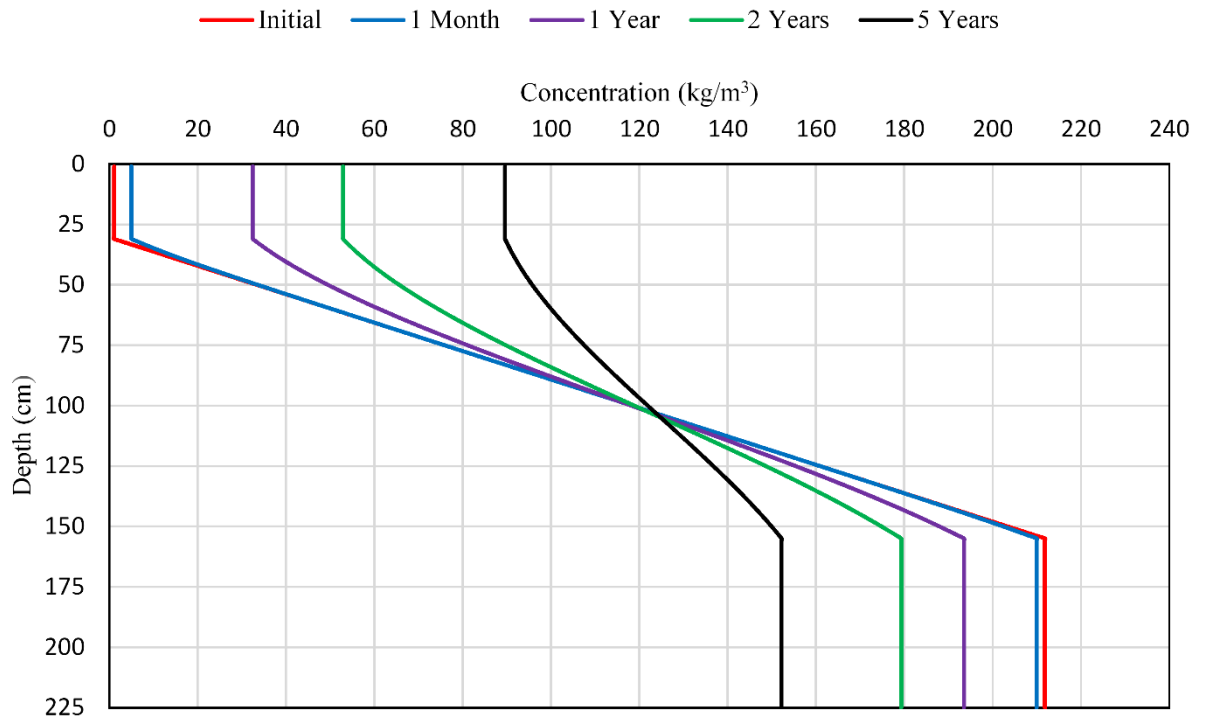


Figure 5.4 Concentration profiles of the solar pond for a month to five years

5.2.2 Heat Extraction

The pond heat extraction method used in this project is pumping of the hot brine from the top of the LCZ through an external heat exchanger and then returning the brine at a reduced temperature to the bottom of the LCZ. The velocity of the brine being pumped needs to be regulated to prevent erosion of the gradient layer.

The useful heat extraction from the solar pond is shown in Figure 5.5. The average heat extraction from the pond is 80 W/m^2 which is about 17.5 % of the average insolation on the pond surface during the summer (June, July and August) of the second year.

The outlet hot brine temperature from the pond was assumed to be equal to LCZ temperature. The pond outlet and inlet temperatures are shown in Figure 5.6. It can be seen that the temperature difference between outlet and inlet is $4\text{-}5^\circ\text{C}$ when the system is ON. The difference in temperatures is reasonable for heat exchanger design.

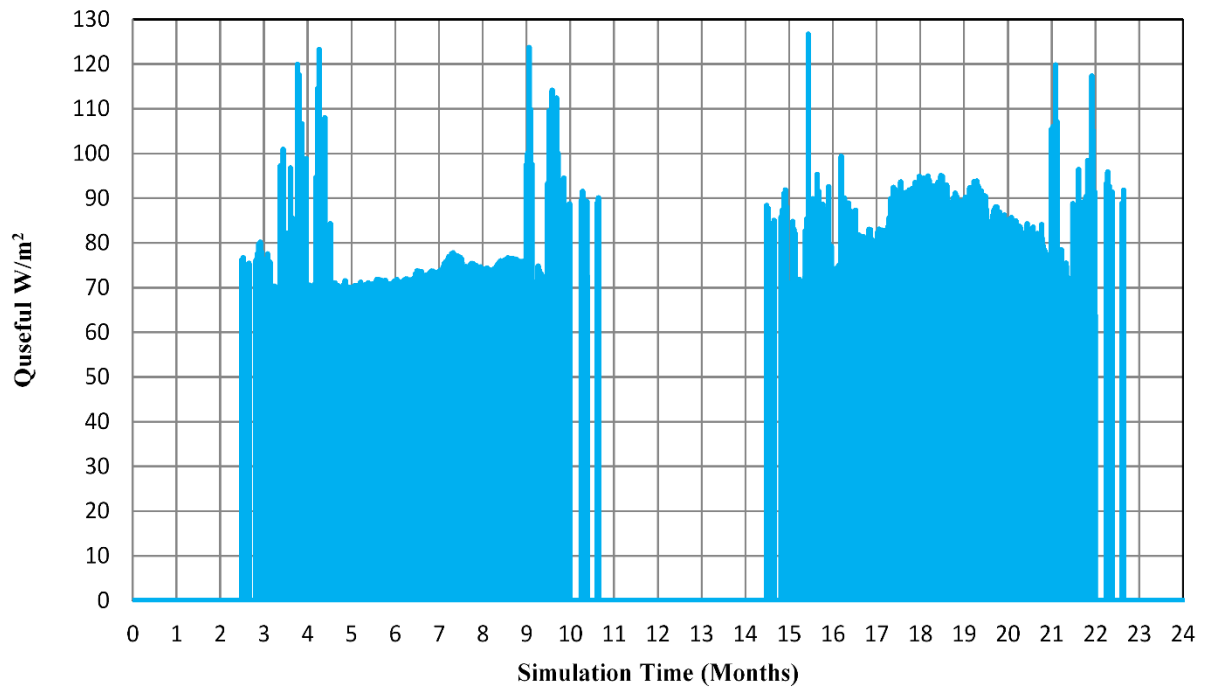


Figure 5.5 Heat extraction from the solar pond

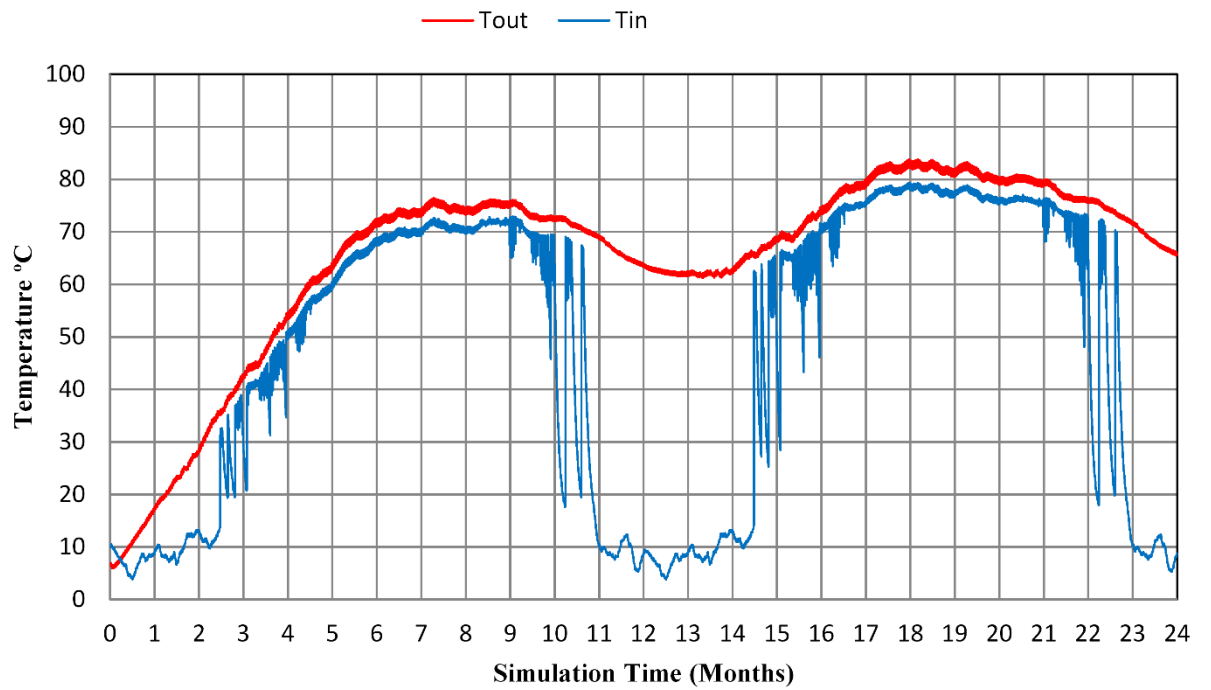


Figure 5.6 Pond outlet and inlet temperatures

5.2.3 Hot Water Inlet Temperature

In the solar pond and heat exchanger loop, the hot brine is withdrawn from the solar pond and pumped it through the external heat exchanger. After that, in the heat exchanger and chiller loop, the output hot water from the heat exchanger is used as an input to the chiller. The hot water inlet temperature is one of the key system variables, because it will drive the chiller and enable it to meet the load. In this project, an absorption chiller is used. 70°C to 95°C is the hot water inlet temperature range required to made the chiller work at its design conditions

The hot water inlet temperature to the absorption chiller is shown in Figure 5.7. It is clear that the hot water inlet temperature only exceeds 70°C for a short period of time during the first year, whereas, the hot water inlet temperature is 70°C- 80 °C most of the summer time during the second simulation year, which is sufficient to make the chiller work properly.

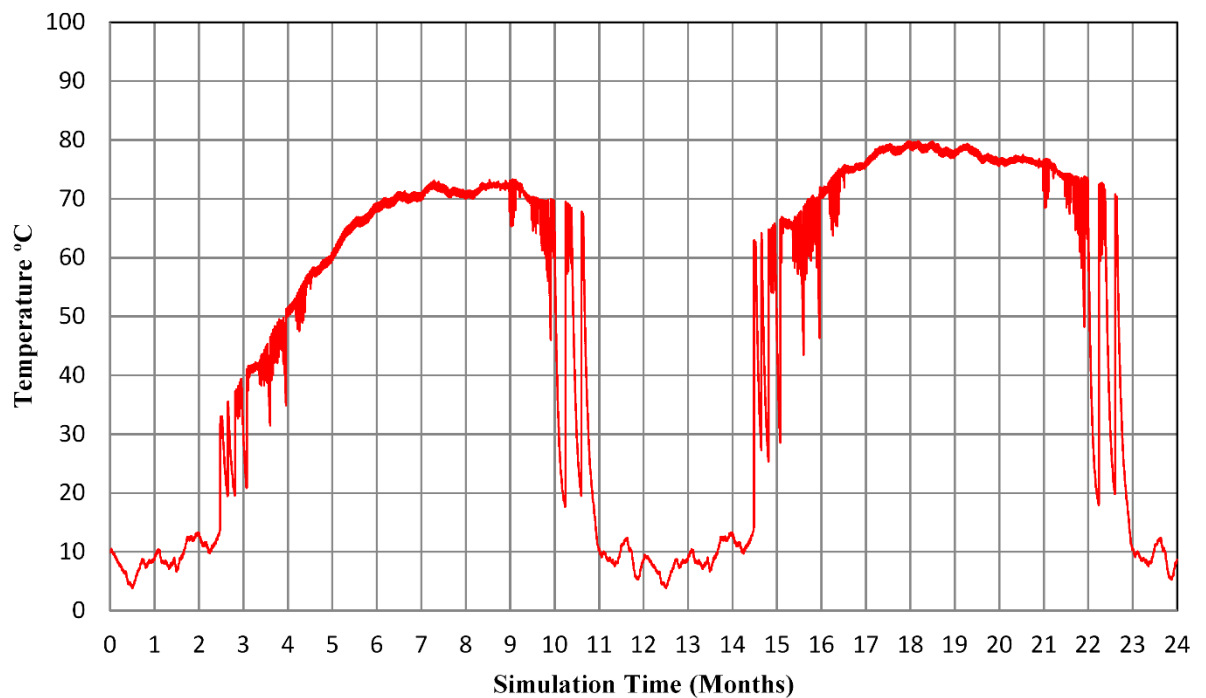


Figure 5.7 Hot water inlet temperature to the absorption chiller

5.2.4 Absorption Chiller

When the hot water inlet temperature is in the range of 70°C to 95°C, and heat energy input is sufficient to drive the chiller at design conditions, then the chilled water outlet temperature will match the set point temperature (7°C). The chilled water outlet temperature is shown in Figure 5.8. It was explained in Chapter Three, that the chiller is controlled by ON and OFF control (thermostat). When the chiller is OFF, the chilled water outlet temperature from TRNSYS follows the ambient temperature, and may become below the set point temperature.

Figure 5.8 show that the chiller is able to meet the load for almost all the time in the second summer.

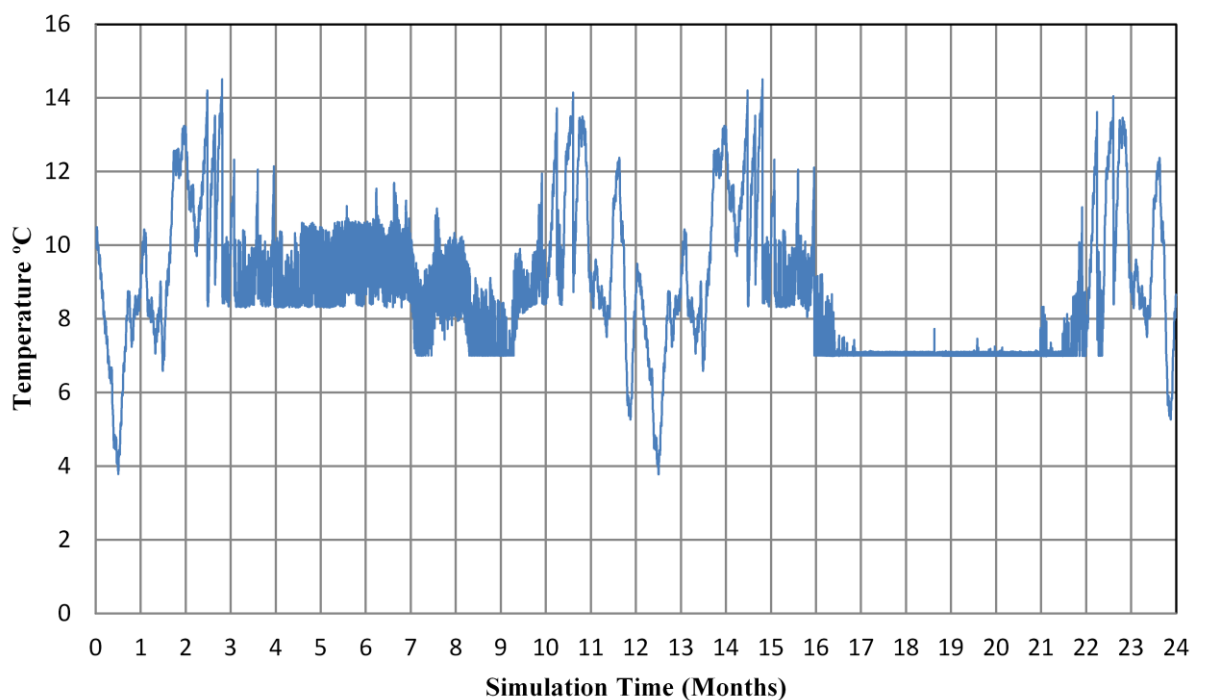


Figure 5.8 Chilled water outlet temperature

The chilled water inlet and outlet temperatures are shown in Figure 5.9. It is noticed that the maximum chilled water inlet temperature during summer of the second year is close to 12.5°C, which is the manufacturer's design inlet temperature. The chilled water inlet temperature for the first year is often over 14°C, which is higher than the design temperature. This is because the hot water inlet temperature is less than the required chiller inlet temperature. Therefore, the chiller is unable to meet the load.

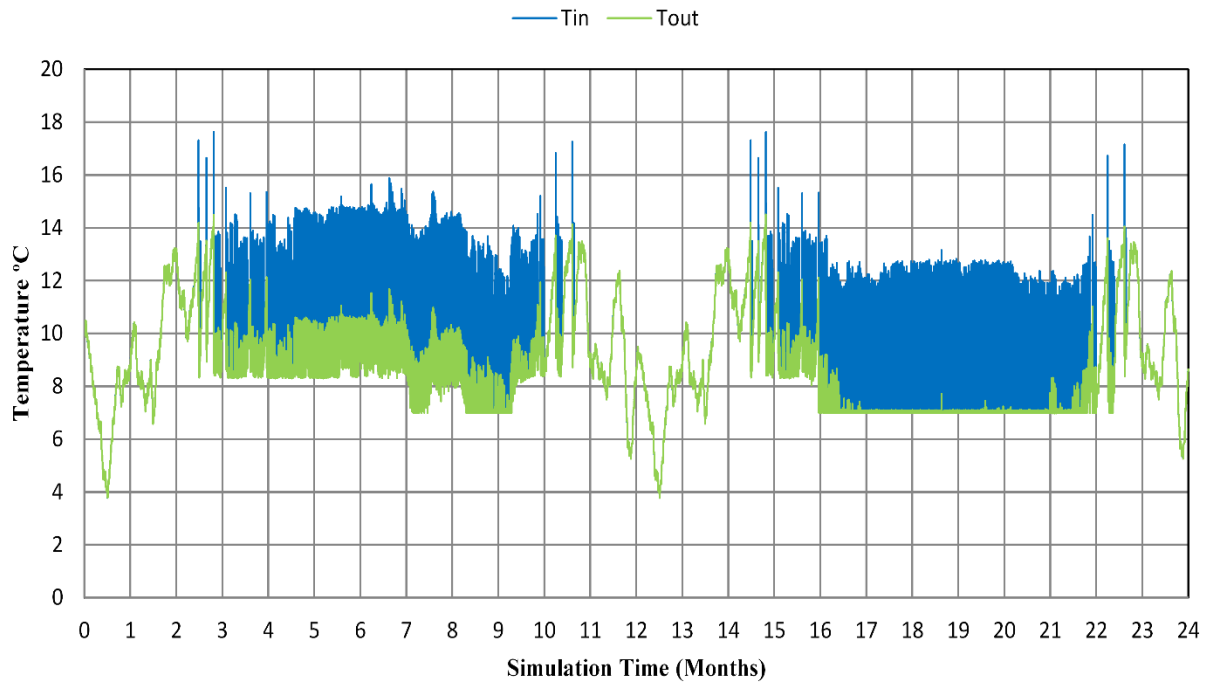


Figure 5.9 Chilled water inlet and outlet temperatures

Figure 5.10 illustrates the coefficient of performance for the absorption chiller. The averaged value of the COP is found to be 0.67 during the summer of the second year. This is a reasonable value of actual COP when compared with the chiller rated COP of 0.7. It is observed that COP may be higher than the rated COP at the beginning of spring and late autumn; this is because the COP depends on water temperatures and load, and can may be more than 0.7 under low load conditions.

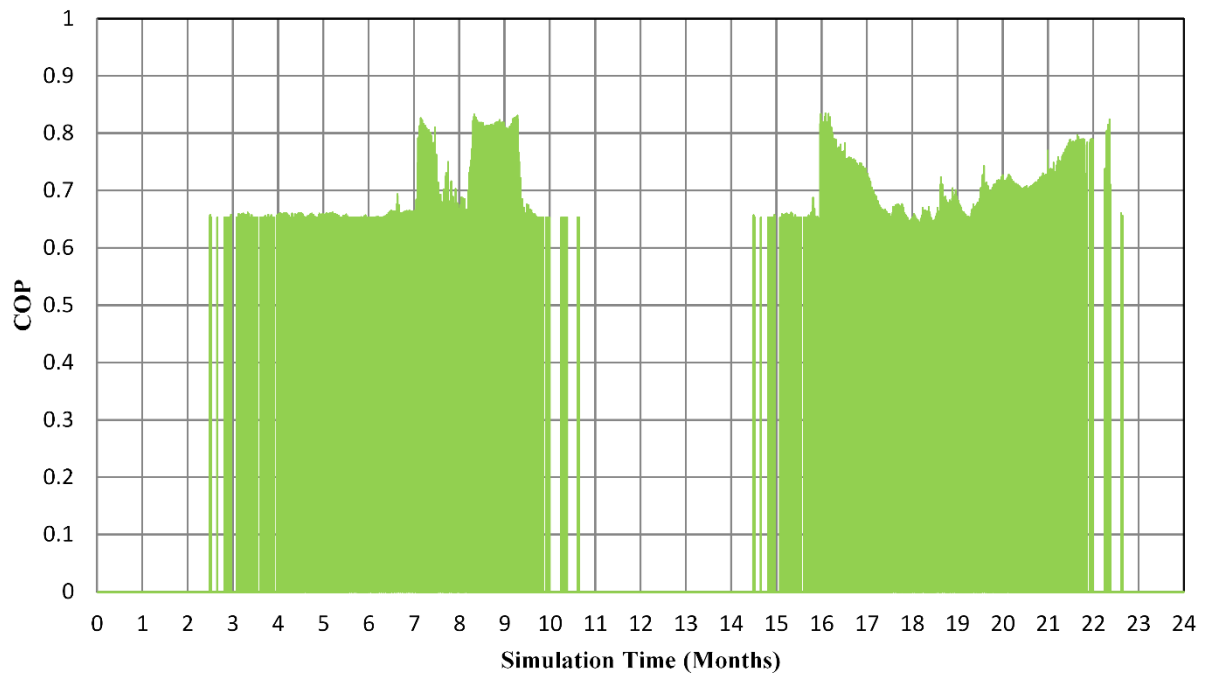


Figure 5.10 Coefficient of performance for the absorption chiller

5.2.5 Room Air Temperature

For building thermal comfort, the room temperature is maintained by the fan air controlled by an ON-OFF thermostat. The cooling system is sized so that the room temperature is always under thermostatic control (less than 25°C) during the summer season. The room temperature and ambient temperature for two years are shown in Figure 5.11. As intended, the maximum room temperature is equal to or below 25°C in the months of May, June, July, August, and September during the second year. In winter, there is no heating and no cooling in the simulation; the room temperature is higher than the ambient temperature, due to the effects of solar and internal heat gains and building thermal capacity.

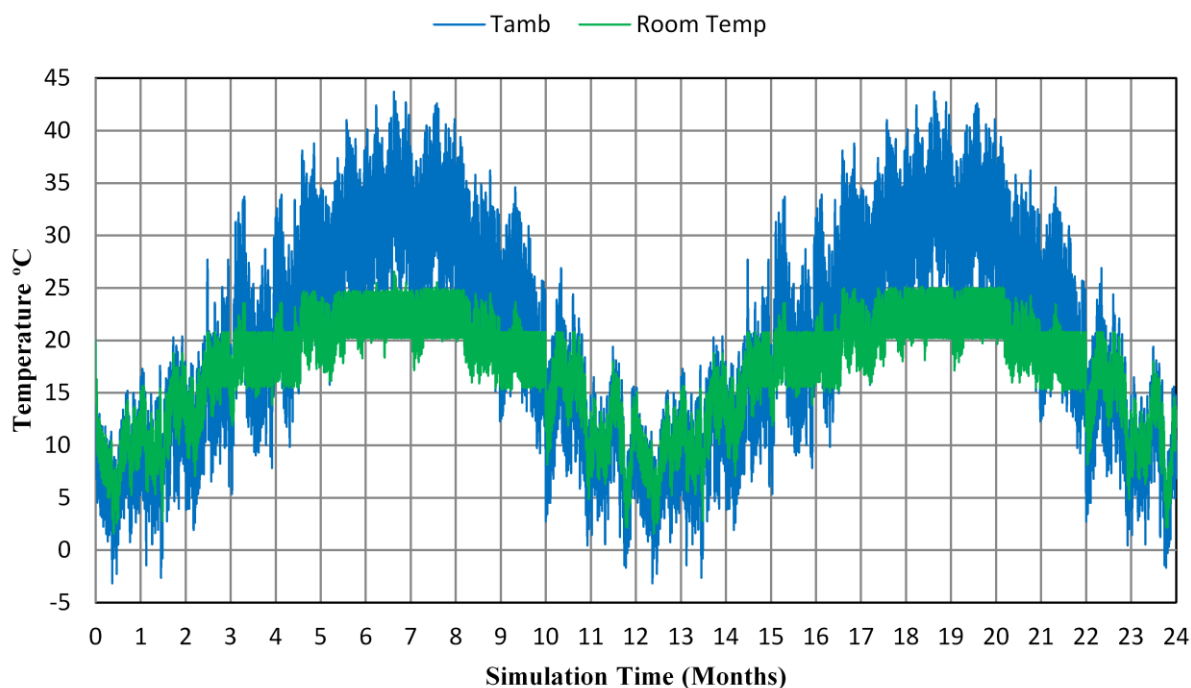


Figure 5.11 Ambient and room air temperatures for two years

5.2.6 Cooling Coil Air and Water Temperatures

A conventional cooling coil model is used in TRNSYS to model building air cooling through chilled water from an absorption chiller. The cooling coil air cools down as it passes across a coil containing a cooler fluid. The cooling coil inlet and outlet air temperatures are shown in Figure 5.12. It was found that the average inlet air temperatures are 23.6°C and the average outlet air temperature is 14.4°C.

The cooling coil inlet and outlet water temperatures are shown in Figure 5.13. During summer of the 2nd year, the average inlet water temperature to the coil is approximately 7°C, which is same as the chiller set point temperature. The average outlet water temperature from the coil is approximately 12.5°C, which is the chiller design inlet temperature. These results are as expected from the system layout.

The maximum cooling coil total heat transfer rate is 24.22 kW which is close to the chiller design capacity as expected.

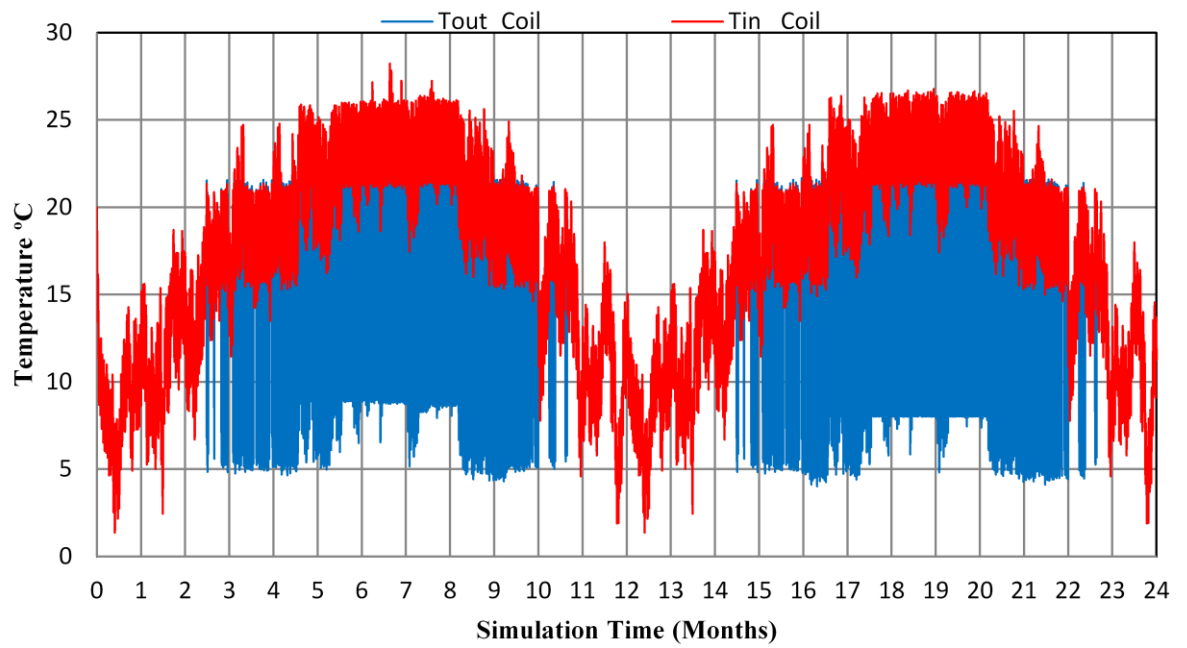


Figure 5.12 Inlet and outlet air temperature for cooling coil

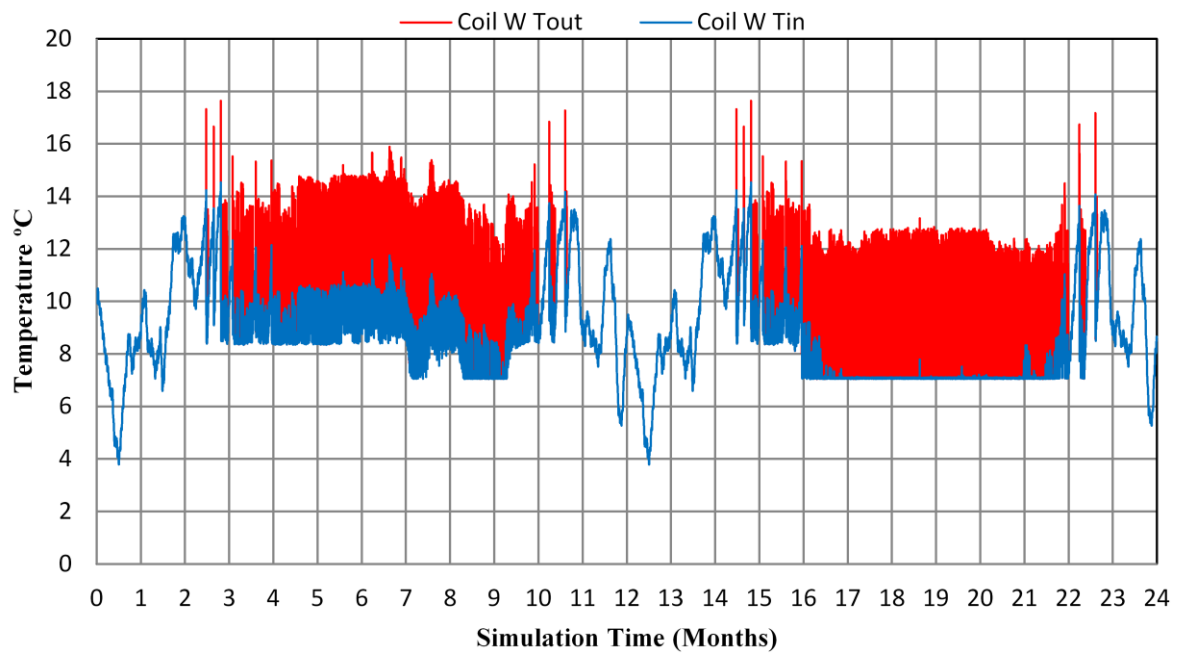


Figure 5.13 Inlet and outlet water temperature for cooling coil

5.2.7 Cooling Tower

The counter flow induced draft cooling tower model T-220 is selected from CTS cooling tower systems, Inc. with rated capacity of 70.4 kW to meet the heat rejection duty (60 kW) at the system design conditions. The cooling tower inlet and outlet temperatures are shown in Figure 5.14. The maximum water inlet temperature is 30.5°C at (13600 hr) in July 2nd year simulation time. The water outlet temperature for the same time is 26.5°C and the wet bulb temperature is 22.5°C. The maximum heat rejected by the cooling tower is 60 kW as expected.

The heat rejected by the cooling tower is equal to the heat input from solar pond to the absorption chiller, heat absorbed from the air in the room, and any energy gain by the system. The energy balance for absorption chiller, which include heat input from pond to the chiller and heat rejected by cooling tower, is described in Appendix B.

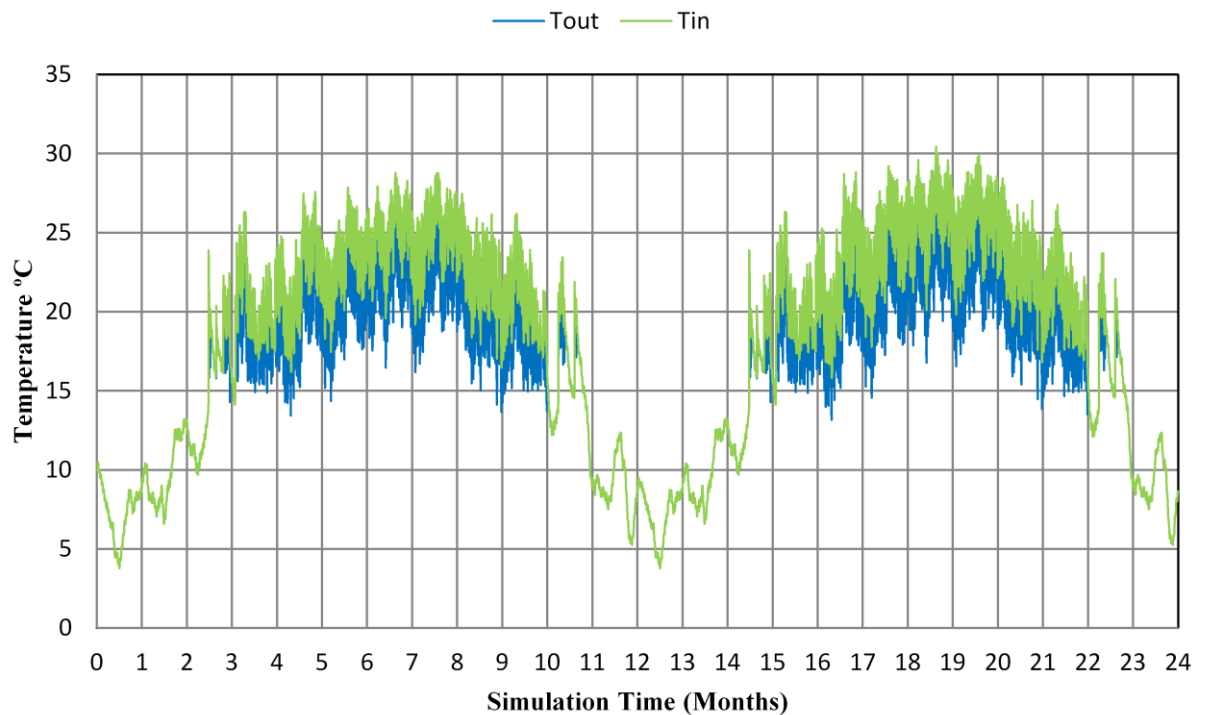


Figure 5.14 Inlet and outlet water temperatures of the cooling tower

5.3 Validation

5.3.1 Introduction

In this section, validation of the salinity gradient solar pond model is carried out. The experimental data for the solar pond temperature distribution represented by Leblanc et al., (2011) was compared to the corresponding numerical results of this study, in order to validate the accuracy of the model. The simulation results of the absorption chiller is also validated with performance data for a commercially-available absorption chiller. Finally, the solar pond cooling system simulation is validated by the energy balance of the system.

5.3.2 Validation of the Solar Pond Model

Validation of a model of a system is the act of comparing some output data from the model with reference data and drawing conclusions from this comparison. Although most models are based on physical laws and material properties, modellers need some experimental data to test the model's predictions. The comparison is used to establish confidence that the model can be used to predict performance where experimental data does not exist. An advantage of modelling is the ability to perform parameter optimisation, which is difficult to do through experiments; however, a validated model allows optimisation with confidence at minimal cost (Kennish, 1978). Due to the absence of experimental studies for a solar pond cooling system, it was decided to validate solar pond and cooling system separately.

The simulated temperature distribution in the solar pond from the MATLAB code was validated with experimental data from the Bundoora solar pond (Leblanc et al., 2011). The reasons to choose the Bundoora experimental salinity gradient solar pond for validation are the small surface area of 53 m², and the level of water in the pond is fixed at 2.05 m from the bottom using an overflow system. The depth of the pond was expected to be close to the current simulation pond model. Table 5.1 shows the differences between the Bundoora pond and the current simulation pond model. The simulation was performed for the period from January 2007 to February 2008. Weather data was obtained from Surface meteorology and solar energy (2016). Figure 5.15 shows the simulated and experimental temperature distributions in the solar pond on 1st February 2008; it can be seen that they are in good agreement. In consequence,

the model is considered a useful tool to predict the performance of the pond and to determine the hot water outlet temperature which is used to drive the chiller.

	Bundoora	Current Simulation Pond Model
location	Bundoora, Melbourne, Australia.	Baghdad, Iraq
hemisphere	Southern hemisphere	Northern hemisphere
area	53 m ²	400 m ²
depth	2.05 m	2.25 m
UCZ	0.15 m	0.3 m
NCZ	1.34 m	1.25 m
LCZ	0.56 m	0.7 m

Table 5.1 The Bundoora experimental pond and current simulation pond model

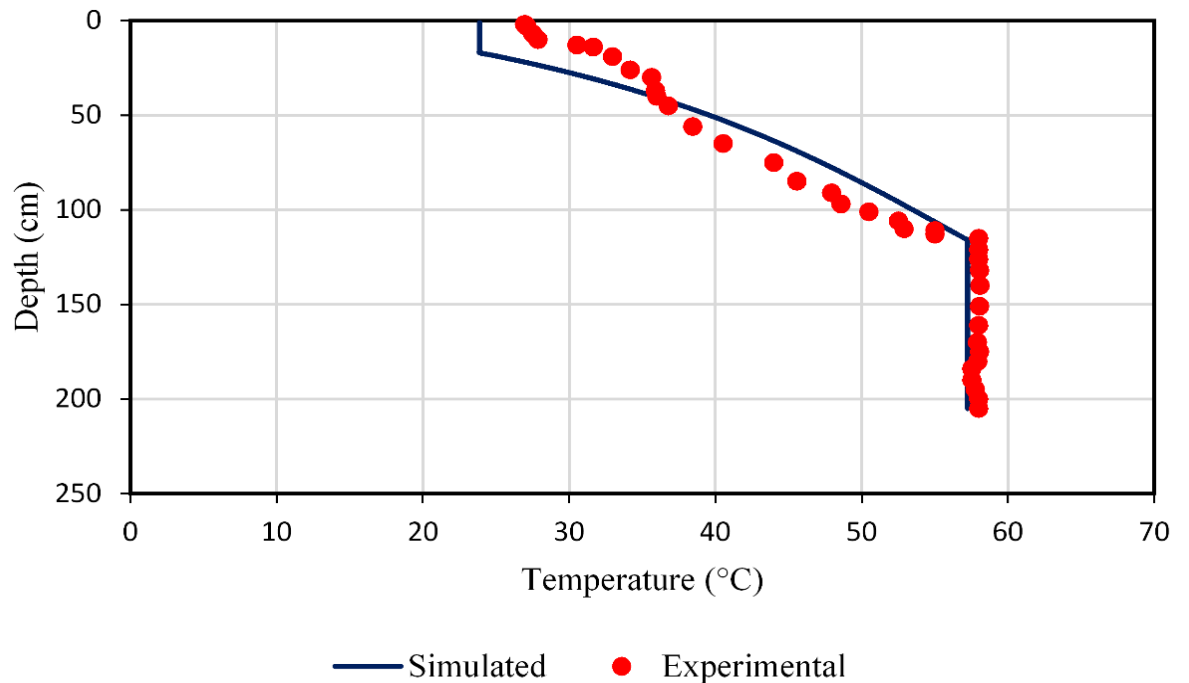


Figure 5.15 Simulated (MATLAB code) and experimental (Leblanc et al., 2011) temperature distributions for Bundoora solar pond on 1st February 2008

A validation has also been done with experimental data from the El Paso solar pond which is a research development and demonstration project operated by The University of Texas at El Paso. The project was initiated in 1983. The El Paso solar pond had been in operation since 1985 (Leblanc et al., 2011). The El Paso solar pond has a surface area of 3000 m² and depth of 3.25 m. The UCZ, NCZ, and LCZ are 0.7 m, 1.2 m and 1.35 m respectively. The simulation was performed with the typical temperature profile of the El Paso solar pond on 1st September 1999. Weather data was obtained from the El Paso TMY2 in TRNSYS. The simulation was also performed with the annual temperature for LCZ and ambient temperature based on 1991- 1993. Figure 5.16 shows the simulated and experimental temperature distributions in the solar pond on 1st September 1999; it can be seen that they are in good agreement in the UCZ and the NCZ but not in the LCZ. It can be seen that the experimental LCZ is not well mixed, whereas the simulated LCZ is assumed to be well mixed as this is the usual assumption in solar pond research. Figure 5.17 shows an annual LCZ temperature variation of El Paso solar pond and the simulated LCZ temperature. It can be seen that they are in reasonably good agreement but the simulated temperature is slightly lower in winter and higher in summer. The experimental and simulated ambient temperatures follow a similar pattern, which may explain the differences in LCZ temperatures. Also, there is no available experimental data for solar pond radiation, which is one of the main factors affecting the LCZ temperature.

It is concluded that the MATLAB code for the solar pond model successfully simulates two existing solar ponds for two different places and pond dimensions.

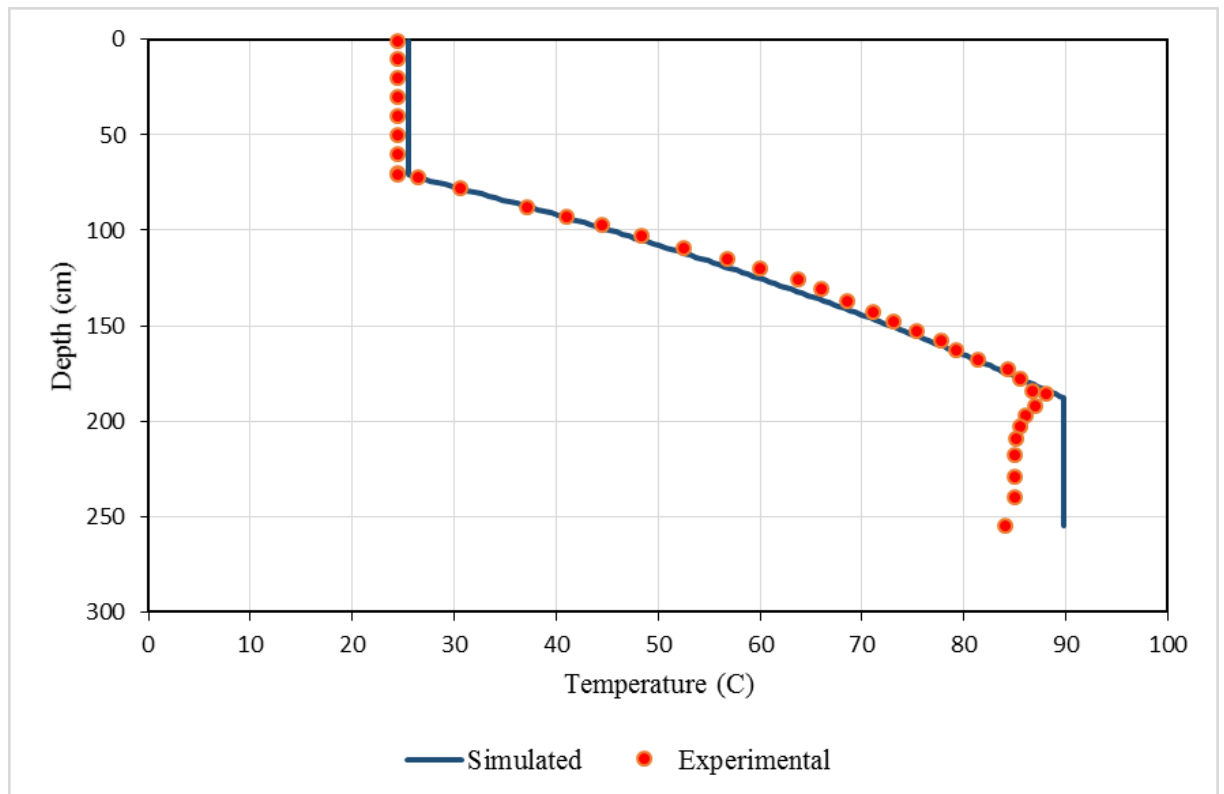


Figure 5.16 Simulated and experimental (Leblanc et al., 2011) temperature distributions for El Paso solar pond on 1st September 1999

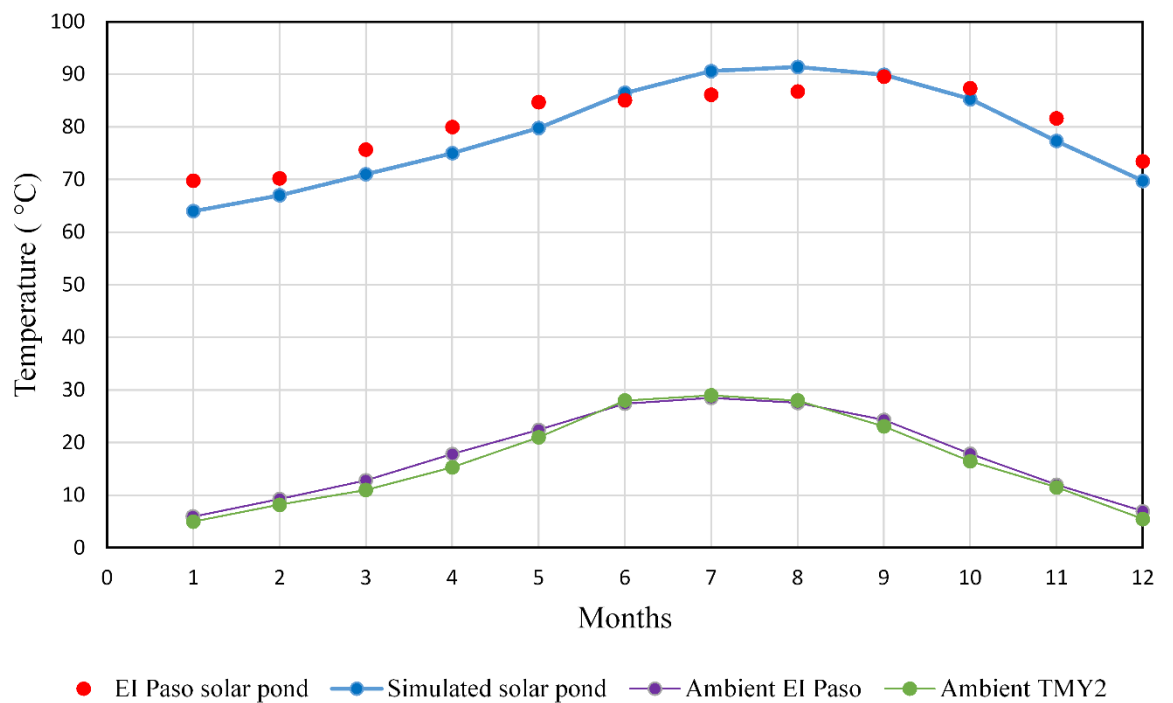


Figure 5.17 Simulated and experimental (Leblanc et al., 2011) annual LCZ temperature profile of the El Paso solar pond and ambient temperature with TMY2

5.3.3 Validation of the absorption chiller

The chiller model is based on the manufacturer's data from the Chart Reader spreadsheet shown in Figure B.2 and B.3 of Appendix B. This shows the cooling capacity and heat input as a function of the hot and cooling water inlet temperatures. All data is for 7 °C chilled water set point temperature and rated chilled, hot and cooling water flow rates.

The chiller model in TRNSYS was validated by setting the water flow rates and auxiliary power input to the rated values, and the chilled water set point temperature to 7 °C. The hot and cooling water inlet temperatures were set to selected values within the ranges covered by the manufacturer's data. For each combination of hot and cooling water inlet temperatures, the chilled water inlet temperature was adjusted until the chiller was fully loaded. The resulting cooling capacity and heat input were noted.

Figure 5.18 and 5.19 show the cooling capacity and heat input for different cooling water inlet temperatures calculated by the model plotted with the manufacturer's data. It may be seen that the plotted points are very close to the manufacturer's data. It was concluded that the chiller model was operating correctly.

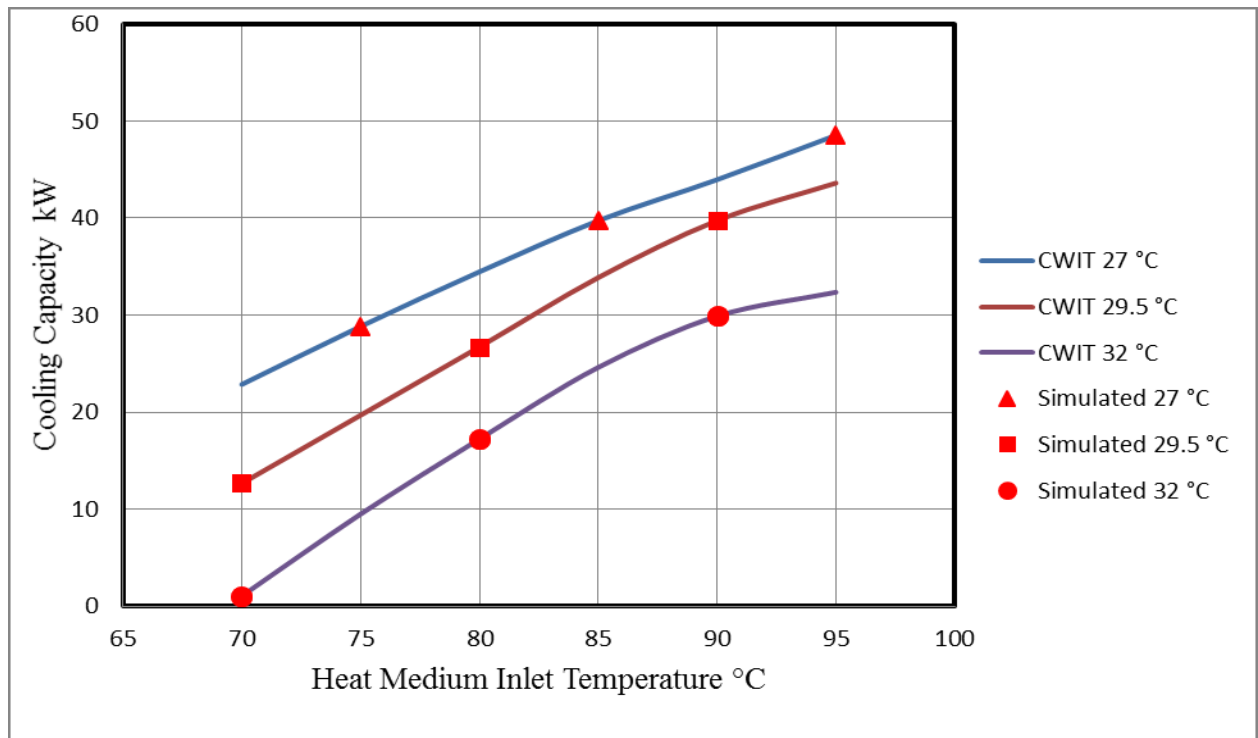


Figure 5.18 Yazaki chiller cooling capacity and simulation model

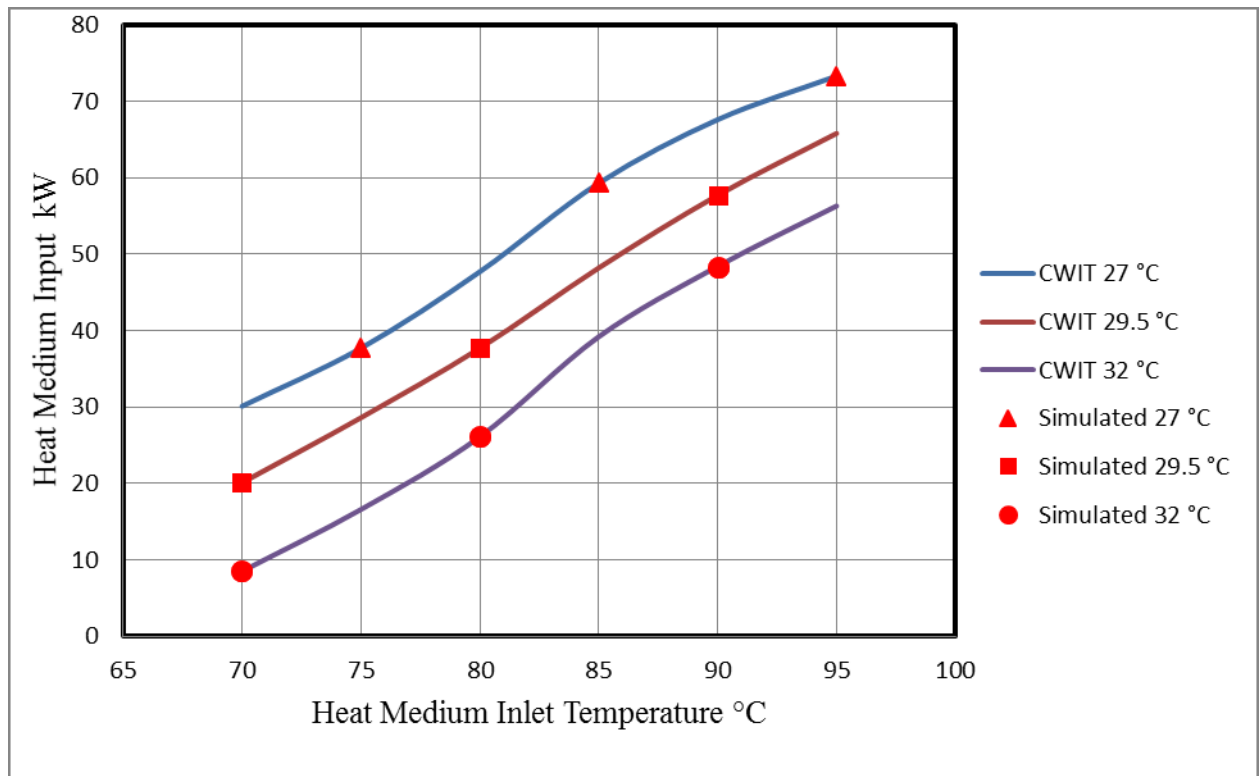


Figure 5.19 Yazaki chiller heat medium input and simulation model

5.3.4 Energy Balance for the Solar Pond Cooling System

The model solar pond cooling system integrated with the building includes many components with energy loss and gain associated with each component. The energy inputs are heat removed from the building, solar energy extracted from the solar pond, heat gains by pipes and electricity used by the pumps, chiller, and fan. The main energy losses are heat rejected at the cooling tower and heat losses from the pipes. The solar pond cooling system simulation is validated by the energy balance of the system.

The total monthly energy input and output for the solar pond cooling system is shown in Figure 5.20. The total monthly input and output increase and decrease together as would be expected from the variation of solar energy available and the cooling load. However, they are not quite equal. The distribution of the annual input and output for the solar pond cooling system energy is shown in Figure 5.21.

Major input energy is from the solar pond (57.5%) and the room cooling load (38.8%), which is 96.3% of the total input. Major output energy is the heat rejected by the

cooling tower, which is about 99% of the total output. The total annual energy input to the system is 135,512 kWh and the total energy output is 132,120 kWh. Annual energy input is more than output and the system surplus energy is 3132 kWh which is about 2 % of the total energy input as shown in Appendix B. This discrepancy shows that there are some energy losses in the simulation which were not accounted for. Annual input and output energies for all components are shown in Table 5.2.

In TRNSYS, the chiller model is in energy balance (see Table B.1 for details). It is not possible to determine where in the rest of the system the energy loss occurs, because TRNSYS does not report energy input and output for the other components. It would be possible to calculate the missing energy inputs and outputs from temperatures, flow rates, etc. but it is not possible to determine whether TRNSYS performs the equivalent calculations correctly. Asim (2016) reported on the energy balance for a solar cooling system modelled in TRNSYS. It was found that the discrepancy cannot be reduced to zero and the TRNSYS technical support were unable to assist; indeed the idea of an energy balance seemed to be new to them. However, 2% is better than would be expected for an experimental study of the energy balance of a cooling system in a building (Asim, 2016).

The absorption chiller monthly energy balance is shown in Appendix B. The input energies to the chiller are electrical, chilled water and hot water energies. The output energy is the cooling water energy. The total annual energy input to the absorption chiller is balanced with the total energy output and the value is 131,201 kWh. Therefore, there is no discrepancy in the chiller energy balance.

Component	Annual Energy (in)	Annual Energy (out)	(in - out) kWh
Chiller	131201.4854	131201.4854	0
Cooling Coil	52689.43	N/A	N/A
Pond Useful Heat	77925.59908	N/A	N/A
Pumps and Fan Electrical Energy	4897.47	N/A	N/A
Cooling Tower	N/A	131625.5736	N/A
Pipe and Fan losses	N/A	754.14	N/A
Total (excluding Chiller)	135512.4991	132379.7136	3132.785472

Table 5.2 Annual input and output energies for all components

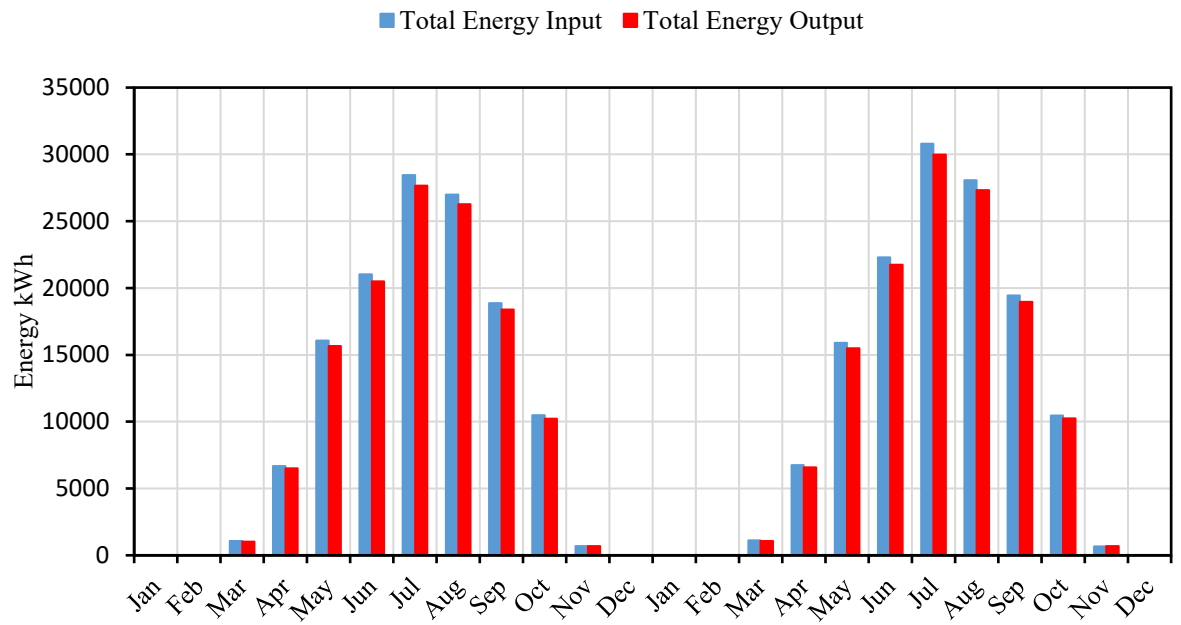


Figure 5.20 Energy balance of the solar pond cooling system

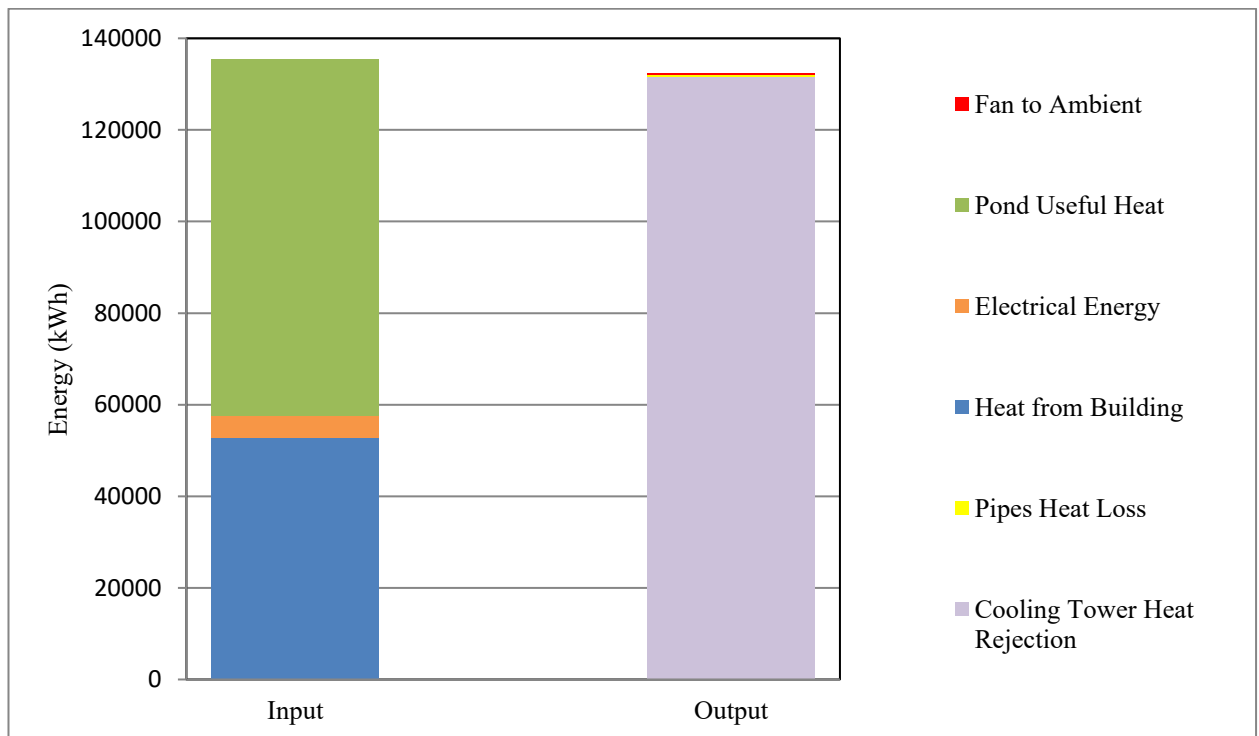


Figure 5.21 Annual input and output energy distribution

5.4 Parameter Variation

The parameter variation analysis of a model is used to investigate how the output of a given numerical model depends on its input factors. This analysis is important in verification and validation of a simulation model.

The characteristics of a solar pond cooling system connected with a building are the combination of variables acting together with a changing pattern due to solar radiation variation and weather conditions. In this section, the effect of varying important parameters such as pond area, thicknesses of upper convective zone, non-convective zone and lower convective zone, and ground conditions on cooling system performance are investigated.

In this research, the computational parameters were selected depending on literature recommendation, hand calculations and trial and error. To start the simulation, feasible initial values for pond and cooling system were assumed. Then the effect of varying of the most important parameters is examined. Finally, the reasonable and optimum parameter values which improve the system performance is adopted.

Many other values were tried in the simulation and the results are not shown in this Thesis because they did not add any significant improvements to the system.

Chilled water outlet temperature is used as the main criterion of the system performance, as it has been found that this is maintained at the set point provided the hot water inlet temperature is high enough and the chiller is not overloaded (see sections 5.2.4 and 5.3.3).

5.4.1 Selection of Required Solar Pond Area

The main contents of this section has been published in Energy Procedia Journal (Kanan et al., 2015).

The basic consideration in any pond design is the pond area. The size of the pond is inseparably related to the demand for heat required by the application, the temperature of the heat required, and the availability of solar radiation.

Effect of Pond Area on Chilled Water Outlet Temperature

The required heat input to drive the absorption chiller at its rated output is 35.2 kW. Different solar pond areas were tested with the same chiller capacity, house and other

components to meet the required heat input. Four different solar pond areas (250 m^2 , 375 m^2 , 400 m^2 , and 500 m^2) were considered. For each pond area, the simulation was run for two years to allow the system to approach its long-term performance.

Figure 5.22 shows the chilled water outlet temperature from the chiller for different solar pond areas for two years simulation time. With 250 m^2 pond area, the chilled water outlet temperature does not stabilise at the set point (7°C) even in the second year. With 400 m^2 or more pond area, the chilled water outlet temperature stabilises at the 7°C set point temperature by the end of the first summer and during the second summer. When the chilled water outlet temperature stabilises at the set point, this shows the system is able to meet the demand for cooling. The 400 m^2 is therefore suggested as a suitable pond area for the 125 m^2 single family house.

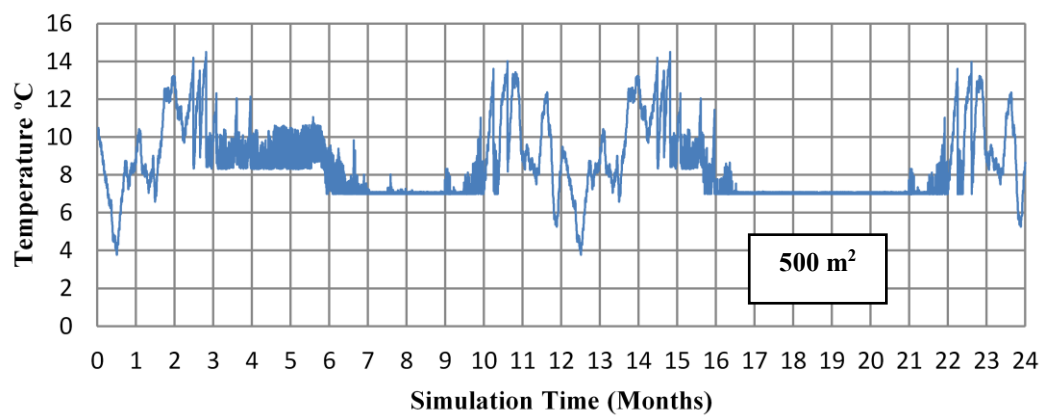
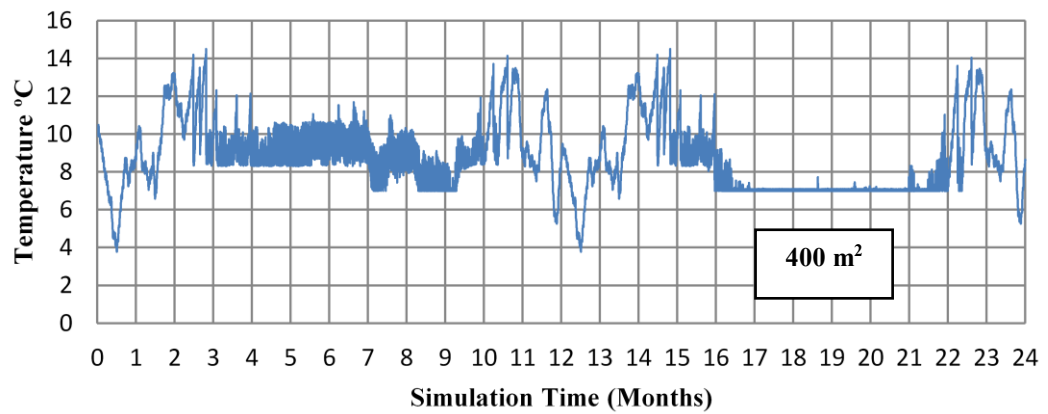
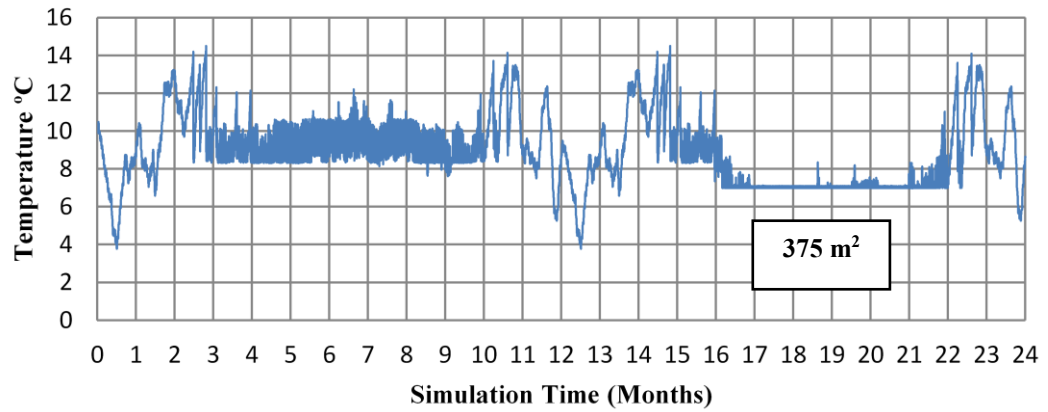
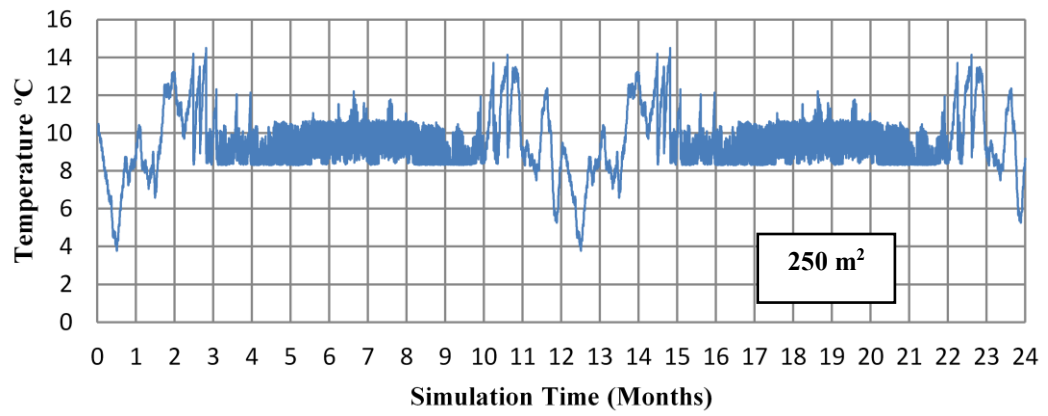


Figure 5.22 Chilled water outlet temperature with different pond area

5.4.2 Solar Pond and Ground Conditions

The main contents of this section have been published in Energy Procedia Journal (Kanan et al., 2016).

In this section, the effect of four ground conditions (soil type, moisture content, sandy soil texture and the depth of the water table) is investigated. Different soil types and water table depths were tested with all other parameters unchanged. It was assumed that there was no insulation between the pond and the ground.

5.4.3 Soil Type

Effect of Soil Type on Chilled Water Outlet Temperature

Different type of soils are used in this study with different soil thermal properties conditions as described in Chapter Three, Table 3.3. Figure 5.23 shows the chilled water outlet temperature from the absorption chiller with different types of soil under solar pond. It can be seen that the chilled water outlet temperature in the case of sandy soil (lower thermal conductivity) (Yari and Javani, 2007) underneath the solar pond stabilised at the set point of (7°C) at the beginning of June in the first simulation year, whereas with clay and sandstones soil (higher thermal conductivity) (AlMaliky, 2011), the chilled water outlet temperature does not stabilise at the set point of (7°C) until a short period of time before the end of the first year summer. During the summer of the second year, the chilled water outlet temperature is approximately matched for the most of the time, but it also shows that the chilled water outlet temperature is more often stabilised at the set point in the case of sandy soil.

Therefore, it is recommended to construct the pond on soil with low thermal conductivity.

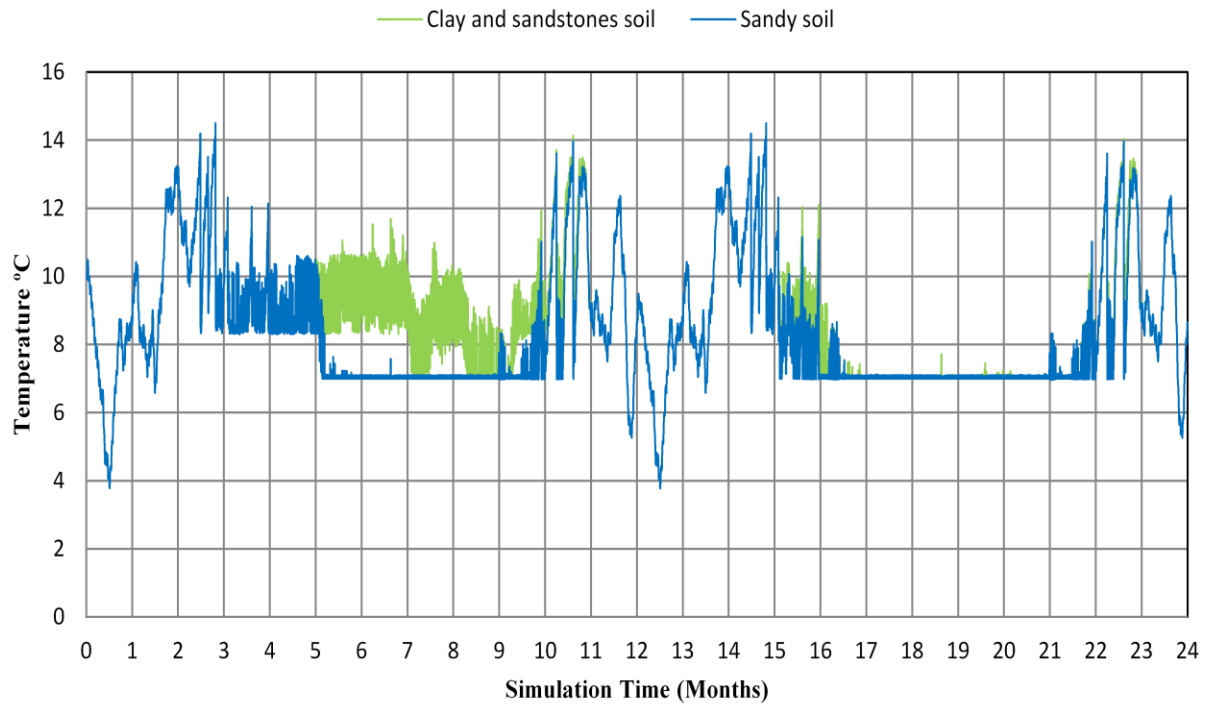


Figure 5.23 Chilled water outlet temperature with different types of soil under solar pond

5.4.4 Moisture Content

Effect of Moisture Content on Chilled Water Outlet Temperature

Soil thermal properties are calculated according to section 3.4.1. The thermal conductivity of the soil increases with increasing moisture content. Figure 5.24 illustrates the chilled water outlet temperature from the absorption chiller with different moisture content for clay and silt 2 soil under the solar pond. The chilled water outlet temperature with 5% moisture content of the soil stabilises at the set point of 7°C from May to October of the second year and by the end of the first year summer. This does not occur with 10% moisture content. It is therefore recommended to search for dry soil before constructing the pond.

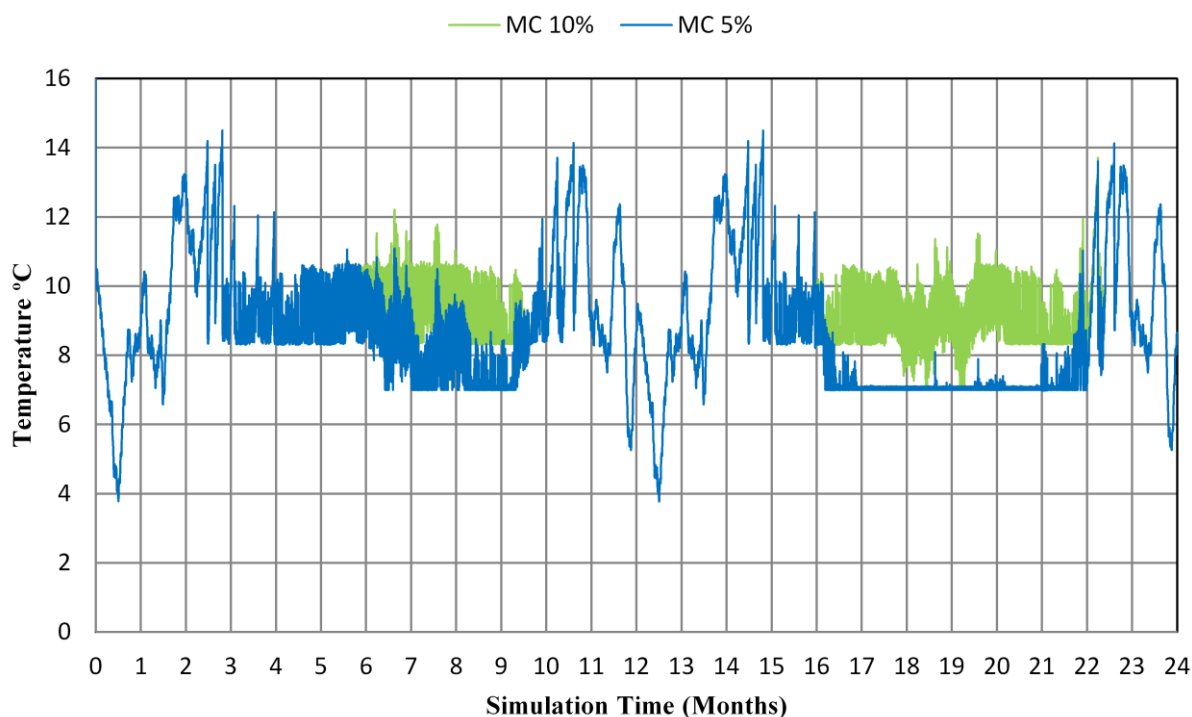


Figure 5.24 Chilled water outlet temperature with different moisture content for clay and silt 2 soil under the solar pond

5.4.5 Sandy Soil Texture

Different sand soil textures are utilized in this study, namely coarse and fine sand soil with dry conditions. The soil thermal properties of coarse and fine sand soil are shown in Table 3.4. The sandy soil texture has only a moderate effect on the soils' thermal properties, much less than the effect of moisture content.

Effect of Sandy Soil Texture on Chilled Water Outlet Temperature

Figure 5.25 shows the chilled water outlet temperature from the absorption chiller with dry fine and dry coarse sand soil texture underneath the solar pond. The chilled water outlet temperature in both cases are almost the same and stabilise at the set point of 7°C in the second year and most of the time in the first year except for May.

During May the chilled water outlet temperature for coarse sand soil is slightly higher than the chilled water outlet temperature in the case of fine sand soil. The maximum difference is about 1.88°C .

It is concluded that dry fine sandy soil is slightly preferable to dry coarse sandy soil.

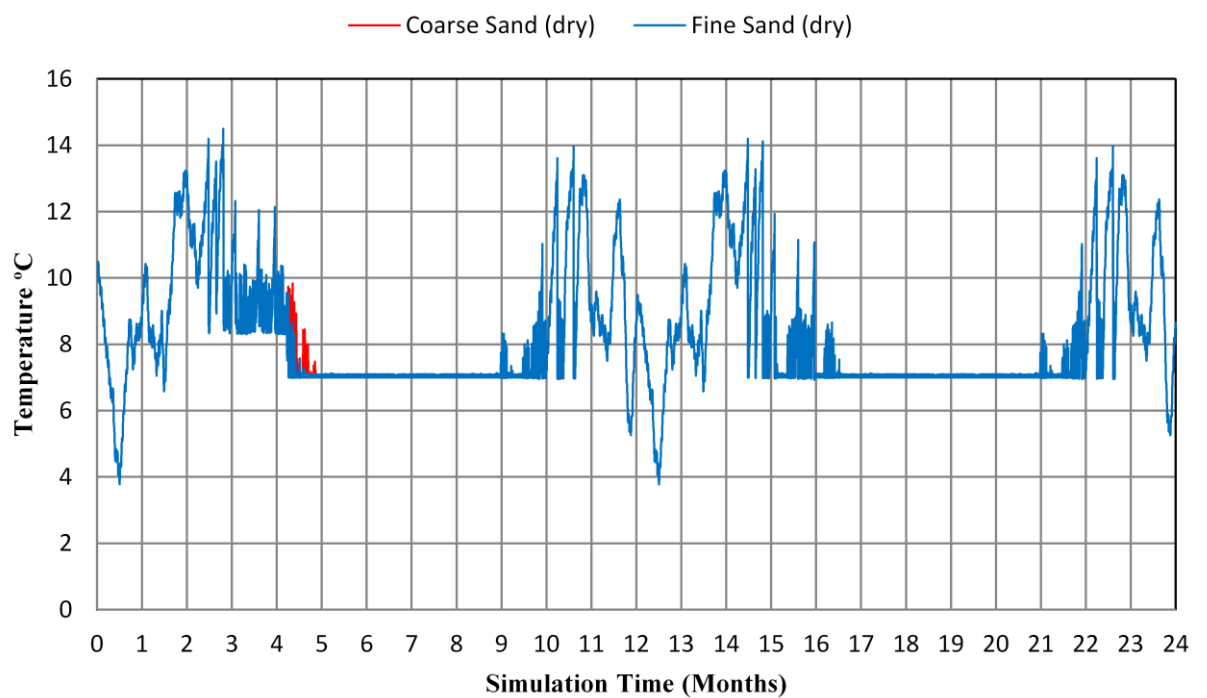


Figure 5.25 Chilled water outlet temperature with dry sand soil texture under the solar pond

5.4.6 Depth of the Water Table

At the non-insulated bottom of the solar pond, heat is lost from solar pond to the ground. The magnitude of heat loss depends on the soil thermal properties and on the depth of the water table underneath the solar pond, which acts as a heat sink. The deeper the water table, the smaller the rate of heat transfer from the pond to the water table is expected to be.

The effect of varying the depth of the water table under the solar pond for clay and sandstones soil has been investigated. The values are 1m, 2m, 3m, 4m, 5m and 10m measured from the bottom of the solar pond.

Effect of Depth of the Water Table on Chilled Water Outlet Temperature

Figure 5.26 illustrates the chilled water outlet temperature from the absorption chiller with different depth of the water table under the solar pond. The chilled water outlet temperature in the cases of 1m and 2 m of water table depth does not stabilise at the chiller set point temperature of 7°C in the first year and even in the second year. While the chilled water outlet temperature in case 3m and 4m of water table depth is tried to stabilise at the set point of 7°C starts from May to October of the second year. The chilled water outlet temperature in cases of 5m and 10m of water table depth stabilises at the set point of 7°C starts from May to October of the second year and by the end of the first year summer. That's clearly shown in Figure 5.27. The chilled water outlet temperature lines with 1 m is behind the lines of 2 m. Therefore, it is invisible in the Figure 5.27.

As expected, it is recommended to search for a site with deep water table under soil before constructing the pond.

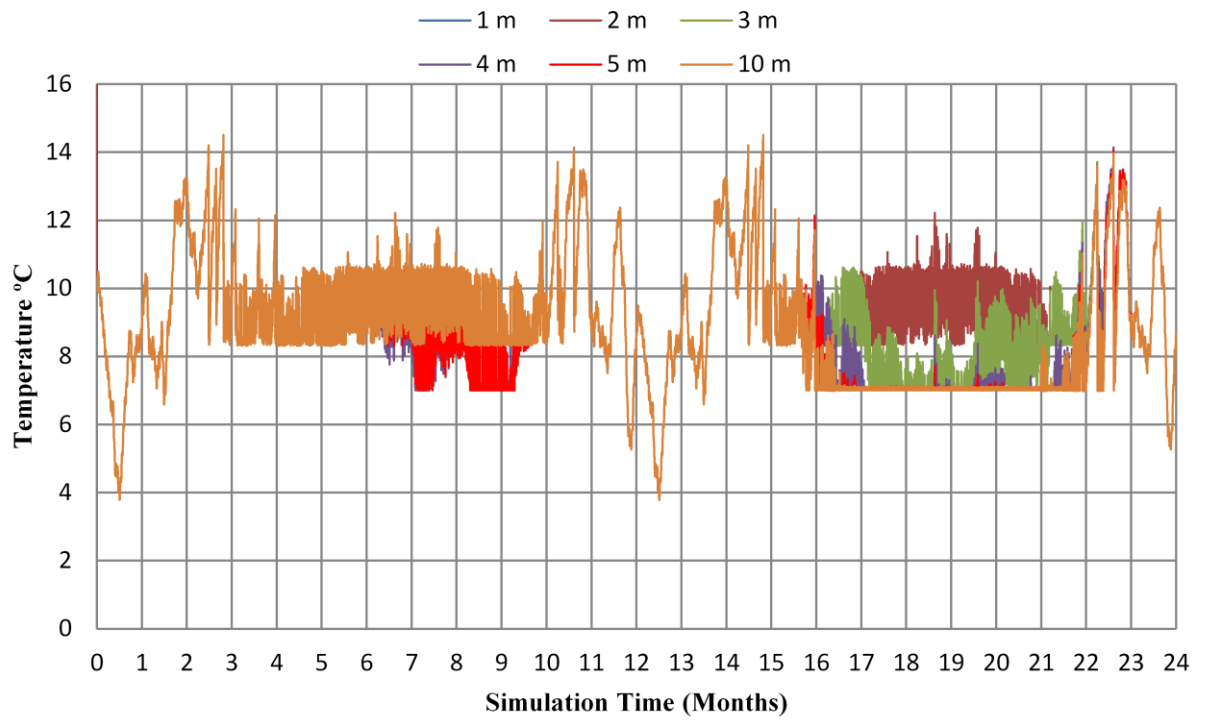


Figure 5.26 Chilled water outlet temperature with different depth of the water table under the solar pond

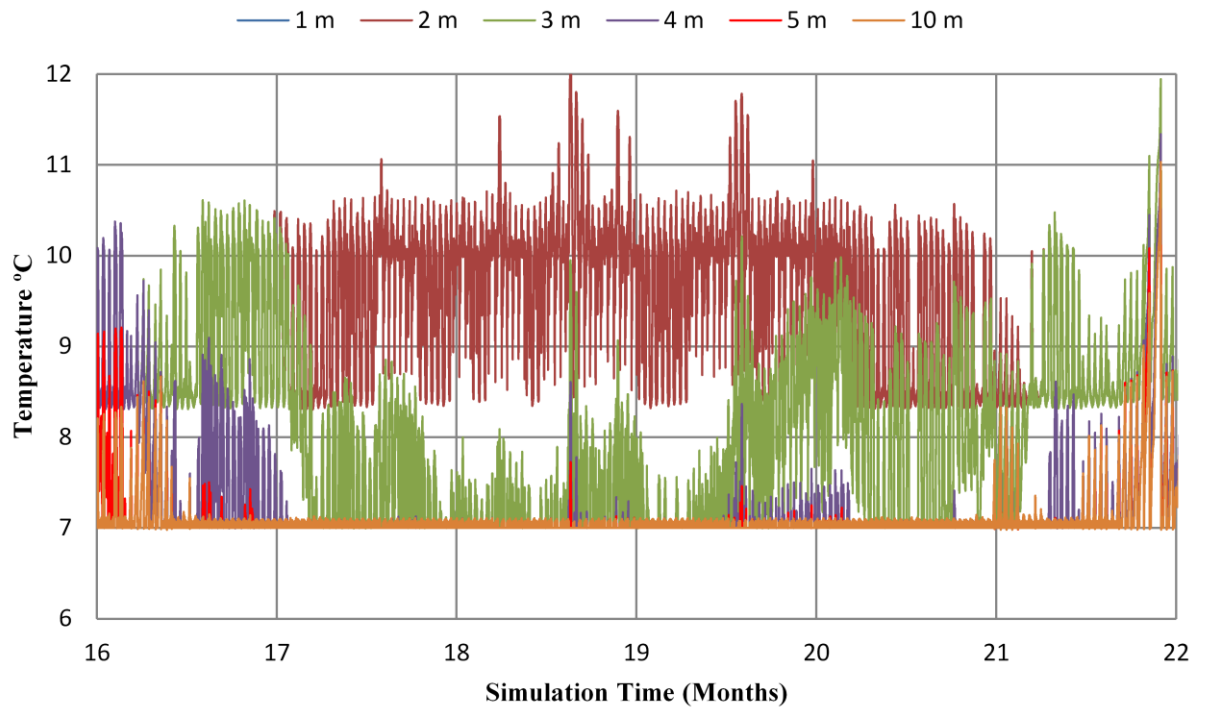


Figure 5.27 Chilled water outlet temperature with different depth of the water table under the solar pond for May to October in the 2nd year.

5.4.7 Ground Conditions Summary

The results presented here were obtained from run of the complete model for two simulated years, to ensure that the system approached its long-term performance.

Four factors were studied for soil underneath the solar pond: moisture content, soil type, sandy soil texture and the depth of the water table. The effect of the four soil factors on the chilled water outlet temperature is shown in Table 5.3.

At 5 m water table depth, soils which are dry or at moderate moisture content (up to 8%) allow the chiller to operate at its set point chilled water outlet temperature most of the time from May to September (3400 hours or more). At higher moisture contents, the chiller's effective operating time is greatly reduced, in some cases to zero. Increasing the depth of the water table beyond 5 m slightly increases the possible operating time. Reducing the depth reduces the effective operating time, in some cases to zero.

Soil Type	Soil Thermal Properties			Moisture Content (%)	Water table depth (m)	No. of hours for chilled water outlet temperature at 7 °C
	Thermal conductivity W/m. °C	Density kg/m ³	specific heat kJ/kg .°C			(May-Sept /2 nd year)
Clay and sandstone	1.7	1470	2.0	4.4	1	0
					2	0
					3	2772
					4	3426
					5	3613
					10	3621
Clay and silt 1	2.15	1350	1.137	5.6	5	3425
Clay and silt 2	1.932	2325	1.007	5	5	3473
	3.152	2255	1.175	10	5	1262
Sand	1.082	1352	1.105	7.9	5	3660
Coarse sand	0.25	1800	0.800	0	5	3660
	3.72	2080	1.483	20.2	5	0
Fine sand	0.15	1600	0.800	0	5	3660
	2.75	2010	1.632	24.6	5	2360

Table 5.3 Number of hours for chilled water outlet temperature at 7°C with different ground conditions.

5.4.8 Solar Pond Optimum Zone Thicknesses

The main contents of this section has been submitted to the Journal of Solar Energy.

The thickness of the zones of a salinity gradient solar pond affects the quantity of solar radiation that penetrates to the bottom of the pond, which in turn affects the LCZ temperature and amount of useful heat collected and then affects the cooling system performance. Therefore, the optimum zone thicknesses for the solar pond connected to the solar air conditioning system have been investigated.

Simulations were performed for various thicknesses of the UCZ, NCZ and LCZ zones. For each simulation, the thickness of one zone was varied while the other zone thicknesses were set to base case values. The zone thicknesses are given in Table 5.4.

Zone	Thicknesses (m)
UCZ (Upper Convective Zone)	0.1 0.3 (base case) 0.5 0.7
NCZ (Non-Convective Zone)	1.0 1.25 (base case) 1.5 2.0
LCZ (Lower Convective Zone)	0.4 0.7 (base case) 1.0 1.3

Table 5.4 Zone thicknesses for simulations

5.4.9 UCZ Thickness

Effect of Varying UCZ Thickness on Chilled Water Outlet Temperature

Figure 5.28 shows the effect of varying UCZ thickness on the chilled water outlet temperature. Four different values (0.1 m, 0.3 m, 0.5 m and 0.7 m) are considered in these figures. NCZ and LCZ were assumed to be 1.25 m and 0.7 m respectively. Increasing the UCZ thickness is expected to reduce the amount of solar radiation that penetrates the NCZ and LCZ, thereby reducing the LCZ temperature and useful heat collected. A thin zone of UCZ is better for the solar cooling system during the summer period of the second year. Because it stabilised the chilled water outlet temperature to the design set point temperature of 7 °C.

The UCZ temperature is not expected to be significantly affected, as the UCZ is well mixed and in contact with the ambient air. The UCZ thickness which is needed in practice, to protect the NCZ from disturbance is about 0.1-0.3 m (Hull, et al., 1988).

0.5 m and 0.7 m UCZ prevent the system bringing chilled water outlet temperature under control. 0.1 m thickness improves the system performance (chilled water outlet temperature under control earlier and for longer). However, a 0.1 m thickness cannot protect the pond from the effect of wind mixing, rain, and evaporation. Therefore the minimum practical thickness, about 0.3 m, is recommended.

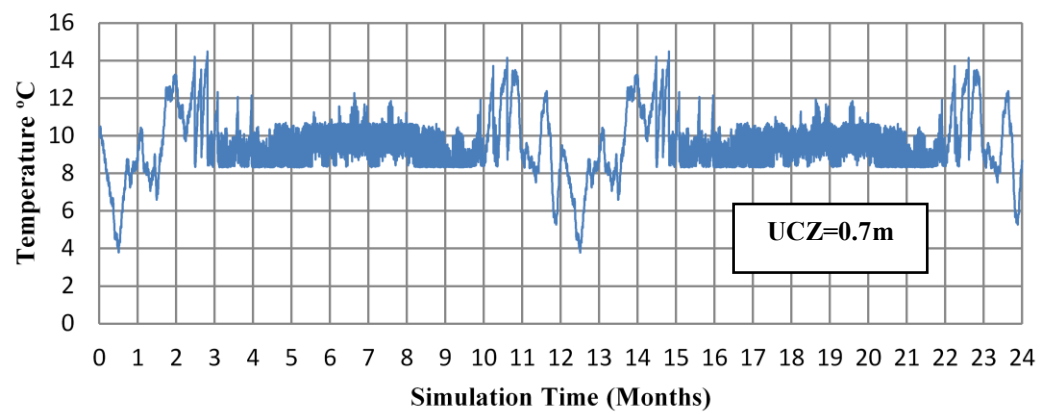
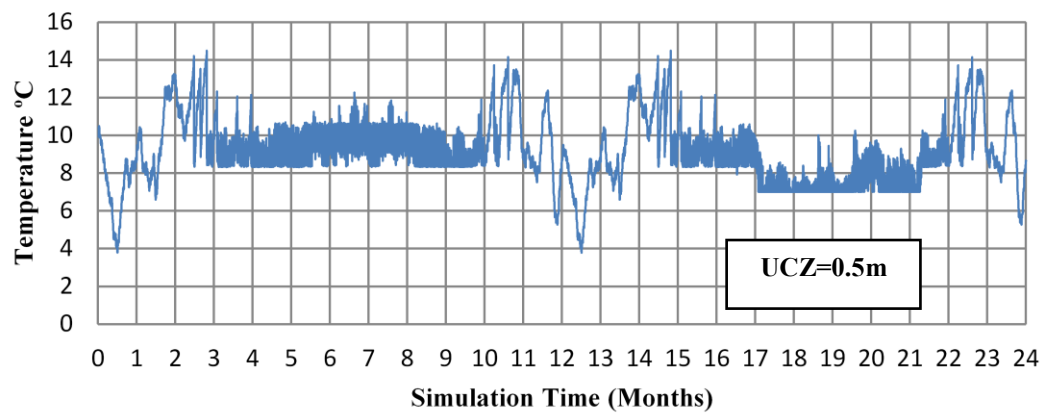
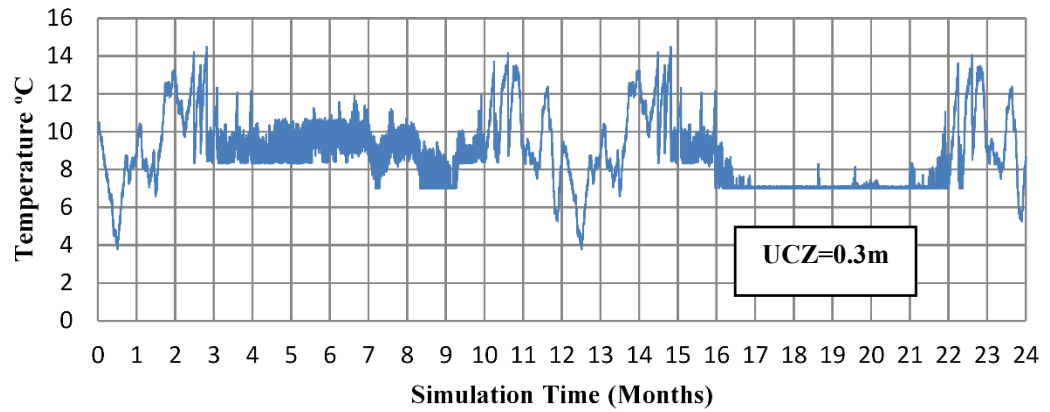
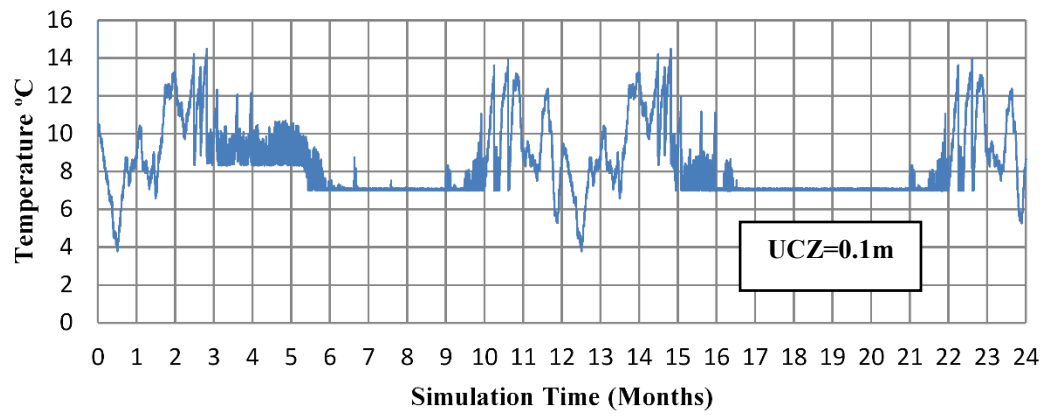


Figure 5.28 Effect of varying UCZ thickness on the chilled water outlet temperature with NCZ=1.25 m and LCZ=0.7 m

5.4.10 NCZ Thickness

Effect of Varying NCZ Thickness on Chilled Water Outlet Temperature

The NCZ in the pond plays an important role in determining the actual thermal performance. It works as a thermally insulating layer between UCZ and LCZ. Increasing the NCZ thickness will have two opposing effects: (1) Improving the thermal insulation, hence tending to increase the LCZ temperature and (2) reducing the amount of solar radiation which reaches the LCZ, hence tending to reduce the LCZ temperature.

Figure 5.29 shows the effect of varying NCZ thickness on the chilled water outlet temperature. The NCZ with different values (1.0 m, 1.25 m, 1.5 m and 2.0 m) are considered in these figures. The thin zone of 1.0 m has a negative impact on temperature storage in LCZ zone and on the solar pond thermal performance. Any other thickness zone higher than 1.0 m will capture a required LCZ temperature to drive the absorption chiller with a design set point temperature of 7 °C. From the simulation of two years and during the summer for the second year, it was found that a suitable thickness of NCZ was 1.25 m. Thickness greater than 1.25 m does not significantly improve performance, and would be more expensive to construct and maintain.

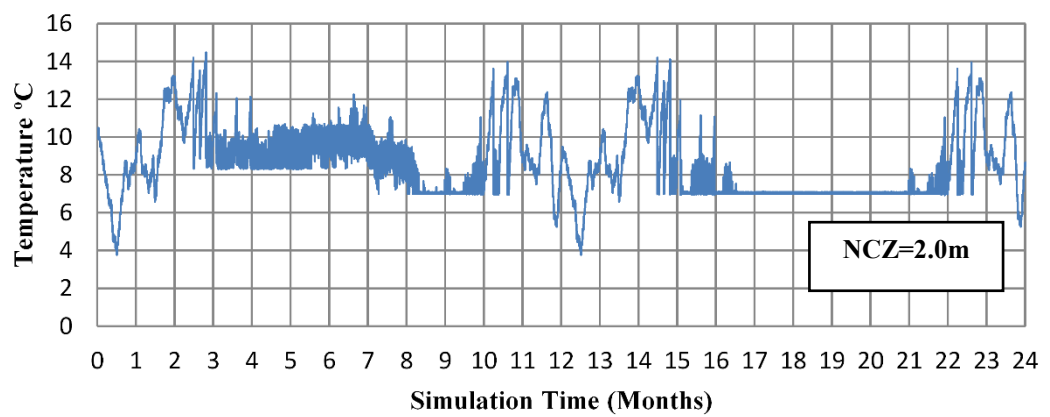
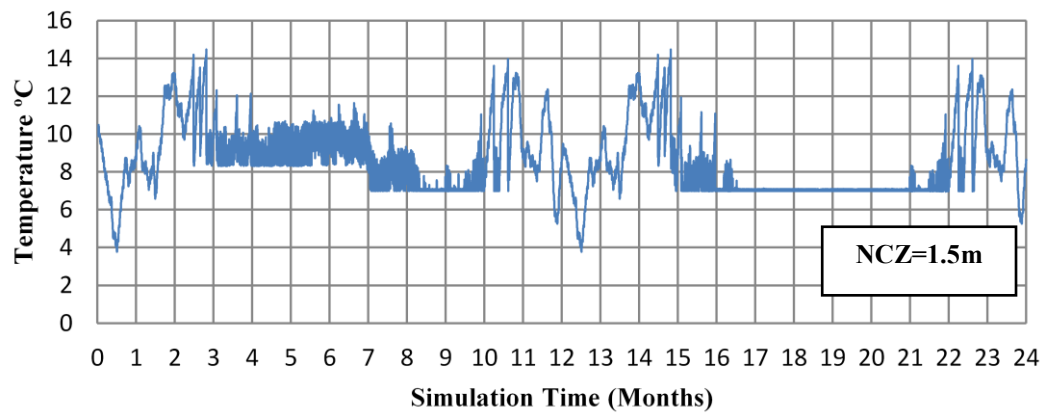
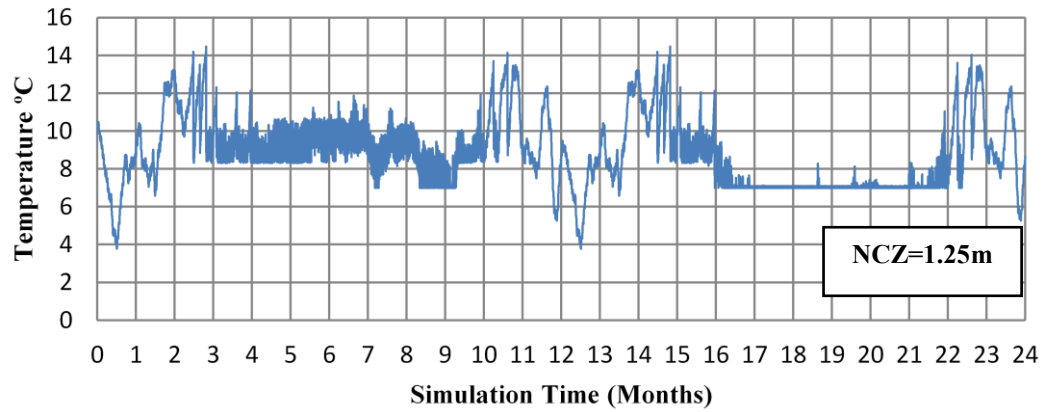
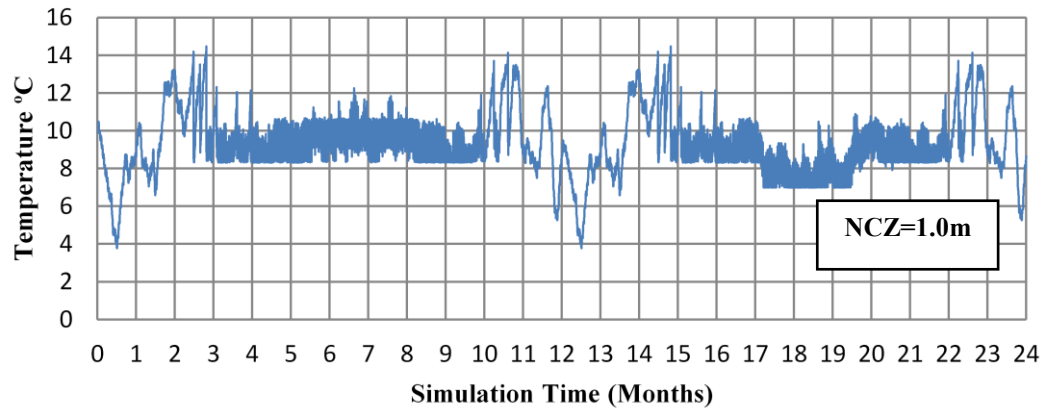


Figure 5.29 Effect of varying NCZ thickness on the chilled water outlet temperature with UCZ=0.3 m and LCZ=0.7 m

5.4.11 LCZ Thickness

Effect of Varying LCZ Thickness on Chilled Water Outlet Temperature

Useful heat is stored and extracted from the lower convective zone of the solar pond. This heat is the result of the energy balance for LCZ. Increasing the thickness of the LCZ will increase its thermal capacity, so it will take longer to heat up and longer to cool down. It will not affect heat loss in the model (except in so far as it affects the LCZ temperature) as no heat loss from the sides has been assumed.

Figure 5.30 presents the effect of varying LCZ thickness on the chilled water temperature. All of the tested thicknesses work fine to provide chiller with a suitable hot water temperature and, as a result, the chilled water outlet temperature reaches set point temperature particular in the second year simulation time. A small thickness leads to more rapid seasonal warm up of the lower convective zone. However, a thin LCZ gives a chance of disturbing the gradient in the NCZ layers. The 0.7 m LCZ thickness was therefore selected as the recommended thickness.

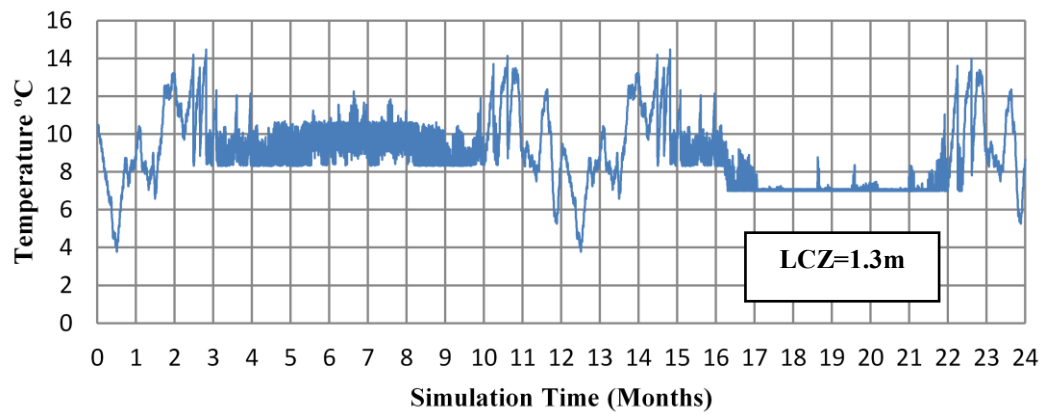
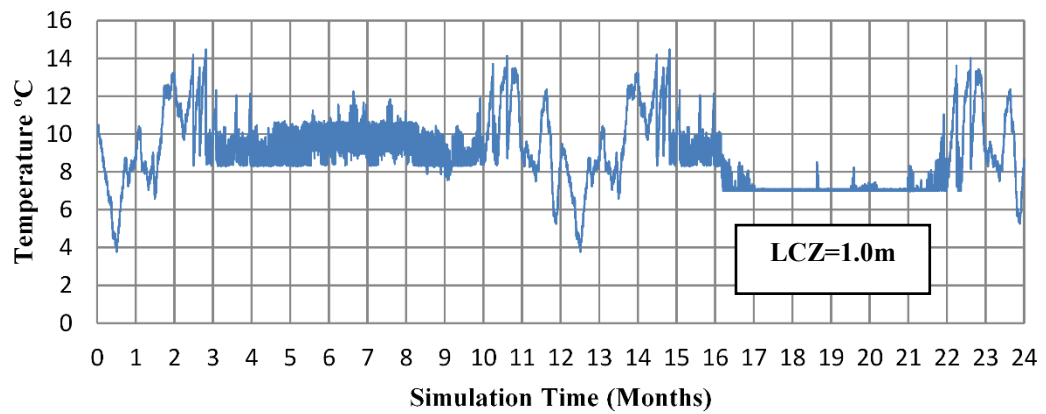
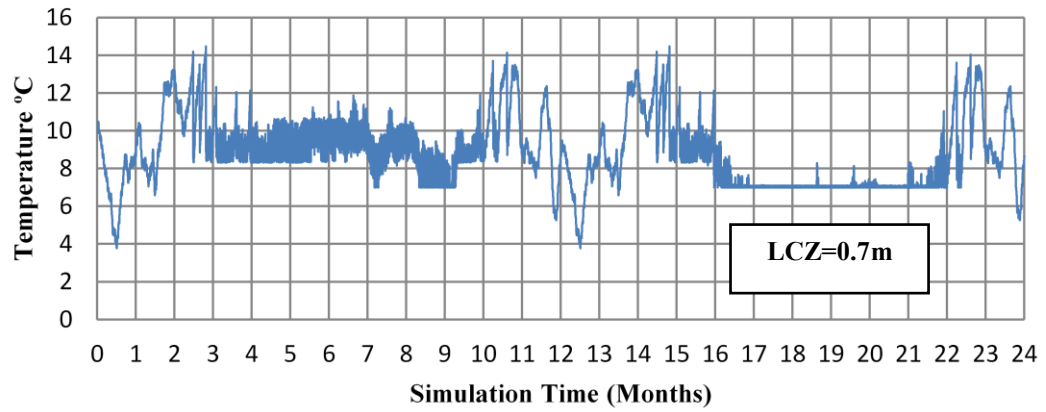
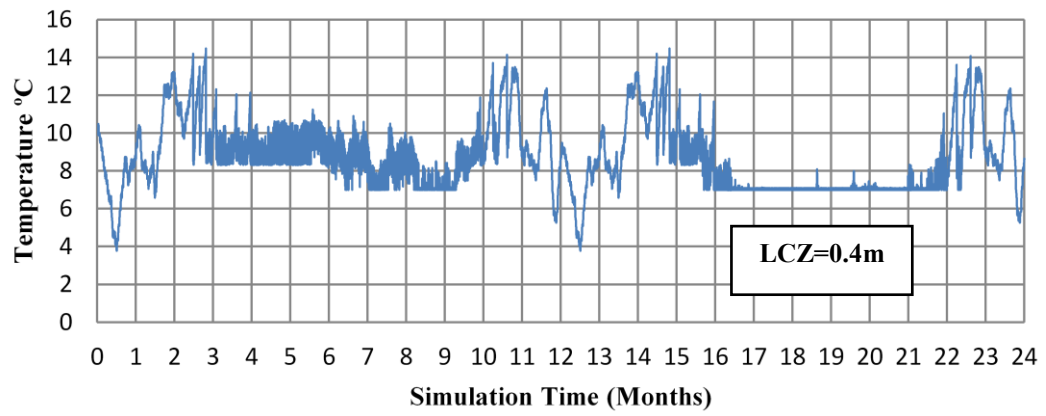


Figure 5.30 Effect of varying LCZ thickness on the chilled water outlet temperature with UCZ=0.3 m and NCZ=1.25 m

5.4.12 Optimum Zone Thicknesses Summary

The results and the number of hours for chilled water set point temperature from May to September, during the second year are summarised in Table 5.5. Nine cases and the base case are considered in the simulation. For the base case, the number of hours for chilled water outlet temperature that meet the set point chiller temperature of 7°C is (3317 hr) which is 90% of the total hours (3672 hr) from May to September. In Table 5.5, there are some hours higher than 3317 hr of the base case. However, it cannot be selected as better as the base case for optimum thicknesses. This is due to many reasons such as, unrealistic thin UCZ layer (case 1), thicker insulation layer of NCZ (case 5, and 6) which would result in increased costs and shallow LCZ thickness (case 7) which may disturb the gradient in the NCZ layers.

Cases	UCZ (m)	NCZ (m)	LCZ (m)	No. of hours for chilled water set point temperature of (7 °C) achieved (May-Sept (3672 hr) during 2 nd year)
1	0.1	1.25	0.7	3498
2	0.5			1470
3	0.7			0
4	0.3	1.0	0.7	422
5		1.5		3498
6		2.0		3500
7	0.3	1.25	0.4	3418
8			1.0	3184
9			1.3	3017
base case	0.3	1.25	0.7	3317

Table 5.5 No. of hours for chilled water set point temperature of (7°C) achieved by varying zone thicknesses

5.5 Heat Exchanger Effectiveness

The effectiveness is the ratio between the actual heat transfer rate and the maximum possible heat transfer rate for the given fluid inlet temperatures, flow rates, and specific heats. Simulations were performed for various values of heat exchanger effectiveness (0.4, 0.6 and 0.8). The effect of varying heat exchanger effectiveness on the chilled water outlet temperature is shown in Figure 5.31. It can be seen that when the effectiveness is high, the chilled water outlet temperature stabilises at the 7°C set point temperature by the end of the first summer and during the second summer. With 0.4 effectiveness, the chilled water outlet temperature does not stabilise at the set point (7°C) in the first year. With 0.8 effectiveness the chilled water outlet temperature stabilises at the design set point for a longer time than 0.4 and 0.6 effectiveness.

The effect of varying heat exchanger effectiveness on the solar pond efficiency is shown in Figure 5.32. It is observed that the solar pond efficiency with 0.8 heat exchanger effectiveness is higher than the efficiency with 0.4 and 0.6 heat exchanger effectiveness. This is because the heat extraction from the solar pond is higher with 0.8 heat exchanger effectiveness.

Referring to Section 3.7.2 and to enable the chiller to provide cooling when required, which is May to September in the second year, it was decided to adopt 0.8 for heat exchanger effectiveness for the calculations in this research.

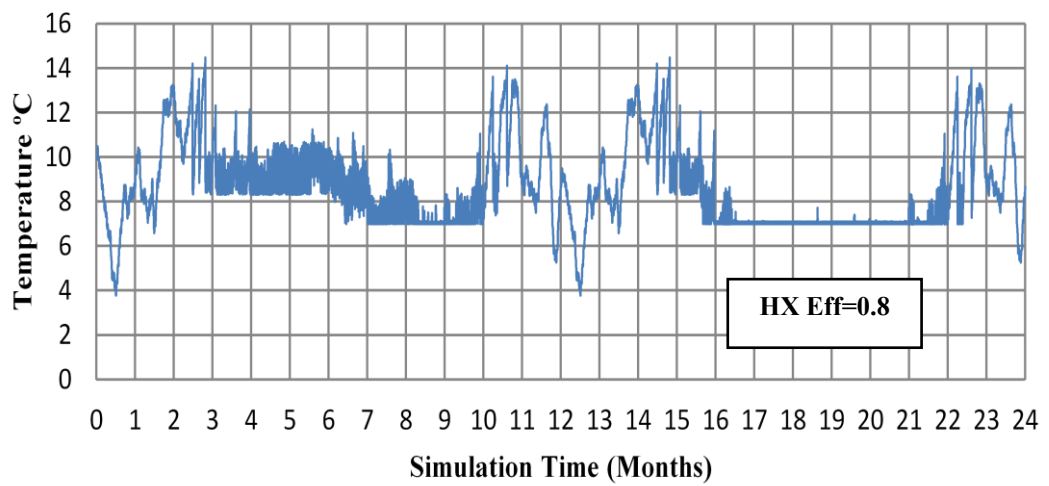
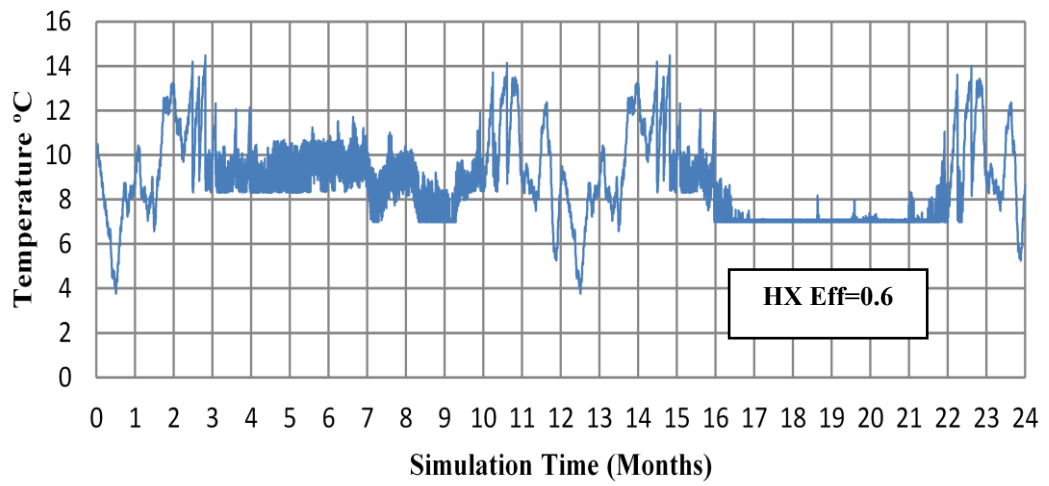
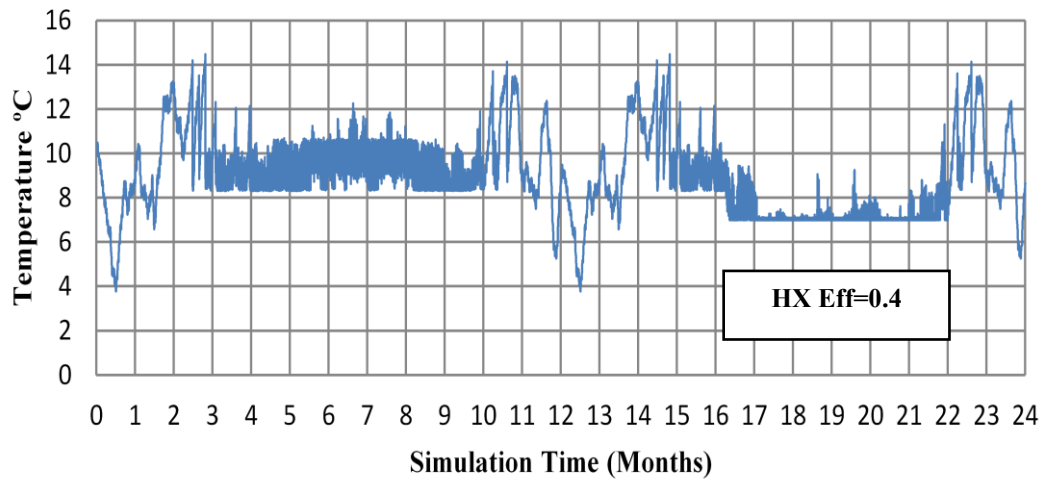


Figure 5.31 Effect of varying heat exchanger effectiveness on the chilled water outlet temperature

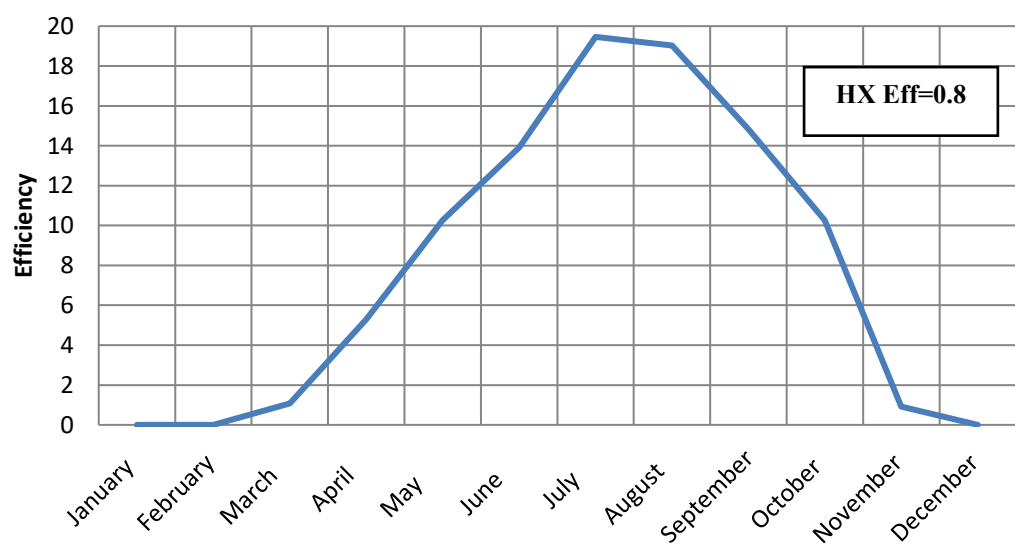
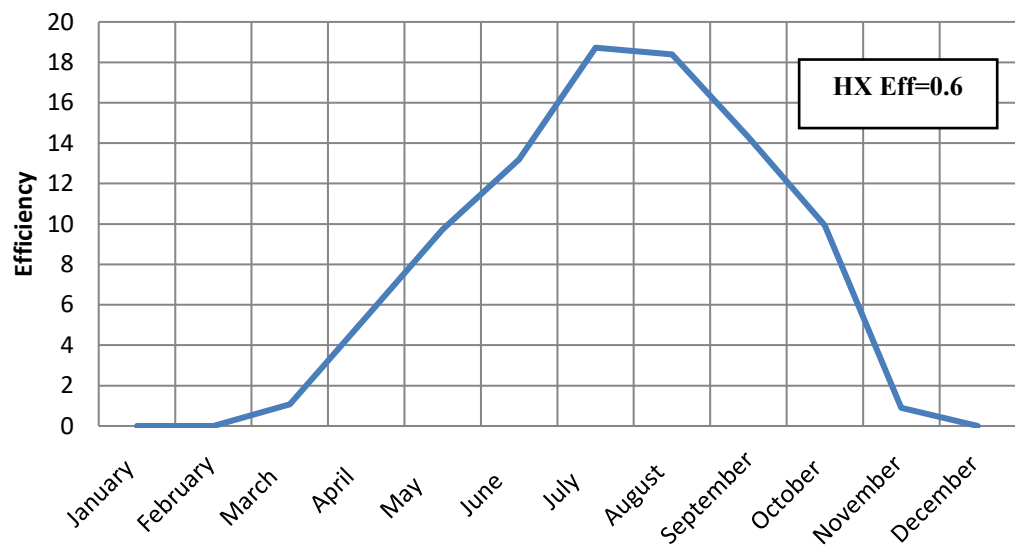
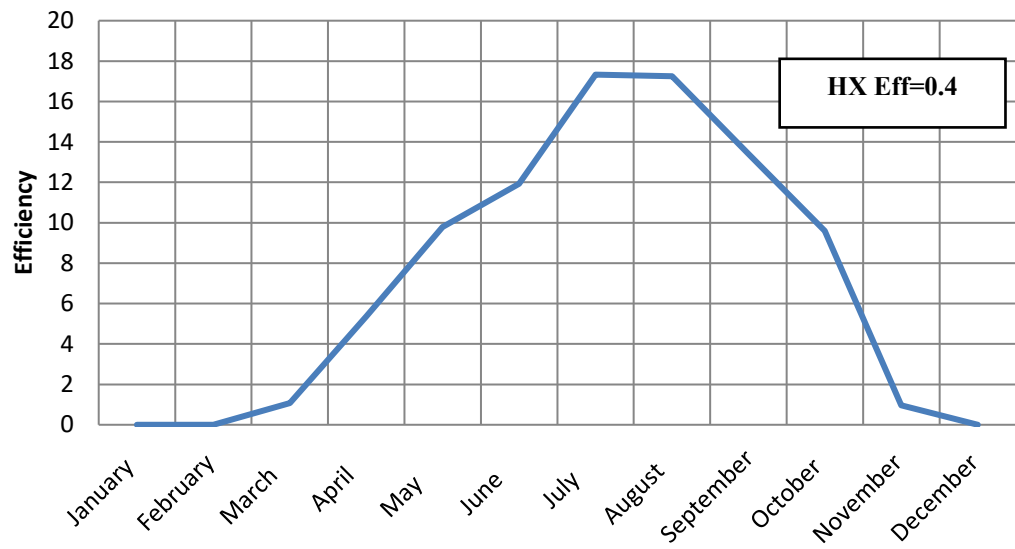


Figure 5.32 Effect of varying heat exchanger effectiveness on the solar pond efficiency

5.6 Electrical Energy Consumption

Electrical energy is required to run pumps for brine and water flow between components, fan for air flow, and the chiller solution pump. The monthly total electrical energy consumption for the solar pond cooling system is shown in Figure 5.33.

The electrical energy supply varies with month in a similar manner to the building cooling load shown in Figure 3.8. In December, January, and February the system is off because the room temperature is lower than the thermostat control temperature 25°C.

The total annual electrical energy consumption for the solar cooling system is 4897 kWh and the total cooling load is 52689 kWh. Electrical energy represents about 9% of the total cooling load. The electricity required to drive the solar pond absorption cooling system is less than the electricity required to drive the equivalent conventional vapour compression cooling system. A comparison has been made between a solar pond cooling system energy consumption and a vapour compression air cooled chiller. (YORK Commercial & Industrial HVAC, 2016) The details of a vapour compression air-cooled chiller are shown in Appendix B. The cooling capacity, total input power, and energy efficiency rating are 24.6 kW, 8.45 kW, and 2.91 respectively.

The power consumption of a vapour compression air cooled chiller for the same number of operating hours (which is from May to the end of October) for a solar cooling system is:

$$8.45 \text{ kW} * 4416 \text{ hr} = 37315 \text{ kWh per season}$$

Annual power consumption for solar absorption chiller = 4897 kWh per season

$$\text{Saving power consumption} = 37315 - 4897 = 32418 \text{ kWh}$$

According to the UK Department of Energy and Climate Change (DECC) (Department for Business, Energy & Industrial Strategy, 2016), a 0.41205 kg of CO₂ emission per each kWh of electricity produced, in 2016.

Therefore,

$$32418 \text{ kWh} * 0.41205 \text{ kg CO}_2 \text{ e/ kWh} = 13357 \text{ kg CO}_2 \text{ e/ season}$$

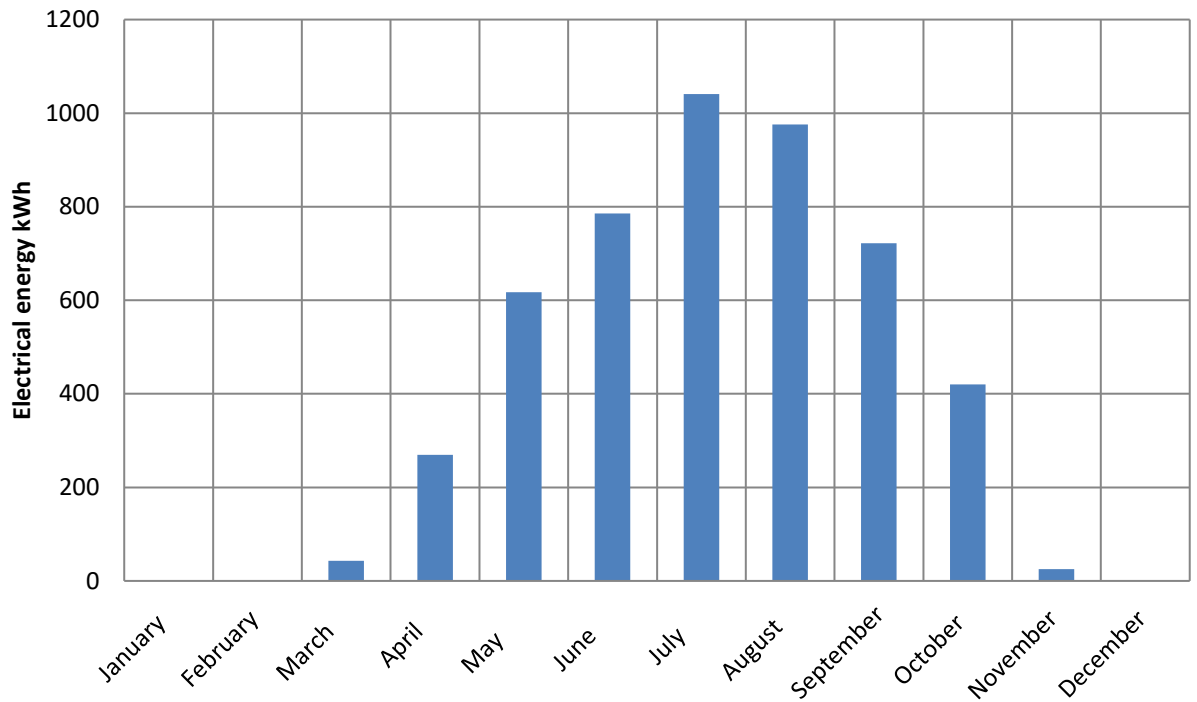


Figure 5.33 Monthly electrical energy consumption for solar pond cooling system

5.7 Conclusion

A solar pond thermal cooling system integrated with a building model for a single family house in Baghdad, Iraq was simulated to maintain a comfortable room temperature. The house was of standard construction and did not include any measures to reduce the cooling load.

The results showed that a solar pond cooling system for a typical existing building in Iraq is feasible. The designed solar pond cooling system successfully maintained the room temperature below 25°C throughout the year without any backup heat source. The final system configuration and equipment sizes are shown in Chapters 3 and 4. The final solar pond powered cooling system for a 125m² house floor area with 100% solar fraction consists of 400 m² of salinity gradient solar pond, and a 24.64kW capacity absorption chiller.

A parametric analysis was performed on the pond area, ground conditions and pond layers thickness. It was found that varying the pond area, ground conditions and pond layers thicknesses affected the pond and system performance.

The annual electricity consumption for the system was 9 % of the building cooling load. The associated electricity demand would be 87% lower than for an equivalent conventional vapour compression cooling system consumption. That makes a reduction in carbon dioxide emissions of 13 tons per season.

The energy balance of the system showed a small discrepancy (approximately 2%) between the annual energy input and output. This discrepancy may occur because the energy balance considers heat flow from the building into the cooling system at the coil and that consider sensible and latent load on the coil.

The strength of these results is that they are based on a detailed dynamic thermal simulation model of the solar pond, cooling system and building using hourly typical weather data, and the details of the pond, cooling system and building are based on published or actual data.

The overall results showed that Iraq's climate has a potential for solar pond powered thermal space cooling systems. It is feasible to use a solar thermal powered cooling system to meet the space cooling load for a single family house in the summer season.

Chapter 6. Conclusions and recommendations

6.1 Introduction

The use of solar energy for cooling purposes is an attractive prospect the key factors for this application are the availability of solar energy at the specific location and suitable cooling technology. This research has studied a salinity gradient solar pond driving an absorption cooling system, as an alternative to conventional electrical powered cooling systems. For a hot climate like that of Iraq, a solar cooling system could be a sustainable, clean, and viable system to meet cooling energy demand.

6.2 Conclusions

6.2.1 Contribution

The main contributions of this project are:

- i. to develop a dynamic model of heat and mass transfer in the solar pond, in MATLAB and couple it to a dynamic thermal simulation of a building with an absorption chiller air conditioning system in the TRNSYS software.
- ii. to use the coupled simulation to study the performance of the system in the climate of Iraq.

These contributions are met with the aim of this study.

6.2.2 Method and Validation

Referring to the first, second and third objectives in Section 1.7, this research has utilized a one-dimensional, time-dependent mathematical model of heat and mass transfer in a solar pond and the ground underneath it to predict the performance of the pond in the hot and sunny climate of Iraq. MATLAB code was written to solve the governing equations for the solar pond and the ground underneath it. Temperature profiles and concentration distributions have been calculated. Predicting the solar pond performance in a hot climate has been investigated and a comparison with experimental solar pond temperature distribution has been performed.

Referring to the fourth objective, coupling the salinity gradient solar pond with absorption cooling system and building in Iraq has been studied. TRNSYS software

was used to model the solar cooling system including the absorption chiller and building. The weather data used was for Baghdad in Iraq.

The accuracy of the solar pond model was investigated by validating the results with published experimental data. The simulated temperature distribution in the solar pond from the MATLAB code was validated with experimental data from the Bundoora solar pond (Leblanc et al., 2011). It is concluded that the simulated and experimental temperature distributions for the solar pond are in good agreement.

The absorption chiller model in TRNSYS and its associated chiller characteristic data file are also validated with performance data for a commercially available absorption chiller, namely Yazaki WFC-SC10. It has been found that they are in excellent agreement.

The energy balance of the system showed a small discrepancy (approximately 2%) between the annual energy input and output which was in the range of acceptable level of accuracy.

6.2.3 Base Case Main Parameter Values and Performance

Referring to the first, second and third objectives in Section 1.7, the simulation was run for two simulated years to allow the system to approach its long-term performance. The second year (representative year) results are adopted because the first year was assumed to be a warm up year.

Constructing a solar pond with an area of 400 m² and with an upper convective zone (UCZ) of 0.3 m, non-convective zone (NCZ) of 1.25 m and lower convective zone (LCZ) of 0.7 m may be considered to be the suitable dimensions for a for the assumed building and location, as it can provide hot saline water with a temperature exceeding 70°C which, in turn, produces sufficient hot water to make the chiller work properly.

For the base case, it is observed that the zone temperatures vary with the simulation time of the two years, depending on the outside air temperature and incoming solar incidence. The temperature of the lower convective zone (LCZ) is observed to be a maximum of 83.8°C in July in the second year. It has been found that the UCZ is close to ambient in winter, but lower in summer, as expected, since ambient relative humidity is high in winter and low in summer, hence evaporation is low in winter and

high in summer. It is also found that the calculated maximum efficiency for the solar pond is 19.5 % in July in the second year.

The average useful heat extraction from the solar pond is 80 W/m^2 which is about 17.5 % of the average insolation on the pond surface during the summer (June, July ,and August) of the second year.

The salt concentration is found low in the UCZ, high in the LCZ, and varies linearly in the NCZ. The salt concentration of the solar pond needs occasional maintenance by flushing the UCZ with water and adding saturated brine to the LCZ.

For the cooling system, it has been found that the hot water inlet temperature to the absorption chiller only exceeded 70°C for a short period of time during the first year, whereas, the hot water inlet temperature is 70°C - 80°C most of the summer time during the second simulation year, which is sufficient to make the chiller work properly. Therefore, the chilled water outlet temperature will match the chiller setpoint temperature (7°C). It was noticed that the maximum chilled water inlet temperature during summer of the second year was close to 12.5°C , which is the manufacturer's design inlet temperature.

The TRNSYS simulation results showed that a final system for the house with a floor area of approximately 125 m^2 consists of 400 m^2 of solar pond area for 24.64 kW absorption chiller capacity. It is concluded from the simulation of the system that, on an annual basis without a backup heat source, 100% of the heat input demand can be covered with solar energy and the system can meet the building cooling loads. The averaged value of the COP is found to be 0.67 during the summer of the second year. As intended, the maximum room temperature is equal or below 25°C in the months of May, June, July, August, and September during the second year.

The cooling coil, cooling tower and their associated pipes, pumps and fans have been sized for the building's design cooling load. It was found that the maximum heat rejected by the cooling tower is 60 kW as expected and the maximum cooling coil total heat transfer rate is 24.22 kW, which is close to the chiller design capacity.

For the base case, the annual electricity consumption for the system was 9 % of the building cooling load. The associated electricity demand would be 87% lower than for

an equivalent conventional vapour compression cooling system consumption. That would make a reduction in carbon dioxide emissions by 13 tons per operating season.

6.2.4 Key Parameter Variations and Effect On Performance

Referring to the fifth objective, a parametric variation analysis has been performed on the pond area, ground conditions, pond layer's thickness, and heat exchanger effectiveness. It was found that varying the pond area, ground conditions and pond layers thickness had an effect on pond and system performance.

Different solar pond areas have been tested with the same chiller capacity, house and other components to meet the required heat input. It was observed that 400 m² was a suitable pond area for the 125 m² single family house.

The effect of four ground conditions (soil type, moisture content, sandy soil texture and the depth of the water table) have been investigated. Based on the results, it can be concluded that the recommended site to construct the pond is on soil with low thermal conductivity. The effect of soil moisture content on the solar pond performance has been tested. It is recommended to search for dry or lower moisture content soil before constructing the pond.

Different sand soil textures have been utilized in this research: namely, coarse and fine sand soil with dry conditions. The results show that the dry, fine sand soil is the best scenario for the solar pond and site selection. Finally, the effect of varying the depth of the water table under solar pond has been examined. It is recommended to search for a site with deep water table under soil before constructing the pond. Enhancing the solar pond performance will also improve the cooling system performance.

The optimum zone thicknesses for the solar pond connected to the solar air conditioning system have been investigated. Simulations were performed for various thicknesses of the UCZ, NCZ and LCZ zones. For each simulation, the thickness of one zone was varied while the other zone thicknesses were set to base case values. It was found that a thin zone of UCZ is better for the solar cooling system during the summer period of the second year. Therefore, the minimum practical thickness about 0.3 m is recommended.

Increasing the NCZ thickness will have two opposing effects: (1) improving the thermal insulation, hence tending to increase the LCZ temperature and (2) reducing

the amount of solar radiation which reaches the LCZ, hence tending to reduce the LCZ temperature. From the simulation of two years and during the summer for the second year, it was found that the suitable thickness of NCZ is 1.25 m.

Increasing the thickness of the LCZ will increase its thermal capacity, so it will take longer to heat up and longer to cool down. In contrast, decreasing the thickness of the LCZ may disturb the gradient zone (NCZ). Therefore, the 0.7 m LCZ thickness has been selected as a reasonable thickness, which is cheaper than the deeper one.

Simulations have been performed for various value of heat exchanger effectiveness (0.4, 0.6 and 0.8). The effect of varying heat exchanger effectiveness on the solar pond cooling system performance has been tested. It was found that with 0.8 heat exchanger effectiveness, the chilled water outlet temperature stabilises at the design set point for a longer time than 0.4 and 0.6 effectiveness. Therefore, It is recommended to adopt 0.8)for heat exchanger effectiveness for the calculations in this research.

6.2.5 Practical Considerations

It is likely that the cooling load could be reduced by insulation for walls, roof and floor by 33% (Aktacir et al., 2010), improved windows including double glazing and / or heat rejecting glass and/ or shading, and modifying the building form, orientation and glazed area to reduce its conduction and solar heat gains. This would reduce the required sizes of the chiller and solar pond. Insulation the base of the pond could reduce the heat loss to the ground however it might be very expensive in large pond area.

6.2.6 Overall Conclusion

Salt gradient solar pond technology is ideally suited to semi-arid areas such as Iraq and countries with similar weather conditions, owing to the abundance of solar radiation, the thermal energy from which can then be employed to generate power for an absorption chiller to produce cool air for a building. Coupling a solar pond with an absorption chiller and building could assist in addressing the single major issue in such areas: that of providing thermal comfort to the occupants.

Based on the results, it can be concluded that Iraq's climate has a potential for solar pond powered thermal space cooling systems. It is feasible to use a solar pond powered cooling system to meet the space cooling load for a single family house in the summer season.

6.3 Recommendations

6.3.1 Recommendations and Practical Suggestions

Referring to section 6.2.2, the accurate energy statistics data for research, updated weather data and many other thermal data for Iraq are not available from any public agency of the country. Therefore, it is recommended to establish a new organisation which should publish authentic and accurate data as suggested above and any related data for research.

Referring to section 6.2.5, using insulation for walls, roof and double glazed windows instead of the currently used single glazed windows can improve comfort, infiltration and heat gains and losses in buildings. Therefore, buildings in Iraq need more attention to energy efficiency, which could be achieved through application building energy code and standard.

Referring to section 6.2.6, although there are some absorption cooling systems already installed in Iraq, it is recommended to promote use of solar absorption systems for cooling buildings in Iraq, because this research shows the feasibility of using solar energy to drive an absorption chiller as a free energy supply, also saving resources of fossil fuel.

6.3.2 Recommendations For Further Research

Further research could be carried out into using more energy efficient building materials, components and designs to reduce the size of the solar pond cooling system. Research could be carried out into the advantages and disadvantages of individual systems or ponds for each building versus shared ones. Shared ones might enable the overall size and cost to be reduced.

Experimental work can be set up to assess the performance of the actual solar pond cooling system and compared with the TRNSYS results for system performance.

The economic analysis of solar pond cooling system can be carried out under Middle East weather conditions. The most economical configuration for solar pond cooling system can be figured out.

The simulation results showed that in the solar pond cooling system, heat energy collected is available and not used in winter months. Research could be carried out into whether this energy can be used for heating the building and/or domestic hot water in winter season.

Further research can be carried out into using backup heat source and optimising the share of solar energy in the total energy supply with minimum solar pond size.

Further research work could be carried out to investigate the effect of different types of collectors and cooling systems on system efficiency, energy consumption and economic analysis to find out the suitable and optimum system for cooling buildings in hot and dry climate.

Further research can be carried out into using other types of ponds as well as NaCl brine.

Further research work could be carried out to investigate a two or three-dimensional pond model and other ground models, such as pond insulation from ground and the depth of the water table is not infinite heat sink.

Research could be carried out into improving chiller and equipment such as alternative air conditioning equipment, cooling tower, fan and other equipment.

Further research could be carried out to investigate the system performance in non-typical weather because weather varies from year to year.

Appendix A

MATLAB Codes

```
mFileErrorCode = 100    % Beginning of the m-file

% --- Solar pond parameters-----
% NCZ elements
n=127.;
%UCZ Thickness
Xucz=0.3;

%NCZ Thickness
Xncz=1.25;

%LCZ Thickness
Xlcz=0.7;
%Xlcz=1.3;

% Ground elements
    %ng=50;
    ng=50;
% Ground Depth
    Lg=5;
    %Lg=10;
%for clay and sandstone soil/Iraq
    kg=1.7;

    ROg=1470;
    Cpg=2000;
%for clay and Silt soil/Iraq
    %kg=2.15;

    %ROg=1350;
    %Cpg=1137;

%for sand soil/
%kg=1.082;
%ROg=1352;
%Cpg=1105;
% for clay and silt soil/Turkey
%kg=2.941;
%ROg=2271;
%Cpg=1137;
%for clay and Silt soil/Turkey 5% moisture content
    %kg=1.9322;

    %ROg=2325.25;
    %Cpg=1007.34;

    %for clay and Silt soil/Turkey 10% moisture content
    %kg=3.152;

    %ROg=2255.5;
    %Cpg=1175;
%for Course Sand (Dry)
%kg=0.25;
```

```
%ROg=1800;
%Cpg=800;
%for Course Sand (Sat.)
%kg=3.72;
%ROg=2080;
%Cpg=1483;

%for Fine Sand (DRY)
%kg=0.15;
%ROg=1600;
%Cpg=800;

%for Fine Sand (Sat.)
%kg=2.75;
%ROg=2010;
%Cpg=1632;

%for Medium Sand (DRY)
%kg=0.27;
%ROg=1700;
%Cpg=800;

%for Medium Sand (Sat.)
%kg=3.34;
%ROg=2080;
%Cpg=1483;


mFileErrorCode = 110    % After setting parameters

% --- Process Inputs -----
% -----

Tamb = trnInputs(1);
HO   = trnInputs(2);
RH   = trnInputs(3);
V    = trnInputs(4);
THi  = trnInputs(5);
tsky = trnInputs(6);
Tin  = trnInputs(7);
mdot = trnInputs(8);

mFileErrorCode = 120    % After processing inputs

% --- First call of the simulation: initial time step (no iterations) ----
% -----
% (note that Matlab is initialized before this at the info(7) = -1 call, but the m-file
is not called)

if ( (trnInfo(7) == 0) & (trnTime-trnStartTime < 1e-6) )

    % This is the first call (Counter will be incremented later for this very first
```

```

call)
    nCall = 0;

    % This is the first time step
    nStep = 1;

    % Initialize history of the variables for plotting at the end of the simulation
    nTimeSteps = (trnStopTime-trnStartTime)/trnTimeStep;
    history.Tamb = zeros(nTimeSteps,1);
    history.HO = zeros(nTimeSteps,1);
    history.RH = zeros(nTimeSteps,1);
    history.V = zeros(nTimeSteps,1);
    history.THi = zeros(nTimeSteps,1);
    history.tsky = zeros(nTimeSteps,1);
    history.To = (zeros(nTimeSteps,1)+7);
    history.TU = (zeros(nTimeSteps,1)+7);
    history.Ti = (zeros(nTimeSteps,1)+7);
    history.TN2 = (zeros(nTimeSteps,1)+7);
    history.Tb1 = (zeros(nTimeSteps,1)+7);
    history.Tg1 = (zeros(nTimeSteps,1)+25);
    history.Tg2 = (zeros(nTimeSteps,1)+25);
    history.Tgi = (zeros(nTimeSteps,1)+25);
    history.qext = zeros(nTimeSteps,1);
    history.q1 = zeros(nTimeSteps,1);

    % No return, we will calculate the solar pond performance during this call
    mFileErrorCode = 130 % After initialization

end

% --- Very last call of the simulation (after the user clicks "OK"): Do✓
nothing-----
% -----

if ( trnInfo(8) == -1 )

    mFileErrorCode = 1000;

    mFileErrorCode = 0; % Tell TRNSYS that we reached the end of the m-file without✓
errors
    return

end

% --- Post convergence calls: store values -----
% -----

if (trnInfo(13) == 1)

    mFileErrorCode = 140; % Beginning of a post-convergence call

    history.Tamb(nStep) = Tamb;

```

```

        history.HO(nStep)      = HO;
        history.RH(nStep)      = RH;
        history.V(nStep)       = V;
        history.THi(nStep)     = THi;
        history.tsky(nStep)    = tsky;
        history.To(nStep+1)    = To;
        history.TU(nStep+1)    = TU;
        history.Ti(nStep)      = Ti;
        history.TN2(nStep+1)   = TN2;
        history.Tb1(nStep+1)   = Tb1;
        history.Tg1(nStep+1)   = Tg1;
        history.Tg2(nStep+1)   = Tg2;
        history.Tgi(nStep+1)   = Tgi;
        history.qext(nStep)    = qext;
        history.q1(nStep)      = q1;

        mFileErrorCode = 0; % Tell TRNSYS that we reached the end of the m-file without
errors
        return % Do not update outputs at this call

end
% --- All iterative calls -----
% -----
% --- If this is a first call in the time step, increment counter ---
if ( trnInfo(7) == 0 )
    nStep = nStep+1;
end

% --- Get TRNSYS Inputs ---

nI = trnInfo(3);      % For bookkeeping
nO = trnInfo(6);      % For bookkeeping

Tamb = trnInputs(1);
HO    = trnInputs(2);
RH    = trnInputs(3);
V     = trnInputs(4);
THi   = trnInputs(5);
tsky  = trnInputs(6);
Tin   = trnInputs(7);
mdot  = trnInputs(8);

mFileErrorCode = 150; % After reading inputs

% --- Calculate Solar Pond performance -----

%elements thickness or space steps
dx=Xncz/(n-2);

%Time steps
%dt=300;
dt=trnTimeStep*3600;

```



```

% Refraction angle and Snell's Law
%TH=11.97;

TH=asind((sind(THi))/(1.333));

% Montly Average Solar Radiation for June
%HO=315;

dxg=Lg/ng;
ws=((kg/(ROg*Cpg))*dt)/(dxg*dxg);

%Fourier Number

w=(0.000000164*dt)/(dx*dx);

%solar radiation inside the pond
for i=1:n;
    x(i)=((i-1)*dx)+Xucz;
    H(i)=(HO/3.6)*(0.36-0.08*log(x(i)/cosd(TH)));
end
    Hb=(HO/3.6)*(0.36-0.08*log((Xucz+Xncz+Xlcz)/cosd(TH)));
%desity ,specific heat and thermal conductivity for sodium chloride Brine at 60C and
salinity 15%

r=1088.6;
cp=3570;
ka=0.637;

%Initial Condition
for i=1:n
    T(i,1)=7;
end
for i=1:ng;
    Tg(i,1)=25;
end
    Tb1(1)=7;
    Tg1(1)=25;
    Tg2(1)=25;

    j= nStep; % Time Loop 1:20

%-----
% Heat loss from the POND'S Surface

tsu(j)= history.TU(nStep);
La=2257.000;
Cs=1.0097;
Patm=101325;
hconv=5.7+(3.8*V);
Pf=(RH/100)*(exp(18.403-(3885/(Tamb+230))))*133.322368;
Ps(j)=(exp(18.403-(3885/(tsu(j)+230))))*133.322368;

```

```

%Convection

qconv(j)=hconv*(tsu(j)-Tamb);

%Evaporation

qe(j)=(La*hconv*(Ps(j)-Pf))/(1.6*Cs*Patm);

%Radiation

qr(j)=0.83*0.0000000567*((tsu(j)+273)^4)-((tsky+273)^4));

%Total heat loss
qloss(j)=qconv(j)+qe(j)+qr(j);
%-----

% Boundary conditions
%   UCZ   UCZ   (BC 1)

T(1,j+1)=(history.TU(nStep))+((dt/(r*cp*Xucz))*(((HO/3.6)-H(1))+((ka/(dx/2)))*
((history.TN2(nStep))-(history.TU(nStep))))-(qloss(j))));

%Internal nodes
%   NCZ   NCZ

for i=2:n-1; % Space Loop

    T(i,j+1)=(T(i,j))+(w*(T(i+1,j)-2*T(i,j)+T(i-1,j)))+(w*(dx/ka))*(H(i-1)-H(i));
end

%   LCZ   LCZ   (BC 2)

% Pond Area= 400 m2

qext= (((mdot/3600)*(cp))*((history.To(nStep))-(Tin)))/(400);

T(n,j+1)=((history.To(nStep))+((dt/(r*cp*Xlcz))*((H(n-1))-((ka/(dx/2))*((history.To
(nStep))-T(n-1,j))))-(qext)-((kg/dxg)*((history.Tb1(nStep))-(history.Tg1(nStep))))));

%-----
% Ground Heat loss
%-----
%Boundary conditions

% first point Layer

Tg(1,j+1)=(history.Tg1(nStep))+((ws)*(history.Tb1(nStep)-(2*(history.Tg1(nStep))+
(history.Tg2(nStep)))));

```

```

%Internal nodes

    for i=2:ng-1; % Space Loop

        Tg(i,j+1)=(Tg(i,j))+((ws)*(Tg(i+1,j)-(2*(Tg(i,j)))+(Tg(i-1,j)))));

    end

% T sink
    Tg(ng,j+1)=25;
%-----
% The bottom of the Pond
%-----
hLCZ=175.289;

Tb(j+1)=(((Hb)+((kg/dxg)*(Tg(1,j+1)))+(hLCZ*(T(n,j+1)))))/((kg/dxg)+hLCZ));


    To= T(n,j+1);
    TU= T(1,j+1);
    Ti= T(i,j+1);
    TN2= T(2,j+1);
    ql= qloss(j);
    Tg1=Tg(1,j+1);
    Tg2=Tg(2,j+1);
    Tgi=Tg(i,j+1);
    Tb1=Tb(j+1);

% --- Set outputs ---

    trnOutputs(1) = To;
    trnOutputs(2) = TU;
    trnOutputs(3) = HO;
    trnOutputs(4) = Ti;
    trnOutputs(5) = TN2;
    trnOutputs(6) = ql;
    trnOutputs(7) = Tb1;
    trnOutputs(8) = Tg1;
    trnOutputs(9) = qext;
    trnOutputs(10)= mdot;


mFileErrorCode = 0; % Tell TRNSYS that we reached the end of the m-file without errors
return

```

```

n=125.;
L=1.25;
dx=L/n;

maxj=8760;
%maxj=105120;
%maxj=210240;
%maxj=518400;
dt=300;
%Salt Diffusivity
DD=0.00000000323;

w=(DD*dt)/(dx*dx);

% desity ,specific heat and thermal conductivity for sodium chloride Brine at 40C and salinity 10%
%r=1063.8;
%cp=3758.3;
%ka=0.566;
% desity ,specific heat and thermal conductivity for sodium chloride Brine at 60C and salinity 15%
r=1088.6;
cp=3570;
ka=0.637;

%Linear concentration distribution
for i=1:n

    RO(i,1)=(1.7*(i-1))+1;

end

for j=1:maxj % Time Loop

    %Boundary conditions
    % UCZ UCZ

    RO(1,j+1)= (((DD*dt)/(dx*0.3))*(RO(2,j)-RO(1,j)))+(RO(1,j));

    for i=2:n-1; % Space Loop
%Internal nodes
% NCZ NCZ
        RO(i,j+1)=(RO(i,j))+(w*(RO(i+1,j)-(2*(RO(i,j)))+(RO(i-1,j))));

    end

% LCZ LCZ
    RO(n,j+1)= (((-DD*dt)/(dx*0.7))*(RO(n,j)-RO(n-1,j)))+(RO(n,j));
end

for i=1:n;
    R(i)=RO(i,maxj);
end

```

Appendix B

Data

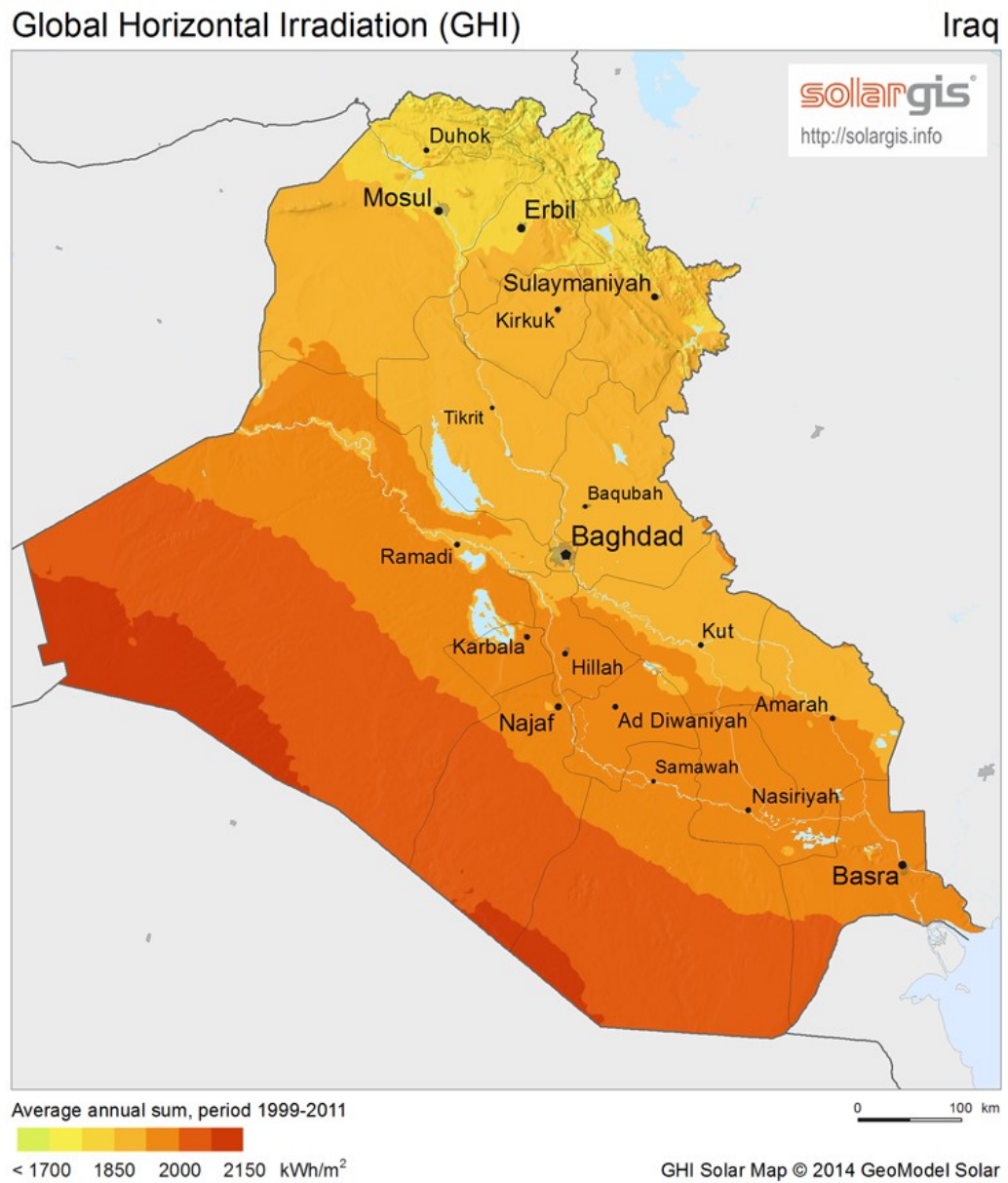


Figure B.1 Iraq global horizontal irradiation

	Energy in			Total Energy in (kWh)	Total Energy out (kWh)	Net (in -out)
Period	Electrical Energy	Chilled Water Energy	Hot Water Energy		Cooling Water Energy	
January	0	0	0	0	0	0
February	0	0	0	0	0	0
March	3.06712963	620.5308322	407.731944	1031.329906	1031.329906	-6.594E-12
April	19.29398148	3902.524731	2564.86472	6486.683434	6486.683434	9.095E-12
May	46.44675926	9397.549085	6174.44639	15618.44223	15618.44223	-2.437E-10
June	60.6712963	12282.10628	8065.39944	20408.17702	20408.17702	-1.903E-09
July	81.43518519	16545.48146	10890.3627	27517.2793	27517.2793	-1.899E-09
August	74.9537037	15594.98244	10474.7331	26144.66919	26144.66919	-3.274E-10
September	53.94675926	10670.75772	7578.13856	18302.84303	18302.84303	0
October	30.48611111	5923.668639	4163.75204	10117.90679	10117.90679	1.655E-10
November	1.840277778	372.6658335	244.639167	619.1452779	619.1452779	-2.728E-12
December	0	0	0	0	0	0
January	0	0	0	0	0	0
February	0	0	0	0	0	0
March	3.06712963	620.5308322	407.731944	1031.329906	1031.329906	-9.322E-12
April	19.29398148	3902.051068	2565.59432	6486.939372	6486.939372	-1.546E-11
May	44.18981481	8806.269179	6549.7058	15400.16479	15400.16479	-4.729E-11
June	56.25	12929.22935	8660.63399	21646.11333	21646.11333	0
July	74.53703704	17908.69521	11867.2072	29850.43943	29850.43943	1.419E-10
August	69.89583333	16076.80308	11047.6114	27194.31027	27194.31027	0
September	51.68981481	10984.41028	7834.47127	18870.57137	18870.57137	0
October	30.09259259	5748.253768	4343.53241	10121.87877	10121.87877	0
November	1.805555556	342.3876571	255.544925	599.7381373	599.7381373	1.364E-12
December	0	0	0	0	0	0

Table B.1 Absorption chiller energy balance

Period	Quseful_in	Total Building_in	Power Consumption	Tower_out	Heat loss	Total Input	Total output	Total (in-out)
January	0.00	0.00	0.00	0.00	0.00	0.00	0.00	0.00
February	0.00	0.00	0.00	0.00	0.00	0.00	0.00	0.00
March	680.77	388.37	42.82	1024.65	47.64	1111.95	1072.29	39.66
April	3973.74	2508.76	269.34	6488.34	119.69	6751.85	6608.03	143.82
May	8844.50	6439.74	616.89	15438.03	99.33	15901.13	15537.37	363.76
June	12984.39	8532.40	785.25	21718.36	80.38	22302.03	21798.74	503.29
July	18041.97	11710.82	1040.54	29980.68	49.79	30793.33	30030.47	762.86
August	16198.34	10897.17	975.75	27313.29	54.74	28071.26	27368.03	703.22
September	11019.52	7714.28	721.59	18930.46	85.70	19455.39	19016.15	439.24
October	5783.24	4258.23	420.09	10139.69	128.80	10461.56	10268.48	193.08
November	399.13	239.67	25.21	592.07	88.11	664.00	680.18	-16.18
December	0.00	0.00	0.00	0.00	0.00	0.00	0.00	0.00
Total 2nd year	77925.60	52689.43	4897.47	131625.57	754.17	135512.51	132379.74	3132.76

Table B.2 Solar pond cooling system energy balance for the second year

		Today's Date: 18/03/2017		Date: <input style="width: 100px;" type="text"/>	
WFC-S Chart Reader, Rev 7B3 ©2009, 2012		MODEL <div style="border: 1px solid black; padding: 2px; display: inline-block;">WFC-SC10</div>		Project Name: <input style="width: 150px;" type="text"/> Unit Identification: <input style="width: 150px;" type="text"/> Prepared By: <input style="width: 150px;" type="text"/>	

VARIABLES					
Chilled Water Flow Rate GPM: <input style="width: 50px; text-align: center;" type="text" value="24.2"/> %: <input style="width: 50px; text-align: center;" type="text" value="100"/> Cooling Water Flow Rate GPM: <input style="width: 50px; text-align: center;" type="text" value="80.8"/> %: <input style="width: 50px; text-align: center;" type="text" value="100"/> Heat Medium Flow Rate GPM: <input style="width: 50px; text-align: center;" type="text" value="38.0"/> %: <input style="width: 50px; text-align: center;" type="text" value="100"/>	Unit Selected: <div style="border: 1px solid black; padding: 2px; display: inline-block;">WFC-SC10</div> Cooling Setpoint °F: <input style="width: 50px; text-align: center;" type="text" value="44.6"/> Heating Setpoint °F: <input style="width: 50px; text-align: center;" type="text" value="na"/> Heat Medium °F: <input style="width: 50px; text-align: center;" type="text" value="190.4"/> Cooling Water °F: <input style="width: 50px; text-align: center;" type="text" value="87.8"/>	Glycol Solution Options Chilled Water Loop none <input style="width: 40px;" type="text"/> 50% <input style="width: 40px;" type="text"/> Cooling Water Loop none <input style="width: 40px;" type="text"/> 0% <input style="width: 40px;" type="text"/> Heat Medium Loop none <input style="width: 40px;" type="text"/> 0% <input style="width: 40px;" type="text"/>			

NOTE: Modified Values displayed are in response to data input above and may not reflect actual performance.
 This data is based upon the UL-listed models only. Metric values are converted from English values.

WORK SHEET DATA							
Specified Values				Modified Values			
Cooling				English		Metric	
Cooling Capacity	120.0	Mbtu/Hr		120.0	Mbtu/Hr	35.2	kW/hr <input style="width: 20px;" type="text"/>
Rated Tons	10.0	Tons		10.0	Tons	10.0	Rated Tons
COP	0.70			0.70		0.70	
Estimated ΔT	9.9	°F		9.9	°F	5.5	°C
Heating							
Heating Capacity	na	Mbtu/Hr		na	Mbtu/Hr	na	kW/hr <input style="width: 20px;" type="text"/>
Estimated ΔT	na	°F		na	°F	na	°C
Heat Medium Loop							
Cooling Mode Heat Input	171.4	Mbtu/Hr		171.4	Mbtu/Hr	50.2	kW/hr <input style="width: 20px;" type="text"/>
Heating Mode Heat Input	na	Mbtu/Hr		na	Mbtu/Hr	na	kW/hr <input style="width: 20px;" type="text"/>
Inlet Temperature	190.4	°F		190.4	°F	88.0	°C
Water Flow	38.0	GPM		38.0	GPM	2.4	l/sec <input style="width: 20px;" type="text"/>
Estimated ΔT	9.0	°F		9.0	°F	5.0	°C
Chilled/Hot Water Loop							
Flow Rate	24.2	GPM		24.2	GPM	1.5	l/sec <input style="width: 20px;" type="text"/>
Estimated ΔT	9.9	°F		9.9	°F	5.5	°C
Cooling Water				Minimum Tower Size:		24 tons	
Total Heat Rejection	291.4	Mbtu/Hr		291.4	Mbtu/Hr	85.4	kW/hr <input style="width: 20px;" type="text"/>
Inlet Temperature	87.8	°F		87.8	°F	31.0	°C
Water Flow	80.8	GPM		80.8	GPM	5.1	l/sec <input style="width: 20px;" type="text"/>
Estimated ΔT	7.2	°F		7.2	°F	4.0	°C

NOTE: For informational purposes only. Yazaki assumes no responsibility for application of this data nor for actual designs created while using this data. Yazaki reserves the right to discontinue or change, at any time, specifications or designs without notice and without incurring obligation or liability.

Figure B.2 Yazaki absorption chiller performance spreadsheet (part 1 of 2)


		Date: <input type="text"/>	
WFC-S Chart Reader, Rev 7B3 ©2009, 2012		Project Name: <input type="text"/>	
MODEL WFC-SC10		Unit Identification: <input type="text"/>	
		Prepared By: <input type="text"/>	
PROJECT DATA REPORT			
NOTE: Modified Values displayed are in response to data input in VARIABLES section of this spreadsheet and may not reflect actual performance. For informational purposes only. This data is based upon the UL-listed models only. Metric values are converted from English values.			
Specified Values		Modified Values	
Cooling		English Metric	
Capacity	120.0 Mbtu/Hr	120.0 Mbtu/Hr	35.2 kW/hr
Chilled Water Temp	44.6 °F	44.6 °F	7.0 °C
Rated Tons	10 Tons	10.0 Tons	10.0 Rated Tons
COP	0.70	0.70	0.70
Heating			
Capacity	na Mbtu/Hr	na Mbtu/Hr	na kW/hr
Estimated ΔT	na °F	na °F	na °C
Heated Water Temp	na °F	na °F	na °C
Chilled Water Loop <i>Water, No Glycol</i>			
Flow Rate	24.2 GPM	24.2 GPM	1.5 l/sec
Evap Pressure Drop	8.1 PSI	8.1 PSI	56 kpa
Estimated ΔT	9.9 °F	9.9 °F	5.5 °C
Water Retention Volume	4.5 Gallons	4.5 Gallons	17 liters
Cooling Water Loop <i>Water, No Glycol</i>		Minimum Tower Size: 24 tons	
Total Heat Rejection	291.4 Mbtu/Hr	291.4 Mbtu/Hr	85.4 kW/hr
Inlet Temperature	87.8 °F	87.8 °F	31.0 °C
Water Flow	80.8 GPM	80.8 GPM	5.1 l/sec
Absorber Pressure Drop	12.3 PSI	12.3 PSI	85 kpa
Condenser Pressure Drop	incl in ABS PSI	incl in ABS PSI	incl in ABS kpa
Estimated ΔT	7.2 °F	7.2 °F	4.0 °C
Water Retention Volume	17.4 Gallons	17.4 Gallons	66 liters
Heat Medium Loop <i>Water, No Glycol</i>			
Cooling Mode Heat Input	171.4 Mbtu/Hr	171.4 Mbtu/Hr	50.2 kW/hr
Estimated Cooling ΔT	9.0 °F	9.0 °F	5.0 °C
Heating Mode Heat Input	na Mbtu/Hr	na Mbtu/Hr	na kW/hr
Estimated Heating ΔT	na °F	na °F	na °C
Inlet Temperature	190.4 °F	190.4 °F	88.0 °C
Water Flow	38.0 GPM	38.0 GPM	2.4 l/sec
Generator Pressure Drop	13.1 PSI	13.1 PSI	90 kpa
Water Retention Volume	5.5 Gallons	5.5 Gallons	21 liters
Electrical		Physical Data	
Power Supply	208-3-60 V-ph-Hz	Dimensions	Width 29.9 Inches 759 mm
Consumption	210 Watts		Depth 38.2 Inches 970 mm
MCA	0.60 Amps		Height 74.8 Inches 1900 mm
MOCP	15 Amps	Weight, Dry	1100 Pounds 500 kgs
		Weight, Operating	1329 Pounds 604 kgs
Noise Level			
Noise Level	49 dB(A)	Chilled/Hot Water Piping	1-1/2 Inches NPT
		Cooling Water Piping	2 Inches NPT
		Heat Medium Piping	1-1/2 Inches NPT
NOTE: For informational purposes only. Yazaki assumes no responsibility for application of this data nor for actual designs created while using this data. Yazaki reserves the right to discontinue or change, at any time, specifications or designs without notice and without incurring obligation or liability.			

Figure B.3 Yazaki absorption chiller performance spreadsheet (part 2-of 2)

Air cooled chiller & heat pump

YLCD-YLHD 0025 to 0150



Technical features

T Three phases supply C/P Hydro Pack H Heat pump

Models			YLCD / YLHD					
			0025 TC	0040 T-TP	0070 T-TP	0100 T-TP	0120 T-TP	0150 T-TP
Performance	Cooling capacity c/o units (1)	kW	24.6	39.8	69.5	98.4	118.5	144.5
	Total Input Power (1)	kW	8.45	15.13	27.36	37.41	44.72	56.67
	EER (1)		2.91	2.63	2.54	2.63	2.65	2.55
	Cooling capacity h/p units (1)	kW	23.6	39.8	67.5	95.4	116.5	142.5
	Heating capacity h/p units (1)	kW	23.4	43.2	72.5	104.6	120.1	159.5
	Total Input Power cool/heat mode (1)	kW	8.14 / 8.18	15.13 / 15.6	26.57 / 26.46	36.27 / 37.63	42.21 / 43.2	60.13 / 59.07
	EER / COP (1)		2.9 / 2.86	2.63 / 2.77	2.54 / 2.74	2.63 / 2.78	2.76 / 2.78	2.37 / 2.7
	Capacity steps	%	100	50-100			25-50-75-100	
	Sound power level	dB(A)	81	83	86	86	86	87
Compressor	Type		Scroll					
	Quantity		1	2	2	4	4	4
Air side heat exchanger	Fans quantity		1	2	2	4	4	4
	Nominal air flow	m ³ /h	8 100	18 000	23 000	36 000		48 000
	Nominal static pressure	Pa	100			200		
	Working ambient temp. cool. / heat. mode		(4) (-18°C) ~ 46°C / -10°C ~ 20°C			-18°C ~ 46°C / -10°C ~ 20°C		
Water side heat exchanger	Type		Single plate heat exchanger			Dual plate heat exchanger		
	Unit water volume	Litres	32	84	92	193	195	214
	Pump Type		Multistage horizontal pump					
	Nominal water flow	l/h	4 300	6 880	12 040	17 030	20 470	24 940
	Available pressure (1) (2)	kPa	208	105	120	187	202	186
	Pressure drop (1) (3)	kPa	-	31	53	54	32	24.5
	Working range water leaving temperature cooling / heating (5)		-5°C ~ 15°C / 30°C ~ 50°C					
	Water connections	inch	1-1/4"	2"		2-1/2"		
	Height	mm	1 526	1 794	1 794	2 460	2 460	2 480
Dimensions & Weight	Width	mm	1 740	2 659	2 659	3 466	3 416	3 768
	Depth	mm	785	897	897	1 101	1 101	1 101
	Weight without pack / pack c/o	kg	- / 390	730 / 770	740 / 780	1 264 / 1 360	1 264 / 1 360	1 680 / 1 776
	Weight without pack / pack h/p	kg	- / 400	750 / 790	760 / 800	1 284 / 1 380	1 284 / 1 380	1 700 / 1 796
El. supply	Voltage / Phases / Frequency	V/ph/hz	400 / 3 / 50 + N + E					

Table B.3 Vapour compression air cooled chiller and heat pump from YORK

Appendix C

Published Papers



SHC 2015, International Conference on Solar Heating and Cooling for Buildings and Industry

The effect of ground conditions under a solar pond on the performance of a solar air-conditioning system

Safwan Kanan^{a*}, Jonathan Dewsbury^a, Gregory F. Lane-Serff^a, Muhammad Asim^a

^a*School of Mechanical, Aerospace and Civil Engineering, University of Manchester, Manchester, M13 9PL, UK*

Abstract

Heat loss through the bottom of a salt gradient solar pond is significant if the bottom of the pond is non-insulated. This loss has an impact on the thermal performance of the solar pond and the solar air conditioning system connected to it. In this paper, a coupled simulation between a transient model of the solar pond and the ground underneath it in MATLAB and of an absorption chiller, air conditioning system and building in TRNSYS is used to investigate the effect of ground conditions on the performance of the complete system. Four factors have been studied for soil underneath the solar pond: moisture content, soil type, sandy soil texture and the depth of the water table. It was found that dry, fine sandy soil with low thermal conductivity is best and that the deeper the water table, the better for system performance.

© 2016 The Authors. Published by Elsevier Ltd. This is an open access article under the CC BY-NC-ND license (<http://creativecommons.org/licenses/by-nc-nd/4.0/>).

Peer-review by the scientific conference committee of SHC 2015 under responsibility of PSE AG

Keywords: Salt gradient solar pond; soil thermal properties; solar air-conditioning system; TRNSYS simulation.

1. Introduction

Air conditioning is essential for residential buildings in hot and dry weather such as the Middle East. An attractive alternative to vapour compression refrigeration for air conditioning could be absorption refrigeration driven by heat energy, particularly solar thermal energy [1]. Different types of solar thermal collectors have been used in such solar air conditioning systems, such as flat plate solar collectors and evacuated tube collectors [2]. A salinity gradient solar pond has been suggested as a combined collector and heat store to drive an absorption chiller.

* Corresponding author. Tel.: +44-782-556-7780.

E-mail address: safwan.kanan@manchester.ac.uk or safwan2smj@yahoo.com

In a salinity gradient solar pond, solar radiation penetrates to the bottom of the pond, which is usually black to absorb as much radiation as possible, and heats it. Heat loss to the surroundings is reduced by the salinity gradient (explained below), so high temperatures can be achieved at the bottom of the pond. Heat can be withdrawn from the bottom of the pond to drive an absorption chiller or other load.

The pond is typically composed of three zones as shown in Figure 1. The topmost zone is the Upper Convective Zone (UCZ), which has the lowest salt concentration and protects the other zones from disturbance by the wind. The middle zone is the Non-Convective Zone (NCZ), which has salt concentration increasing with depth. The increase in density due to increasing salt concentration is greater than the decrease due to increasing temperature. Thus convection currents are suppressed and, as the thermal conductivity of water is fairly low, the NCZ acts as an insulator over the bottom zone. The bottom zone is the Lower Convective Zone (LCZ), which has the highest salt concentration and temperature, and stores heat to supply the load.

Solar ponds are usually contained in earth excavations, and the heat loss to the ground can have an important influence on the performance of the pond. Saxena et al. [3] investigated the effect of water table depth on solar pond thermal performance. Simulation analysis indicated that the deeper the water table, the lower the heat losses and the higher the temperature achieved by the pond. Zhang and Wang [4] studied the time-dependent ground heat storage capacity, its relations to the parameters of the pond and the properties of soil beneath the pond, and its effects on the transient behaviour of the solar pond. They concluded that the ground thermal properties and the depth of the water table had a significant influence on the transient behaviour.

In this article the effect of four ground conditions (moisture content, soil type, sandy soil texture and the depth of the water table) is investigated using a coupled simulation between a transient model of the solar pond and the ground underneath it in MATLAB and of an absorption chiller, air conditioning system and building in TRNSYS. Different soil types and water table depths were tested with all other parameters unchanged. It was assumed that there was no insulation between the pond and the ground.

Nomenclature

Greek letters

C_p	specific heat capacity for brine (J/kg °C)	θ_r	angles of refraction
C_{pg}	specific heat capacity for soil (J/kg °C)	ρ	brine density (kg/m ³)
C_{pgd}	dry specific heat capacity for soil (J/kg °C)	ρ_g	soil density (kg/m ³)
C_{pgc}	corrected specific heat capacity for soil (J/kg °C)	ρ_{gd}	dry soil density (kg/m ³)
C_{pw}	specific heat capacity for water (J/kg °C)	ρ_{gc}	corrected soil density (kg/m ³)
H_o	insolation incident on horizontal surface (W/m ²)	ρ_w	water density (kg/m ³)
H_x	incoming radiation flux at depth x (W/m ²)	ω	moisture content (% of total weight)
H_b	incoming radiation flux at bottom of the pond (W/m ²)		
h	convection heat transfer coefficient for LCZ (W/m ² °C)		
k	thermal conductivity (W/m °C)		
k_g	soil thermal conductivity (W/m °C)		
L_g	depth of water table (m)		
LCZ	Lower Convective Zone		
NCZ	Non-Convective Zone		
T	temperature (°C)		
T_b	temperature at the bottom (°C)		
T_g	ground or soil temperature (°C)		
UCZ	Upper Convective Zone		
x	distance from the surface of the solar pond (m)		
X	layer thickness (m)		

2. Mathematical modelling

The governing equations of one-dimensional heat transfer for the salinity gradient solar pond and the ground underneath it are solved numerically by an explicit finite difference method, to determine the temperature distributions within the pond and the ground, as shown in Figure 1. The code is written in MATLAB. The most important output from the code is the temperature of the lower convective zone at the bottom of the pond, which is used to drive the absorption chiller. The model of the chiller, air conditioning system and building is developed within the TRNSYS simulation environment [5], which calls the MATLAB code at each time step to couple the pond to the rest of the system.

2.1. Solar pond and ground model

The simulation model is one-dimensional (neglecting heat loss from the sides of the pond) and is modified from [3, 6]. The vertical coordinate (x) is measured as positive downward, and $x = 0$ at the surface of the pond as shown in Figure 1.

Ambient conditions (temperature, humidity, wind speed and solar radiation) are taken from an hourly weather data file. The solar radiation penetrating the water decays exponentially with depth and is given by Equation (1) [7].

$$\frac{H_x}{H_0} = \left\{ 0.36 - 0.08 \ln \left(\frac{x}{\cos \theta_r} \right) \right\} \quad (1)$$

The heat flow equation for the solar pond in the NCZ is given by Equation (2) [8].

$$\rho C_p \left(\frac{\partial T}{\partial t} \right) = k \left(\frac{\partial^2 T}{\partial x^2} \right) - \frac{\partial H(x,t)}{\partial x} \quad (2)$$

Energy balances for the UCZ and LCZ are used as boundary conditions for Equation 2.

Assuming no insulation between the pond and the soil, the heat transfer between the bottom of the solar pond and the soil is given by Equation (3). [9]

$$k_g \left(\frac{\partial T_b}{\partial x_g} \right) + h(T_b - T_{LCZ}) = H_b \quad (3)$$

The heat flow equation through the soil underneath the solar pond is given by Equation (4) [9].

$$\rho_g C_{p_g} \left(\frac{\partial T_g}{\partial t} \right) = k_g \left(\frac{\partial^2 T_g}{\partial x_g^2} \right) \quad (4)$$

The sink temperature of the last layer is equal to the ground water table temperature.

$$T_{SINK} = T_{water\ table} \quad (5)$$

2.2. System description

The simulated solar cooling system is shown in Figure 2. It consists of a single effect vapour absorption water chiller with a rated capacity of 7 TR, and set point of 7°C, thermally powered by the salinity gradient solar pond through a heat exchanger. The chiller requires an inlet hot water temperature of 70°C or more to operate [10]. Chilled water is passed through a cooling coil, and the cool air distributed by a fan to a 125 m² single family house in Baghdad, Iraq (33.32° N, 44.42° E), based on a typical new house. The heat rejected from the chiller is dissipated

to the environment by a wet cooling tower. Pumps are used to circulate hot, chilled and cooling water, and a controller provides automatic operation of the system. Real component data is utilised in the simulation. The MATLAB code for the pond and soil are called by TRNSYS using the Type 155 component. The simulation was run for two simulated years to allow the system to approach its long-term performance.

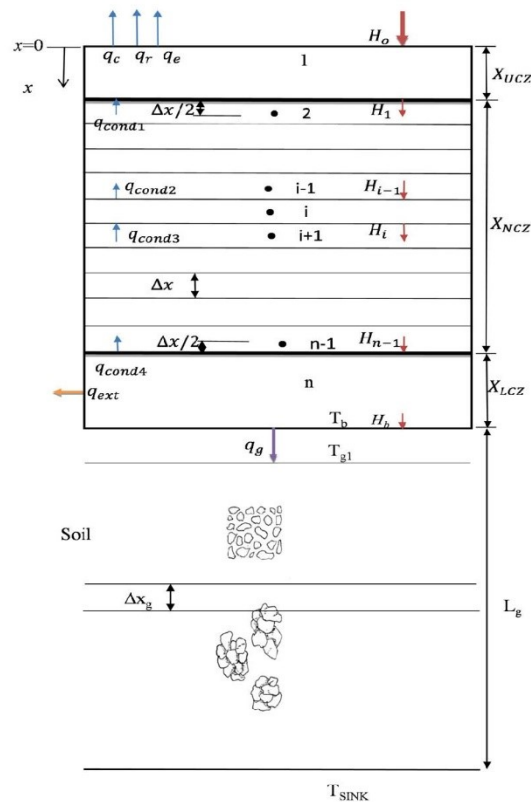


Fig. 1. Solar pond and ground model

2.3. Soil thermal properties

Soil is a porous medium and is thus composed of solids and pores. The solids comprise mineral substances and organic matter; the pores may be filled with air or water in any of its three phases (liquid, vapour or ice) [11].

Heat loss from the solar pond to the ground is by unsteady conduction and is affected by the soil's thermal conductivity, density and specific heat [12]. Obtaining accurate values for thermal properties of the soil requires a detailed site survey. Thermal properties of granular soils (sand, clay, silt) may be estimated from the sand and clay content, dry density, and moisture content. In this study, analytical equations were used to calculate the thermal properties of the soil based on soil type, dry density and moisture content.

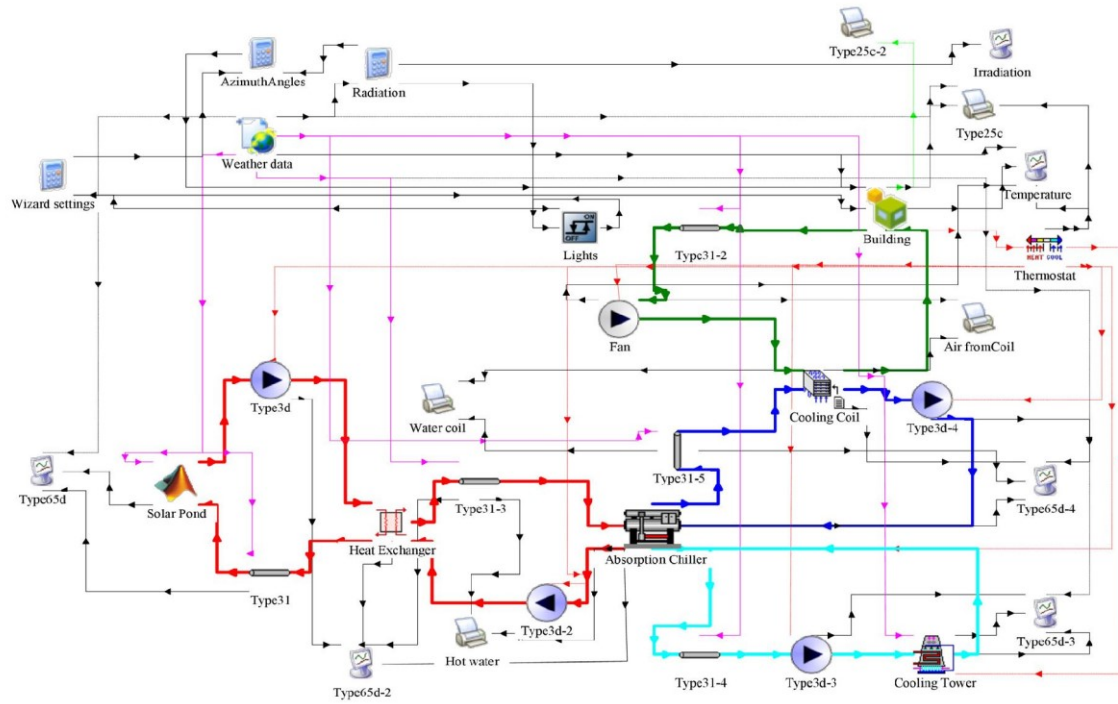


Fig. 2. TRNSYS model

The thermal conductivity of the soil (k_g) was calculated from the equations given by [13] as follows:

$$k_g = 0.14423(0.9 \log \omega - 0.2) 10^{0.000624 \rho_{gd}} \quad \text{for silt and clay soils} \quad (6)$$

$$k_g = 0.14423(0.7 \log \omega + 0.4) 10^{0.000624 \rho_{gd}} \quad \text{for sand soils} \quad (7)$$

The dry specific heat ($C_{p_{gd}}$) and dry soil density (ρ_{gd}) of the soil must be corrected for moisture content as follows [13]:

$$C_{p_{gc}} = [\omega C_{p_w} + (100 - \omega) C_{p_{gd}}] / 100 \quad (8)$$

$$\rho_{gc} = [\omega \rho_w + (100 - \omega) \rho_{gd}] / 100 \quad (9)$$

All values are used in this study are listed in Tables 1 and 2. There is a wide variation of thermal conductivity with soil type and, especially, moisture content. There is less variation of density and specific heat.

Table 1. Soil thermal properties. [13][14][15]

				Calculated soil properties			Experimental soil properties	
		Unit	Clay and Silt [13]	Clay and silt 2 (calculated) 5% moisture	Clay and silt 2 (calculated) 10% moisture	Sandy soil [14]	Clay and sandstones [15]	Clay and silt 1 [15]
Thermal conductivity	k_g	W/m. °C	2.941	1.932	3.152	1.082	1.7	2.15
Dry density	ρ_{gd}	kg/m ³	2395	2395	2395	1382	-	
Moisture	ω	%	8.87	5	10	7.9	4.4	5.6
Dry specific heat	Cp_{gd}	kJ/kg. °C	0.84	0.84	0.84	0.84	-	
Corrected density	ρ_{gc}	kg/m ³	2271	2325.25	2255.5	1352	1470	1350
Corrected specific heat	Cp_{gc}	kJ/kg. °C	1.137	1.007	1.175	1.105	2.0	1.137

Table 2. Soil thermal properties with a different texture. [16]

Soil type	Moisture content %	Density kg/m ³	Thermal conductivity W/m. °C	Specific heat kJ/kg. °C
Coarse sand(dry)	0	1800	0.25	0.800
Coarse sand (sat.)	20.2	2080	3.72	1.483
Fine sand (dry)	0	1600	0.15	0.800
Fine sand (sat.)	24.6	2010	2.75	1.632

3. Results

The results presented here were obtained from simulation of the complete model for two simulated years, to ensure that the system approached its long-term performance.

Four factors were studied for soil underneath the solar pond: moisture content, soil type, sandy soil texture and the depth of the water table. The absorption chiller required an inlet hot water temperature of 70°C or higher (based on manufacturer performance) to work at its design conditions. The effect of the four soil factors on the chiller inlet hot water temperature is shown in Table 3.

At 5 m water table depth, soils which are dry or at moderate moisture content (up to 8%) allow the chiller to be operate most of the time from May to September (3400 hours or more). At higher moisture contents, the chiller's possible operating time is greatly reduced, in some cases to zero.

Increasing the depth of the water table beyond 5 m slightly increases the possible operating time. Reducing the depth reduces the possible operating time, in some cases to zero.

Table 3. Number of hours for chiller inlet hot water temperature above 70°C with different ground conditions.

Soil Type	Soil Thermal Properties			Moisture Content (%)	Water table depth (m)	No. of hours for chiller inlet hot water temperature above 70 °C (May-Sept /2 nd year)
	Thermal conductivity W/m. °C	Density kg/m ³	specific heat kJ/kg . °C			
Clay and sandstone	1.7	1470	2.0	4.4	1	0
					2	0
					3	2772
					4	3426
					5	3613
					10	3621
Clay and silt 1	2.15	1350	1.137	5.6	5	3425
Clay and silt 2	1.932	2325	1.007	5	5	3473
	3.152	2255	1.175	10	5	1262
Sand	1.082	1352	1.105	7.9	5	3660
Coarse sand	0.25	1800	0.800	0	5	3660
	3.72	2080	1.483	20.2	5	0
Fine sand	0.15	1600	0.800	0	5	3660
	2.75	2010	1.632	24.6	5	2360

4. Conclusions

A coupled simulation between MATLAB and TRNSYS has been used to develop a model for a salinity gradient solar pond and the ground beneath it, with the pond driving an absorption chiller to cool a building through an air conditioning system.

The thermal conductivity of the soil varies considerably with soil type and, especially, moisture content. There is less variation of density and specific heat. It was found that the solar pond and absorption chiller could be used to cool a single family house during the summer period in Iraq, but not for all soil types and ground conditions. Dry, fine sandy soil with low thermal conductivity was better than the other types of soil. The deeper the water table, the better the system performance.

The ground conditions should be investigated before constructing a solar pond. It may be necessary to insulate the pond from the ground, particularly in case of a high soil moisture content or a shallow water table.

Acknowledgements

This research is funded by Ministry of Higher Education and Scientific Research (MoHESR) of Iraq.

References

- [1] Malzoumi M, Naghashzadegan M, Javaherdeh K. Simulation of solar lithium–water absorption cooling system with parabolic trough collector. *Energy Convers Manage* 2008; **49**:2820–32.
- [2] Sarbu, Ioan, and Calin Sebarchievici, Review of solar refrigeration and cooling systems, *Energy and Buildings*, 2013; **67**:286-297.
- [3] Saxena, A. K., S. Sugandhi, and M. Husain, Significant depth of ground water table for thermal performance of salt gradient solar pond. *Renewable Energy* 2009; **34**(3): 790-793.
- [4] Zhang, Z. M., and Y. F. Wang. A study on the thermal storage of the ground beneath solar ponds by computer simulation. *Solar Energy* 1990; **44**, no. 5: 243-248.

- [5] Klein, S.A. et al, 2010, TRNSYS 17: A Transient System Simulation Program, Solar Energy Laboratory, University of Wisconsin, Madison, USA, <http://sel.me.wisc.edu/trnsys>.
- [6] Kanan, S.; Dewsbury, J.; Lane-Serff, G. Simulation of Solar Air-Conditioning System with Salinity Gradient Solar Pond, Energy Procedia 2015; **79**, 746-751.
- [7] Bryant, H. C., and Ian Colbeck., A solar pond for London. Solar Energy 1977; **19**(3): 321-322.
- [8] Rubin, H., Benedict, B.A., Bachu, S., Modeling the performance of a solar pond as a source of thermal energy. Solar Energy 1984; **32**, 771-778.
- [9] Sodha MS, Kaushika ND, Rao SK, Thermal analysis of three zone solar pond. Energy Research 1981; **5**:321–40.
- [10] Yazaki. WFC – SC chiller and chiller specifications; available at www.yazaki.com.
- [11] Behari, Jitendra. Microwave dielectric behaviour of wet soils. Vol. 8. Springer Science & Business Media, 2006.
- [12] Ochsner, T.E., R. Horton, and T. Ren, A New Perspective on Soil Thermal Properties. Soil Sci. Soc. Am. J., 2001; **65**(6):1641-1647.
- [13] Hepbasli, A., Performance evaluation of a vertical ground-source heat pump system in Izmir, Turkey. International Journal of Energy Research, 2002; **26**(13): 1121-1139.
- [14] Yari, M. and N. Javani, Performance assessment of a horizontal-coil geothermal heat pump. International Journal of Energy Research, 2007; **31**(3):288-299.
- [15] AlMaliky, Salam J. Bash. Investigation of the readiness of ground soils for the installation of ground heat exchange systems in Baghdad city. Journal of Geography and Geology 2011; **3**, no. 1: 200-206.
- [16] Clarke, Barry G., Ali Agab, and Duncan Nicholson. Model specification to determine thermal conductivity of soils. Proceedings of the ICE-Geotechnical Engineering 2008; **161**, no. 3: 161-168.



Available online at www.sciencedirect.com

ScienceDirect

Energy Procedia 91 (2016) 702 – 706

Energy

Procedia

SHC 2015, International Conference on Solar Heating and Cooling for Buildings and Industry

TRNSYS simulation of a solar cooling system for the hot climate of Pakistan

Muhammad Asim^{a*}, Jonathan Dewsbury^a, Safwan Kanan^a

^a School of Mechanical Aerospace and Civil Engineering, University of Manchester Oxford road, Manchester M13 9PL, UK

Abstract

Cooling is a basic need for buildings in hot and sunny climates. In most countries the major source of cooling is electrical power based. During summer in hot climates there is an increase in electricity consumption due to cooling load. Pakistan is facing an electricity shortage crisis, which becomes worse in summer due to the high demand for cooling. The annual average insolation for Pakistan is 5-6 kWh/m²/day, reaching 6-8 kWh/m²/day in summer with sunshine of 10-13 hours a day, which gives suitable conditions for solar powered cooling system operation. TRNSYS software provides the possibility to simulate a complete solar air conditioning system integrated with a building. In this study, TRNSYS is used to model an absorption chiller operated by hot water from an evacuated tube collector. It is found that, with a hot water storage tank, a collector area of 12 m² is sufficient to maintain the temperature in a room in a typical house at or below 26°C during the cooling season.

© 2016 The Authors. Published by Elsevier Ltd. This is an open access article under the CC BY-NC-ND license (<http://creativecommons.org/licenses/by-nc-nd/4.0/>).

Peer-review by the scientific conference committee of SHC 2015 under responsibility of PSE AG

Keywords: Solar Cooling Pakistan; TRNSYS Simulation; Solar Thermal Cooling

1. Introduction

Pakistan has a generally hot and sunny climate, and many buildings use electrically powered air conditioning for much of the year. Most of the electricity system is dependent on fossil fuels (Fig.1(a)), which are expensive and damage the environment by their emissions (including greenhouse gases) [1]. Pakistan is an energy deficient country, where the majority of the population has inadequate provision of basic energy facilities like electricity and

* Corresponding author. Tel.: +44-772-200-3224;
E-mail address: Muhammad.asim@manchester.ac.uk

gas [2]. The current electricity shortage crisis started in 2007 and has affected the operation of cooling systems, causing discomfort in buildings, particularly in summer [3].

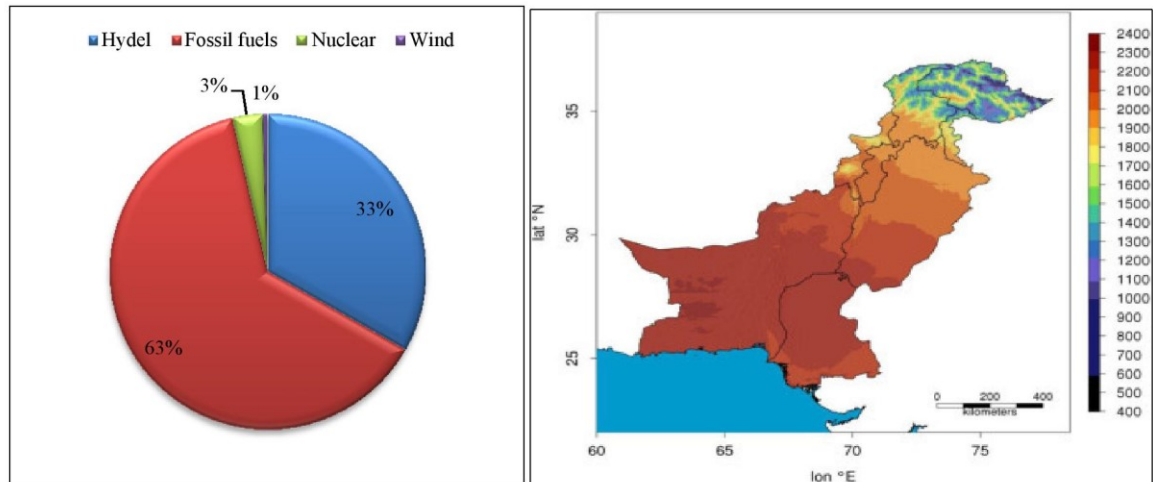


Fig. 1: Pakistan's (a) electricity generation by fuel type; (b) solar energy potential

The annual mean global insolation in Pakistan is 5-6 kWh/m²/day, with 10 - 13 sunshine hours per day, which gives suitable conditions for solar powered cooling system operation[4]. The multi-year (2000-2012) mean of annual global horizontal irradiance for Pakistan is shown in Fig.1 (b)[5]. A clean and sustainable cooling system, such as solar energy cooling, can provide an alternative green source for comfort in buildings.

TRNSYS is a widely used, thermal process simulation program. It was originally developed by the members of the solar energy laboratory at the University of Wisconsin for solar energy applications, and can now be used for a wider variety of thermal processes. The first version was released in 1977 [6]. TRNSYS has the capability of interconnecting system components in any desired manner, solving the system differential equations, and producing information output. Component models may be selected from the libraries, or written by the user and linked to the main TRNSYS model [7].

The aim of this research is to use a TRNSYS simulation to determine whether it is feasible to use a system comprising an evacuated tube solar collector driving an absorption chiller, to maintain a comfortable temperature in a typical single family house in Pakistan during the cooling season.

Nomenclature

COP	Co-efficient of Performance
kW	Kilo Watt
kWh	Kilo Watt hour
TRNSYS	TRaNsient SYstem Simulation
TESS	Thermal Energy System Specialists
TR	Ton of Refrigeration

2. System description and modelling

The building comprises one room of a typical single-storey house in Pakistan, with one single-glazed window and one timber door. The room is of brick and concrete construction, uninsulated. The cooling system comprises an

evacuated tube solar collector which supplies hot water to an absorption chiller, which in turn supplies chilled water to an air cooling coil. A fan circulates room air through the cooling coil. The chiller rejects heat to ambient air through a cooling water circuit using a dry cooling tower. A stratified tank stores hot water from the collector to allow the chiller to operate when there is insufficient solar energy available (which is mainly at night).

Pumps circulate water through the system. The solar collector circuit is controlled so that it operates when heat is available and required by the chiller or storage tank; the rest of the system operates continuously during the cooling season to maintain the room temperature at the set point.

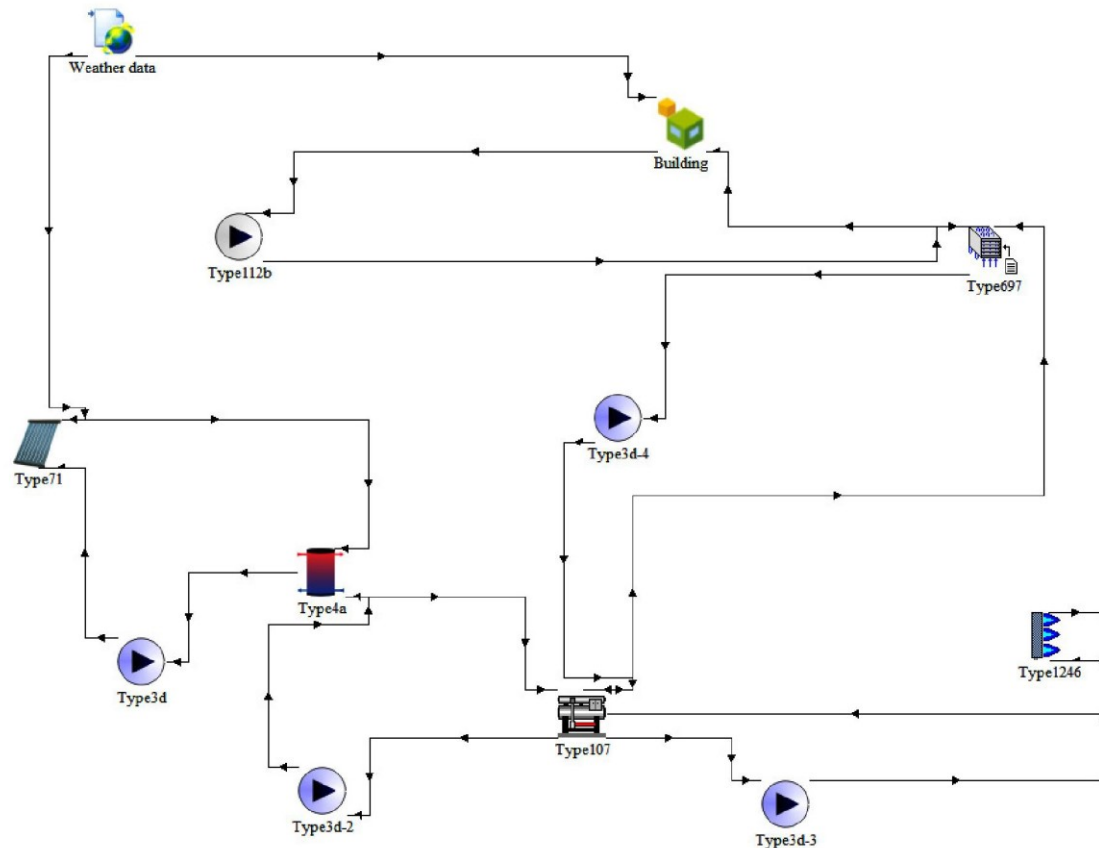


Fig.2: TRNSYS model of building integrated solar thermal cooling system

Sketchup was used to model the room geometry. The model was imported to TRNSYS; building constructions and the components of the solar thermal energy and cooling systems were selected from the libraries. The components were integrated in operational order and the cooling system connected with the building (Fig.2). (Note that the lines in Fig.2 represent logical connections in the simulation model, not necessarily physical connections.)

An absorption chiller capacity of 3.52 kW (1 TR) is chosen to match the cooling load of the space (a single room); other component sizes were optimized to maintain the room temperature set point throughout the summer season. The chiller model is a scaled-down version of a realistic, larger, absorption chiller. In practice, a single larger chiller would probably be used to cool several rooms. TRNSYS Type 107 can simulate any cooling capacity chiller and this small size chiller (3.52kW) was used by references [8, 9]. Simulation was performed for one year starting on 1st January. Key parameters are given in Table 1.

Table 1. System key parameters

Description	Specification
Room floor area	14 m ²
Cooling set point	26°C
Operation hours	Continuous
Solar fraction	100%
Design cooling load	2 kW
Chiller type	Hot water fired absorption
Chiller capacity	3.52 kW (1TR)
Collector type	Evacuated tube
Collector area	12 m ²
Collector slope	0
Hot water storage tank volume	2 m ³
Weather data	TMY2, Lahore, Pakistan

The storage tank size is chosen to ensure that the system can meet the cooling load at all times without an auxiliary heat input. Topics for further research could include reducing the tank size by, for example, changing the system temperatures or using an auxiliary heat input.

3. Results

The TRNSYS simulation was run with 15 minute time step and results were obtained. The selected system successfully maintained the room temperature below set point 26°C, even when the ambient temperature was more than 40°C, during peak summer season (Fig. 3). The other key results during the summer (April –September) for the cooling season are presented in Table 2. All the energies are stated per m² of collector area.

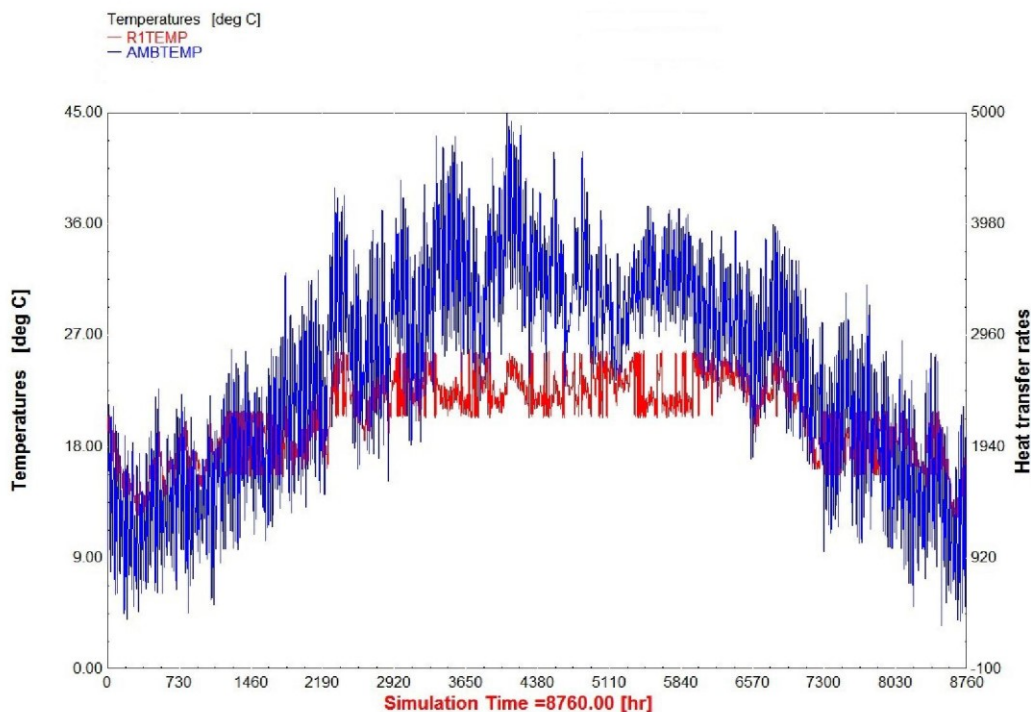


Fig.3. Simulated room temperature and ambient temperature for one year

Table 2. Simulation Results

Period	Specification
Collector efficiency (%)	75
Chiller COP	0.60
Total Chiller yield (kWh/m ²)	790
Total room cooling load(kWh/m ²)	479
Total electrical energy consumption (kWh/m ²)	67
Total pipes and tank heat loss (kWh/m ²)	6.5

The results are presented in term of collector area so easy to compare with any other result (similar or different capacity) as collector area is key parameter for solar thermal cooling system design. The comparison of these results with the similar capacity references [8, 9] showed a better energies per collector area.

4. Conclusions

According to TRNSYS simulation of solar powered absorption cooling system, using TMY2 data of Lahore, following conclusions are established.

- The evacuated tube solar collector yield is sufficient to meet the system required thermal energy input during the cooling season.
- The stratified hot water tank stores heat efficiently, with losses of less than 1% of total input energy.
- The electrical energy supply to the system is about 14% of the cooling load.
- The equipment sizes could reasonably be accommodated in the building, and could be reduced by measures to reduce the cooling load.
- Pakistan's climate has the potential for use of solar powered thermal cooling systems in summer.

References

1. British Petroleum, *Statistical review of world energy June 2014*. 2014.
2. Muneer, T. and M. Asif, *Prospects for secure and sustainable electricity supply for Pakistan*. Renewable and Sustainable Energy Reviews, 2007. **11**(4): p. 654-671.
3. Pasha, Hafiz A and Wasim Saleem, *The Impact and Cost of Power Load Shedding to Domestic Consumers*. The Pakistan Development Review, 2013. **52**(4): p. 355-373.
4. Nasa. *Surface Meteorology and Solar Energy*. Renewable Energy Source website 2014 [cited 2014 30-11-2014]; 6.0:[]
5. Stöckler, Steffen, Christoph Schillings and Birk Kraas, *Solar resource assessment study for Pakistan*. Renewable and Sustainable Energy Reviews, 2016. **58**: p. 1184-1188.
6. Duffie, John A and William A Beckman, *Solar Engineering of Thermal Processes, Fourth Edition*. 2013, USA: John Wiley & Sons. 928.
7. S.A. Klein, W.A. Beckman, J.A. Duffie, *TRNSYS version 17 program manual*, S.E. Laboratory, Editor. 2010: University of Wisconsin, Madison.
8. Assilzadeh, F, Sa Kalogirou, Y Ali, and K Sopian, *Simulation and optimization of a LiBr solar absorption cooling system with evacuated tube collectors*. Renewable Energy, 2005. **30**(8): p. 1143-1159.
9. Ozgoren, Muammer, Mehmet Bilgili and Osman Babayigit, *Hourly performance prediction of ammonia–water solar absorption refrigeration*. Applied Thermal Engineering, 2012. **40**: p. 80-90.



Available online at www.sciencedirect.com

ScienceDirect

Energy Procedia 79 (2015) 746 – 751

Energy

Procedia

2015 International Conference on Alternative Energy in Developing Countries and
Emerging Economies

Simulation of Solar Air-Conditioning System with Salinity Gradient Solar Pond

Safwan Kanan^{a*}, Jonathan Dewsbury^a, Gregory F. Lane-Serff^a

^a*School of Mechanical, Aerospace and Civil Engineering, University of Manchester, Manchester, M13 9PL, UK*

Abstract

In hot dry climates, due to the high demand for space air conditioning during summer and the abundance of solar radiation, solar air conditioning is a promising approach to reduce the energy consumption and negative environmental impact of buildings. Solar cooling systems have used various types of collectors to drive chillers. In this paper, a salinity gradient solar pond is suggested as a collector to drive an absorption chiller, to provide cool air for a house during hot and dry weather. A coupled simulation between MATLAB and TRNSYS has been used to solve the problem. MATLAB code was written to solve the governing equations for the salinity gradient solar pond and the ground underneath it. TRNSYS software was used to model the solar cooling system including the absorption chiller and building. The weather data used was for Baghdad in Iraq. It was found that the salinity gradient solar pond could be used to drive the absorption chiller and produce cool air for a single family house during the summer period. Different solar pond areas were tested with the same chiller capacity. It was found that a solar pond area of approximately 400 m² was required to provide satisfactory cooling for a typical house with a floor area of approximately 125 m².

© 2015 The Authors. Published by Elsevier Ltd. This is an open access article under the CC BY-NC-ND license (<http://creativecommons.org/licenses/by-nc-nd/4.0/>).

Peer-review under responsibility of the Organizing Committee of 2015 AEDCEE

Keywords: Salinity gradient solar pond; solar cooling; solar thermal energy; TRNSYS simulation.

1. Introduction

Air conditioning of residential and commercial buildings is essential in hot and dry weather such as in the Middle East. A common solution to provide thermal comfort is a conventional air conditioning system

* Corresponding author. Tel.: +44-782-556-7780.

E-mail address: safwan.kanan@manchester.ac.uk or safwan2smj@yahoo.com

using electricity from power stations burning fossil fuel. The electricity consumption for air conditioning in Saudi Arabia exceeds 70% of the electricity consumption during the summer months [1]. The financial and environmental cost of this makes renewable energy sources attractive for buildings.

Nomenclature		Greek letters	
C_p	specific heat capacity for brine (J/kg °C)	θ_r	angles of refraction
C_{pg}	specific heat capacity for soil (J/kg °C)	ρ	brine density (kg/m ³)
E	rate of solar irradiance absorption per unit volume of water (W/m ³)	ρ_g	soil density (kg/m ³)
H_o	insolation incident on horizontal surface (W/m ²)		
H_x	incoming radiation flux at depth x (W/m ²)		
H_b	incoming radiation flux at bottom of the pond (W/m ²)		
h	convection heat transfer coefficient for LCZ (W/m ² °C)		
k	thermal conductivity (W/m °C)		
k_g	soil thermal conductivity (W/m °C)		
L_g	depth of water table (m)		
LCZ	Lower Convective Zone		
NCZ	Non-Convective Zone		
T	temperature (°C)		
T_b	temperature at the bottom (°C)		
T_g	ground or soil temperature (°C)		
UCZ	Upper Convective Zone		
x	distance from the surface of the solar pond (m)		
X	layer thickness (m)		

One of the possible options is to use solar thermal energy to drive an absorption chiller. Different types of solar thermal collectors have been used in such solar cooling system, such as: flat plate solar collector and evacuated tube collectors. [2]

A salinity gradient solar pond has also been suggested as a combined collector and heat store to drive an absorption chiller. As well as cooling of buildings, solar pond technology has various other applications such as industrial process heating, heating of buildings, refrigeration, desalination and salt production, and power generation.

A solar pond is an artificial large body of liquid (usually water) that collects and stores solar thermal energy. The solar radiation landing on the surface of the pond penetrates the liquid and falls on the blackened bottom which is thereby heated. If the liquid is homogeneous then convection currents will be set up and the heated liquid will travel towards the surface and dissipate its heat to the atmosphere. In a salinity gradient solar pond these convection currents are prevented by having a concentration gradient of salt, the concentration and solution density being highest at the bottom and lowest at the top. Typically ponds are composed of three zones as shown in Figure 1. The topmost zone is the Upper Convective Zone (UCZ), which has low salt concentration. The middle zone is the Non-Convective Zone (NCZ) or insulation layer, which has salt concentration increasing with depth. Water in the NCZ does not rise if it is

hotter than the water immediately above because the water above has a lower salt concentration and is, therefore, less dense. Similarly, water in the NCZ does not fall if it is cooler than the water immediately below, because the water below has a higher salt content and is, therefore, denser. Thus, convection motions are hindered and upwards heat transfer from the lowest zone, the Lower Convective Zone (LCZ), is only by conduction. Heat may be extracted from the LCZ to drive an absorption chiller. The other main components of the solar cooling system are a cooling tower to reject heat to the ambient, a fan and cooling coil for distributing cool air inside the building, a heat exchanger between the solar pond and the chiller, pumps and controls.

Weinberger [3] studied the thermal energy balance for a large solar pond in 1964. Rabl and Nielsen [4] developed the model of Weinberger with a two-zone pond. Hull [5], Rubin et al. [6], and Kurt et al. [7] used a finite difference method to solve the partial differential energy equation for the solar pond. The thermal performance of solar pond can be significantly affected by heat loss through the bottom. Saxena et al. [8] investigated the effect of water table depth on solar pond thermal performance. Simulation analysis indicates that deeper the water table, the lower the heat losses and the higher the temperature achieved by the pond. Ranjan and et al. [9] mention some instances of utilization of solar ponds for refrigeration and air-conditioning. Tsilingiris [10, 11] investigated the possibility of using solar ponds as low-cost solar collectors combined with an absorption chiller in a large scale solar cooling system. The analysis is based on the combination of a steady state solar pond mathematical model with operational characteristics of a commercial absorption chiller.

In the current paper, a coupled simulation between a transient model of the solar pond and the ground in MATLAB and of the chiller, air conditioning and building in TRNSYS is used to investigate the performance of the complete system.

2. Mathematical Modelling

2.1. Solar pond and ground model

The simulation model is one-dimensional and is modified from [8, 12]. The vertical coordinate (x) is measured as a positive downward, and $x = 0$ at the surface of the pond as shown in Figure 1. The heat flow equation for the solar pond is given by Eq. (1). [6]

$$\rho C_p \left(\frac{\partial T}{\partial t} \right) = k \left(\frac{\partial^2 T}{\partial x^2} \right) + E(x, t) \quad (1)$$

The rate of solar energy absorption by the fluid per unit volume can be expressed by Eq. (2).

$$E = - \frac{\partial H(x, t)}{\partial x} \quad (2)$$

The solar radiation penetrating the water decays exponentially with depth and is given by Eq. (3). [15]

$$\frac{H_x}{H_o} = \left\{ 0.36 - 0.08 \ln \left(\frac{x}{\cos \theta_r} \right) \right\} \quad (3)$$

The heat flow equation through the soil underneath the solar pond is given by Eq. (4). [13]

$$\rho_g C_{pg} \left(\frac{\partial T_g}{\partial t} \right) = k_g \left(\frac{\partial^2 T_g}{\partial x_g^2} \right) \quad (4)$$

Assuming no insulation between the pond and the soil, the heat transfer equation between the bottom of the solar pond and soil is given by Eq. (5). [13]

$$k_g \left(\frac{\partial T_b}{\partial x_g} \right) + h(T_b - T_{LCZ}) = H_b \quad (5)$$

Fig. 2. TRNSYS model

The complete simulated solar cooling system consisted of a single effect vapour absorption water chiller with rated capacity of 7 TR and based on [14], thermally powered by the salinity gradient solar pond. Chilled water is passed through a cooling coil, and the cool air distributed by a fan to a 125 m² single family house in Baghdad, Iraq (33.32° N, 44.42° E), based on typical house. The heat rejected from the chiller is dissipated to the environment by a wet cooling tower. Pumps are used to regulate the flow rate, and a controller provides automatic operation of the system. Real component data is used in the simulation. The MATLAB code for the pond and soil are called by TRNSYS [16] using the Type 155 component as shown in Figure 2.

3. Results and Discussion

Figure 3 shows the chilled water outlet temperature for different solar pond areas for two years simulation time. With 250 m² pond area, the chilled water outlet temperature does not stabilise at the set point (7°C) even in the second year. With 400 m² or more pond area, the chilled water outlet temperature

stabilises at the 7°C set point temperature by the end of the first summer and during the second summer. 400 m² is therefore suggested as a suitable pond area for this 125 m² single family house.

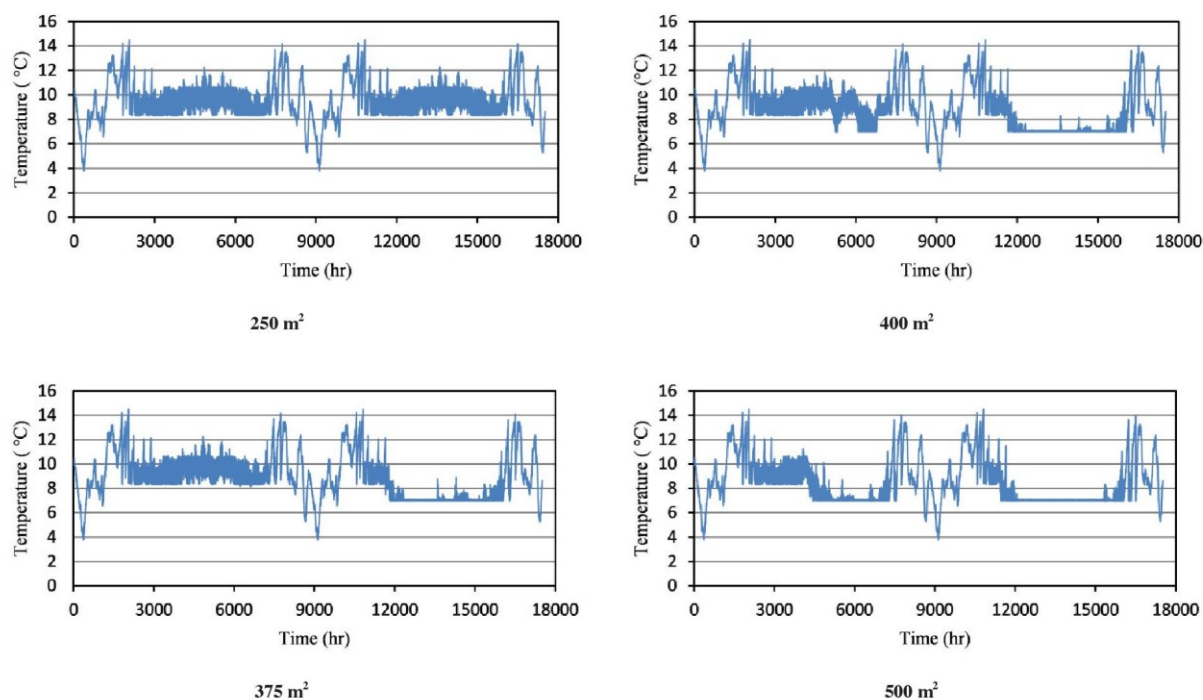
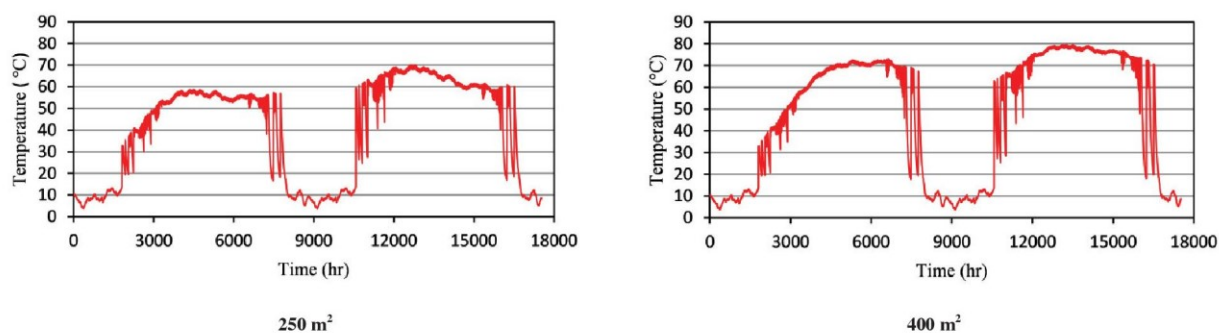


Fig. 3. Chilled water outlet temperature with different pond area

Figure 4 shows hot water inlet temperature to the absorption chiller with different solar pond areas. It can be seen that the larger the solar pond area, the higher the temperature achieved for the same amount of heat extracted from pond. Comparing Figures 3 and 4, it is found that when the hot water inlet temperature is 70°C or higher, then the absorption chiller works normally and the chilled water outlet temperature is close to the set point temperature.



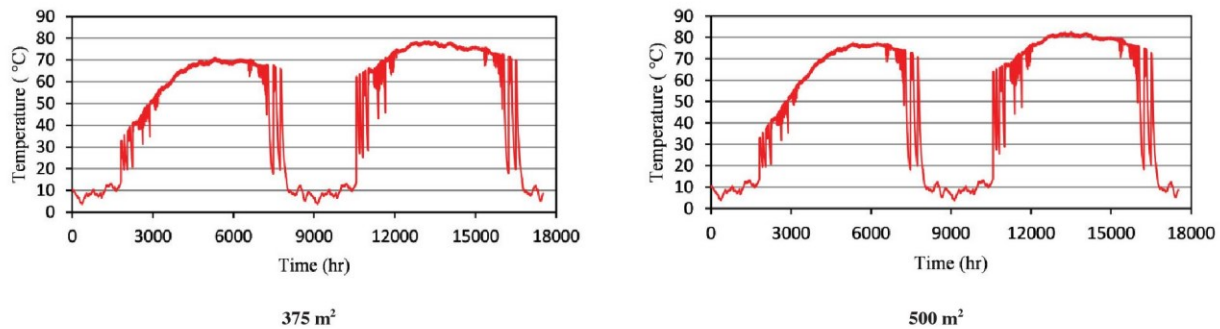


Fig.4. Hot water inlet temperature with different pond area

4. Conclusions

A coupled simulation between MATLAB and TRNSYS has been used to develop a model for a solar pond and cooling system. It was found that the salinity gradient solar pond could be used to drive an absorption chiller and produce cool air for a single family house during the summer period in Iraq. Different solar pond areas were tested with the same chiller capacity. It was found that a solar pond area of approximately 400 m² was required to provide satisfactory cooling for a typical new house with a floor area of approximately 125 m². A hot water inlet temperature of 70°C or higher made the absorption chiller work at its design condition.

Acknowledgements

This research is funded by Ministry of Higher Education and Scientific Research (MoHESR) of Iraq.

References

- [1] Al-Mogbel et al., The potential of solar adsorption air conditioning in Saudi Arabia. *Proceedings of 5th International Conference solar air conditioning*, 2013, Germany.
- [2] Sarbu, Ioan, and Calin Sebarchievici, Review of solar refrigeration and cooling systems, *Energy and Buildings*, **67** (2013); 286-297.
- [3] Weinberger H., The physics of the solar pond. *Solar Energy* 1964; **8**(2):45-56.
- [4] Rabl, A., & Nielsen, C. E. Solar ponds for space heating. *Solar Energy* 1975; **17**(1), 1-12.
- [5] Hull, J.R., Computer simulation of solar pond thermal behaviour. *Solar Energy* 1980; **25**:33-40.
- [6] Rubin, H., Benedict, B.A., Bachu, S., Modeling the performance of a solar pond as a source of thermal energy. *Solar Energy* 1984; **32**, 771-778.
- [7] Kurt, Hüseyin, Mehmet Ozkaymak, and A. Korhan Binark. Experimental and numerical analysis of sodium-carbonate salt gradient solar-pond performance under simulated solar-radiation. *Applied Energy* 2006; **83**(4):324-342.
- [8] Saxena, A. K., S. Sugandhi, and M. Husain, Significant depth of ground water table for thermal performance of salt gradient solar pond. *Renewable Energy* 2009; **34**:3: 790-793.
- [9] Ranjan, K. R., and S. C. Kaushik, Thermodynamic and economic feasibility of solar ponds for various thermal applications: A comprehensive review. *Renewable and Sustainable Energy Reviews* 2014; **32**: 123-139.
- [10] Tsilingiris, P. T., Large scale solar cooling design using salt gradient solar ponds. *Renewable energy* 1991; **1**:2: 309-314.
- [11] Tsilingiris, P. T., The absorption chiller in large scale solar pond cooling design with condenser heat rejection in the upper convecting zone. *Solar energy* 1992; **49**, no. 1: 19-27.
- [12] Kanan, S., Dewsbury, J., Lane-Serff, G., A Simple Heat and Mass Transfer Model for Salt Gradient Solar Ponds, World Academy of Science, Engineering and Technology, International Science Index 85, *International Journal of Mechanical, Aerospace, Industrial and Mechatronics Engineering* 2014; **8**(1): 27 - 33.
- [13] Sodha MS, Kaushika ND, Rao SK, Thermal analysis of three zone solar pond. *Energy Research* 1981; **5**:321-40.
- [14] Yazaki, WFC – SC chiller and chiller specifications; available at www.yazaki.com.
- [15] Bryant, H. C., and Ian Colbeck., A solar pond for London. *Solar Energy* 1977; **19**:3: 321-322.
- [16] Klein, S.A. et al, 2010, TRNSYS 17: A Transient System Simulation Program, Solar Energy Laboratory, University of Wisconsin, Madison, USA, <http://sel.me.wisc.edu/trnsys>.

A Simple Heat and Mass Transfer Model for Salt Gradient Solar Ponds

Safwan Kanan, Jonathan Dewsbury, Gregory Lane-Serff

Abstract—A salinity gradient solar pond is a free energy source system for collecting, converting and storing solar energy as heat. In this paper, the principles of solar pond are explained. A mathematical model is developed to describe and simulate heat and mass transfer behaviour of salinity gradient solar pond. MATLAB codes are programmed to solve the one dimensional finite difference method for heat and mass transfer equations. Temperature profiles and concentration distributions are calculated. The numerical results are validated with experimental data and the results are found to be in good agreement.

Keywords—Finite Difference method, Salt-gradient solar-pond, Solar energy, Transient heat and mass transfer.

I. INTRODUCTION

THE solar pond is described as an artificial large body of water reservoir that collects and stores solar energy. It is about 1 to 3 meters deep, and the bottom of the pond is usually painted black. The solar radiation landing on the surface of the pond penetrates the liquid and falls on the blackened bottom which is thereby heated. If the liquid is homogeneous which means no density gradient, convection currents will be set up and the heated liquid being lighter will travel towards the surface and dissipate its heat to the atmosphere. In a solar pond these convection currents are prevented by having a concentration gradient of salt, the solution's concentration and density being highest at the bottom and lowest at the top. Typically ponds are composed of three zones as shown in Fig. 1. The first zone is Upper Convective Zone (UCZ), which is cold, close to the ambient temperature; and has low salt concentration (almost fresh water). The thickness of this surface layer varies from 0.1 to 0.4m. The second zone is Non-Convective Zone (NCZ) or (insulation layer), which has salt density increasing with depth. The thickness of NCZ ranges from 0.6 to 1.0m. Hot water in one layer of NCZ cannot rise because of its high relative density (due to its salt content) and water above is lighter (low density). Similarly, water cannot fall because the water below it has a higher salt content and is heavier (high density). Therefore convection motions are hindered and heat transfer from the hot third zone,

Lower Convective Zone (LCZ) or (storage layer) to the cold UCZ can only happen through conduction. Given the moderately low conductivity of water, the NCZ layer acts as a transparent insulator, permitting solar radiation to be trapped in the hot bottom layer, from which useful heat is withdrawn [1]. Its thickness depends on the temperature and the amount of the thermal energy to be stored. Because of large storage of heat and small diurnal fluctuation in temperature, solar ponds have a variety of applications such as; electrical power generation, water desalination, heating and cooling of buildings and industrial process heating.

Weinberger [2] investigated the thermal energy balance for a large solar pond in 1964. The analytical solution of the partial differential equation for the transient temperature distribution was obtained by superimposing the effects of the radiation absorption at the surface, in the body of the water and at the bottom. Rabl and Nielsen [3] developed the model of Weinberger into a two-zone pond containing a LCZ and NCZ. Analytical solution methods are very useful for simple cases, however, when the model has complex boundary conditions, numerical methods should be utilized.

There have been several efforts for the numerical solution of the partial differential energy equation governing solar pond in the literature. Hull [4], Rubin et al. [5], and Kurt et al. [6] have used a finite difference method, while Jayadev et al. [7] and Panahi et al. [8] have applied a finite element technique.

In this paper, a one dimensional finite difference method for heat and mass transfer are used to solve the governing equations for solar pond located in Baghdad (33.3250° N, 44.4220° E) Iraq. Temperature distribution for one month and for whole year has been found. Salt concentration profile for pond had been considered.

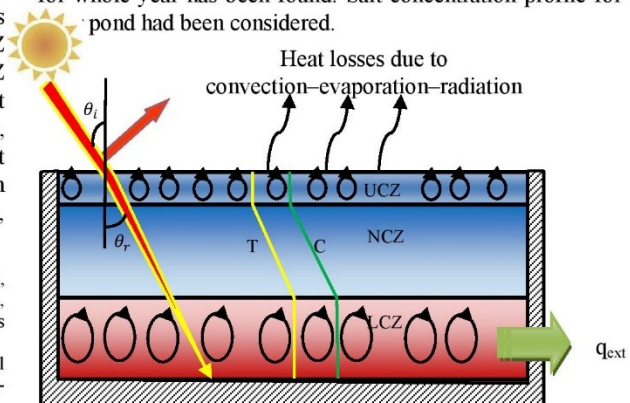


Fig. 1 Schematic view of the salt gradient solar pond

Safwan Kanan is currently a PhD researcher with School of Mechanical, Aerospace and Civil Engineering, The University of Manchester, M13 9PL, Manchester, UK (e-mail: safwan.kanan@postgrad.manchester.ac.uk). He was lecturer with the Erbil Technical Institute, Erbil, Iraq

J. Dewsbury, is Lecturer with School of Mechanical, Aerospace and Civil Engineering The University of Manchester, M13 9PL, Manchester, UK (e-mail: j.dewsbury@manchester.ac.uk).

G. Lane-Serff is Senior Lecturer with School of Mechanical, Aerospace and Civil Engineering, The University of Manchester, M13 9PL, Manchester, UK (e-mail: gregory.f.lane-serff@manchester.ac.uk).

II. MATHEMATICAL FORMULATION

The solution of the heat equation for salt gradient solar pond uses the following assumptions in the mathematical model developed to simulate the solar pond:

1. The pond consists of three zones; the upper convective zone, the non-convective zone and lower convective zone.
2. The horizontal temperature variations are considered small enough so that they are negligible. Therefore, the temperature and salinity distributions within the pond are one dimension.
3. The temperature and density in upper convective zone and in lower convective zone are uniform and perfectly mixed.
4. The heat losses from the walls are neglected.
5. The bottom surface is blackened in order to maximize the radiation absorption. Therefore, the radiation energy reaching the LCZ is completely absorbed by the solution and the bottom of the pond.

A. Solar Radiation in Solar Pond

The solar radiation, penetrating into the water body, decays exponentially with depth, as fluid layers absorb energy. The rate of decay is a function of the wavelength of the radiation and for the whole spectrum of wavelengths.

This exponential formula was proposed by Bryant and Colbeck, [9] and seems to be in very good agreement with [3] model.

$$\frac{H_x}{H_o} = \left\{ 0.36 - 0.08 \ln \left(\frac{x}{\cos \theta_r} \right) \right\} \quad (1)$$

where H_o is the monthly average insolation incident on horizontal surface in W/m^2 and H_x is the incoming radiation flux at depth x in W/m^2 . θ_r = angle of refraction at the pond's surface, which can be calculated from Snell's Law [10].

$$\frac{\sin \theta_i}{\sin \theta_r} = 1.333 \quad (2)$$

where θ_i is the angle of incidence of direct radiation to a horizontal plane with normal (zenith angle).

$$\cos \theta_i = \cos \delta \cos \phi \cos \omega + \sin \delta \sin \phi \quad (3)$$

where δ is the angle of declination, ϕ the angle of latitude, and ω the hour angle. The declination angle δ is defined in degrees by [10].

$$\delta = 23.45 \sin \left(\frac{360(284+N)}{365.25} \right) \quad (4)$$

N is the day of the year.

The hour angle ω is an angular measure of time considered from noon based on local time h , and is defined as:

$$\omega = \frac{2\pi(h-12)}{24} \quad (5)$$

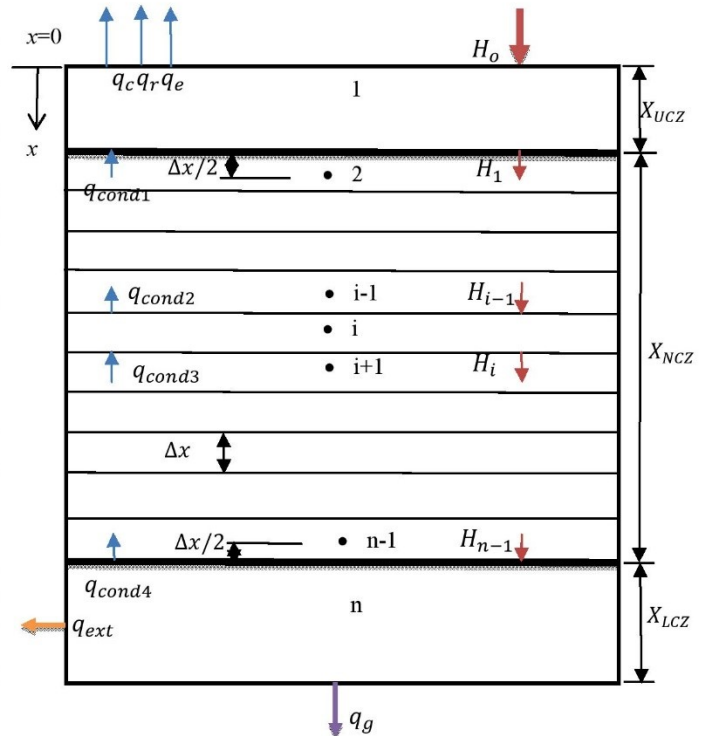


Fig. 2 Solar pond's mathematical model

B. Heat Transfer Model

In the vertical system of Cartesian coordinates with (x) measured as a positive downward and $x = 0$ at the surface of the pond as shown in Fig. 2. The mathematical model developed in the present work is based upon an energy balance over a fluid layer. Incoming energy to the layer and radiant energy absorbed by the layer equals the loss of energy from the layer and energy accumulation in the layer with time. Based upon energy conservation, the energy balance for UCZ, NCZ and LCZ are expressed as follows.

1. Energy Balance for UCZ

The energy flows in solar pond's surface can be written as: Energy in = Energy out + Energy stored

$$[H_o + q_{cond1}] = [H_1 + q_{loss}] + \rho C_p \frac{\partial T}{\partial t} X_{UCZ} \quad (6)$$

where q_{loss} is the total heat loss from the pond's surface due to convection, evaporation and radiation.

$$q_{loss} = q_c + q_r + q_e \quad (7)$$

The convection heat transfer from the upper layer to the atmosphere depends mainly on the wind speed and the temperature difference between the atmosphere and the pond's water surface.

$$q_c = h_c(T_1 - T_a) \quad (8)$$

where convection heat transfer coefficient is given by. [11]

$$h_c = 5.7 + 3.8 V \quad (9)$$

where V is the average monthly wind speed recorded in Table I from NASA data website [12].

The radiation heat loss equation may be written as the following:

$$q_r = \sigma \epsilon_w \{ (T_1 + 273)^4 - (T_{sky} + 273)^4 \} \quad (10)$$

where ϵ_w is the emissivity of water which is assumed to be 0.83 and σ is the Stefan-Boltzmann's constant.

The sky temperature value may be found by several equations, such as: [13]

$$T_{sky} = T_a - (0.55 + 0.061 \sqrt{P_1})^{0.25} \quad (11)$$

The heat loss from the surface due to the evaporation phenomenon is given by [11].

$$q_e = \frac{L_v h_e (P_1 - P_a)}{1.6 C_s P_{atm}} \quad (12)$$

where

$$P_1 = \exp \left(18.403 - \frac{3885}{T_1 + 230} \right) \quad (13)$$

$$P_a = RH * \exp \left(18.403 - \frac{3885}{T_a + 230} \right) \quad (14)$$

TABLE I
WEATHER DATA FOR BAGHDAD IRAQ BASED ON THE MONTHLY AVERAGE
FROM NASA[12]

Months	Insolation kWh/m ² /day	T_a °C	V m/s	RH %
January	2.96	9.77	3.67	58.0
February	4.03	11.5	4.00	47.0
March	4.98	16.2	4.20	38.0
April	5.39	23.0	4.26	29.9
May	6.48	29.1	4.53	22.3
June	7.56	33.3	4.88	17.1
July	7.00	36.1	4.76	16.2
August	6.71	35.7	4.65	17.1
September	5.55	32.0	4.34	19.4
October	3.98	26.2	4.13	27.2
November	2.98	17.8	3.76	42.3
December	2.62	11.5	3.71	55.7

The finite difference for upper convective zone heat (6) can be written as:

$$T_1^{j+1} = T_1^j + \frac{\Delta t}{\rho C_p X_{UCZ}} \left[(H_o - H_1) + k \left(\frac{T_2^j - T_1^j}{\Delta x} \right) - q_{loss}^j \right] \quad (15)$$

where ρ , C_p and k are density, specific heat and thermal conductivity of sodium chloride brine.

Equation (15) is the first upper boundary condition for solar pond as defined in Fig. 2.

2. Energy Balance for NCZ

The NCZ has been divided into different layers (2 to n-1) which the energy equation is formulated below. The energy balance for any layer in the NCZ can be written as:

$$[H_{i-1} + q_{cond3}] = [H_i + q_{cond2}] + \rho C_p \frac{\partial T}{\partial t} \Delta x \quad (16)$$

The temperature for any layer through NCZ in finite difference form can be obtained from (16) as:

$$T_i^{j+1} = T_i^j + \frac{\Delta t}{\rho C_p \Delta x} \left[(H_{i-1} - H_i) + k \left(\frac{T_{i+1}^j - T_i^j}{\Delta x} \right) - k \left(\frac{T_i^j - T_{i-1}^j}{\Delta x} \right) \right] \quad (17)$$

The temperatures of NCZ can be calculated from above equation as internal nodes for the solar pond model.

3. Energy Balance for LCZ

From Fig. 2, the energy conservation equation for LCZ with a thickness of X_{LCZ} can be written as:

$$[H_{n-1}] = [q_{cond4} + q_{ext} + q_g] + \rho C_p \frac{\partial T}{\partial t} X_{LCZ} \quad (18)$$

In (18), the left hand side is the radiation energy entering the control volume of LCZ; and in the right hand side, the first term is the heat loss to the non-convective zone at the interface, the second term is the useful heat extracted from the solar pond, the third term is the heat loss to the ground, the forth term is the energy stored within the LCZ layer. The conduction heat loss from LCZ to NCZ at the interface is given as:

$$q_{cond4} = -k \frac{\partial T_n^j}{\partial x} \Big|_{x=X_{UCZ}+X_{NCZ}} \quad (19)$$

The ground heat loss can be written as:

$$q_g = -k_g \frac{\partial T_n^j}{\partial x} \Big|_{x=X_{UCZ}+X_{NCZ}+X_{LCZ}} \quad (20)$$

Using (19) and (20) in (18) and simplifying, gives the temperature of the LCZ, explicitly at the time of j+1 as:

$$T_n^{j+1} = T_n^j + \frac{\Delta t}{\rho C_p X_{LCZ}} \left[(H_{n-1}) - k \left(\frac{T_n^j - T_{n-1}^j}{\Delta x} \right) - q_{ext}^j - U_g (T_n^j - T_g^j) \right] \quad (21)$$

where U_g is the ground overall heat transfer coefficient and it can be obtained from Hull [14].

$$U_g = \frac{k_g}{L_g} + b k_g \frac{p}{A} \quad (22)$$

where b is an empirical parameter, equal to 1.37 for vertical wall solar pond [14]; p and A are the pond perimeter and area; k_g is the ground thermal conductivity; L_g can be considered as the distance of water table from the bottom of the pond; T_g can be taken as the ground water temperature.

C. Mass Transfer Model

There are several physical processes occurring in the operation of a solar pond. Convective mass-transfer occurs in the LCZ and UCZ and diffusive mass-transfer in the NCZ. The density gradient could be develop by molecular diffusion. In the proposed model, the total mass of the system in the control volume is constant, and the mass transfer is only the result of molecular diffusion. The mass-transfer processes are assumed to be independent of the thermal processes. Based upon these assumptions, one dimensional mass diffusion in the x -direction for a differential volume-element of thickness, Δx , is given as follows:

$$-\frac{\partial J}{\partial x} = \frac{\partial \rho(x,t)}{\partial t} \quad (23)$$

The Fick's law of diffusion state that the diffusion flux J is proportional to the density gradient by

$$J = -D \frac{\partial \rho(x,t)}{\partial x} \quad (24)$$

Substituting from (24) into (23) assuming constant salt diffusivity D in m^2/s , the mass transfer differential equation can be written as:

$$\frac{\partial}{\partial x} \left(D \frac{\partial \rho(x,t)}{\partial x} \right) = \frac{\partial \rho(x,t)}{\partial t} \quad (25)$$

The salinity can be defined as the ratio of concentration to density of the salt water [1].

$$S(x,t) = \frac{C(x,t)}{\rho(x,t)} \quad (26)$$

So that the (25) can be written as

$$\frac{\partial}{\partial x} \left(D \frac{\partial C(x,t)}{\partial x} \right) = \frac{\partial C(x,t)}{\partial t} \quad (27)$$

where S is the salinity % and C is the salt concentration, kg/m^3 , the diffusion coefficient of salt water (brine), D is $3 \times 10^{-9} \text{ m}^2/\text{s}$, according to [15].

The mass transfer partial differential (27) can be discretized to

$$D \frac{C_{(i-1)}^j - 2C_{(i)}^j + C_{(i+1)}^j}{\Delta x^2} = \frac{C_{(i)}^{j+1} - C_{(i)}^j}{\Delta t} \quad (28)$$

Then

$$C_{(i)}^{j+1} = \frac{D \Delta t}{\Delta x^2} [C_{(i-1)}^j - 2C_{(i)}^j + C_{(i+1)}^j] + C_{(i)}^j \quad (29)$$

This equation is representing a concentration profile for internal nodes in the NCZ. The initial conditions are assumed to be $10 \text{ kg}/\text{m}^3$ at the UCZ and $178 \text{ kg}/\text{m}^3$ at the LCZ with linear distribution in the NCZ.

For the mass transfer equation, the two boundary conditions are:

At the top of the pond, the mass balance gives:

$$D \frac{\partial C}{\partial x} = \frac{\partial C}{\partial t} X_{UCZ} \text{ (B.C.1)} \quad (30)$$

At the bottom of the pond

$$-D \frac{\partial C}{\partial x} = \frac{\partial C}{\partial t} X_{LCZ} \text{ (B.C.2)} \quad (31)$$

III. NUMERICAL SIMULATION

The governing equations (15), (17), (21), (29), (30) and (31) obtained from the heat and mass transfers are solved numerically to determine the temperature and concentration profiles within the pond. The method used in generating solutions to the one dimensional temperature and density finite-difference equations is explicit because unknown nodal variables for a new time are calculated using the known values of the parameters at a previous time. A finite-difference form of the differential equation is derived by integration over the control volume surrounding the typical node (i), as shown in the grid of Fig. 2. MATLAB codes have been written to solve these equations. The NCZ was divided into (n-1) equal size layers, where (n=100) was assumed. A space step of Δx is 0.01 m and a time step Δt of 300 sec were used in the code. The UCZ and LCZ are considered as a single grid points. The numerical stability criterion of explicit formulation is $\tau = \alpha \Delta t / \Delta x^2 \leq 0.5$, where α is thermal diffusivity. The mass transfer equation is of exactly the same form as the one dimension unsteady heat-conduction equation: the same mathematical techniques are applicable for its solution. The results are calculated with constant ambient temperature for each months and the monthly averaged insolation incident on a horizontal surface. The effect of night and day to day variations for solar radiation was neglected due to the monthly average data taken from NASA website. For example, during June is $7.56 \text{ KW}/\text{m}^2/\text{day}$ for 22 years and 33.3°C for ambient temperature. In the simulation, input data are 2 m depth of the pond, $3 \times 10^{-9} \text{ m}^2/\text{s}$ thermal diffusivity, and $0.566 \text{ W}/\text{m}^\circ\text{C}$ thermal conductivity of salt water. The density of salt water and specific heat at constant pressure at 40°C and salinity 10% NaCl by mass are $1063.8 \text{ kg}/\text{m}^3$, $3758.3 \text{ J}/\text{kg}^\circ\text{C}$ respectively. The thermal diffusivity is $1.4156 \times 10^{-7} \text{ m}^2/\text{s}$ at the same temperature and salinity. The thickness of UCZ was taken to 0.3 m , the NCZ is 1 m and the LCZ is 0.7 m .

In ground heat loss $k_g = 2.15 \text{ W}/\text{m}^\circ\text{C}$ [16] and $T_g = 23.2^\circ\text{C}$ at $L_g = 6 \text{ m}$ depth [17].

The output of the MATLAB codes are the temperature and concentration profiles of the pond. The simulation has been run for a year starting from 1st January until the 30th of January for the next year. The results of temperature for the current month are used as the initial conditions for next month. The computer program has been successfully validated by comparing the calculated temperature distribution with available experimental data for specific period of time and a good agreement was achieved from this comparison.

IV. RESULTS AND DISCUSSION

A. Temperature Distribution inside the Solar Pond

Temperature profiles as a function of the pond's depth for selected city are shown in Fig. 3. The initial pond's temperature is assumed to be 25°C. The average ambient temperature is 33.3°C and the average monthly solar radiation is 7.56 kW/m²/day. It is observed that temperature increases with respect to depth of the gradient zone NCZ of the solar pond, after 30 June. The maximum temperature at the LCZ in the pond is exceed 66°C with included the heat loss to the ground and from the surface. This profile in LCZ temperature is agreed with physical and experimental data of solar pond.

Fig. 3 illustrates the temperature profiles development for the pond. It shows the temperature distribution for different selected days. After fifteen days of simulation the temperature in the LCZ is increased with respect to time and depth exceeding 50°C. If the simulation carries on for next month the temperature will be increased and also the useful heat that extracted from the pond. This heat can be used for any suitable applications such as electrical power generation, and heating and cooling of buildings. The increase in temperature in any day of the simulation is due to accumulated heat absorbed in LCZ from the previous day.

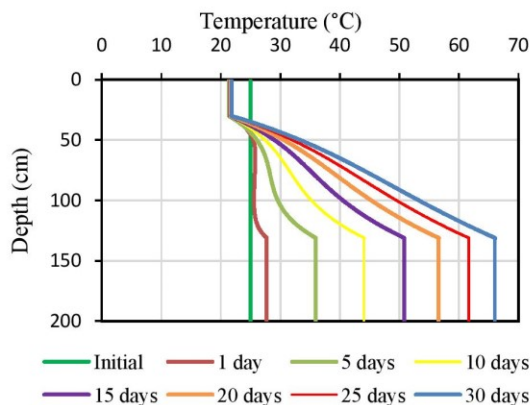


Fig. 3 Temperature profile development for solar pond during June.

B. Concentration Profile inside the Solar Pond

The UCZ has low salt concentration 10 kg/m³ and the LCZ has the high salt concentration 178 kg/m³ and the NCZ is assumed to have linear distribution. Fig. 4 shows the salt concentration profile inside the solar pond. The code was run for one month start from 1st of June until the 30th. It is obvious there is a small change in concentration profile inside the pond, that's means the pond is stable and the salt concentration gradient does not need any maintenance during short period of operation.

The code was also run for one year and two years stating from initial distribution for concentration. It is observed that the salt concentration for UCZ is increased after one year of simulation and increased more after two year, whereas the salt concentration for LCZ is decreased for one and two years.

This is because of the diffusion of salt concentration inside the solar pond and the mass transfer will occur from the high concentration to low concentration varying with the time and it is assumed that the fluid at rest (velocity is zero). If this phenomenon still happens inside the solar pond, the stratification of the NCZ layer will be disturbed. Therefore the stratified regions on the solar pond need maintenance by flushing the UCZ and adding saturated brine in the LCZ.

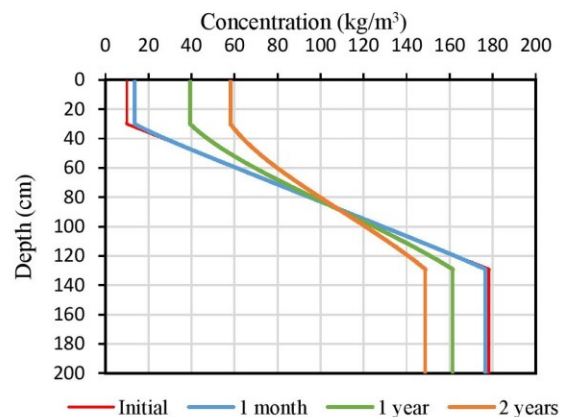


Fig. 4 Salt concentration profile in the solar pond

C. Validation of Temperature Distribution

In order to check the accuracy of the numerical code specifically developed for the solution of the problem considered in the present study, the temperature distribution is validated with experimental temperature data from Pyramid Hill solar pond. It has been constructed at Pyramid Salt's facility at Pyramid Hill in northern Victoria, Australia with a surface area of around 3000 m². Fig. 5 shows temperature distribution inside the solar pond on 3rd February 2006 for present numerical study and experimental data published by [18]. Weather data for specific location is found from Bureau of meteorology [19]. The monthly averaged insolation incident on a horizontal surface is 8.4 kWh/m²/day and the average ambient temperature is 29°C.

The dimensions of pond's layers were UCZ=0.8 m, NCZ=0.7 m and LCZ=0.8 m. The bottom of the solar pond was insulated with 100 mm thick expanded polystyrene (EPS) insulation to reduce the average heat loss by 42% [18]. It can be seen that the temperature profile of present study and experimental data show a good agreement.

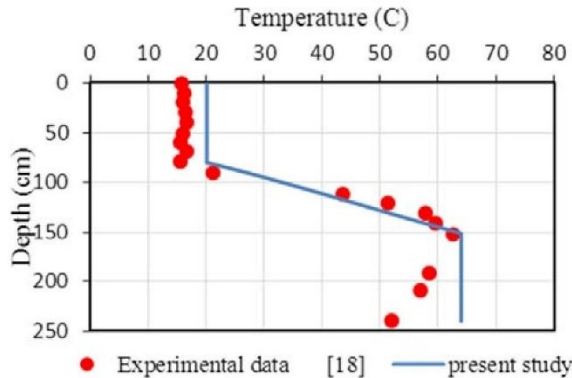


Fig. 5 Validation of temperature distribution with experimental data of [18]

D. Effect of NCZ and LCZ Thicknesses on the Temperature

The NCZ of the solar pond can act as a thermal insulator and the LCZ is the region where the thermal energy is stored. To better understand the effects of the thicknesses of NCZ and LCZ on the thermal behaviour of the solar pond during the storage of solar energy as thermal energy in the bottom of the pond, it has reproduced in Fig. 6 the temperature distribution in a salt-gradient solar pond with different thicknesses of NCZ, (0.7m, 1m and 1.3 m) and LCZ thicknesses are (1m, 0.7 m and 0.4 m) respectively. The thickness of UCZ is fixed to 0.3 m.

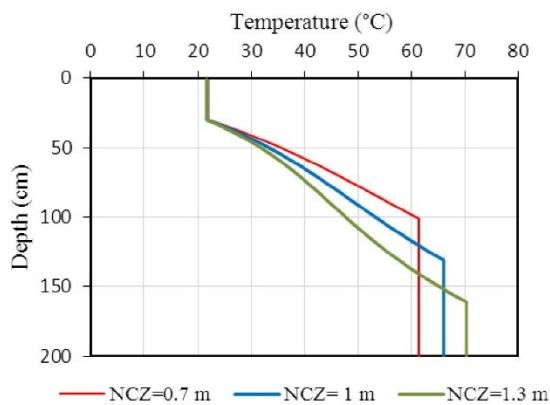


Fig. 6 Effect of the thickness of NCZ and LCZ on the temperature profile at the end of June

Fig. 6 shows that there is a decrease of the temperature of the NCZ due to the increase of its thickness which increases the insulation property and subsequently reduces the upwards heat losses. In addition, the decrease of the thickness of LCZ will increase the storage temperature in this zone.

E. Heat Extracted from the Solar Pond

The code was run from 1st of January until the 30th of January for next year. Heat was extracted from the solar pond after four months (no load) from simulation start point. The heat extracted was different from one case to another

depending on the load applications. From these amounts of heat extracted from the pond and depending on the surface area of solar pond, the heat supplied to different types of applications can be calculated.

Fig. 7 illustrates the annual LCZ temperature profile at the end of each month with the ambient temperature. It can be seen that the LCZ temperature increased to peak in July and then decreased to point higher than its initial value. The LCZ temperature depended on the solar radiation absorbed by the LCZ, ambient and initial temperatures of each months and the amount of heat extracted from the solar pond.

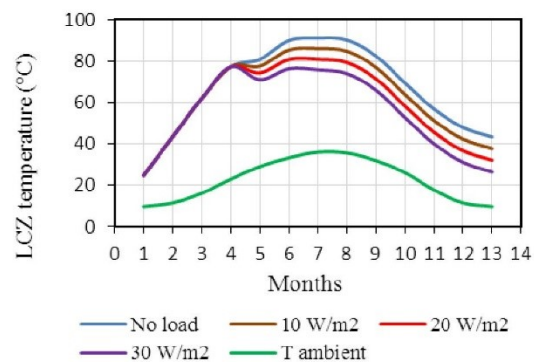


Fig. 7 Annual LCZ temperature with heat extracted from the solar pond

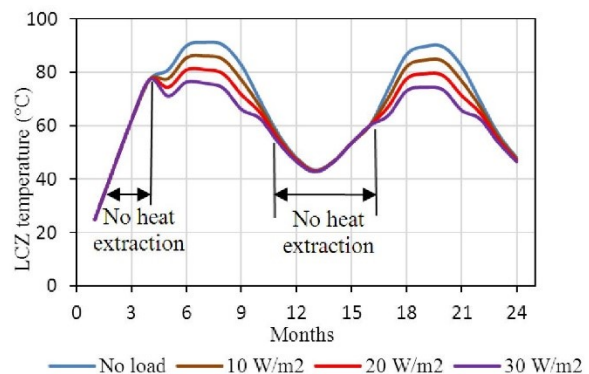


Fig. 8 LCZ temperature for two years with heat extraction

In Fig. 8, the simulation for solar pond was run for two years started from 1st of January until the 30th December for the next year. No heat extracted during the first four months and also from October to April for next year. Different heat extracted applied for solar pond depending on the load demand for different applications. The minimum LCZ temperature is 42 °C in December first year and the maximum LCZ temperature is 91°C in June first year.

V. CONCLUSIONS

This paper has presented heat and mass transfer mathematical model for salt gradient solar ponds.

Temperatures distribution and concentration profile are calculated. Temperature distribution has been compared and validated with experimental data. The results have showed a good approximation and agreement. The following conclusions seem to be pertinent:

- Solar ponds are reliable solar collector-storage systems which can provide thermal energy during summer. So that it could be used to supply energy for different applications.
- The solar pond cannot work without a stable concentration profile. This means, the concentration should be increase downwards to prevent any gravitational overturn. In contrast, a weak salt gradient cause's instability in solar pond and this leads to effect on solar pond's insulation so that energy will be lost through the surface of the pond.
- The maximum LCZ temperature is 91°C in July without heat extraction from the pond whereas the maximum LCZ temperature is 76° C in June with 30 W/m² heat extraction. Total power output from a typical pond's area (100*100) m² is 300 KW.
- LCZ temperature is decreased when NCZ thickness decrease and it is increased when LCZ thickness decrease.

NOMENCLATURE

Symbol	Quantity	Units
A	Pond's area	m ²
b	Empirical parameter (22)	
C	Salt concentration	kg/m ³
C_p	Specific heat capacity of salt water	J/kg °C
C_s	Humid heat capacity of air	J/kg °C
D	Coefficient of salt diffusion	m ² /s
h	Local time	hours
h_c	Convective heat transfer coefficient	W/m ² °C
H_O	Monthly average insolation incident on horizontal surface	W/m ²
H_x	Incoming radiation flux at depth x	W/m ²
J	diffusion flux	kg/m ² s
k	thermal conductivity of NaCl brine	W/m °C
k_g	Ground thermal conductivity	W/m °C
L_v	Latent heat of evaporation of water	J/kg
L_g	distance of water table from the bottom of the pond	m
N	Day of the year	
p	Perimeter of the pond	m
P_l	Vapor pressure of water at the surface temperature	Pa
P_a	Partial pressure of water vapor in the ambient air	Pa
P_{atm}	Atmospheric pressure	Pa
q_c	Convection heat transfer	W/m ²
q_{cond}	Conduction heat transfer	W/m ²
q_e	Evaporation heat transfer	W/m ²
q_{ext}	Heat extracted from the pond	W/m ²
q_g	Heat loss to the ground	W/m ²
q_{loss}	Total heat loss from the pond's surface	W/m ²
q_r	Radiation heat transfer	W/m ²
RH	Relative humidity	%
S	Salinity	kg/m ³

T	Temperature	°C
T_a	Ambient temperature	°C
T_g	Ground water temperature	°C
t	Time	s

REFERENCES

- [1] C. Angeli, & E. Leonardi "A one-dimensional numerical study of the salt diffusion in a salinity-gradient solar pond". *International journal of heat and mass transfer*, 47(1), pp.1-10, (2004).
- [2] Weinberger H. "The physics of the solar pond". *Solar Energy*, 8(2), pp.45-56, (1964).
- [3] Rabl, A., & Nielsen, C. E. "Solar ponds for space heating" *Solar Energy*, 17(1), pp.1-12, (1975).
- [4] Hull, J.R., "Computer simulation of solar pond thermal behaviour" *Solar Energy*, 25, pp.33-40, (1980).
- [5] Rubin, H., Benedict, B.A., Bachu, S., "Modeling the performance of a solar pond as a source of thermal energy" *Solar Energy*, 32, pp.771-778, (1984).
- [6] Kurt, Hüseyin, Mehmet Ozkaymak, and A. Korhan Binark. "Experimental and numerical analysis of sodium-carbonate salt gradient solar-pond performance under simulated solar-radiation." *Applied energy* 83(4), pp. 324-342, (2006).
- [7] Jayadev, T. S., and Jon Henderson. "Salt concentration gradient solar ponds-modeling and optimization." *Proceedings of International Solar Energy Society*. Atlanta, vol. 1, pp. 1015-1019, (1979).
- [8] Panahi, Zahra, J. Clair Batty, and J. P. Riley. "Numerical simulation of the performance of a salt-gradient solar pond." *J. Sol. Energy Eng. : (United States)* 105(4), (1983).
- [9] Bryant, H. C., and Ian Colbeck. "A solar pond for London?" *Solar Energy* 19(3), pp.321-322, (1977).
- [10] Jafarzadeh, Mohammad Reza. "Thermal behavior of a small salinity-gradient solar pond with wall shading effect." *Solar Energy* 77(3), pp.281-290, (2004).
- [11] Kishore, V. V. N., and Veena Joshi. "A practical collector efficiency equation for nonconvecting solar ponds." *Solar Energy* 33(5), pp. 391-395, (1984).
- [12] <http://www.eso.org/gen-fac/pubs/astclim/espas/world/ION/ion-cloud.html>
- [13] Kurt, Hüseyin, Fethi Halici, and A. Korhan Binark. "Solar pond conception—experimental and theoretical studies." *Energy conversion and management* 41(9), pp. 939-951, (2000).
- [14] Hull, John R., J. Nielsen, and Peter Golding. "Salinity gradient solar ponds." (1988).
- [15] Srinivasan, J. "Solar pond technology." *Sadhana (Academy Proceedings in Engineering Sciences)*. Vol. 18. Indian Academy of Sciences, 1993.
- [16] AlMaliky, Salam J. Bash. "Investigation of the Readiness of Ground Soils for the Installation of Ground Heat Exchange Systems in Baghdad City." *Journal of Geography and Geology* 3(1), pp.200, (2011).
- [17] Abdkaramallah, Abdulhassan, Hussen, Hasanen. M., Hoshi, Hisham A., "Experimental model of ground-source heat pump." *The 7th Jordanian International Mechanical Engineering Conference (JIMEC'7)*, Sept. (2010).
- [18] Leblanc, Jimmy, Aliakbar Akbarzadeh, John Andrews, Huanmin Lu, and Peter Golding. "Heat extraction methods from salinity-gradient solar ponds and introduction of a novel system of heat extraction for improved efficiency." *Solar Energy*, 85(12), pp. 3103-3142, (2011).
- [19] <http://www.bom.gov.au/climate/data/>

References

- Agyenim, F., Knight, I. & Rhodes, M. (2010) Design and experimental testing of the performance of an outdoor LiBr/H₂O solar thermal absorption cooling system with a cold store. *Solar energy*, 84(5), 735-744.
- Akbarzadeh, A., Andrews, J. & Golding, P. (2005) Solar pond technologies: a review and future directions.
- Aktacir, M. A., Büyükalaca, O. & Yılmaz, T. (2010) A case study for influence of building thermal insulation on cooling load and air-conditioning system in the hot and humid regions. *Applied Energy*, 87(2), 599-607.
- Alagao, F., Akbarzadeh, A. & Johnson, P. (1994) The design, construction, and initial operation of a closed-cycle, salt-gradient solar pond. *Solar Energy*, 53(4), 343-351.
- Al-Karaghoul, A., Al-Hamdani, N. & Al-Sinan, W. (1989) Iraqi solar house cooling season performance evaluation. *Solar & wind technology*, 6(1), 29-40.
- Allouhi, A., Kousksou, T., Jamil, A., Bruel, P., Mourad, Y. & Zeraouli, Y. (2015) Solar driven cooling systems: An updated review. *Renewable and Sustainable Energy Reviews*, 44, 159-181.
- AlMaliky, S. J. B. (2011) Investigation of the readiness of ground soils for the installation of ground heat exchange systems in Baghdad city. *Journal of Geography and Geology*, 3(1), p200.
- Almeida, P., Carvalho, M., Amorim, R., Mendes, J. F. & Lopes, V. (2014) Dynamic testing of systems—Use of TRNSYS as an approach for parameter identification. *Solar Energy*, 104, 60-70.
- Al-Mutaz, I. & Al-Anezi, A. (1999) Determination of Silica Scale Potential in Reverse Osmosis Pretreatment. *In: International Desalination Association, San Diego Conference Proceedings*, 1999.
- Alsammarae, A., I RAQ's Electrical System. 2005. p. 36.
- Anderson CC. (1958) 'Limnology of shallow saline meromictic lake'. *Limnol Oceanogr*; 3:25-69.
- Angeli, C. & Leonardi, E. (2004) A one-dimensional numerical study of the salt diffusion in a salinity-gradient solar pond. *International journal of heat and mass transfer*, 47(1), 1-10.

- Arias, D. A. (2006) Advances on the coupling between a commercial CFD package and a component-based simulation program. *In: Second National IBPSA-USA Conference (SimBuild 2006)*, Cambridge, MA, 2006.
- Armanasco, F., Colombo, L. P. M., Lucchini, A. & Rossetti, A. (2015) Performance analysis of a solar cooling plant based on a liquid desiccant evaporative cooler. *International Journal of Refrigeration*, 53, 163-176.
- Aryo-group (2012) Aryo-group. Available at: <http://www.aryo-group.com/index.php/en/> (Accessed: 1 October 2014).
- ASHRAE, A. (2005) Handbook of fundamentals. American Society of Heating Refrigerating and Air Conditioning Engineers, Atlanta, GA.
- Asim, M. (2016) Simulation of solar powered absorption cooling system for buildings in Pakistan. University of Manchester.
- Atkinson, J. F. & Harleman, D. (1983) A wind-mixed layer model for solar ponds. *Solar Energy*, 31(3), 243-259.
- Balaras, C. A., Grossman, G., Henning, H.-M., Ferreira, C. A. I., Podesser, E., Wang, L. & Wiemken, E. (2007) Solar air conditioning in Europe—an overview. *Renewable and sustainable energy reviews*, 11(2), 299-314.
- Barron, R. F. (1999) *Cryogenic heat transfer*: CRC Press.
- Beckman, W. A., Klein, S. A. & Duffie, J. A. (1977) Solar heating design, by the f-chart method. *NASA STI/Recon Technical Report A*, 78, 31071.
- Behari, J. (2006) *Microwave dielectric behaviour of wet soils* (Vol. 8): Springer Science & Business Media.
- Bhatia. (2015). Overview of Vapor Absorption Cooling Systems. Available at: <https://www.cedengineering.com/userfiles/Vapor%20Absorption%20Machines.pdf>, (Accessed: 20 July 2015).
- Birol, F, World Energy Outlook 2015. International Energy Agency, Paris, France, , 2015.
- Boudhiaf, R., Moussa, A. B. & Baccar, M. (2012) A two-dimensional numerical study of hydrodynamic, heat and mass transfer and stability in a salt gradient solar pond. *Energies*, 5(10), 3986-4007.
- BP Statistical Review of World Energy (2015) Available at: <https://www.bp.com/content/dam/bp/pdf/energy-economics/statistical-review-2015/bp-statistical-review-of-world-energy-2015-full-report.pdf> (Accessed: 5 August 2016).

- BP Energy Outlook (2016) Available at: <https://www.bp.com/content/dam/bp/pdf/energy-economics/energy-outlook-2016/bp-energy-outlook-2016.pdf> (Accessed: 12 August 2016).
- Bryant, H. & Colbeck, I. (1977) A solar pond for London? *Solar Energy*, 19(3), 321-322.
- Bureau of Energy Efficiency (2004) Available at: <https://beeindia.gov.in/sites/default/files/3Ch4.pdf> (Accessed: 18 August 2016).
- Cengel, Y. & Özişik, M. (1984) Solar radiation absorption in solar ponds. *Solar Energy*, 33(6), 581-591.
- Cengel, Y. A., Klein, S. & Beckman, W. (1998) *Heat transfer: a practical approach* (Vol. 141): McGraw-Hill New York.
- Chattree, M. & Sengupta, S. (1985) Heat transfer and evaporation from heated water bodies. *Journal of heat transfer*, 107(4), 779-787.
- Chepurniy, N. & Savage, S. (1975) Effect of diffusion on concentration profiles in a solar pond. *Solar Energy*, 17(3), 203-205.
- Chinn, A., Akbarzadeh, A., Andrews, J., Malik, N. & Fonseca, T. (2001) Solar Pond Technology and its Role in Salinity Mitigation.
- Choudhury, B., Saha, B. B., Chatterjee, P. K. & Sarkar, J. P. (2013) An overview of developments in adsorption refrigeration systems towards a sustainable way of cooling. *Applied Energy*, 104, 554-567.
- Clarke, B. G., Agab, A. & Nicholson, D. (2008) Model specification to determine thermal conductivity of soils. *Proceedings of the Institution of Civil Engineers-Geotechnical Engineering*, 161(3), 161-168.
- Clintberg, B. (2005) Lesson 54: Snell's law. Available at: http://www.studyphysics.ca/newnotes/20/unit04_light/chp1719_light/lesson54.htm, (Accessed: 26 October 2016).
- Collins, R. & Fredrickson, D. (1985) The advanced Alice Springs solar pond. *Ext. Abst. Intersol*, 85, 327.
- CtrlTech. (2014). Industrial Dehumidifier. Available at: <http://www.dehumidifier-uae.com/industrial-dehumidifier-in-uae>, (Accessed: 25 August 2016).
- Cussler, E. L. (2009) *Diffusion: mass transfer in fluid systems*: Cambridge university press.

- Department for Business, Energy & Industrial Strategy (2016) Greenhouse gas reporting - conversion factors 2016. Available at: <https://www.gov.uk/government/publications/greenhouse-gas-reporting-conversion-factors-2016> (Accessed: 1 November 2016).
- Dickinson, W. C., Clark, A. & Iantuono, A. (1976) Shallow solar ponds for industrial process heat: the ERDA--SOHIO project. California Univ., Livermore (USA). Lawrence Livermore Lab.
- Dorgan, C. B., Leight, S. P. & Dorgan, C. E. (1995) *Application guide for absorption cooling/refrigeration using recovered heat*: American Society of Heating, Refrigerating, and Air-Conditioning Engineers.
- Duffie, J. A. & Beckman, W. A. (1980) *Solar Engineering of Thermal Processes*, New York: John Wiley & Sons. Inc.
- Elata, C. & Levin, O. (1965) Hydraulics of the solar pond. *Congr. Int. Assoc. Hydraulic Res.*, 11th.
- Elhadidy, M. & Nimmo, B. (1983) The influence of bottom and side wall heat loss on solar pond performance. *ASHRAE Trans. (United States)*, 89(1A).
- El-Sebaili, A. A., Aboul-Enein, S., Ramadan, M. R. I., & Khallaf, A. M. (2011). Thermal performance of an active single basin solar still (ASBS) coupled to shallow solar pond (SSP). *Desalination*, 280(1), 183-190.
- Elwell, D. L., Short, T. H., & Badger, P. C. (1977). Stability criteria for solar/thermal-saline/ponds. In *International Solar Energy Society, Annual Meeting* (Vol. 1, pp. 16-29).
- Fasfous, A., Asfar, J., Al-Salaymeh, A., Sakhrieh, A., Al_hamamre, Z., Al-bawwab, A. & Hamdan, M. (2013) Potential of utilizing solar cooling in The University of Jordan. *Energy conversion and management*, 65, 729-735.
- Fernandes, M. S., Brites, G. J. V. N., Costa, J. J., Gaspar, A. R., & Costa, V. A. F. (2014). Review and future trends of solar adsorption refrigeration systems. *Renewable and Sustainable Energy Reviews*, 39, 102-123.
- Florides, G., Kalogirou, S., Tassou, S. & Wrobel, L. (2002) Modelling and simulation of an absorption solar cooling system for Cyprus. *Solar Energy*, 72(1), 43-51.
- Folchitto, S. (1991) Seawater as salt and water source for solar ponds. *Solar Energy*, 46(6), 343-351.

- Fong, K., Chow, T. T., Lee, C. K., Lin, Z. & Chan, L. (2010) Comparative study of different solar cooling systems for buildings in subtropical city. *Solar Energy*, 84(2), 227-244.
- Forejt, L., Hensen, J., Drkal, F. & Barankova, P. (2006) Weather data around the world for design of field hospital HVAC. *In: Proceedings international air-conditioning and ventilation conference*, 2006.
- Garg, H. (1987) Solar ponds. *Advances in Solar Energy Technology*. Springer.
- Garg, H., Bandyopadhyay, B., Rani, U. & Hrishikesan, D. (1982) Shallow solar pond: state-of-the-art. *Energy Conversion and Management*, 22(2), 117-131.
- Garrison, T. (2007) *Oceanography: an invitation to marine science*. 6th edn, California: Thomson Brooks.
- Gasulla, N., Yaakob, Y., Leblanc, J., Akbarzadeh, A. & Cortina, J. L. (2011) Brine clarity maintenance in salinity-gradient solar ponds. *Solar Energy*, 85(11), 2894-2902.
- Ghafoor, A. & Munir, A. (2015) Worldwide overview of solar thermal cooling technologies. *Renewable and Sustainable Energy Reviews*, 43, 763-774.
- Giestas, M., Pina, H. L., Milhazes, J. P. & Tavares, C. (2009) Solar pond modeling with density and viscosity dependent on temperature and salinity. *International Journal of Heat and Mass Transfer*, 52(11), 2849-2857.
- Golding, P. (1982) *A Salty Solution: The Laverton Solar Ponds*: Department Mechanical Engineering, University of Melbourne.
- Gommed, K. & Grossman, G. (2007) Experimental investigation of a liquid desiccant system for solar cooling and dehumidification. *Solar Energy*, 81(1), 131-138.
- Grossman, G. (2002) Solar-powered systems for cooling, dehumidification and air-conditioning. *Solar energy*, 72(1), 53-62.
- GVB3/16 CIBSE Guide B3: Air Conditioning and Refrigeration (2016) Available at: <http://www.cibse.org/knowledge/knowledge-items/detail?id=a0q20000008JuBbAAK> (Accessed: 5 November 2015).
- Hartmann, N., Glueck, C. & Schmidt, F. (2011) Solar cooling for small office buildings: Comparison of solar thermal and photovoltaic options for two different European climates. *Renewable Energy*, 36(5), 1329-1338.
- Hawladar, M. N. A. & Brinkworth, B. (1981) An analysis of the non-convecting solar pond. *Solar Energy*, 27(3), 195-204.
- Haynes, W. M. (2014) *CRC handbook of chemistry and physics*: CRC press.

- Henning, H.-M. (2007) Solar assisted air conditioning of buildings—an overview. *Applied thermal engineering*, 27(10), 1734-1749.
- Henning, H.-M. (2007) *Solar-assisted air conditioning in buildings: a handbook for planners*: Springer Verlag Wien.
- Henning, H.-M. & Döll, J. (2012) Solar systems for heating and cooling of buildings. *Energy Procedia*, 30, 633-653.
- Hepbasli, A. (2002) Performance evaluation of a vertical ground-source heat pump system in Izmir, Turkey. *International Journal of Energy Research*, 26(13), 1121-1139.
- Herold, K. E., Radermacher, R. & Klein, S. A. (1996) *Absorption chillers and heat pumps*: CRC press.
- Hirschmann J. Suppression of natural convection in open ponds by a concentration gradient. In: U.N. Conf. New Sources of Energy. 1961. p. 487.
- Holman, J. (2002) Heat transfer 9th Edition. *New York, Boston, McGraw-Hill, Inc*, 168-169.
- Holman, J. P. (2010) *Heat transfer*: McGraw-Hill.
- Hong, T., Chang, W.-K. & Lin, H.-W. (2013) A fresh look at weather impact on peak electricity demand and energy use of buildings using 30-year actual weather data. *Applied Energy*, 111, 333-350.
- Hull, J. & Kasza, K. (1985) Heat extraction from salt gradient solar ponds for agricultural purposes. Argonne National Lab., IL (USA).
- Hull, J., Liu, K., Sha, W., Kamal, J. & Nielsen, C. (1984) Dependence of ground heat loss upon solar pond size and perimeter insulation calculated and experimental results. *Solar Energy*, 33(1), 25-33.
- Hull, J. R. (1978) The effects of radiation absorption on convective instability in salt-gradient solar ponds. *Proc. Am. Sec. ISES Meet*, 37-40.
- Hull, J. R. (1980) Membrane stratified solar ponds. *Solar Energy*, 25(4), 317-325.
- Hull, J. R. & Nielsen, C. E. (1989) Steady-state analysis of the rising solar pond. *Solar energy*, 42(5), 365-377.
- Hull, J. R., Nielsen, J. & Golding, P. (1988) Salinity gradient solar ponds.
- Huppert, H. E. & Turner, J. S. (1981) Double-diffusive convection. *Journal of Fluid Mechanics*, 106, 299-329.

- Hussen, H. M. & Hisham, A. (2010) Experimental Model of Ground-Source Heat Pump System. *In: The 7th Jordanian International Mechanical Engineering Conference (JIMEC'7)*, 27-29.
- Hwang, Y., Radermacher, R., Alili, A. A. & Kubo, I. (2008) Review of solar cooling technologies. *HVAC&R Research*, 14(3), 507-528.
- IIT Kharagpur (2009) Available at: <http://nptel.ac.in/courses/112105128/> (Accessed: 10 April 2015).
- Iraq-Climate. (1988). Iraq Index. Available at: <http://data.mongabay.com/history/iraq/iraq-climate.html>, (Accessed: 27 July 2015).
- Iraqi Meteorological Organisation and Seismology (2013) Available at: <http://meteoseism.gov.iq/index.php?name=Pages&op=page&pid=75>, (Accessed: 26 October 2016).
- Issa, R. I. (1986) Solution of the implicitly discretised fluid flow equations by operator-splitting. *Journal of computational physics*, 62(1), 40-65.
- Jaefarzadeh, M. R. (2004) Thermal behavior of a small salinity-gradient solar pond with wall shading effect. *Solar Energy*, 77(3), 281-290.
- Jassim, S. Z. & Goff, J. C. (2006) *Geology of Iraq*: DOLIN, sro, distributed by Geological Society of London.
- Yari, M., Javaani, N., Ansari, A., & Moradian, H. (2005). Design and installation of the first geothermal heat pump in Iran. In *Proceedings World Geothermal Congress, Antalya, Turkey* (pp. 24-29).
- Jassim, S. Z., & Goff, J. C. (Eds.). (2006). *Geology of Iraq*. DOLIN, sro, distributed by Geological Society of London.
- Joudi, K. A. & Abdul-Ghafour, Q. J. (2003) Development of design charts for solar cooling systems. Part I: computer simulation for a solar cooling system and development of solar cooling design charts. *Energy Conversion and Management*, 44(2), 313-339.
- Joudi, K. A. & Abdul-Ghafour, Q. J. (2003) Development of design charts for solar cooling systems. Part II: Application of the cooling f-chart. *Energy Conversion and Management*, 44(2), 341-355.
- Kalogirou, S. A. (2004) Optimization of solar systems using artificial neural-networks and genetic algorithms. *Applied Energy*, 77(4), 383-405.

- Kalogirou, S. A. (2013) *Solar energy engineering: processes and systems*: Academic Press.
- Kamal, W. A. (1992) A solar pond for air conditioning a small family house in Qatar. *Engineering Journal of Qatar University*, Vol. 5, p. 163-176.
- Kanan, S., Dewsbury, J. & Lane-Serff, G. F. (2015) Simulation of Solar Air-Conditioning System with Salinity Gradient Solar Pond. *Energy Procedia*, 79, 746-751.
- Kanan, S., Dewsbury, J., Lane-Serff, G. F. & Asim, M. (2016) The Effect of Ground Conditions under a Solar Pond on the Performance of a Solar Air-conditioning System. *Energy Procedia*, 91, 777-784.
- Karakilcik, M., Dincer, I. & Rosen, M. A. (2006) Performance investigation of a solar pond. *Applied Thermal Engineering*, 26(7), 727-735.
- Kennish, W. J. (1978) *An approach to the validation of computer simulation codes*: Department of Energy.
- Kishore, V. & Joshi, V. (1984) A practical collector efficiency equation for nonconvecting solar ponds. *Solar Energy*, 33(5), 391-395.
- Klein, S. (2010) A Transient System Simulation Program (TRNSYS 17) Manual. *Thermal Energy System Specialists. Madison, USA*.
- Klein, S. & Beckman, W. (1971) TRNSYS, a Simulation program. *ASHRAE Trans*, 76.
- Klein, S., Cooper, P., Freeman, T., Beckman, D., Beckman, W. & Duffie, J. (1975) A method of simulation of solar processes and its application. *Solar Energy*, 17(1), 29-37.
- Klein, S., Duffie, J., Beckman, W. & Bradley, D. (2010) TRNSYS 17. *A Transient System Simulation Program (Solar Energy Laboratory, University of Wisconsin, Madison, USA, 2009)*.
- Klein, S. A., Beckman, W. & Duffie, J. (1976) A design procedure for solar heating systems. *Solar Energy*, 18(2), 113-127.
- Kooi, C. F. (1979). The steady state salt gradient solar pond. *Solar Energy*, 23(1), 37-45.
- Kreith, F., Manglik, R. & Bohn, M. (2010) *Principles of heat transfer*: Cengage learning.
- Kumar, A. & Kishore, V. (1999) Construction and operational experience of a 6000 m² solar pond at Kutch, India. *Solar energy*, 65(4), 237-249.

- Kurt, H., Halici, F. & Binark, A. K. (2000) Solar pond conception—experimental and theoretical studies. *Energy conversion and management*, 41(9), 939-951.
- Kurt, H., Ozkaymak, M., & Binark, A. K. (2006). Experimental and numerical analysis of sodium-carbonate salt gradient solar-pond performance under simulated solar-radiation. *Applied energy*, 83(4), 324-342.
- Lazzarin, R. M. (2014) Solar cooling: PV or thermal? A thermodynamic and economical analysis. *International Journal of Refrigeration*, 39, 38-47.
- Leblanc, J., Akbarzadeh, A., Andrews, J., Lu, H. & Golding, P. (2011) Heat extraction methods from salinity-gradient solar ponds and introduction of a novel system of heat extraction for improved efficiency. *Solar Energy*, 85(12), 3103-3142.
- Leshuk, J., Zaworski, R., Styris, D. & Harling, O. (1978) Solar pond stability experiments. *Solar Energy*, 21(3), 237-244.
- Lide, D. R., & Bruno, T. J. (2012). CRC handbook of chemistry and physics. CRC Press LLC.
- Li, Z. & Sumathy, K. (2000) Technology development in the solar absorption air-conditioning systems. *Renewable and sustainable energy reviews*, 4(3), 267-293.
- Lizarte, R., Izquierdo, M., Marcos, J. & Palacios, E. (2013) Experimental comparison of two solar-driven air-cooled LiBr/H₂O absorption chillers: Indirect versus direct air-cooled system. *Energy and Buildings*, 62, 323-334.
- Lu, H. & Swift, A. (1996) Reconstruction and operation of the El Paso Solar Pond with a geosynthetic clay liner system. American Society of Mechanical Engineers, New York, NY (United States).
- Lu, H., Swift, A. H., Hein, H. D. & Walton, J. C. (2004) Advancements in salinity gradient solar pond technology based on sixteen years of operational experience. *Journal of solar energy engineering*, 126(2), 759-767.
- Lu, H., Walton, J. C. & Swift, A. H. (2001) Desalination coupled with salinity-gradient solar ponds. *Desalination*, 136(1), 13-23.
- MacAdams, W. H. & McAdams, W. H. (1954) *Heat transmission*: McGraw-Hill New York.
- Martínez, P. J., Martínez, J. C. & Lucas, M. (2012) Design and test results of a low-capacity solar cooling system in Alicante (Spain). *Solar Energy*, 86(10), 2950-2960.

- Mehdizadeh, M. & Ahmadi, G. (2014) Two-Dimensional Computer Simulation of Salinity Gradient Solar Pond Operation. *In: ASME 2014 4th Joint US-European Fluids Engineering Division Summer Meeting collocated with the ASME 2014 12th International Conference on Nanochannels, Microchannels, and Minichannels, American Society of Mechanical Engineers, V01CT24A005-V01CT24A005.*
- Ministry of Construction & Housing (2009) Available at: http://www.imariskn.gov.iq/sites/default/files/syosat_eskan.pdf (Accessed: 1 November 2015).
- Meyer, K. (1981) One-dimensional model of the dynamic layer behavior in a salt-gradient solar pond. Los Alamos National Lab., NM (USA).
- Mohamed, H., Chang, J. D. & Alshayeb, M. (2015) Effectiveness of High Reflective Roofs in Minimizing Energy Consumption in Residential Buildings in Iraq. *Procedia Engineering*, 118, 879-885.
- MOTHER, the and Publications, O. (1980) Mother earth news. Available at: <http://www.motherearthnews.com/renewable-energy/solar-pond-zmaz80mjzraw> (Accessed: 1 November 2016).
- Nakahara, N., Miyakawa, Y. & Yamamoto, M. (1977) Experimental study on house cooling and heating with solar energy using flat plate collector. *Solar Energy*, 19(6), 657-662.
- Nielsen, C., Rabl, A., Watson, J. & Weiler, P. (1977) Flow system for maintenance of salt concentration gradient in solar ponds—test in isothermal pond. *Solar Energy*, 19(6), 763-766.
- Noro, M. & Lazzarin, R. (2014) Solar cooling between thermal and photovoltaic: An energy and economic comparative study in the Mediterranean conditions. *Energy*, 73, 453-464.
- Ochsner, T. E., Horton, R. & Ren, T. (2001) A new perspective on soil thermal properties. *Soil Science Society of America Journal*, 65(6), 1641-1647.
- Onwubiko, C. (1984) Effect of evaporation on the characteristic performance of the salt-gradient solar pond. *Solar Energy*, 84, 6-11.
- Ouni, M., Guizani, A. & Belguith, A. (1998) Simulation of the transient behaviour of a salt gradient solar pond in Tunisia. *Renewable Energy*, 14(1), 69-76.
- Patankar, S. (1980) *Numerical heat transfer and fluid flow*: CRC press.

- Patankar, S. V. & Spalding, D. B. (1972) A calculation procedure for heat, mass and momentum transfer in three-dimensional parabolic flows. *International journal of heat and mass transfer*, 15(10), 1787-1806.
- Pesaran, A. A. (1994) *A review of desiccant dehumidification technology*: National Renewable Energy Laboratory.
- Platten, J. & Costesèque, P. (2004) Charles Soret. A short biography. *The European Physical Journal E*, 15(3), 235-239.
- Rabl, A. & Nielsen, C. E. (1975) Solar ponds for space heating. *Solar Energy*, 17(1), 1-12.
- Rebai, L. K., Mojtabi, A., Safi, M. & Mohamad, A. (2006) A linear stability study of the gradient zone of a solar pond. *Journal of solar energy engineering*, 128(3), 383-393.
- Rubin, H., Benedict, B. A. & Bachu, S. (1984) Modeling the performance of a solar pond as a source of thermal energy. *Solar Energy*, 32(6), 771-778.
- Rudoy, W. & Cuba, J. F. (1979) *Cooling and heating load calculation manual*: ASHRAE.
- Sarbu, I. & Sebarchievici, C. (2013) Review of solar refrigeration and cooling systems. *Energy and Buildings*, 67, 286-297.
- Saxena, A., Sugandhi, S. & Husain, M. (2009) Significant depth of ground water table for thermal performance of salt gradient solar pond. *Renewable Energy*, 34(3), 790-793.
- Schladow, S. G. (1988) Simulation of Dynamics of the Double-Diffusive System. *Journal of Hydraulic Engineering*, 114(1), 1-20.
- Schmitt, D. D., Klein, S. A. & Reindl, D. T. (2000) Automated generation of hourly design sequences. Univ. of Wisconsin, Madison, WI (US).
- Schwerdt, P. & Ali, A. H. H. (2014) German/Egyptian demonstration project on solar cooling in a hot arid climate. *Energy Procedia*, 48, 991-996.
- Seinfeld, J. H. & Pandis, S. N. (2016) *Atmospheric chemistry and physics: from air pollution to climate change*: John Wiley & Sons.
- Sekret, R. & Turski, M. (2012) Research on an adsorption cooling system supplied by solar energy. *Energy and Buildings*, 51, 15-20.
- Sherman, B. S. & Imberger, J. (1991) Control of a solar pond. *Solar Energy*, 46(2), 71-81.

- Shirtcliffe, T. (1969) An experimental investigation of thermosolutal convection at marginal stability. *Journal of Fluid Mechanics*, 35(04), 677-688.
- Singh, T., Singh, A. & Kaushika, N. (1994) Investigations of thermohydrodynamic instabilities and ground storage in a solar pond by simulation model. *Heat Recovery Systems and CHP*, 14(4), 401-407.
- Sodha, M., Kaushik, N. & Rao, S. (1981) Thermal analysis of three zone solar pond. *International Journal of Energy Research*, 5(4), 321-340.
- Spalding, D. (1972) A novel finite difference formulation for differential expressions involving both first and second derivatives. *International Journal for Numerical Methods in Engineering*, 4(4), 551-559.
- Srinivasan, J. (1993) Solar pond technology. *Sadhana*, 18(1), 39-55.
- Stolzenbach KD, Dake JMK, Harleman DRF. Prediction of temperature in solar ponds. In: Annu. Meeting, Solar Soc. 1986.
- Suárez, F., Tyler, S. W. & Childress, A. E. (2010) A fully coupled, transient double-diffusive convective model for salt-gradient solar ponds. *International Journal of Heat and Mass Transfer*, 53(9), 1718-1730.
- Subhakar, D. & Murthy, S. S. (1993) Saturated solar ponds: 1. Simulation procedure. *Solar Energy*, 50(3), 275-282.
- Sundaram, T. (1974) Transient thermal response of large lakes to atmospheric disturbances. In: IN: PROCEEDINGS, SEVENTEENTH CONFERENCE ON GREAT LAKES RESEARCH, PART 2, 1974.
- Surface meteorology and solar energy (2014) Available at: <https://eosweb.larc.nasa.gov/sse/> (Accessed: 26 October 2016)
- Swinbank, W. C. (1963) Long-wave radiation from clear skies. *Quarterly Journal of the Royal Meteorological Society*, 89(381), 339-348.
- Systems, C.T. (2007) Cooling tower systems, Inc. - water cooling tower model: T-220. Available at: <http://www.coolingtowersystems.com/t220towerspec.php> (Accessed: 10 January 2016).
- Tabor, H. (1961) Large-area solar collectors (Solar Ponds) for power production', UN Conf. *New Sources of Energy, Publication S/47, Rome*.
- Tabor, H. & Matz, R. (1965) A status report on a solar pond project. *Solar Energy*, 9(4), 177-182.
- Tabor, H. (1981). Solar ponds. *Solar Energy*, 27(3), 181-194.

- Taga, M., Matsumoto, T. & Ochi, T. (1990) Studies on membrane viscosity stabilized solar pond. *Solar Energy*, 45(6), 315-324.
- Thevenard, D. J. & Brunger, A. P. (2002) The development of typical weather years for international locations: part I, algorithms. *ASHRAE Transactions*, 108, 376.
- Tsilingiris, P. T. (1992). The absorption chiller in large scale solar pond cooling design with condenser heat rejection in the upper convecting zone. *Solar energy*, 49(1), 19-27.
- Tundee, S., Terdtoon, P., Sakulchangsattajai, P., Singh, R. & Akbarzadeh, A. (2010) Heat extraction from salinity-gradient solar ponds using heat pipe heat exchangers. *Solar Energy*, 84(9), 1706-1716.
- Tybout, R. A. (1967) A recursive alternative to Weinberger's model of the solar pond. *Solar Energy*, 11(2), 109-111.
- Ullah, K., Saidur, R., Ping, H., Akikur, R. & Shuvo, N. (2013) A review of solar thermal refrigeration and cooling methods. *Renewable and Sustainable Energy Reviews*, 24, 499-513.
- US Department of Energy. Weather Data Sources. Energy Efficiency & Renewable Energy (2016) 22-April-2015]; Available from: http://apps1.eere.energy.gov/buildings/energyplus/weatherdata_sources.cfm.
- Usmanov, Y., Eliseev, V. & Umarov, G. Y. (1971) Optical characteristics of a solar pond.[Absorption of solar radiation in a saline-solar pond]. *Appl. Solar Energy (USSR)(Engl. Transl.);(United States)*, 7(3).
- Usmanov, Y. U., Umarov, G. Y. & Zakhidov, R. (1969) Salt-water ponds as solar-energy accumulators. *Appl. Solar Energy (USSR)(Engl. Transl.);(United States)*, 5(2).
- Van Doormaal, J. & Raithby, G. (1984) Enhancements of the SIMPLE method for predicting incompressible fluid flows. *Numerical heat transfer*, 7(2), 147-163.
- Versteeg, H. K. & Malalasekera, W. (2007) *An introduction to computational fluid dynamics: the finite volume method*: Pearson Education.
- Vitner, A., Sarig, S. & Reisfeld, R. (1988) The self-generation mechanism of a laboratory scale saturated solar pond. *Solar energy*, 41(2), 133-140.
- Wang, Y. & Akbarzadeh, A. (1983) A parametric study on solar ponds. *Solar Energy*, 30(6), 555-562.
- Ward, D. S. (1979) Solar absorption cooling feasibility. *Solar Energy*, 22(3), 259-268.

- Ward, D. S., Weiss, T. A. & Löf, G. O. (1976) Preliminary performance of CSU Solar House I heating and cooling system. *Solar Energy*, 18(6), 541-548.
- Weinberger, H. (1964) The physics of the solar pond. *Solar Energy*, 8(2), 45-56.
- WILO (2013) Heating, air-conditioning, cooling. Available at: <http://www.wilo.co.uk/home/products-expertise/heating-air-conditioning-cooling/air-conditioning-cooling/#.WBpuRCQnnEY> (Accessed: 9 July 2016).
- World weather information service - home (2014) Available at: <http://worldweather.wmo.int/en/home.html> (Accessed: 26 October 2016).
- Wright, J. & Loehrke, R. (1976) The onset of thermohaline convection in a linearly-stratified horizontal layer. *Journal of Heat Transfer*, 98(4), 558-563.
- Wrobel, J., Walter, P. S. & Schmitz, G. (2013) Performance of a solar assisted air conditioning system at different locations. *Solar Energy*, 92, 69-83.
- Yari, M. & Javani, N. (2007) Performance assessment of a horizontal-coil geothermal heat pump. *International journal of energy research*, 31(3), 288-299.
- Yazaki (2008) Available at: <http://www.yazakienergy.com/> (Accessed: 21 November 2014).
- YORK Commercial & Industrial HVAC (2016) Available at: http://www.johnsoncontrols.com/nl_nl/-/media/jci/be/netherlands/products/files/be_york_chillers_and_heatpumps_en_2016.pdf (Accessed: 1 November 2016).
- Zangrando, F. (1979) Observation and Analysis of a Full-Scale Experimental Salt Gradient Solar Pond.
- Zangrando, F. (1980) A simple method to establish salt gradient solar ponds. *Solar Energy*, 25(5), 467-470.
- Zangrando, F. (1991) On the hydrodynamics of salt-gradient solar ponds. *Solar Energy*, 46(6), 323-341.
- Zhai, X. & Wang, R. (2009) A review for absorbtion and adsorbtion solar cooling systems in China. *Renewable and Sustainable Energy Reviews*, 13(6), 1523-1531.
- Zhang, Z. & Wang, Y. (1990) A study on the thermal storage of the ground beneath solar ponds by computer simulation. *Solar Energy*, 44(5), 243-248.